Model-based Control of Laboratory HVAC Systems

by

Osman Ahmed

A dissertation submitted in partial fulfillment

of the requirement for the degree of

Doctor of Philosophy

(Mechnical Engineering)

at the

UNIVERSITY OF WISCONSIN - MADISON

1996

In the name of Allah, Most Gracious, Most Merciful

Read! in the name of thy Lord and Cherisher
Who created man
From a clot of congealed blood.
Proclaim! And thy Lord is most bountiful.
He, who taught the use of knowledge with the pen.
Taught men that which he knew not.

(Meaning of Verses 1-5: Chapter Read (96):Holy Qur'an)

In loving memory of my late parents,
Anjuman Ara Begum and Syed Ahmed
who inspired me to pursue Ph.D. program
and passed away during the course of this research.

Acknowledgments

Acknowledgments here are more than a formality. No words can explain the gratitude I have for so many individuals who have helped me in so many ways. I can make only a feeble attempt.

I feel fortunate to have pursued this research at the Solar Energy Laboratory, University of Wisconsin- Madison, in a congenial atmosphere. Professors William A. Beckman, John W. Mitchell and Sanford A. Klein have created an outstanding research environment conducive to an open exchange of ideas and academic excellence.

Prof. Beckman's interest in my research and encouragement are much appreciated. With deep sincerity, I thank Prof. Sanford Klein for his constant guidance and suggestions. He provided invaluable assistance in developing simulation program and resolving many programming issues. Without the support of Prof. John Mitchell, It would have been next to impossible to complete this research. His constant inspiration and personal dedication were exemplary in keeping me focused. I remain grateful to him for his profound contribution in guiding me. It is my privilege to have found in Prof. Mitchell both a guide and a mentor.

Thanks are due to Landis & Gyr management for giving me an opportunity to pursue the Ph.D. program and for providing financial support throughout the course of this research. I also received unquestioned support and assistance whenever I needed it throughout the Landis & Gyr organization,

and I am thankful for that help. I am particularly grateful to my present and past supervisors, and my colleagues and my friends at the Laboratory Business Division for their unparalleled support and encouragement.

It is now time to reflect on the value of my family. I am highly grateful to all my relatives and friends for their continued encouragement. In the course of this project, I was often challenged to find time for research in between a full time job and a family. It was difficult. My family sacrificed a lot in sharing my dream to pursue higher studies. I am grateful to my wife, Aftab, and my children, Aadil and Aaqib, for their personal dedication, understanding and sacrifice. In times of frustration, it was Aftab's encouragement kept me going; while in times of accomplishments, the whole family was brought together. To me, the real value of this research is not in its conclusions and findings, but in the process of arriving at an end. This process of patience, endurance and perseverance, I hope, will make me humble and encourage me to share my experience and knowledge with my children and others.

Finally, a couple of happy notes. My eldest son, Aadil is very happy that I have completed my research. Now, we will have more time together. My little son, Aaqib did not want me to complete my research. He thought I was getting a medical degree and would be able to give him shots. Well, just recently, he realized that I will be getting a doctorate in engineering and he can perfectly say "Doctor in Philosophy".

Abstract

The laboratory (lab) environment is unique in terms of the comfort and safety requirements and operation dynamics. The goal of the lab heating, ventilating and air conditioning (HVAC) and associated control systems are to maintain comfort and safety. The lab safety constraint requires effective control of contaminants generated within the fume hood and the lab space. A proper fume hood exhaust captures and exhausts contaminants generated within the fume hood. Contaminant leakage from the lab is prevented by lowering the space pressure compared to the adjacent space and thus inducing infiltration.

The volume flow rate of lab supply air needs to be high for effective ventilation and the safety criteria require that 100% of the supply air come from outdoors. This air flow is thermally treated which increases the lab energy cost. The lab variable air volume (VAV) HVAC system saves energy by reducing the supply air flow when the total lab exhaust decreases but challenges the lab control system because the operating states in a lab VAV vary over wide ranges. The lab HVAC system consists of several multiple, coupled, non-linear and conflicting loops. Present lab control systems use several feedback controllers which work well at the conditions of tuning and at peak operating conditions. However, they exhibit poor performance at other operating points and due to component non-linearity re- tuning becomes necessary. The lab HVAC system commissioning is challenging and expensive due to the complex process of feedback loops tuning.

This research proposes a model-based combined feedforward and feedback control strategy for lab HVAC system. The method adds an adaptive feedforward element to the existing feedback controller. The feedforward controller has identification and control algorithms. The identification algorithm captures and identifies the process characteristics and up-dates such characteristics on a regular interval. They are passed to the control block which generates the required control signal for given room conditions (i.e. space temperature and pressure). A memory based General Regression Neural Network (GRNN) that is simple to implement is used for identification and control of HVAC components and shows promising results. Any residual control signal needed to reach a steady state is provided by the feedback controller. The tuning of the combined approach will be simple and cost effective.

The operation of the combination and feedback controllers are compared for pressure, heating and cooling sequences under wide operating conditions using simulations. A lab emulator based on experiments was developed and tested for this purpose. In all cases, the proposed system performed well compared to the feedback only method in terms of providing stability and accuracy. The combined algorithm does not require additional sensors and is compatible with available HVAC controller hardware platforms. Implementation is expected to be practical and simple. Additional benefits of the proposed system includes lowering commissioning and operation cost as it needs less tuning and trouble shooting. The proposed system for a VAV lab offers customer value in terms of reducing cost, enhancing performance and maintaining lab safety and comfort.

Table of Contents

List of Figures

List of Tables

Nomenclature

a	Damper/ valve installed authority
A	Area ft^2, m^2
ach	Room air change per hour rate
Bi	Biot number
c	Specific heat kJ/kg.K, Btu/lbm.R
C	Capacitance kJ/kg.K, Btu/lbm.R
C_s	Control signal
C_1	Ratio of conduction heat transfer coefficient between thermostat and panel wall and thermostat thermal capacitance 1/minutes
C_2	Ratio of convection heat transfer coefficient between thermostat and room air and thermostat thermal capacitance 1/minutes
D_g	Derivative gain constant in PID controller
e	Error between setpoint and observed value
FF	Feedforward
Fo	Fourier number
FFPI	Combined feedforward and feedback
GRNN	General regression neural network
HVAC	Heating, ventilating, and air conditioning
h	Enthalpy kJ/kg, Btu/lbm

hc	Convection coefficient	W/(m^2.K), Btu/(h.ft^2.^{o}F)
I_g	Integral gain constant in PID controller	
k	Thermal conductance	W/(m.K), Btu/(h.ft.^{o}F)
K	Friction coefficient	
K_l	Envelope leakage constant	
K_o	Frictional coefficient when damper or valve is fully open	
L	Length	m, ft
Lab	Laboratory	
Δl	Wall thickness	m, ft
m	Mass	lbm, kg
$\dot{m}$	Rate of mass flow	lbm/sec., kg/sec.
n	Flow exponent	
P	Pressure	inches of water, kPa
ΔP	Pressure differential	inches of water, kPa
PI	Proportional-integral	
PID	Proportional-integral-derivative	
PPI	Proprietary proportional-integral	
P_g	Proportional gain constant in PID controller	
$\dot{q}_{gen}$	The rate of generation of internal heat	W, Btu/min
$\dot{q}_{load}$	Room thermal load	W, Btu/min
$\dot{q}_{tr}$	Rate of heat transfer by conduction	W, Btu/min
r	Normalized actuator position (0-1)	
r_a	Command actuator position	
R	Gas constant	kJ/kg.K, Btu/lbm.R

Rt	Thermal resistance	m^2.K/W, (h.ft^2.^oF)/Btu
S_t	Sample time	seconds
t	time	
Tau	Mass-capacitance	W-sec/K, Btu/^oF
t_o	Dead time	seconds
T	Temperature	^oC, ^oF
U	Total internal energy	kJ/kg, Btu/lbm
UO	Overall heat transfer coefficient	W/(m^2.K), Btu/(h.ft^2.^oF)
V	Volume	m^3, ft^3
VAV	Variable air volume	
$\dot{v}$	Volumetric flow rate	m^3/min, ft^3/min
$\dot{w}_f$	Non- linear valve/ damper parameter	
w.c.	Inches of water column gauge	
w.g.	Inches of water column gauge	
x	Space coordinate to indicate the direction of heat flow	
X	Random GRNN input vector	
X	Given sample of GRNN input vector	
X_i	ith observed sample of GRNN input vector X	
Y	Random GRNN output scalar	
Y	Desired GRNN output for given input vector **X**	
$\hat{Y}$	Estimate of desired GRNN output, **Y**	
Y_i	ith observed sample of GRNN output scalar Y	

Greek symbols:

ε	Coil effectiveness	
α	Thermal diffusivity	m^2/s, ft^2/s
λ	Damper leakage constant	
ρ	Density	kg/m^3, lbm/ft^3
τ	Time constant	seconds

Subscript:

a	Air
ad	Adjacent space
cl	Ceiling
Coil	Coil
dfo	Damper fully open
e	Exhaust
ex	General exhaust
f	Fluid (water)
fh	Fume hood
fl	Floor
gen	Generation
i	In
o	Out
p	Constant pressure
pw	Panel wall
r	Room
rad	Radiant wall
s	Supply

sp	Setpoint
ss	Steady state
st	Thermostat
$t\text{-}t_o$	Sample time equals to current sample time t preceded by dead time t_o
v	Constant volume
w	Wall surface

Chapter 1
Introduction

1.1 Research Objectives:

The objectives of this research are:

- To develop laboratory HVAC control strategies that enhance control performance while reducing energy cost and satisfying the safety and comfort constraints.

- To implement these strategies in a practical, simple and cost effective manner.

1.2 Research Buildings and Laboratories:

A recent Department of Energy (DOE) survey (DOE 1994) estimates that there are 19,000 buildings classified as "Laboratories" in the U.S.A. covering a total floor space of 510 million sq. ft. According to a Dodge Construction report (Dodge 1995), from 1986 to 1991, the total lab construction projects consist of 8221 buildings, 121 million sq. ft of floor area and a construction cost of 15.5 billion dollars. The statistics indicate a robust growth in the lab market as industries and educational institutions continue to invest in research and development.

Research buildings are complex in both design and function. Construction costs are between \$144 to \$275/ft^2 (Brower 1990) compared to \$89/ft^2 for hospitals (Means 1991), which is the second highest considering all building categories. Such high costs reflect the specialized nature of research

buildings in terms of functions, service utilities, safety, security and host of other features.

The laboratory is an integral part of the research building. The use of hazardous materials in a lab environment introduces the elements of safety and is unique in its design and operation. There are differences between a lab and an office space due to the health and safety factors as explained in the following.

Health and safety:

West (1978) discussed the use of primary-secondary barrier systems to contain hazardous materials within the lab and discharge the contaminants using environmentally safe practices. While the primary barriers ensure the safety of the lab workers, the secondary barriers protect the health of the non-lab personnel and the environment. The local exhaust devices are used as primary barriers whereas architectural features such as space layout, lab envelope materials, airlock, and the pressure gradients between the lab and the adjacent space act as the secondary barriers. The fume hood is discussed later in this Chapter.

The concept of a secondary barrier is shown in Figure 1.1. The lab space pressure, P is kept lower than the adjacent space pressure, P_{ad}. This is ensured by supplying less volume of air into the lab than the total lab exhaust. The difference between the lab supply and exhaust flows produces infiltration from the adjacent area and prevents leakage from the lab. The lab exhaust is a result of fume hood exhausts and the exhaust from the lab

space, often known as general exhaust. The conditioned air supplied to the laboratory maintains comfort and safety. The supply air volume flow rate is controlled to maintain pressure differential across the lab envelop while the discharge air temperature is usually modulated to maintain space temperature.

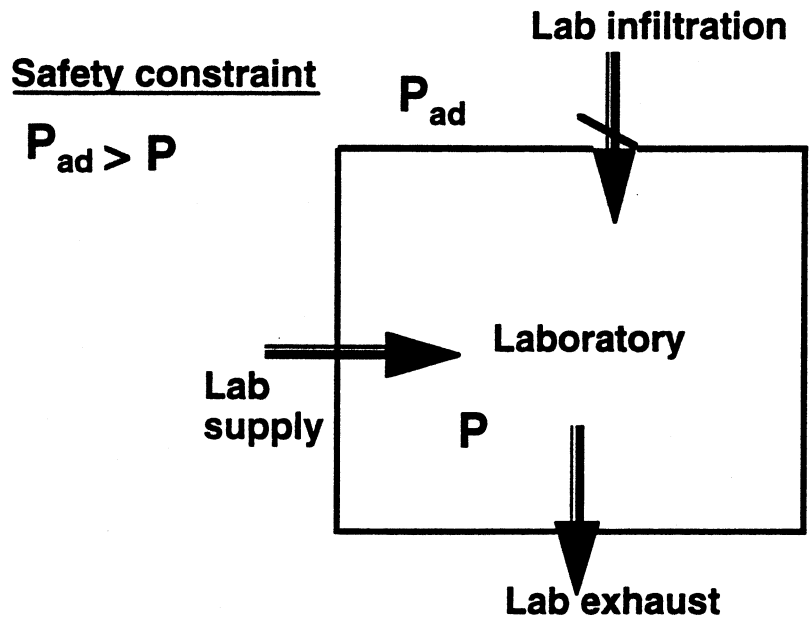

Figure 1.1: Concept of Lab de-pressurization and secondary barrier

Separate mechanical systems are used to serve lab and non-lab spaces to prevent cross-contamination. The building HVAC and HVAC control systems are responsible for maintaining both the primary and secondary barriers.

1.3 Lab HVAC Systems

The reliability, redundancy, flexibility and monitoring requirements for lab HVAC systems differ from those for commercial space. Moreover, the lab safety and comfort requirements put additional constraints on the HVAC systems. The type of HVAC system, termed a central system usually found in research buildings is shown in Figure 1.2 (Hrkman, 1996).

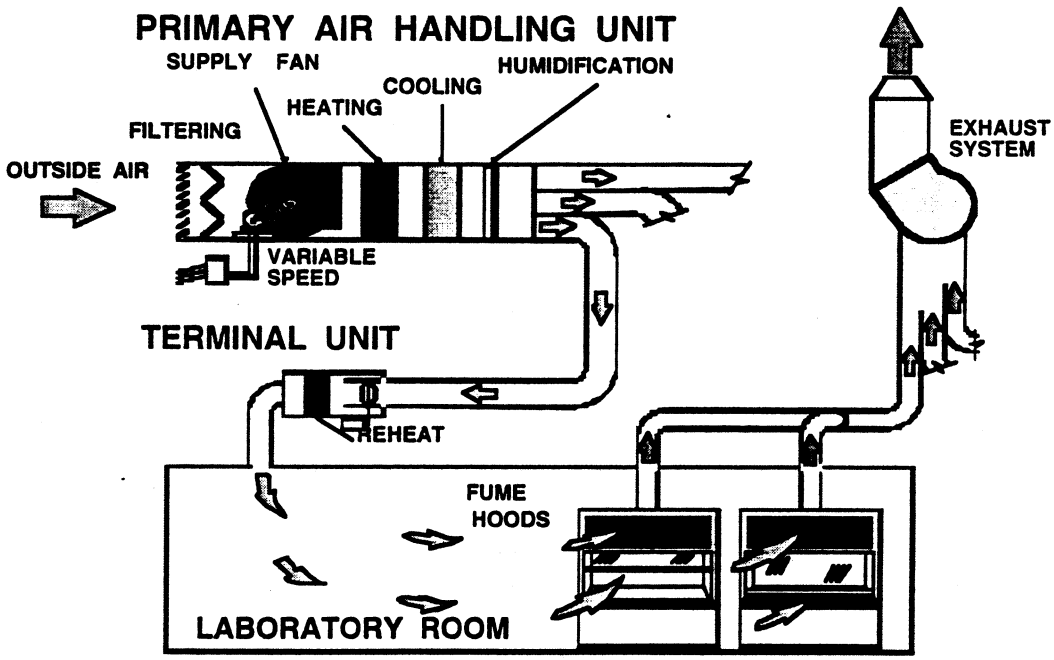

Figure 1.2: A Central Laboratory HVAC System

The central lab HVAC system treats outside air and then distributes it to different labs through ductwork. The primary air handling unit contains cooling/heating coils and maintains specified values of the supply air temperature and the humidity. In most cases, 100% outside air is drawn in

by the air handler, conditioned and then introduced to the lab space. On the exhaust side, a central fan exhausts air from the fume hoods and labs and discharges it to the atmosphere at a specified discharge velocity.

The fume hood exhaust system operates as a stand-alone system. The operation of the fume hood is independent of the central HVAC system and largely dictates the operation of the rest of the lab HVAC system. This research study addresses that the fume hood operation that puts dynamic constraints on the rest of the lab HVAC system that need to be satisfied.

Fume hood:

A fume hood is used in a lab as a safety device for containment (ASHRAE Applications 1995). A sketch of a fume hood is shown in Figure 1.3. Protective glass sashes are placed in front of the fume hood. The fume hood operates by keeping the hood interior pressure negative with respect to the lab space. The result is that room air is exhausted through the fume hood, which in the process picks up the contaminants, dilutes and then discharges them into the atmosphere. Safe hood operation requires that an average velocity of 60 - 125 fpm (SAMA 1980; Caplan and Knutson 1984) of the entering air at the face of the fume hood be maintained.

Current safe practice of fume hood operation is based on maintaining a constant face velocity (Miller and Williams 1988; Caplan and Knutson 1978). The face velocity is kept constant by varying the exhaust air flow rate as the sash open area changes. The strategy also reduces the energy

consumption. This type of fume hood is known as variable air volume (VAV) fume hood.

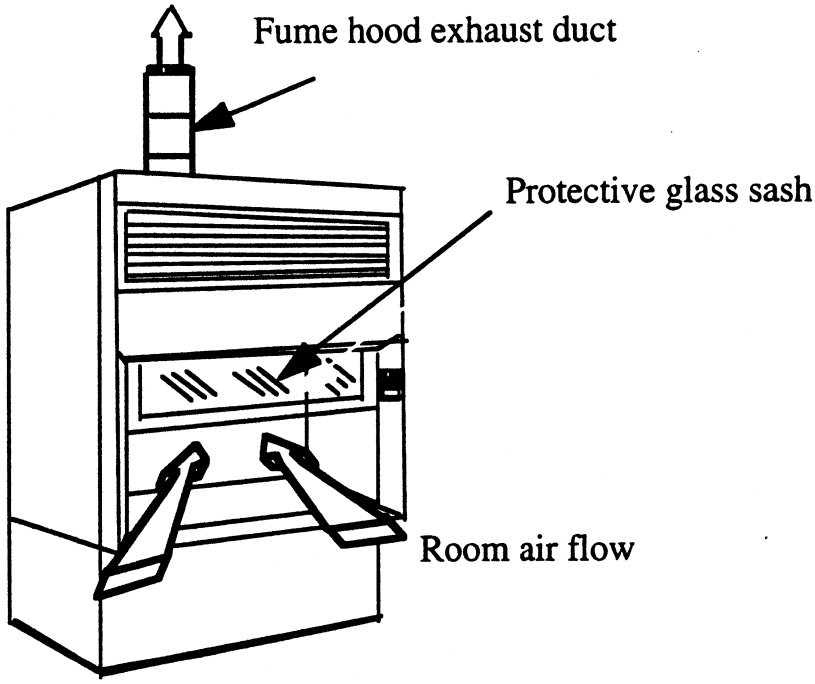

Figure 1.3: Schematic of a fume hood

Unique characteristics of lab HVAC systems:

Thermal load:

The purpose of the HVAC system is to meet the space thermal load, which can be cooling or heating, by maintaining a constant space temperature and humidity. The thermal load in a conventional office space is generally cooling whereas both cooling and heating loads may be significant for the lab space.

The lab supply air flow varies with the total lab exhaust in order to maintain a desirable pressure differential between the lab and the adjacent space. The supply air is usually maintained at 55°F to satisfy the space cooling load. However, when the supply flow rate increases significantly as a result of increases in fume hood exhausts, reheating is required to maintain the lab temperature at the setpoint. The heating load imposed by the fume hood exhausts is often referred as the ventilation load.

The thermal load in a lab space can change within seconds due to the changing exhaust flow rate of the fume hood (Neuman 1989). In addition to the thermal load, two other factors are unique for lab HVAC systems; 100% outdoor air is required since recirculation is not permitted (NFPA 1984; FDA 1976) and distribution in lab space is critical in order to keep the average room air velocity near the fume hood within 50% of the fume hood average face velocity (Knutson 1987).

Thermal comfort:

The thermal comfort criteria for lab researchers is the same as for office workers (ANSI/ASHRAE 1995; Vance 1990). The temperature setpoint in lab buildings usually varies from 78 to 68 °F for summer and winter conditions with a humidity range of 40-55% RH (Vance 1990; Carpenter 1990; Carnes 1984; Wenz 1989). From the process point of view, however, different ranges and much closer tolerances may be required with respect to both humidity and temperature (Neuman 1989; Anderson 1987). Published data for the pharmaceutical industry shows that 72 °F ± 2 °F is often maintained with the relative humidity requirements as low as 30-40%

(Accatatta 1987 and Viscovitch 1987). In critical applications, such as clean rooms, tolerances in temperature of 0.2 ^{o}F and 1% to 2.5% RH are reported (Naughton 1990; Gerbig 1981).

Safety criteria:

The lab HVAC system maintains a lower pressure in the lab space compared to the adjacent spaces. The pressure differential induces infiltration into the lab space and prevents leakage of any contaminants. A properly maintained pressure differential is critical for both lab safety (Anderson 1987) and fume hood containment (Knutson 1987; Schuyler 1990; Ahmed and Bradley 1990). The value of pressure differential varies with application and a range of 0.005 to 0.05 inches of water (w.c.) have been reported (Wenz 1989; Neuman and Rousseau 1986; Esmond 1989; Baylie and Schultz 1994).

1.4 Opportunity for Energy Conservation:

A constant air volume lab system, in parallel to the constant air volume fume hood operation, draws and exhausts a constant volume of air based on the maximum design condition and requires 100% outdoor air. The yearly energy cost of conditioning commercial space is about $2.00-3.00/ sq. ft (DOE 1991; DOE/HUD 1990). In contrast, the energy costs for a constant volume lab is in the range of $6.00 to $10.00/ sq. ft (Nelson 1986; Neuman and Rousseau 1986). Published documents report that a typical laboratory building is six to ten times more energy intensive for the same size of offices (Moyer 1983). Energy costs can be reduced, however, if the supply air volume is varied depending upon the activity in the lab space, similar to the VAV fume hood operation. The total VAV approach saves energy and also

increases VAV hood containment efficiency (Neuman and Rousseau 1986; Davis and Benjamin 1987; Neuman and Guven 1988). The VAV lab HVAC system is explored in this proposal.

1.5 VAV HVAC Systems:

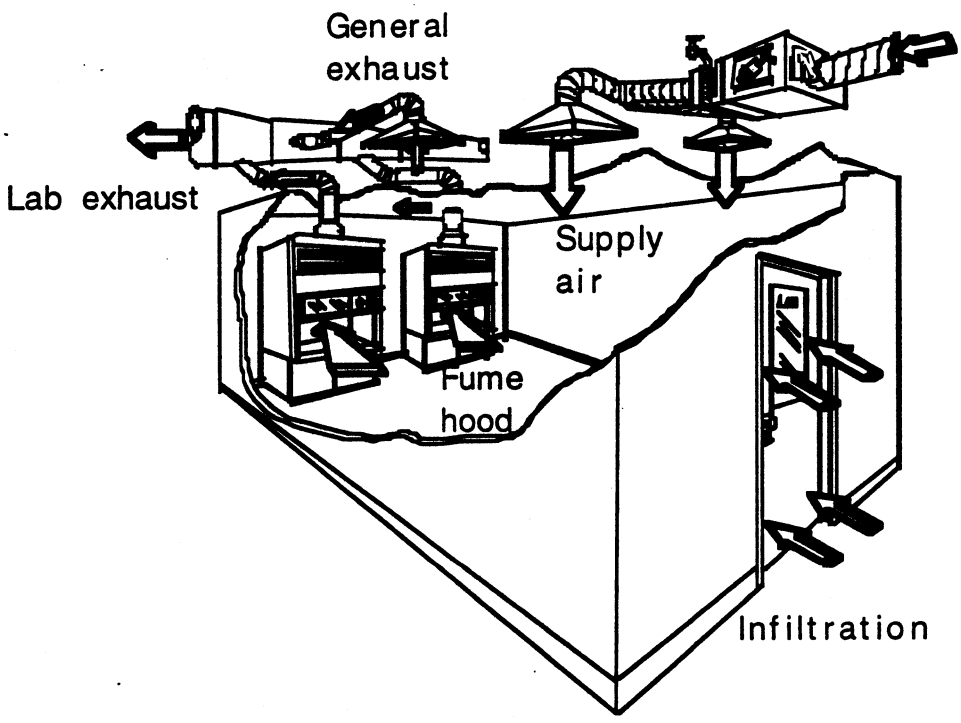

Figure 1.4: Schematic of a VAV laboratory HVAC system

Figure 1.4 shows a schematic of a VAV lab module (Hrkman, 1996). Each zone modulates the supply air volume in response to the total lab exhaust in order to maintain lower lab pressure compared to the adjacent space and induce infiltration. The supply air system serving lab space also has a re-heat coil in order to satisfy the unusual high ventilation load as explained earlier. The lab space may also produce excessive heat due to experiments or the operation of autoclave, hot plate etc. In such circumstances, the general

exhaust damper is opened and more cold air (55 ^{o}F) is introduced into the space to offset the cooling load.

Interaction between thermal comfort and lab safety:

The interaction between the thermal comfort and pressurization is complex and can be best illustrated by two examples.

Example 1 A lab maintains a steady temperature, and minimum total lab exhaust and supply flows. The differential between the total exhaust and the supply is fixed. The supply air temperature is also constant to offset the lab cooling load. The fume hoods are at minimum open positions and the general exhaust damper is closed. At a given instant, both of the fume hoods are fully opened and exhausts increase to a maximum. The supply air flow rate also increases accordingly to maintain the fixed differential. The sudden increase in the volume flow rate of supply air at a constant temperature will rapidly cool the lab space and cause discomfort. The room thermostat will eventually sense the temperature deviation and will signal for more heat.

In this example, the thermal comfort is influenced by the fume hood operation and the safety constraint of maintaining a constant flow differential between the total exhaust and the supply flow rates.

Example 2 In this case, the lab is under the same steady state condition as cited above. However, experiments using autoclaves and ovens outside the fume hoods add heat energy into the room and the lab space needs cooling. The additional cooling can be added by introducing more supply air into the

space. However, that would increase the pressure in the lab because the fume hoods are at minimum open positions and maintaining minimum exhaust flows. Under these circumstances, the general exhaust must be opened to allow more supply air flow rate.

The above example shows the impact of unusual cooling loads in a lab space on safety by changing the required total exhaust and supply flows.

1.6 VAV lab HVAC Control Systems:

Figure 1.5 shows an overall control system for a VAV lab. There are three distinct control loops working together to maintain the lab space comfortable and safe. The fume hood and the general exhaust control loops operate independent of each other, but are controlled to maintain the room pressure differential with respect to the adjacent space. The supply control loop is dependent upon the fume hood and general exhaust control systems and, to ensure safety, lags by keeping the lab space pressure always lower than the adjacent spaces. The fume hood controller controls the fume hood loop while the room controller is responsible for controlling the supply air, general exhaust and room temperature and humidity. Both these controllers are local area network devices reporting to the building automation system. Figure 1.5 also shows different sensors that measure system state variables (Hrkman, 1996). Each individual local air flow control loop has a flow measuring device. The room temperature sensor measures room temperature. In addition, duct air discharge air temperature is also measured. Finally, the pressure differential (DP) across the control dampers are also included.

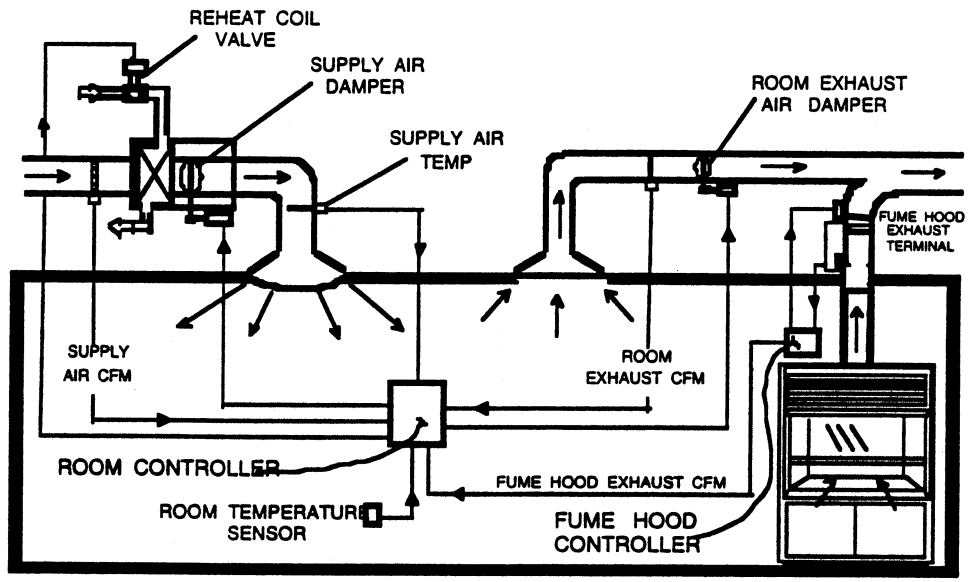

Figure 1.5: A Typical VAV Laboratory HVAC Control System

The essence of the lab control system is a feedback loop that uses a proportional-integral-derivative (PID) algorithm to compute the controller output signal based on the error between the measured process variable and the setpoint. The temperature, humidity, general exhaust flow and supply flow loops work locally to maintain their own individual setpoints. The supply flow rate setpoint is determined in the room controller by adding the general exhaust flow and the fume hood exhaust flow setpoints.

Fume hood control system:

Although the scope of the proposed research does not include the fume hood control system, it needs a brief introduction due to it's influence on the lab's control system. Figure 1.6 shows a schematic of a fume hood control system.

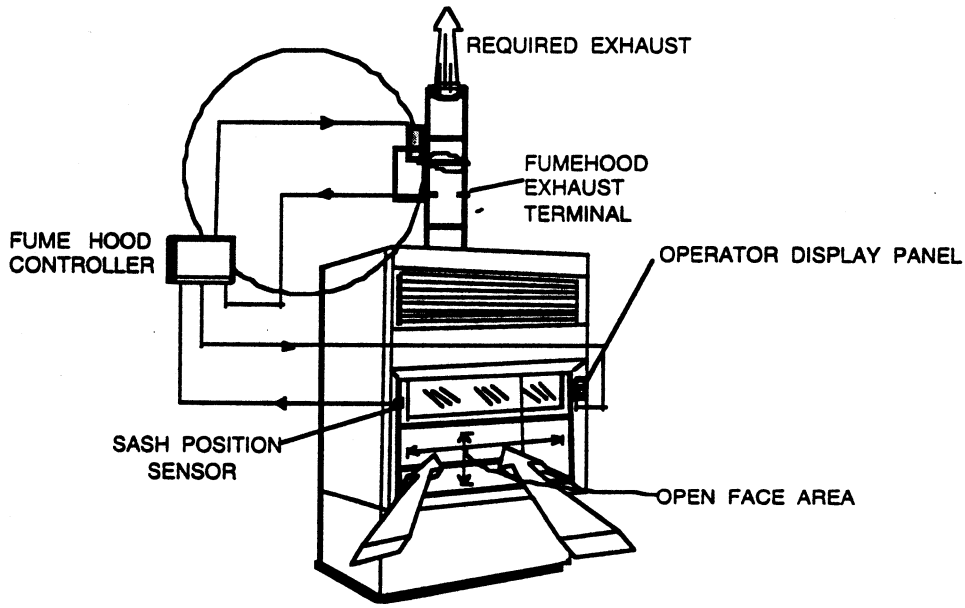

Figure 1.6: Fume hood control system

The objective of the fume hood controller is to maintain a constant average face velocity setpoint irrespective of the sash positions. In reaction to the sash movements, the controller has to respond within 2-3 seconds (Ahmed and Bradley 1990) to ensure fume hood safety and maintain a constant face velocity. Due to the practical difficulty in measuring the actual face velocity, the controller uses the total fume hood exhaust flow rate as its proces

variable. The setpoint is computed as the maximum between a minimum value and the product of the face velocity setpoint and the sash flow area. The sash flow area is calculated by measuring the position of the sash using a position sensor.

The fume hood controller then executes a feedback loop that generates an error between the exhaust flow rate setpoint and the actual exhaust flow rate. The control output then either modulates a damper actuator or a variable speed drive. A damper is used as a control to vary the fume hood exhaust flow when multiple fume hoods are exhausted by a single fan. When each fume hood is connected to an individual exhaust fan, variable speed drive varies the fume hood exhaust by modulating the fan motor speed.

In case of a variable speed drive (Ahmed et al. 1992), a feedforward path generates a control signal based on the pre-calibrated control signal-exhaust flow setpoint relationship. This feedforward signal reduces the controller response time and also simplifies tuning for the PID loop.

Room pressure control:

There are three common methods of room pressure control schemes in use today; 1) direct pressure, 2) flow tracking and 3) cascaded control. All three methods modulate the rate of supply flow. However, with such modulation, the direct pressure control maintains a fixed pressure differential, the flow tracking control holds a constant difference between the total lab exhaust and supply flow rate and the cascaded control varies the difference based on the

measured pressure differential. The response time requirement for lab pressure is usually in the range of seconds.

The major problems in using the direct pressure method are: a) finding a suitable location for the pressure sensor; b) the inability to control when the lab entrance door is open; c) the accuracy and the repeatability of measuring low pressure differentials in the range of 0.005 to 0.05 inches of water (w.c.). Although straightforward, the success of the flow tracking largely depends on the selection of a difference between exhaust and supply flow rates, which is difficult to determine. The cascaded control combines the merits of both the direct pressure and flow tracking but costs more and is more complex to operate.

Comfort control:

The most common method of temperature control is shown in Figure 1.5 in the form of a local feedback loop. Recently, in response to the increase in ventilation load due to the change in the fume hood exhaust flows, an anticipatory control strategy has been employed in a feedforward path (Marsh 1988). The strategy estimates the heating load based on the total fume hood exhaust flow rate and introduces heat into the lab before the thermostat is able to notice the drop in the space temperature. The strategy is employed to avoid large swings in room temperature.

1.7 HVAC Process Dynamics and VAV Laboratory:

HVAC systems are composed of a large number of sub-systems and each exhibits time-varying and non-linear characteristics (Chen and Lee 1990).

Kelly (1984) used 1000 differential and algebraic equations to describe a typical five-zone commercial HVAC system dynamically. For a lab space, the dynamics of HVAC process will include room thermal characteristics, air and water distribution pipes and ducts, HVAC system components such as valves, dampers and coils, control components like actuators, sensors, digital/ pneumatic interface and controllers. Each sub-system and system component exhibits different time lags which makes the indoor climate control complicated (Athienitis 1990). Like most chemical processes, HVAC systems have recycle loops (Stoecker 1971) which makes dynamic process complex. Borreson (1981) listed additional complexities associated with HVAC controls as:

1. Wide operating range.
2. Varying system gains.
3. Coupling of the control loops; i.e. interaction between the flow and the temperature loops or between the temperature and the humidity loops.

The dynamics of the HVAC system introduces an extreme challenge in a VAV lab environment. This is due to the sudden change in the lab operating conditions. The change occurs as a result of fume hood operation or generation of internal load. The internal load can change from 2 to 70 watt/sq.ft within seconds (Neuman 1989). The response time of the HVAC zone controllers, therefore, has to be within seconds to maintain room temperature. In contrast the steady heat load in a commercial space varies within 5 to 10 watt/sq.ft (ASHRAE Applications Handbook 1995).

The sudden change in heat load or sudden opening or closing of fume hood sashes means large change in supply and general exhaust flow rates. As sashes open, additional supply flow is required to maintain the space pressurization. However, as the supply flow rate is increased, heating is usually required to elevate the supply air temperature from 55 ^{o}F. An increase in supply flow is also required when the internal load increases to offset the additional thermal load. One method of defining the room air flow is in terms of room air change per hour (*ach*). The air change per hour is defined as the room air flow rate in cu.ft/ hour divided by the room volume.

$$ach = \frac{Room\ air\ flow\ rate\ (cu.\ ft/hour)}{Room\ volume\ (cu.\ ft)}\ (1/hour) \qquad (1.1)$$

The *ach* in a lab may vary from minimum of 6 to 10 ach to a maximum of 60 ach or more (ASHRAE Applications Handbook 1995; Davis and Benjamin 1987). The resultant effect is that room air flows requirement vary widely in a laboratory environment within a very short period. The task of a good lab controller, therefore, will be to provide accurate and stable control over a wide range of operations.

1.8 Summary:

An attempt is made in this introductory chapter to illustrate the uniqueness of the lab space the HVAC system and HVAC control systems in research buildings. The lab space is unique in terms of the safety requirements and flexibility. The HVAC system must respond to meet varying loads and maintain safety and comfort. The HVAC control systems must maintain the room temperature, humidity and the pressure differential accurately and

quickly to maintain the comfort and safety criteria. In certain applications, the space variables (i.e. temperature) have to be maintained within close tolerance.

Although VAV has been introduced to save energy cost, it introduces new control challenges required to produce stable and accurate performance over a wide range of operating conditions. The control scheme has to be cost effective and easy to implement and operate.

Chapter 2
Literature Survey

2.1 Overview

The purpose of this literature survey is to establish the significance of laboratory VAV HVAC systems, review the options available for the lab VAV control system and select a suitable control topology for further investigation. The literature survey is split into several sections. The first section discusses relevant literature to illustrate that the VAV saves energy costs for labs but adds challenges to the control performance. The next section focuses on the control approaches applied to HVAC systems in general. Both conventional feedback controllers and advanced control methods are included in this section. The applications of the neural network in HVAC controls is the subject of third section. The fourth section introduces memory based neural networks and compares their performance with the popular method of back propagation in neural network. The last section reviews literature on combined feedforward and feedback methods of control in order to enhance laboratory VAV HVAC system performance.

In closure, based on the literature review, a control topology is proposed for a lab HVAC control system based on combined feedforward and feedback approaches and using a specific paradigm of memory based neural network (i.e. General Regression Neural Network).

2.2 VAV Laboratory HVAC System:

Long before the energy "crisis" of early 1970's, laboratory building owners and operators explored VAV as an option to significantly reduce energy cost

but they stayed away from VAV due to safety concerns and complexity associated with the VAV system. Petersen (1964) described such concern for VAV during discussion after his presentation. He cited the disadvantages of the VAV system such as increased maintenance, complexity, difficulty with balancing, system instability and complex controls in a VAV system that often lead to unsatisfactory operation.

Such concerns were expressed even for applications of VAV in commercial space as discussed by Lujan (1977). Lujan indicated that problems with VAV includes noise and poor performance of control and control equipment. Streets and Setty (1983) looked into VAV as an energy conservation option for a large institutional research building and decided not to pursue VAV for control performance concerns.

It is only in the later part of 1980's, with the advent of distributed digital controllers, the VAV become a reality. Since then VAV has showed a significant acceptance by the industry. A precondition of a VAV lab is to have a Variable Air Volume fume hood controller since the fume hood operation and flows basically dictate the lab operation. A VAV fume hood controller was introduced in early 1980's as documented in published literature (Farho et al. 1984; Bentsen 1985; Wiggin and Morris 1985). Early versions of fume hood controllers are being continually modified and improved. Their use in laboratories has greatly increased lately as reported by Lacey (1989) and Rabiah et al. (1989). In their investigations, both Lacey and Rabiah et.al conducted extensive tests in order to evaluate the performance of different kinds of VAV fume hood controllers. They

concluded that some of the controllers were able to respond quickly (within a few seconds) to a change in the sash position in order to maintain constant face velocity. Maintaining constant velocity is the objective of the VAV fume hood controllers as discussed in the Introduction chapter and is a safety criterion as found from early research (Knutson 1987).

In 1986, Neuman and Rousseau (1986) simulated various VAV schemes for different kinds of labs and compared energy costs to a constant volume system for a small lab system consisting of 14 fume hoods. The first scheme was based on variable volume fume hood operation. The second scheme only looked into a VAV system for a clean lab without any fume hoods. Both fume and general exhaust were considered in the third scheme. The last scheme considered a special type of fume hood known as auxiliary air where unconditioned supply air is directly fed into the hood in proportion to the hood exhaust. In order to keep a minimum dilution rate, the authors suggested a minimum hood flow of 20% of the design flow at all times. An economic analysis showed that compared to a constant volume system, the third scheme can save significant energy with an internal rate of return on capital of 35.6% and a payback of 3 Years.

Neuman and Guven (1988) simulated a 200,000 square foot research building in San Diego in order to compare the VAV strategy to a constant volume one. They found that the life cycle cost of the VAV system to be $11 million compared to $18 million for a constant volume system. The payback period for the VAV system was less than six months.

As the VAV systems are being built and operated, the owners of such facilities have shared their experience on the VAV labs. Davis and Benjamin (1987) and McDiarmid (1990) expressed satisfaction with the performance of VAV labs in terms of both reducing energy cost and maintaining cost and safety. However, their findings were based on design operating conditions and did not include dynamics and part load performance.

Shumaker (1989) reported a case study on a VAV system in a research and teaching lab building having a total of 198 fume hoods. Although significant savings in fan energy were reported, the author also pointed out difficulties with holding discharge air temperature, pressure and exhaust air pressure to steady values.

The implementation of VAV system is reported by Doyle et al. (1993) for a retrofit of an industrial research facility. The facility is a 1.2 million square foot corporate research campus and the lab spaces contain more than 500 fume hoods. Projected annual savings in operating cost due to VAV system is about $480,000 compared to existing constant volume system.

Recent literature (Varley 1993; Hitchings and Shull 1993; Rabiah and Welkenbach 1993; Parker et al. 1993) report the use of VAV labs in different kinds of applications including academic institutions, manufacturing facilities and research labs. These papers, however, also point out that the actual operation in labs may vary significantly in terms of flow requirements due to the change in fume hood operation.

It seems that although the VAV strategy is a valuable option for lab buildings to cut energy cost, further improvement is necessary in terms of system performance. Rizzo (1994) pointed out a painstaking process of commissioning VAV labs as a part of a retrofit project of a hospital research facility. Several pre-requisites for the success of a VAV lab operation have been cited (Richardson 1994) which includes expected change in the room internal load and room *ach*.

In spite of the recent success of the VAV system, its role and applications have been limited to labs where critical safety and close tolerances in room temperature and pressure are not expected. The constant volume system remains as a choice for more critical applications such as microelectronics laboratory, clean rooms, clinical supply labs, biological safety labs etc. (Naughton 1990; Simons and Davoodpour 1994; Crane 1994; Bossart and McGinley 1994). The VAV has not yet proven to be a strong contender for these critical application labs where performance is critical.

2.3 HVAC control methods and issues

The literature related to control issues specific to laboratory environment is very limited. This section reviews this literature and then focuses on the control methods for HVAC system in general. It is hoped that a general review will help in identify current control methods, issues, and research trends and in selecting a suitable control topology for present research.

2.3.1 Laboratory control issues

Marsh (1988) discussed various control loops in a VAV laboratory employing PID controller. Three distinct control loops are discussed: fume hood exhaust, supply flow for pressurization, and temperature control. In the case of temperature control, a general exhaust loop is used for cooling while a heating coil is used to provide room heat. The author cited that the difficult control factor in VAV laboratories is to maintain a stable discharge air and room air temperatures due to large swing in room air flows.

The problems associated with the tight pressure control has been discussed by Hitchings (1994). The author commented that often the direct digital control system (DDC) sampling rate is inadequate to capture the short fluctuations in the room pressure. In most cases, by increasing the sample time to gain stability, the accuracy is sacrificed.

Tuning remains a major hurdle for successful implementation in a laboratory control system (Anderson 1987). Cart mounted stand alone computers have been used as adaptive control tuning systems to tune the individual loops for some time in the field. Such practice is an exception rather than norm in the industry due to the cost constraint. Anderson suggested that in the future a better cost effective method of tuning should be available in the field for safe lab operation.

Atkinson and Martino (1989) documented the HVAC control system for semiconductor manufacturing cleanrooms including commissioning process of the control system. They mentioned that achieving pressurization in the

cleanroom was most difficult due to the interaction of multiple control loops. In order to improve the commissioning process, additional sensors were suggested.

2.3.2 HVAC control methods and issues

Modern HVAC controllers usually employ some form of a feedback mechanism. A good example is a room temperature control where the error between the actual room temperature and the setpoint is used by the controller to vary the supply air flow rate. Most of these controllers use DDC as hardware/ software platform and employ PI (Proportional-Integral) or PID (Proportional-Integral-Derivative) as the feedback algorithm (Haines and Hittle 1983; Goldschimdt 1986; Guang and Geary 1993). The PID stands for Proportional-Integral-Derivative. The advantages of PID are its simplicity of implementation and the distinct effect the three terms of a PID provides to the control signal. The proportional term generates a control signal proportion to the error. The integral term produces a control signal proportional to the integral of the error over some time. and eliminates control offset. The derivative term creates a control signal which is proportional to the rate of change of error. and works as an anticipator. The signals from three different terms are added to produce the resultant control signal. The PID algorithm is further explored and discussed in detail in following chapters.

In most simple and single control loops, the PID works well. However, researchers have continued to explore means of improving the performance

of PID or looking into other alternatives for more complex and cascaded loops.

In an earlier paper, Chapman (1964) discussed the linear control theory and its applications and limitations to the HVAC systems. The author mentioned that the feedback controller (i.e. PID) for HVAC applications assume that the system is first order and linear or can be approximated as linear. However, most HVAC systems are non-linear in nature and are higher than first order. Tuning, therefore, is of paramount importance for good controller performance as the author noted. Nordeen (1995) recently cited the problems with PI/PID loops due to non linear valve/damper characteristics, time lags and interacting processes. Avery has discussed as how the interaction of multiple control loops can destabilize the VAV control strategy of an air handling unit.

Shavit and Brandt (1982) modeled a discharge air system and evaluated the performance using a PI controller. The PI controller was tuned by trial and error. They found that the performance of the system was at best when the damper and valve were fully open. However, the performance deteriorated at the other operating points. Also, the control of the variable volume of water flow through the heating coil needed different gains.

A similar study for a discharge air temperature control was reported by Nesler and Stoecker (1984). The authors selected the tuning parameters based on observed discharge air temperature response from an actual air handler and tuned the loop by trial and error at a fixed operating conditions.

Only the steam flow rate through the coil heat exchanger was varied. The authors reported good results in terms of both speed and accuracy. However, they noted that a controller with slight overshoot and quick settling time may better maintain stability through changing seasons and occupancy schedules.

Krakow et al. (1995) applied PID a controllers to compressor and evaporator fans in order to control humidity. They found that the best humidity control was achieved for the tuned conditions while the performance was poor for other operating conditions. The authors also noted that coupling of humidity and temperature control loops added complexity in tuning. The use of a PID gain scheduler was suggested by the authors. A similar conclusion was drawn by Mehta (1987) when he applied a PI controller to a fan-coil system.

A Z-transform based approach has been proven useful for PID tuning (Rohrer and Stoecker 1986). However, such an analysis is limited to linear systems and requires actual time constant data, which is difficult to obtain in cascaded loops.

Dexter and Haves (1989) have summarized the problems with the current feedback control approach. Excessive commissioning time and effort are needed to achieve desired control performance. According to the authors, the performance may be affected by the non-linearity in the system, wide range of operating conditions, time varying delays and time constants, operation near the limits of the control range due to non-linear valve and

damper actuators and change in operation mode i.e., change over from heating and cooling.

In order to circumvent the problems with the PID feedback control approach, attempts have been made to look into other control methods for improvement. To facilitate tuning of PID loops, several approaches have been attempted. The loop tuners are designed to reduce commissioning cost by eliminating trial and error process of tuning that is prevalent in the HVAC industry. Almost all major control companies offer a loop tuner to help operations and field staff in tuning loops. Most of them work on one single control loop only, use open loop response, and assume first order linear system.

Kamimura et al. (1994) developed a computer aided tuning software. The software is based on classical control theory using frequency domain analysis method such as Bode diagram and delivers tuning parameters. Again, the software is applicable for only a single-input single-output model and requires the transfer function of the system.

A closed loop tuning process was presented (Schei 1992) in which the system is excited to generate limit cycle oscillations at cross over frequency and critical frequency. The frequencies can be determined if the transfer function of the system is known. The results showed that the performance of the control system using frequency analysis to tune the PID loop was good. However, at low frequency, poor performance was reported. In addition, the knowledge of transfer function, generation and verification of desired

oscillations and then the technique to find the right tuning parameters are serious challenges to actual implementation of the closed loop tuning.

Besides the improvement in the tuning process for PI and PID loops, significant attempts have been made in the areas of adaptive control of HVAC systems. Äström (1983) presented a detailed survey on adaptive control. He listed three basic types of adaptive control mechanism: gain scheduling; model reference (MRAC); and self-tuning controller. The block diagrams for three types of mechanisms are shown in Figure 2.1.

All three methods use the basic feedback loop. In case of gain schedule, proper schedule variables are selected based on which controller parameters are obtained. Gain scheduling is open loop compensation and, therefore many operating conditions are needed for controller gain requiring extensive simulation data. The MRAC scheme includes a process model that tells how the process ideally should respond to the command signal. This scheme essentially has two loops, which are an inner feedback loop and an outer loop that adjusts the parameters of the controller such that the error between the process and the model output becomes smaller. In the case of a self-tuning controller, the inner loop consists of the process and an ordinary linear feedback controller. The controller parameters are adjusted by the outer loop, which is composed of a recursive parameter estimation and a design calculation.

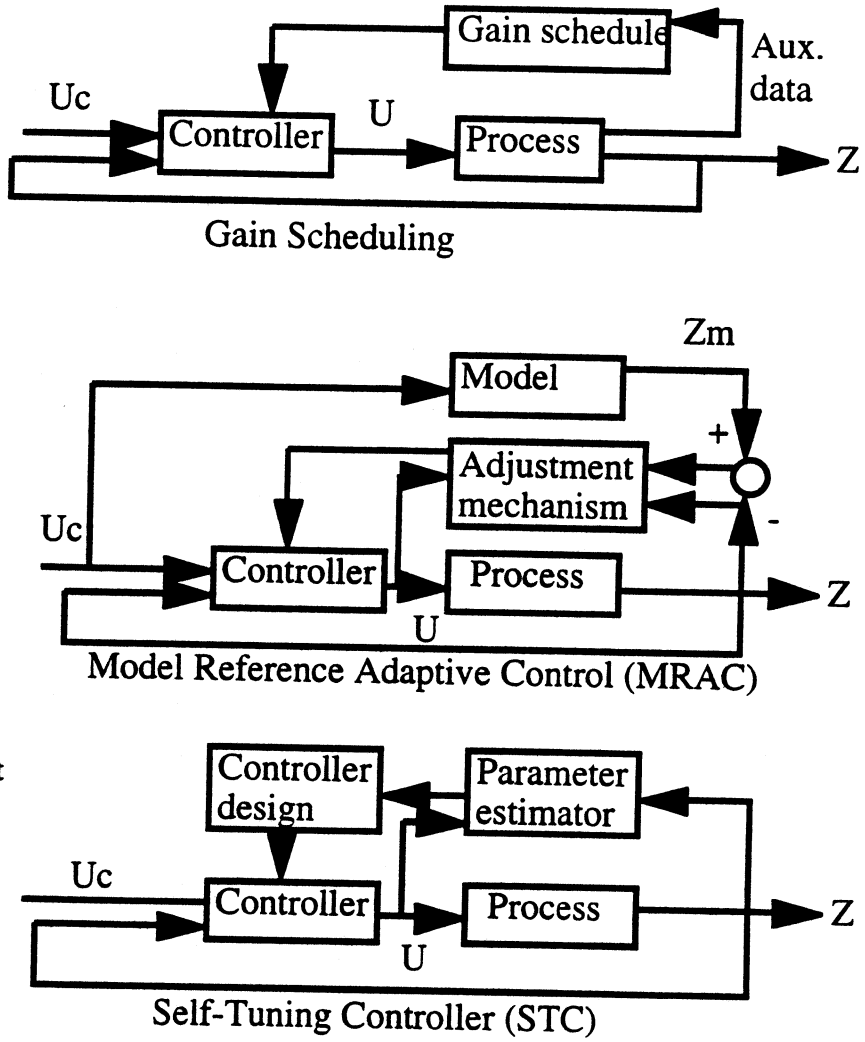

Figure 2.1: Adaptive Control Schemes

Clarke and Gawthrop (1979) implemented a micro-processor based self tuner for a room heating control system to maintain desired temperature. The self-tuner performed well in the mid-range of the heating valve. However, the performance was inadequate in other operating ranges due to the non-linearity of the valve and pronounced saturation properties.

Nesler (1985) used a self tuning controller to control the discharge air temperature from a multi-zone air handling unit. The controller was based on proportional-integral (PI) algorithm and the gains of the PI loop were changed using a RLS parameter estimation. The author pointed out that the success of the adaptive scheme is limited due to system non-linearity.

Kurz et al. (1980) used both recursive least squares (RLS) and recursive maximum likelihood (RML) methods of parameter estimation in an adaptive control system. The system was then applied to control the air temperature of a climate chamber. Although the scheme performed well, the authors noted that application of such scheme is only suited for tuning of digital control algorithms for slowly time variant and weak non-linear processes.

MacArthur et al. (1989) compared normal PI and PID controllers with an adaptive scheme of updating the gains of the controller for constant volume zone temperature control with a heating coil. The process was assumed to be a second order system. The overall strategy allowed the user to select the normal or learning mode of operation. In the learning mode, the controller excites the system by superimposing a perturbation signal on the process setpoint. These excitation results were used for rapid identification of the gains.

The response of a self tuning single loop digital controller (SLDC) was studied by Underwood (1989). The SLDC updated the gains of a PID controller based on system's open loop response until a pre-defined performance index was met. The SLDC was only activated when the

discharge air temperature deviated from the setpoint by certain amount. The performance index was defined as a linear combination of response time, integrated error between the setpoint and discharge air temperature, and the percentage overshoot. The system included an air heating loop and consisted of a heating coil, valve, and sensors measuring discharge air temperature, air and water flow rates. The author concluded that, although attractive, the SLDC was not responsive to the change in a operating range due to the process non-linearity.

Li and Wepfer (1987) used recursive estimation methods for a single-zone HVAC system. Instead of a real system, a simulated system based on the detailed HVAC models was used. The authors compared several algorithms and selected the recursive maximum likelihood based on its performance. For a given sinusoidal input of zone load, the system variables (i.e. temperature and humidity) were expressed as linear equations in terms of control input. The equation constants were recursively updated to track the simulated system's performance as close as possible. On the basis of the results the authors concluded that the RML is preferred for de-coupled systems and suited for long-term load management problems. The authors pointed out that although simple, RLS requires that disturbance sequences be strictly random in order to avoid biased estimates. This requirement limits the applications of RLS. They noted that even for a simple HVAC system, RML method may converge slowly and exhibits computational difficulties.

Bristol (1975) highlighted the use of pattern recognition as an alternative to parameter identification in adaptive control. He stressed the point that a

practical model used in the identification of a process must be simple to provide precise control. On the other hand, if the models are too simple, then the identification will lack precision. Pattern recognition between the input-output relationship can be used to characterize the transient nature of the dynamic system.

Most of the publications on adaptive control for HVAC systems are related to self-tuning controllers. The various schemes used for estimating the tuning parameters are sensitive to process non-linearity, only applicable for small systems and computationally inadequate for on-line implementation.

Dexter and Haves (1989) used a robust self-tuning predictive controller for HVAC applications based on the generalized predictive control algorithm (Dexter 1983). The authors used a simple room and cooling/heating coils as a plant. The HVACSIM+ (U.S. Dept. of Commerce 1984) computer simulation program was used to generate the data for use by the controller. The parameters were updated based on the UD filter form of the recursive least squares algorithm, using a simple form of variable exponential forgetting (Corless and Leitmann 1984). The authors noted success with the predictive approach except for handling short-term dynamics of the plant.

Argüello-Serrano and Vélez-Reyes (1995) recently published a paper on utilizing state feedback control theory to design a non-linear HVAC control system. One of the features of this approach the estimate of the thermal load and its use as a disturbance. The method linearized the HVAC model around an operating point, checked for stability and observability conditions and

then applied the Lyapunov based design method (Chen 1970) for inclusion of disturbance rejection. The linear state feedback control law was then formulated which yields an algebraic Riccati equation. The solution was found using an iterative procedure developed by Kleinman (1968). The authors noted that the availability of a load estimate helped to maintain setpoint tracking and disturbance rejection created by the thermal loads. The method described has merits from design perspective. However, on-line implementation will be difficult considering linearization around the balance point and achieving the solution by an iterative search algorithm.

2.4 Neural Network and HVAC Control Applications

Wasserman (1989) defined neural networks as "Biologically inspired; that is they are composed of elements that perform in a manner that is analogous to the most elementary functions of the biological neuron. ...Artificial networks exhibit a surprising number of the brain's characteristics. For example, they learn from experience, generalize from previous examples to new ones, and abstract essential characteristics from inputs containing irrelevant data."

A simple structure of single neuron unit is shown in Figure 2.2 (Dayhoff 1990). The inputs are connected to a processing unit j that typically uses a sigmoidal function in the form of following equation to produce an output, OUT

$$OUT = f(Sum) = \frac{1}{1 + e^{-\sum_i x_i W_{ji}}} \qquad (2.1)$$

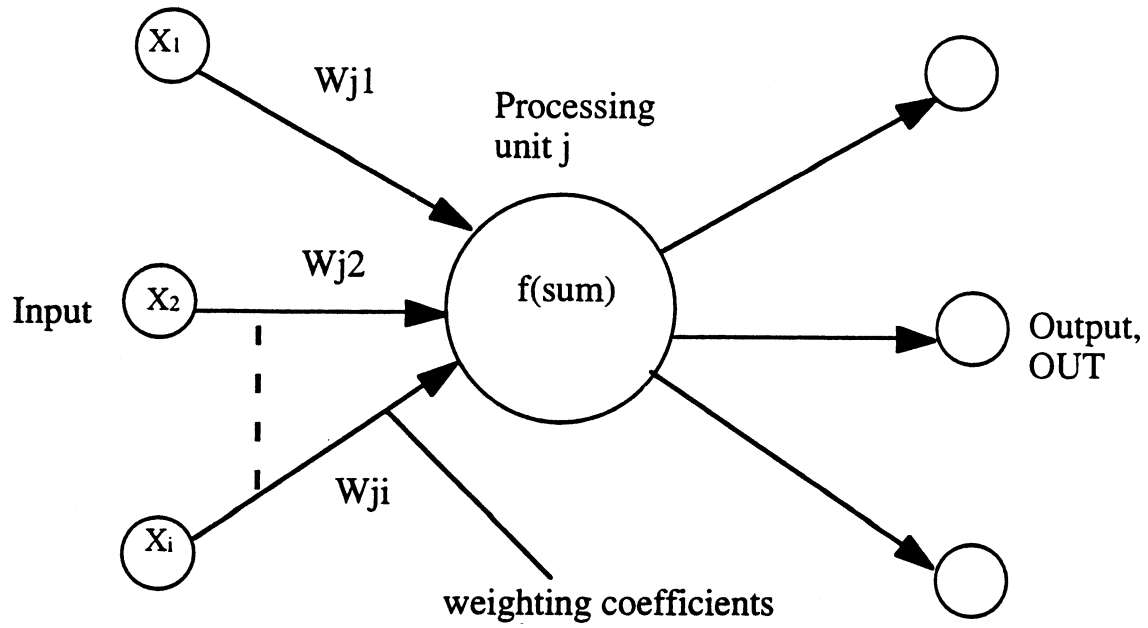

Figure 2.2: Processing unit of an artificial network

Due to its non-linearity and end saturation characteristics, the above function represents most real systems. Figure 2.3 shows a diagram of a network with three fully interconnected layers of neurons (Rumelhart et al. 1989). A fundamental aspect of neural networks is that they are never pre-programmed but are trained.

Narendra and Mukhopadhyay (1992) pointed out the advantage of using a neural network in a control system is its ability to handle complex, non-linear characteristics and system uncertainty. They noted that while the conventional adaptive control methods are suitable for dynamically changing processes and disturbances, the methods lack the memory of the optimal control parameters corresponding to different configurations of the plant.

Neural networks, on the other hand, due to their superior pattern recognizing ability, can classify the different plant configurations and choose the optimal control parameters.

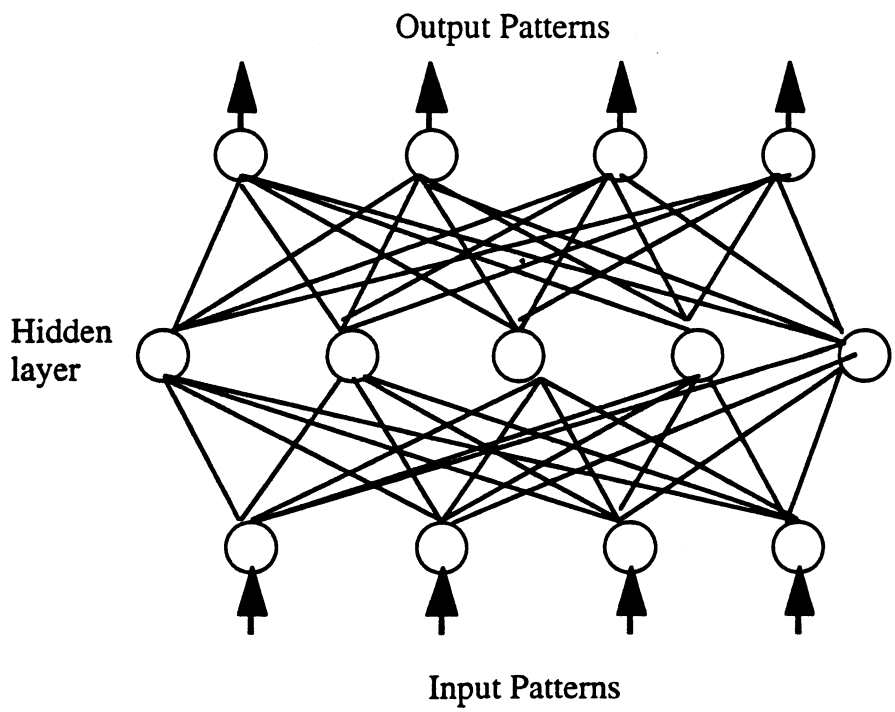

Figure 2.3: A network with three fully interconnected layers

One of the essential properties of a neural network is its ability to generate input/output maps which can approximate any function with any desired accuracy under mild assumptions (Antsaklis 1992). Such a property is utilized for almost all control applications including optimization, adaptation and system identification (Dayhoff 1990; Psaltis et al. 1987; Narendra 1992; Wills et al. 1991).

The type of neural network most commonly used in control is the feedforward multilayer neural network, where no information is fed back during the operation (Dayhoff 1990). In the feedforward architecture shown in Figure 2.3, the network predicts an output vector based on the given input vector for the trained values of weighting factors. During training, feedback architecture is used for supervised learning. The most popular algorithm for feedback is Back Propagation (Psaltis 1987).

A two-layer Back Propagation network for training is shown in Figure 2.4 (Rumelhart 1989). The training involves presenting a set of target input-output pairs to the net. The network uses the initial weights to compute the output, compares that with the target output and then back-propagates the error through the network to adjust the weights. The sequence is repeated until the error between the network output and the target output is minimized. There are several adjustment mechanisms used to accelerate the learning process including optimal gradient, parallel search, Newton's direction, and recursive least squares (Tao and Jurik 1989). The above architecture has been implemented for static systems identification in which the input-output relationship is time-invariant. The relationship changes in the case of a dynamical systems.

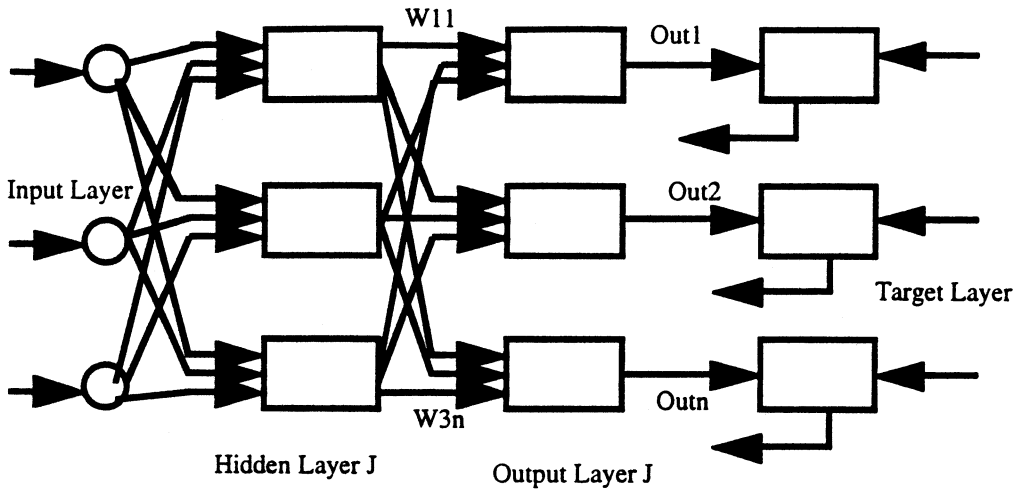

Figure 2.4: Two-Layer Back propagation Network

In most control systems the role of the neural network is to duplicate the plant dynamics so that a required control action can be generated for the desired plant output by inverting the model. The inversion of input-output mapping produces an input for a desired output. A large number of publications present results of using different neural network topologies for adaptively tracking dynamical systems. For example, Ngueyn and Widrow (1990) used a method of dynamical systems identification as shown in Figure 2.5. They used back propagation feedback architecture for the training of the neural network for dynamical system identification. Once a neural network emulator was able to represent the system, it was used to train a controller that satisfied the control objectives. The plant in this system was chosen to be a truck backing process for docking. It took the authors about 200,000 runs to train the controller. The long and laborious process of network training for dynamical systems identification is a major hurdle in implementing a neural network.

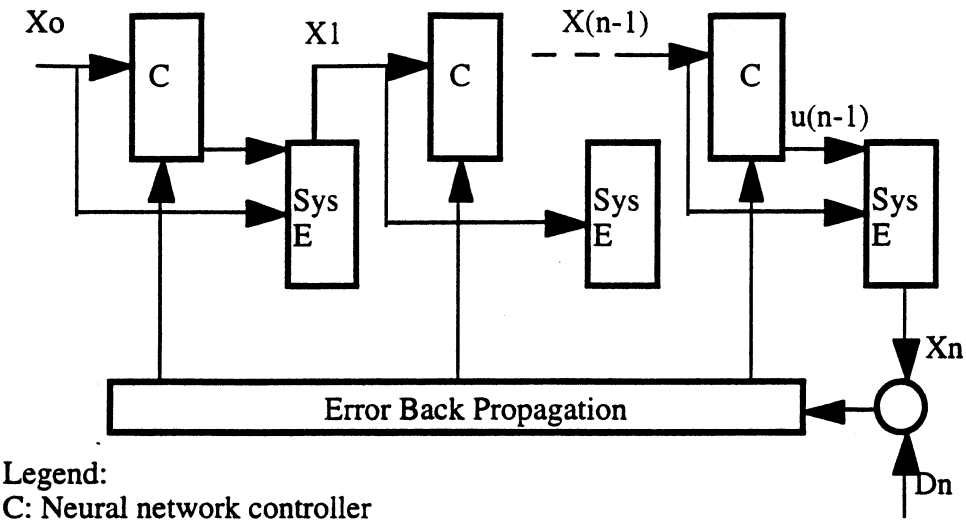

Legend:
C: Neural network controller
Sys E: System Emulator
Xi: State variables
Ui: Control input
Dn: desired output

Figure 2.5: Dynamic Systems Identification

Kraft and Campagna (1990) compared traditional adaptive control methods such as self-tuning regulator and MRAC with neural network in order to track a simple signal created by passing a square wave through first order filter. No *a priori* knowledge of the system other than the system order was assumed. The results showed that both the neural network and the MRAC performed better compared to the self tuning controller (STC) method. The STC did not adapt well when the plant was non-linear. Moreover, the STC needed a change when the system was expected to follow a different reference input. The MRAC method tracked the system non-linearity well but was slow in convergence and sensitive to noise after many control cycles. Although slow to train, the neural network exhibited superior performance in tracking non-linear elements, was insensitive to noise and was easy to implement due to its computational simplicity.

Bhat et al. (1990) modeled a chemical process system via neural computation. The authors first identified a steady state input-output relationship between the feed composition and the product concentrations of constant stirred tank reactor (CSTR). Back propagation method was used and 10,000 iterations were needed to train the network. The authors then studied the dynamic response of pH in a CSTR using back propagation. In this case for a given time window, the current pH and feed composition and future pH values were the input. The future value of the pH was the net output. The network was trained for different sets of initial/ final state conditions.

Using a static mapping technique, Swinarski (1991) was able to generate optimal tuning parameters for a PID controller of a feedback loop. He used the Ziegler and Nichols (1942) procedure to generate optimal values of parameters for various values of open loop output of a first order system. The network was trained using output vector as input and the tuning parameters as the desired output.

Ding and Wong (1990) used a neural network to determine the water low rates of a large dual-temperature hydronic system in response to the heating/cooling demand. The neural network was first trained based on the simulated input-output relationship between the thermal load and the demand for chilled and hot water supplies.

Huang and Nelson (1994) developed a method to determine the delay time of a HVAC control loop using a feedforward neural network with back propagation as a learning method. The input to the network has samples of both input control signal and output or process variable and its output was the delay time. The delay time was defined as the time period in which the normalized values of both input control signal and the process variables are identical. Thus, it became a pattern matching problem for the neural network to find out when the inputs and outputs are similar. A general delta rule was used for the network with learning momentum. Both simulated and experimental results showed encouraging results. The authors suggested that the next step will be to explore on-line implementation of the method for a fuzzy assisted tuner.

A novel idea was presented by Curtiss et al. (1993) for a neural network assisted PID controller. The neural network again used single pass feedforward architecture with back propagation as a learning algorithm. The inputs to the network are the error used by the feedback loop, the sum of the error, the gain constants and the PID output signal. The network output is a control signal that is added to the PID output. The objective was to minimize the cost function that consists of overshoot, settling time and tracking setpoint. The network showed promising results with simulated data. However, actual implementation of the network remains a concern for the authors due to large data required for training and the complexity with the training algorithm.

Recently, Curtiss (1996) reported on modifications to the network assisted PID controller mainly to facilitate implementation. Instead of using a large amount of past data, the neural network only used the data from the last sample time to predict the current control signal. If the neural network prediction was good, the control signal was added to the PID. Otherwise, only the PID control signal was used. The prediction is judged based on the performance of the control loop over the past several time steps. The training is done on-line using a very small data set. Instead of using all past data, the network only uses those data for which the prediction from the network was not satisfactory.

The concept of control with neural networks is strikingly different from the traditional methods of adaptive control. Instead of the complex computations needed for the adaptive schemes, the neural networks learn the process from input-output data representations. The network structures are simple to implement yet they can identify a wide variety of non-linear processes with desired accuracy.

2.5 General Regression Neural Network

In spite of the reported successes, there are certain limitations that restrict the practical implementation of the back propagation method in control. Training is time consuming and requires a large data set. The configuration of the network architecture is not established, and the selection of the number of layers, number of neurons, learning coefficients, and initial values of weighting coefficients need consideration.

In contrast to the back propagation method which must learn the input-output characteristics, a memory based network is described here that captures the input-output (linear or non-linear) characteristics by regression techniques. This general regression neural network (GRNN) requires that only a single parameter be estimated for implementation, and unlike back propagation does not involve an iterative training process. The theoretical basis is a Parzen window estimation (Parzen 1962) and the first reported neural network application was by Specht (1991). Compared to the conventional regression technique, the GRNN does not require *a priori* specification of the regression equation. In addition, compared to other non-linear regression techniques, bounds of the independent variables, initial values and convergence criteria do not have to be selected. This makes on-line implementation of GRNN relatively straightforward.

The GRNN is derived from a probability neural network (PNN) presented by Specht (1990). The concept of PNN is identical to GRNN except that the output from PNN is binary using Bayes theory of probability (Mood and Graybill 1962). Hence, PNN is used for classification, mapping and associative memory problems.

A GRNN is based on the estimation of a probability density function. According to Specht (1991), this is a one-pass learning algorithm with a highly parallel structure. Even with sparse data in a multidimensional measurement space, the algorithm provides smooth transitions from one

observed value to another. The algorithmic form can be used for any regression problem in which an assumption of linearity is not justified. The parallel network form should find use in applications such as learning the dynamics of a plant model for prediction or control. If the joint probability density function of a vector random variable, X, and a scalar random variable, Y are known, then the conditional probability density function and the expected value can be computed. In this case, the joint probability density functions will be estimated from examples using non-parametric estimates. The resulting regression equation can be implemented in a parallel, neural-network-like structure. The structure of data are determined directly from past data, the structure is developed and generalized without feedback.

The theory for the GRNN will be outlined. The estimated value of **Y** for a given **X** is given by a basic equation for general regression as

$$E(\boldsymbol{Y} \mid \boldsymbol{X}) = \frac{\int_{-\infty}^{\infty} \boldsymbol{Y} f(X,Y)\,dy}{\int_{-\infty}^{\infty} f(X,Y)\,dy} \qquad (2.2)$$

where,

$E[\boldsymbol{Y}|\boldsymbol{X}]$ = conditional mean of **Y** on **X**.

f(X,Y)=known joint continuous probability density function

When the density function f(X,Y) is not known, it must be estimated from a sample observations of X and Y. For a non parametric estimate of f(X,Y),

the GRNN uses the Parzen estimation (Parzen 1962), f'(X,Y) which is given by the following expression for observed sample values X_i and Y_i of vector X and scalar Y.

$$f'(X,Y) = \frac{1}{(2\pi)^{(p+1)/2}\,\sigma^{(p+1)}} \cdot \frac{1}{n} \sum_{i=1}^{n} f_X \cdot f_Y \qquad (2.3)$$

where,

$$f_X = exp[-\frac{(X - X_i)^T (X - X_i)}{2\sigma^2}$$

$$f_Y = exp[-\frac{(Y - Y_i)^2}{2\sigma^2}$$

n is the number of sample observations

p is the dimension of the X vector.

σ is a smoothing parameter.

Combining equations 2.2 and 2.3, interchanging the order of integration and summation and performing integration yields an estimate for the desired mean **Y** at any given value of **X**.

$$\hat{Y}(X) = \frac{\sum_{i=1}^{n} Y_i \, exp(-\frac{D_i^2}{2\sigma^2})}{\sum_{i=1}^{n} exp(-\frac{D_i^2}{2\sigma^2})} \qquad (2.4)$$

where the scalar function D_i^2 is given by

$$D_i^2 = (X - X_i)^T (X - X_i) \tag{2.5}$$

Equations 2.4 and 2.5 are the essence of the GRNN method. The estimate $\hat{Y}(X)$ is essentially is a weighted average of all the observed samples, Y_i, where each sample is weighted exponentially according to its Euclidean distance D_i from each X_i. In that sense, D_i resembles the weighting coefficients of a back propagation scheme. For small values of the smoothing parameter, σ, the estimated density assumes non-Gaussian shapes but with the chance that the estimate may vary widely between the known points. When σ is large, a very smooth regression surface is achieved. In the case when an input is outside the range of observed samples, the GRNN will predict an output based on the nearest samples in the observed data.

When using measured data, it is necessary to find the optimum value of σ as, usually, the parent distribution between X and Y is usually not known. As a preprocessing step, all input variables are normalized to obtain the same scale using the ranges of observed samples. The value of σ can be then calculated by a simple yet effective scheme known as "Holdout" method which is one of several methods available to find an optimum value of the smoothing parameter, σ. In the Holdout method, one sample at a time is removed from the set and the network is constructed using the remaining samples. The network is then used to estimate $\hat{Y}$ for the removed sample. Each estimate $\hat{Y}$ is compared with the actual Y and the mean squared error

between the estimate and the actual value is computed and stored. The process is repeated for each sample. The value of σ is chosen so as to minimize the mean squared error. The Holdout method is formulated as a single parameter minimization problem in comparison to the training process in back propagation which is computationally intense and inherently slow.

A GRNN is shown in Figure 2.6, in which equation 2.4 is represented in a neural network architecture. For a given X, the connections between the input and the first layers computes the scalar D_i. Based on observed samples X_i and smoothing parameter σ, the negative exponent of $\frac{D_i^2}{2\sigma}$ is computed. A node in the second layer sums up the exponential values for all samples.

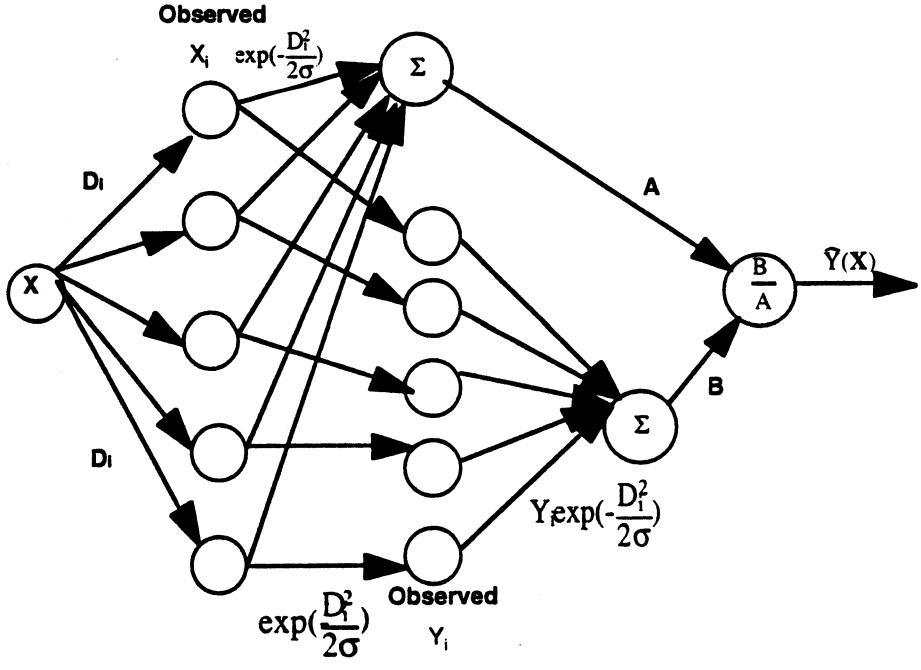

Figure 2.6: General Regression Neural Network architecture

In other nodes the product of the exponent value and the corresponding observed output Y_i for each sample observation are computed. The node in the third layer adds up all the product values, which is then supplied to the output node where the ratio between the sum of the exponent and the product values is calculated. The weighting coefficients between the layers are only dependent upon the observed samples of X_i, Y_i and smoothing parameter σ. As a result, instead of training the weighting coefficients, only a suitable single value of σ is needed to predict the output. The GRNN is thus able to represent the characteristics in a much short time than with a back propagation method.

Both static and dynamic mapping evaluation were performed by Specht and excellent results were obtained. In case of a static mapping a simple linear model with a saturated output at both ends was identified with only five sample points. A five dimensional dynamic model was chosen with cyclic output and the results were compared with a regular back propagation algorithm. The GRNN was able to identify the dynamic model with only 1000 time steps while the back propagation required 10 times more time steps to achieve the same accuracy. With only 10 input patterns, the GRNN was capable of capturing the dynamic model with only twice the error compared to 1000 patterns.

A relevant application of GRNN has been reported in a medical Journal (Buchman et al. 1994). In this report a linear statistical model is compared with the neural network models in order to predict the survival of a patient taken to the intensive care unit (ICU). Neural network models included a

back propagation network, probabilistic neural network and GRNN. Past data for 491 patients with ICU length of stay three days who survived at least an additional four days were used to develop the models. The patient data included age, antibiotic group, volume of red blood cells, maximum heart rate, minimum systolic blood pressure, white blood cell counts and five other medical factors. The models were designed to produce an output ranging from 0 to 1 where 0 means that the patient is discharged from the ICU before the end of the seventh full day and 1 indicates the patient is alive in the ICU through the seventh full day. The results were classified between 0 and 1. A zero value indicated false positive meaning patients predicted to be in the ICU through the seventh day actually was discharged while one meant true positive which is just the opposite of the false positive condition.

The results indicated that all three neural network models outperformed the linear parametric model by a margin of at least three to one. The authors pointed out that the advantage of GRNN over the back propagation neural network is that it does not require training. GRNN is also computationally efficient and a priori knowledge is not required as in the case of a regression.

An application of a PNN has been recently reported by National Institute of Standards and Technology (NIST) scientists (Grother and Candela 1993). They have used a NIST database consisting of binary 128 by 128 pixel images from the sample forms of 2100 writers. For the study samples are drawn randomly from the first 250 writers to yield a training set of 7480 digits. Several statistical classifiers such as Euclidean Minimum Distance,

Quadratic Minimum Distance, Normal, k-nearest neighbor and Weighted Several Nearest Neighbors were compared with the neural network classifiers termed Multi Layer Perceptron, Radial Basis Function and PNN. The results showed that PNN and nearest neighbor classifiers performed best in terms of accuracy. In contrast to the other neural network classifiers, the PNN needed no training. However, the rate of extracting characters for classification was slowest for PNN compared to other classifiers. The authors suggested that significant time was spent by the PNN to reduce the dimension of the feature before character extraction.

The memory based neural networks, PNN and GRNN, are capable of identifying system characteristics based on observed samples with relative ease. Due to large memory requirements, their effective applications will be limited to the cases where a large data set is not required to identify the system characteristics.

2.6 Combined feedforward and feedback control method

A combined feedforward and feedback control topology is an alternative to feedback, adaptive and other advanced control methods. The goal of the combined approach is to provide superior setpoint tracking with the feedforward element while the feedback element will provide steady state disturbance rejection capability.

There is considerable published literature on the combined approach and only a few applications are reviewed here. A general combined approach is presented by Psaltis et al. (1987) and shown in Figure 2.7. For the

feedforward block, the authors recommended using a neural network which will be trained on-line using a back propagation algorithm.

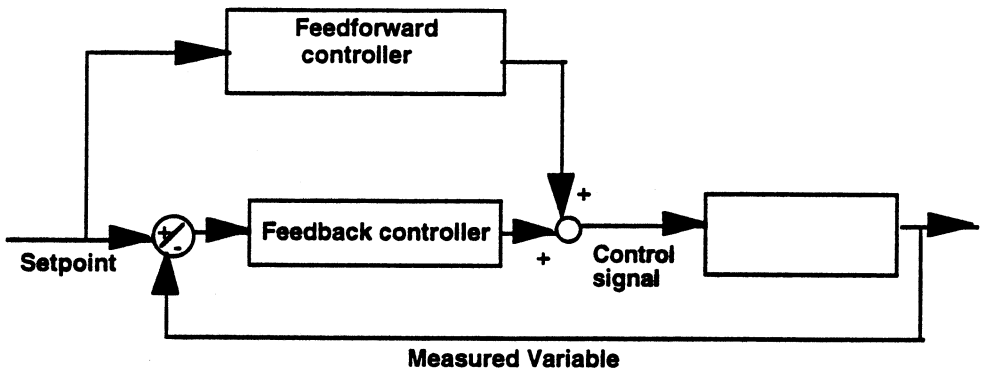

Figure 2.7: Combined feedforward and feedback topology

The authors noted that by adding the feedforward block the speed of response will be increased, and when the feedforward is block is fully trained the majority of the control signal will be generated by the feedforward controller. This will leave only a small steady state error to be handled by the feedback loop.

Kraft and Campagna (1989) proposed a similar control topology as shown in Figure 2.4. The feedforward element in this case was based on a cerebellar model articulation controller (CMAC) neural network. The combined control topology was compared with a self tuning regulator (STR) and a Lyapunov-based model reference adaptive controller (MRAC). The comparisons were made for a low order control system considering linear and non-linear with noisy disturbance. The combined feedforward and feedback approaches worked very well in the presence of noise for both linear and non-linear systems. The authors commented that the combined

approach is most favorable from the implementation point of view due to its simple algorithm.

A combined feedforward and feedback approach has been successfully implemented for the control of semiconductor wafer temperature (Norman and Boyd 1992). A physical model based feedforward block was developed for a rapid thermal process where single wafers are heated, processed and cooled in small reaction chambers. The process is usually completed within a few seconds. The physical model correlated the distribution of radiant heat in the reaction chamber by means of lamp array and distribution of temperature.

The linear feedback loop was able to reject steady state disturbances due to small temperature error. The experimental results showed good wafer temperature distributions with the combined approach.

Combined feedforward and feedback controllers have been successfully used in NASA Deep Space Network (DSN) antennas project (Gawronski and Mellstrom 1994). The authors noted that a simple and reliable choice to track accurately fast moving objects is to augment feedforward with a PI controller. Recently, Gawronski et al. (1995) added a model based, linear quadratic Gaussian controller to the combined feedforward and PI controller to improve the disturbance rejection property further. However, the author noted that such addition increased controller complexity.

It is expected that a combined feedforward and feedback approach for laboratory HVAC system may be appropriate. While the feedforward controller may respond quickly and exhibit superior setpoint tracking ability, the feedback controller may reject steady state disturbance.

2.7 Closure

The VAV lab system is growing in popularity in the lab industry due to its ability to conserve energy. However, VAV poses new challenges to the control system to maintain space temperature, humidity and pressure within close tolerance in critical applications. The response time in a lab system must be in the range of seconds instead of minutes as in conventional buildings. The current method of feedback controller using PI or PID loops have inherent problems dealing with higher order non-linear systems, a wide range of operations, variable system gains and multiple interacting loops which are the characteristics of a lab environment. Tuning of PI/PID loops remains as a major commissioning issue. Available tuning process are valid for single loops and often require trial and error to tune multiple, interconnected loops.

The classical methods such as a recursive algorithm or generalized predictive method are more suited for linear or near linear small systems. Adaptive control does not seem to be an attractive option for on-line implementation due to the solution complexities, large computer memory and detailed system modeling requirements.

As an alternate solution the combined feedforward and feedback control as shown in Figure 2.7 can be further explored for lab HVAC system. The advantage of feedforward for tracking the state variables setpoints is well established for many industrial applications. For lab applications, the command tracking will reduce the swing in state variables, thereby increasing the comfort level. Since it by-passes the feedback loop, the controller response time also decreases. Moreover, if the feedforward path works well, the tuning of the feedback loop is simplified as it can then be designed to handle the disturbance rejection based on a small consistent error between the setpoint and the state variable. Simplified tuning and elimination of re-tuning will offer major cost advantages to the lab owners both in terms of commissioning and operation.

The task of the feedforward controller is to generate control signals to the control equipment such that the setpoints of the manipulated variables are achieved. Any remaining minor discrepancies between the state variable setpoint and the actual value will be handled by the local feedback loop. The feedforward controller will perform best if it can invert the control equipment dynamics such that for a given value of manipulated variable, the required signal to achieve that value is produced. For example, a damper/actuator assembly produces an output of air flow for a control signal input by modulating the damper position. If the input-output relationship of the damper is inverted, then the controller will be able to generate the required control signal for the desired air flow rate. Since the characteristics of the control equipment vary over time, some means of adaptation is necessary for recognizing such change.

The model reference adaptive control is suitable for such tasks. However, development of models of various types of control equipment are a challenge for the method since HVAC models are complex. The drawback of a model based scheme is also significant in the case of a retrofit job (Crawford et al. 1991). In most retrofit instances, it will be costly and next to impossible to identify all of the types of damper/actuator assembly for proper modeling. For example, the characteristics of a linear butterfly damper differ significantly from a quick opening non-linear damper. Furthermore, the HVAC process input-output relationship usually is a result of highly coupled multiple components, which makes the modeling also difficult. As an illustration, the supply air temperature from a hot water coil depends on the characteristics of air flow damper/actuator, water flow valve/actuator and the coil.

The neural network is a possible approach to accommodate the uncertainties in the HVAC system characteristics. The strength of the network approach is the independence of the model and the capability of mapping the input-output pattern. Hence, if a network is trained using the process input-output data, the inverse of the process can be used to generate the required input control signals.

Before the neural network can be selected for this project, two more issues need to be resolved. The first issue concerns whether a single neural network is feasible to characterize the whole HVAC process involving all the control equipment. The second issue is whether dynamic system

identification is necessary for the HVAC control equipment. The network implementation depends on these issues.

The implementation, considering the whole HVAC process, will require a large amount of data and time. The implementation will also be substantial if the dynamical system is considered as wide operating and the initial conditions need to be included in the training set. The use of dynamical systems identification is necessary when the objective is to produce time-variant control signals such that the performance objective is achieved by the neural network controller. In the publications cited, the dynamical systems were considered for identification. However, the training periods were large and the studies were limited to simulation.

The objective of this research is to find a solution which can be implemented in real controller. A practical means of the HVAC process identification will be proposed by using multiple neural networks that replicate the characteristics of the control equipment. With individual networks for dampers/actuators and coil valve/actuator assembly the implementation will be simplified. Considering the overall control scheme, the networks using feedforward architecture will be able to generate near-optimal control signals for desired setpoints of the manipulated variables. Hence, the dynamical systems identification will be not necessary which further simplifies the implementation.

It is proposed that GRNN will be used as individual an control equipment identifier. A large data set is not required for static mapping of HVAC

equipment i.e. valve/damper characteristics and hence, GRNN will be a viable option. Besides, GRNN does not require training and a single smoothing factor can be initially determined based on the size of the input data set. Therefore, a combined feedforward and feedback controller will be proposed using the GRNN as system identifier for the lab HVAC system. Such an architecture is presented in detail in the following chapter.

Chapter 3
Development of An Emulator

3.1 Need for an emulator

In order to develop and test new control strategies for a laboratory, at least two options are available. The first is to use an actual laboratory in which control systems are installed, new control strategies are implemented and data are gathered to evaluate the HVAC system performance. The second option is to create an emulator using software that can simulate the performance of the laboratory and HVAC systems. The control strategies can be then implemented into the emulator for both development and testing purposes.

The first option is costly and difficult to achieve in terms of constructing a test lab or finding an existing one. In addition, safety is essential and application of any unproved solution technique for lab HVAC operating systems is risky. Any lab operator may be cautious and hesitant to allow testing of a new control strategy in an existing operating laboratory. It may be also difficult to conduct controlled experiments in an active laboratory and to collect experimental data.

The second option involves developing a mathematical algorithm that emulates a lab, HVAC and control systems. With the use of an emulator, the element of risk is eliminated. Using an emulator it is relatively easy to test and compare different control strategies. Based on above consideration, a

decision was made to develop an emulator for laboratory and its operating HVAC system. Validation of emulator components, when necessary, is achieved by judging the simulated results obtained under simple limiting conditions. An experimental validation of room models which are unique to the laboratory is described in Chapter 4.

3.2 Overview

This chapter describes the development of an emulator in terms of governing mathematical models, underlying assumptions, significance and any other boundary constraints. The emulator imitates the behavior of a laboratory environment and associated HVAC system. Figure 3.1 shows a schematic of a laboratory HVAC system showing all the physical variables. Laboratory pressure and temperature, P and T are the environmental variables which are being maintained within the specified limits. The conditioned supply air is sent to the laboratory at a pressure P_S, temperature T_S and at a volumetric flow rate of $\dot{v}_s$. The heating coil entering and leaving water temperatures are $T_{f,i}$ and $T_{f,o}$ while the water flow rate through the coil is $\dot{v}_f$. The total fume hood exhaust volumetric flow rate, $\dot{v}_{fh}$, is exhausted at room pressure and temperature. The general exhaust of $\dot{v}_{ex}$ also is exhausted at room pressure and temperature. There is infiltration from adjacent space at P_{ad} and T_{ad}.

Providing safety and comfort are the two basic functions of a laboratory HVAC system. The safety constraint is satisfied by exhausting effluents through the fume hood exhaust and by preventing any leakage from the laboratory. The fume hood is controlled to maintain a constant average face

velocity of entering room air which is exhausted through the hood. Keeping the laboratory pressure (P) low than the adjacent space pressure (P_{ad}) will ensure that nothing leaks out of the laboratory. However, in certain laboratories such as clean room the interior pressure is kept higher than the adjacent space ($P>P_{ad}$) to prevent the flow of any foreign particles from the adjacent space and to keep the interior space free of impurity.

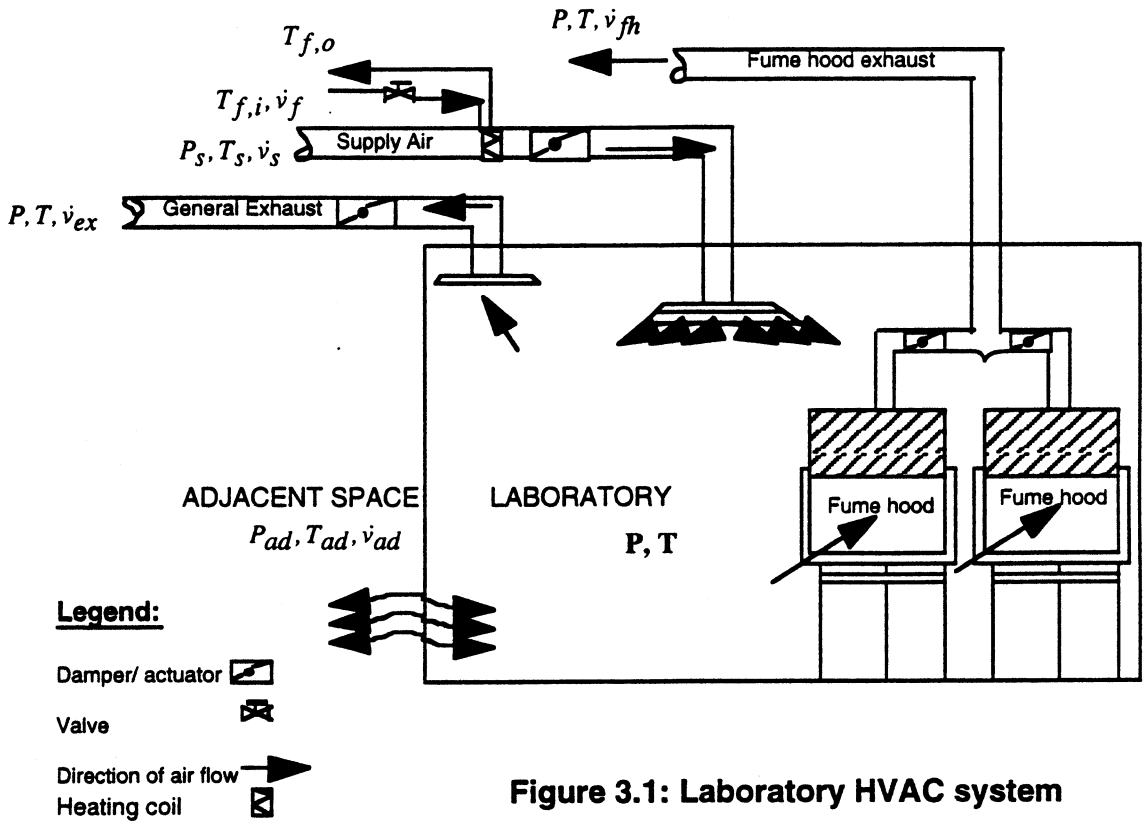

Figure 3.1: Laboratory HVAC system

The pressure differential between the laboratory and the adjacent space is achieved by maintaining a difference between the supply flow rate and the total laboratory exhaust so that there is always infiltration from the adjacent space. The supply air ($\dot{v}_s$), usually discharged at 55 ^{o}F (T_S), also supplies the cooling load. Since the supply flow tracks the lab exhaust, in the case when fume hood exhaust increases substantially, the supply flow rate may also increase more than needed for cooling. The supply air is controlled by

tempering with the auxiliary heating typically provided by the duct heating coil. When the fume hood exhaust is at a minimum, the cooling loads may require more supply air than the fume hood exhaust. However, the supply flow cannot be increased without increasing the exhaust from the lab to maintain the negative pressure in the laboratory. Additional exhaust from the laboratory takes place by opening the general exhaust damper.

What is described above are most common sequences of operations of laboratory VAV HVAC system. These illustrate the intricacies of controlling the laboratory HVAC system in order to maintain both safety and comfort constraints at the same time.

The objective of the control system is to maintain the values of selected physical variables, known as process variables, within specified ranges. For example, referring to Figure 3.1, laboratory temperature, T and pressure differential, P_{ad}-P, (denoted as ΔP), are typical process variables in a lab control system. In addition, some physical variables known as control variables are measured and controlled by the control system. In a lab control system, the volumetric flow rates of supply air, $\dot{v}_s$, general exhaust, $\dot{v}_{ex}$ and coil water, $\dot{v}_f$ are typical control variables.

The overall functional relationship between the emulator and the HVAC controller is shown in Figure 3.2. The controller receives the sensor signals from the emulated laboratory HVAC system, executes the algorithm and returns the appropriate signals to the control equipment. Upon receiving the signals from the controller, the emulator approximates the response of an

actual system and creates the necessary values of observed variables which are in turn fed back to the controller.

Hence, the goal of the emulator is to replace a real laboratory system. The controller configuration shown in Figure 3.2 duplicates an actual controller with separate input and output modules. The input module receives signals from different sensors in terms of current or voltage i.e. 4-20 mA or 0-10 volts. The controller then converts the signals to value of physical variables like temperature and flow. The controller, using the algorithm, then calculates the value of the control variables such as the valve or damper position. However, the value is converted again to a suitable signal which can be read by the control equipment. Since the purpose of the input and output modules is to translate the electrical signal into a value, creating such modules will not be necessary for simulation purposes.

A detailed schematic showing the connections between the controller and sensors and controller and control equipment is depicted in Figure 3.3. The diagram shows the information in the form of electrical signal flows from the sensors to the controller. The controller uses such information to control the equipment in order to achieve the desired control goals. The controller receives the measured values of fume hood exhaust, general exhaust, supply air, supply air temperature and room temperature. The control strategy uses the sensor information to generate the appropriate control signals. The control signals are then sent to the fume hood exhaust, supply and general exhaust dampers and reheat coil valves. The damper regulates the flow and, simultaneously, the discharge temperature of supply air is varied by

modulating the reheat coil valve. The control strategy for existing and proposed systems are discussed in depth in Chapters 6 and 7.

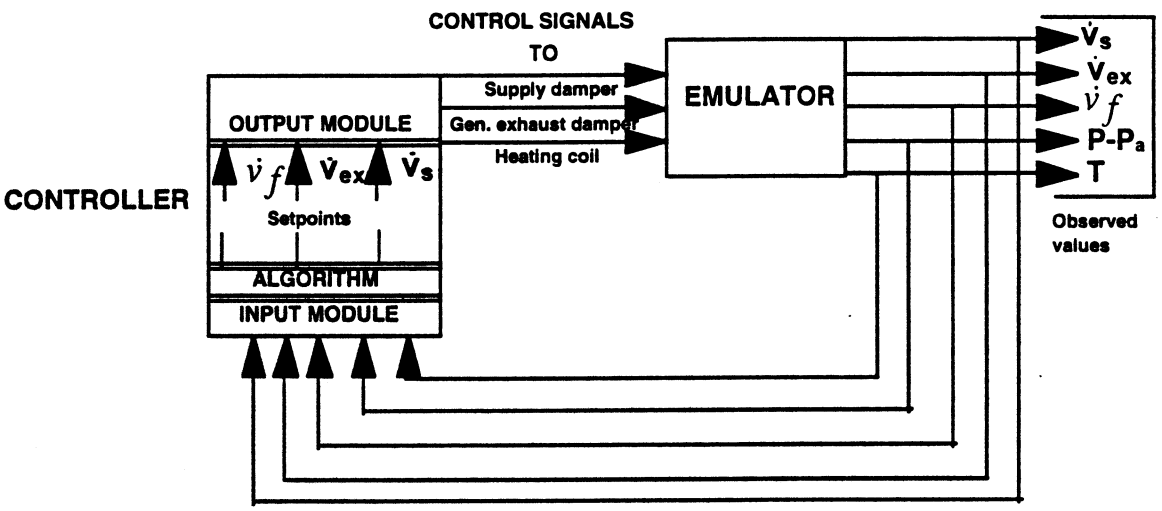

Figure 3.2 Functionality of Emulator

What is shown in Figures 3.1 to 3.3 is a representative VAV laboratory system configuration. Figure 3.1 shows a laboratory HVAC system and physical variables. Figure 3.2 illustrates the role of emulator in approximating the response of physical variables upon receiving control signals from the controller. A typical laboratory control system is depicted in Figure 3.3 indicating the sensor locations and control equipment. In a specific laboratory system both the sensors and components will vary depending upon specific objectives. The illustrations in Figures 3.1 to 3.3 serve the purpose of indicating the typical relationships between a lab system and controller and ensure that the emulator preserves such relationships with the controller.

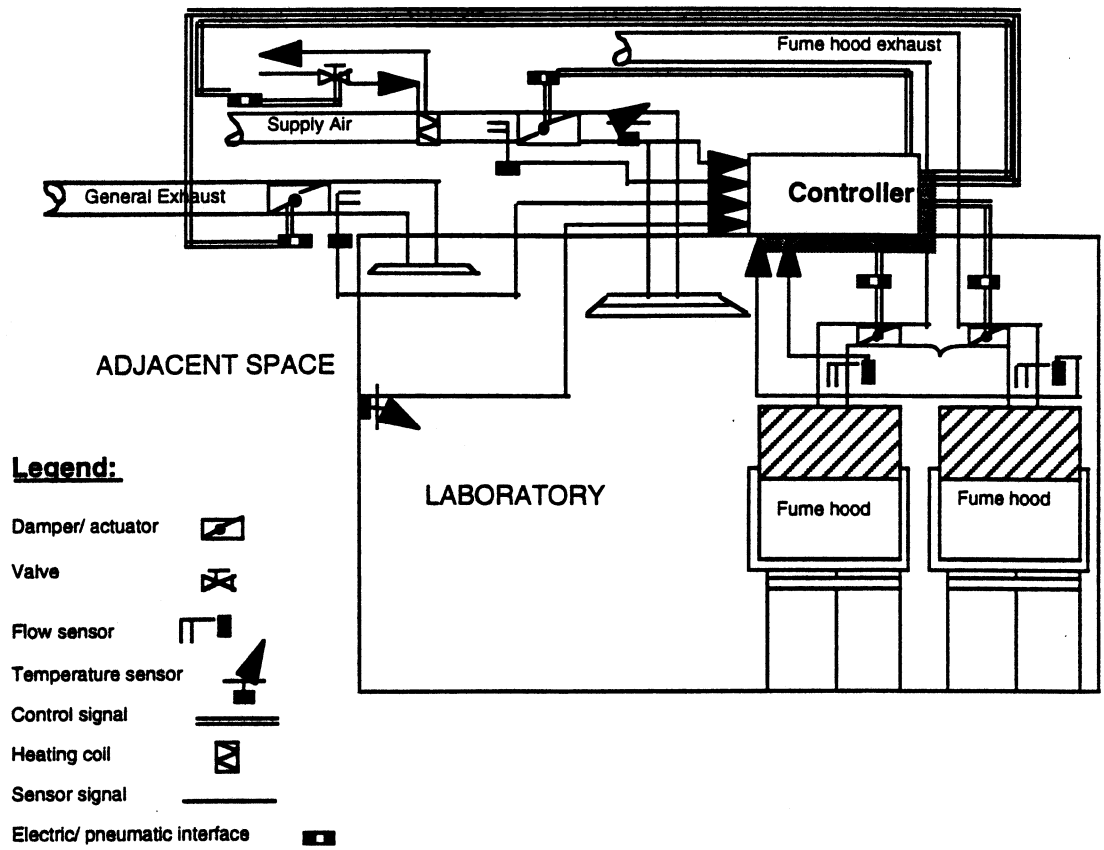

Figure 3.3: Laboratory HVAC Control System

The emulator components are described in detail in sections 3.3 to 3.9. The emulator system consists of a room, heating coil, valve and damper, actuators and sensors. As a part of the emulator development process, simulations are carried out to validate component models, and results are presented as appropriate throughout this chapter. The validation is intended to ensure that the models yield expected results under limiting or simple conditions. The conditions are so chosen that intuitive explanations using

common sense are possible. Experimental validation of the room models is described in Chapter 4.

3.3 Room Model

The purpose of the room model is to emulate the response of environmental parameters such as temperature and pressure when both the room model and the real lab are subjected to the same forcing functions. The room model is developed based on following assumptions and the room air is selected as the control volume.

1. air is an ideal gas and the effect of humidity on propoerties is negligible ,
2. lab air temperature and pressure are spatially uniform at any instant of time,
3. adjacent space temperatures and pressures are constant,
4. supply duct pressure is constant,
5. internal heat generation is purely sensible, and
6. heat conduction is one dimensional through the walls.

Conservation of mass:

$$\frac{dm}{dt} = \dot{m}_i - \dot{m}_e = \dot{m}_S + \dot{m}_{ad} - \dot{m}_e \qquad (3.1)$$

Equation 3.1 is a simple expression for room mass balance. It relates the change of air mass stored in the room to inflows and outflows. The right hand side of the equation represents mass influx and efflux while the left

hand side indicates mass storage with respect to time. The term $\dot{m}_e$ is the total exhaust flow from fume hoods and genreral exhaust.

Also, the mass flow is related to the volumetric flow rate and density by

$$\dot{m} = \dot{v}\rho \tag{3.2}$$

Using the ideal gas law,

$$\rho = \frac{P}{RT} \tag{3.3}$$

Therefore, the mass flow in terms of pressure, temperature, and volume flow rate is

$$\dot{m} = \frac{P\dot{v}}{RT} \tag{3.4}$$

The above expression shows the dependence of mass flow rate on both pressure and temperature. The density of air ρ is usually treated as a constant in HVAC system studies, but it is important to include the variation in density in the laboratory control studies. Using equations 3.3 and 3.4, equation 3.1 becomes

$$\frac{d(PV/RT)}{dt} = \frac{P_s\dot{v}_s}{RT_s} + \frac{P_{ad}\dot{v}_{ad}}{RT_{ad}} - \frac{P\dot{v}_e}{RT} \tag{3.5}$$

Differentiating P and T with respect to time and canceling the gas constant, R, on both sides results in

$$V\left[\frac{1}{T}\frac{dP}{dt}-\frac{P}{T^2}\frac{dT}{dt}\right]=\frac{P_s\dot{v}_s}{RT_s}+\frac{P_{ad}\dot{v}_{ad}}{RT_{ad}}-\frac{P\dot{v}_e}{RT} \qquad (3.6)$$

Equation 3.6 has two time derivative expressions, one for room pressure, P, and temperature, T, respectively. In order to find the room pressure and temperature time variant response, an energy balance on the room air is needed.

Conservation of Energy:

$$\frac{dU}{dt}=\sum h_i\dot{m}_i-h_e\dot{m}_e+\dot{q}_{gen}+\dot{q}_{tr} \qquad (3.7)$$

The first two terms on right hand side are energy influx and efflux respectively due to air flow. The third and fourth terms are the rate of heat generation in the room and the transfer through room envelopes respectively. The term on left is the time derivative of the room air energy. Equation 3.7 can be further expanded in terms of specific internal energy as

$$m\frac{du}{dt}+u\frac{dm}{dt}=\sum h_i\dot{m}_i-h_e\dot{m}_e+\dot{q}_{gen}+\dot{q}_{tr} \qquad (3.8)$$

Taking derivatives of left hand side of equation 3.8, for constant room volume V and introducing the ideal gas equation for internal energy $u= c_vT$, the following equation is obtained.

$$\frac{PV}{RT}c_v\frac{dT}{dt}+\frac{c_vV}{RT}\frac{dP}{dt}-c_vT\frac{PV}{RT^2}\frac{dT}{dt}=\sum h_i\dot{m}_i-h_e\dot{m}_e+\dot{q}_{gen}+\dot{q}_{tr} \qquad (3.9)$$

Canceling the first and third terms on the left hand side, introducing inflows and outflows in terms of volumetric rates, and expressing enthalpy of air, for an ideal gas with a constant specific heat as $dh = c_p dt$,

$$c_v V \frac{dP}{dt} = \frac{P_s \dot{v}_s}{RT_s} c_p T_s + \frac{P_{ad} \dot{v}_{ad}}{RT_{ad}} c_p T_{ad} - \frac{P \dot{v}_e}{RT} c_p T + \dot{q}_{gen} + \dot{q}_{tr} \quad (3.10)$$

Equation 3.10 can be simplified to,

$$c_v V \frac{dP}{dt} = \frac{P_s \dot{v}_s}{R} c_p + \frac{P_{ad} \dot{v}_{ad}}{R} c_p - \frac{P \dot{v}_e}{R} c_p + \dot{q}_{gen} + \dot{q}_{tr} \quad (3.11)$$

Solving Equations 3.6 and 3.11 simultaneously will yield the room pressure and temperature response. Room energy and mass balances show that the response of room pressure and temperature are coupled. The coupling is critical to the investigation the pressure and thermal dynamics of a lab environment.

In Equations 3.7 to 3.11, the term $\dot{q}_{tr}$ represents heat transfer through the room envelope. The mode of heat transfer through room envelope is assumed to be conduction through wall with surface convection to room air. Radiation between surfaces is neglected. The envelope usually consists offour walls, a ceiling and a floor. The rate of heat transfer from surface to room air is calculated using simple convection relations.

$$\dot{q}_{tr} = \sum h c_a A_w (T_u - T) \quad (3.12)$$

where, subscript u represents the u th component of room envelope. More explicitly, the above equation can be written as

$$\dot{q}_{tr} = \sum_{j=1,4} hc_{r,w}(T - T_{w,j}) + hc_{r,fl}(T - T_{fl}) + hc_{r,cl}(T - T_{cl}) \qquad (3.13)$$

Envelope transient:

The transient heat transfer through the room envelope can be handled in many ways. The choice of method willdepend upon the type of envelope, simplicity and the accuracy desired. In a research laboratory, the envelope may vary from concrete walls to pre- fabricated steel panel walls. For steel panels walls, simple lumped- capacitance models for the unsteady heat transfer are justified since the resistance of steel is negligible compared to the surface and insulation resistance. In a panel wall, the insulation between the steel sheets provides negligible capacitance and significant resistance while the steel panels have high capacitance. The Biot number, which is a ratio between surface to internal resistance, is defined as, $Bi = \frac{hc\,L}{k}$, is used as a criteria in using the lumped capacitance model. If the Biot number is less than 0.1, lumped analysis is valid (Incropera and Dewitt 1985). For panel walls, the Biot number is considerably less than 0.1 which makes lumped analysis method a reasonable choice.

For concrete wall construction, however, the Biot number is larger than 0.1. Hence, an alternative method is needed to calculate the heat transfer across the concrete walls or similar structures. A transient numerical scheme is a preferred method of choice for determining the temperature distribution and heat flow through simple regular shaped solids like walls and floors. In

addition to the lumped capacity and numerical methods, a third method of treating room thermal storage is considered in a most simplistic way. Instead of treating walls, floor and ceiling separately, an equivalent single thermal mass is considered which exchanges energy with the room through an overall thermal resistance. The rational for having this approach is to produce meaningful results in a short and simple fashion for evaluation of control strategies or control components selection. To summarize the applicability of three methods, a numerical scheme based on finite differencing is needed to treat heavy construction envelopes such as concrete walls. A lumped capacitance method is suitable for lighter panel walls. An equivalent single wall model provides a quick method of analyzing lab dynamics. The results of finite differencing scheme verification are included in next section. The verification of equivalent single wall approach is considered along with the overall room models verification discussed in room model section below. The lumped capacitance model is used to validate the experimental results which is the subject of the next chapter. A discussion of three methods of treating envelope transient are discussed as follows.

Finite Differencing Scheme:

The basic one dimensional transient equation for heat flows through an envelope, by conduction, such as walls, ceiling and floor, can be expressed as

$$\frac{\partial^2 T_u}{\partial X^2} = \frac{1}{\alpha}\frac{\partial T_u}{\partial t} \qquad (3.14)$$

where,

$$\alpha = \frac{k}{\rho c}$$

Equation 3.14 can be solved using an implicit finite differencing scheme (Incropera and Dewitt 1985) as,

For any interior nodes, m:

$$T_m^{P+1}(1+2Fo) - Fo(T_{m+1}^{P+1} + T_{m-1}^{P+1}) = T_m^P \qquad (3.15)$$

where,

$Fo = \frac{\alpha \Delta t}{\Delta x^2}$, Δx = Nodal interval in space coordinate x

p is time step, and m is spatial step in the direction of heat flow.

Equation 3.15 can be modified to satisfy the necessary boundary conditions. The most common boundary conditions result from the envelope being exposed to the room and the adjacent space.

For the surface node, 1 next to the room:

$$T_1^P = T_1^{P+1}\,[1 + 2FoBi + 2Fo] - 2Fo\left[TBi + T_{1+1}^{P+1}\right] \qquad (3.16)$$

For the surface node, M next to the adjacent space :

$$T_M^P = T_M^{P+1}\,[1 + 2FoBi + 2Fo] - 2Fo\left[T_{ad}Bi + T_{M-1}^{P+1}\right] \qquad (3.17)$$

Although computationally more intensive, the implicit scheme provides for an unconditionally stable solution when compared to an explicit scheme. Moreover, since the number of nodes for the room envelope considered were relatively low for the cases studied, the computational effort is a non-

issue. It should be noted here that in equation 3.13, the temperatures $T_{w,j}$, T_{fl} and T_{cl} are to be determined by expressions given in 3.17.

Lumped-capacitance method:

The lumped capacitance model can be described with the help of a simple sketch of the plane wall and the corresponding thermal circuit. Referring to Figure 3.4, two energy equations can be written for $T_{w,1}$ and $T_{w,2}$ for the metal wall on the room side,

$$(T - T_{w2})hc_{rm} - (T_{w2} - T_{w1})\frac{k_i}{L_i} = (\rho C \Delta l)_{pw}\frac{dT_{w2}}{dt} \qquad (3.18)$$

For the metal wall on the outer side,

$$(T_{ad} - T_{w1})hc_{ad} - (T_{w1} - T_{w2})\frac{k_i}{L_i} = (\rho C \Delta l)_{pw}\frac{dT_{w1}}{dt} \qquad (3.19)$$

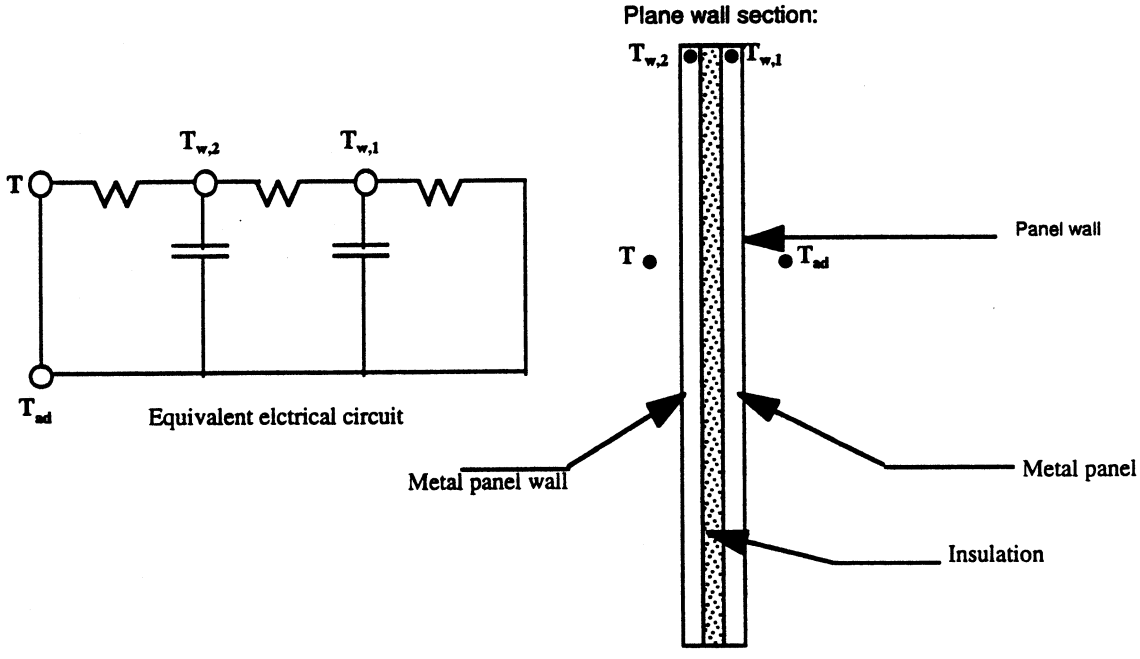

Figure 3.4 Modeling of lumped- capacity system

In equations 3.18 and 3.19, the derivative terms represent thermal capacitances in the equivalent electrical network. The three resistances are expressed as algebraic terms on the left hand side of the equations. Similar expressions for floor and ceiling can be also developed. The lumped capacitance network can be used to calculate the surface temperature of each component (i.e. $T_{w,2}$ in Figure 3.4) and subsequently the heat exchange rate between the component and the room. Hence, $\dot{q}_{tr}$ in equation 3.11 can be calculated by determining wall, floor and ceiling surface temperatures. Further details of the lumped capacitance method are described in Chapter 4 as a part experimental validation of room model.

Single equivalent wall model:

Instead of treating each of the envelope components separately, an approximate imaginary thermal mass can be used which exchanges heat with the room comparable to that of ceiling, walls and floor combined. The basic method used here also uses a thermal network as shown in Figure 3.5.

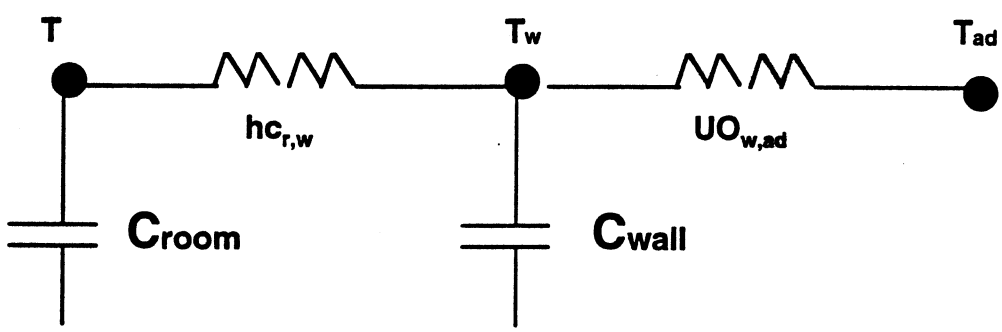

Figure 3.5 Thermal network for single equivalent wall

The wall surface temperature, T_W can be expressed as

$$Tau_W \frac{dT_W}{dt} = hc_{r,w} A_W (T - T_W) + R_{tw,ad} (T_{ad} - T_W) \quad (3.20)$$

where, the wall resistance $R_{tw,ad}$ is given by the total resistances less the convection resistance

$$R_{tw,ad} = \frac{1}{Uo_{w,ad}} - \frac{1}{hc_{r,w}} \quad (3.21)$$

The equivalent wall surface temperature, T_W can be solved for using numerical integration and used to compute the rate of heat transfer between room and equivalent wall.

3.4 Infiltration:

In a lab, the pressure differential across the room envelope rather than the room absolute pressure, P, is critical as it determines whether the room pressure is higher or lower than the adjacent space and thus the direction of the airflow. Higher room pressure prevents air flow from the adjacent space, which is a requirement for clean room operation. The pressure inside the laboratory is usually kept slightly lower than the pressure in adjacent spaces to prevent leakage of air from the lab. Lower room pressure is often termed as negative pressure or de-pressurized. The pressure differential in a lab causes infiltration from the adjacent space. The infiltration equation is based on the assumption of orifice flow. The infiltration through envelope holes and cracks is adequately expressed by an equation of the type shown in

previous studies (Shah 1980; ASHRAE 1989). The infiltration equation is presented as

$$\dot{v}_{ad} = K_l (\Delta P)^n \qquad (3.22)$$

The purpose of the above equation is to couple the volumetric flow rate of infiltrating air and differential pressure across the envelope. Equation 3.22 is coupled with equations 3.6 and 3.11 in terms of $\dot{v}_{ad}$ and Pad.

3.5 Model verification:

The room models constitute conservation of mass and energy principles, represented by equations 3.6 and 3.11, single equivalent wall model for envelope transient, indicated by equations 3.20 and 3.21 and the infiltration equation 3.22. The models are simulated using several simple forcing functions and the results are analyzed. For each simulation, the transient solution at the final state is compared with the steady- state solution to ensure the accuracy of the transient behavior. The values of simulation parameters and some physical variables which are kept fixed are shown in Table 3.1. The value of the envelope leakage constant K_l is calculated based on the procedure described in ASHRAE Fundamentals (1993). The K_l value of $1000 \frac{cfm}{(w.c.)^{0.65}}$ represents a moderately tight envelope. Both the overall equivalent wall heat transfer coefficient, UO_{ad} and time constant, Tau_w are approximated assuming that the wall is made of eight inches of lightweight concrete using values from ASHRAE Fundamentals (1993).

Table 3.1

List of Simulation Parameters and Fixed Variables

Name	Symbol	Value	
		Inch- pound	SI
Envelope leakage constant	K	1000 $\frac{cfm}{(w.c.)^n}$	1165.79 $\frac{L/sec.}{(kPa)^n}$
Flow exponent	n	0.65	0.65
Supply pressure	P_S	408.0 (w.c.)	101.526 (kPa)
Adj. space pressure	P_{ad}	408.0 (w.c.)	101.526 (kPa)
Adj. space temperature	T_{ad}	70 (^oF)	21 (^oC)
Overall heat transfer coefficient between adjacent space and the wall surface	$U_{w,ad}$	0.30 $(\frac{Btu}{hr-sq.\,ft-^o F})$	1.70 $(\frac{W}{m^2-^o C})$
Equivalent thermal capacitance	Tau_w	5000 $(\frac{Btu}{^o F})$	9489.31 $(\frac{kJ}{^o K})$
Connective heat transfer coeff. between room and the wall surface	$hc_{r,w}$	1.46 $(\frac{Btu}{hr-sq.\,ft-^o F})$	8.29 $\frac{W}{m^2-^o C}$ $(\frac{W}{m^2-^o C})$

Following are the three examples of verification process of the room models. For each example, two sets of plots are presented: one to indicate the

response of observed variables and the other represents mass flow rates of air streams in and out of the laboratory. Figures 3.6 and 3.7 show the

response of room temperature and gauge pressure (P_{ad}-P) due to the increase in exhaust flow rate.

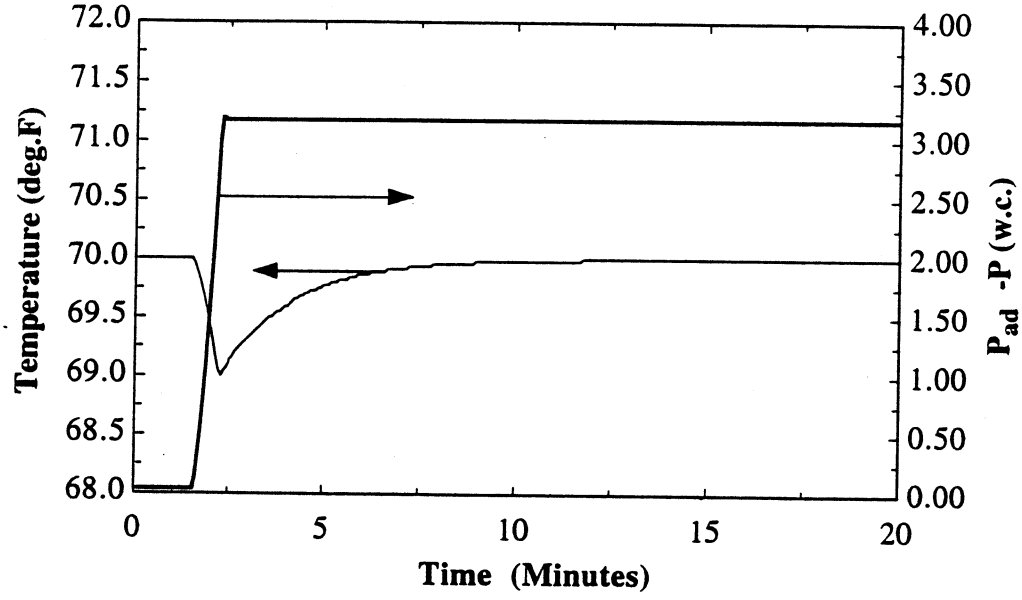

Figure 3.6: Validation of room model: Effect of increase in exhaust flow

The exhaust flow rate is increased linearly from 450 cfm at 1.53 min. and to 2450 cfm in 40 seconds. The supply flow rate, $\dot{v}_s$, the discharge air temperature, T_s, and the rate of internal load generation, $\dot{q}_{gen}$, are constant at 297 cfm, 70 ^{o}F and 82.50 Btu/min. The room temperature drops momentarily and then rises back to the steady state value of 70 ^{o}F. The room pressure, P drops substantially making the gauge pressure, ΔP very positive and reaches a steady value with the steady state of the exhaust flow rate. The supply flow is constant so that the pressure drops to a level such that the infiltration equals the difference between exhaust and supply. The observation in this example is logical since with the increase in the exhaust flow rate, the room pressure will drop making the ΔP (P_{ad} -P) more

positive. As the exhaust flow rate increases, the room temperature will decrease momentarily as a substantial increase in ventilation compared to what is required to keep the room thermally balanced at 70 ^{o}F.

However, the rise in exhaust flow rate causes the air from the adjacent space to infiltrate to preserve the law of mass conservation. Figure 3.7 depicts the increase in the mass flow rate of the infiltrating air as the exhaust mass flow rate increases. The result is that the room temperature returns to a steady state value equal to the adjacent temperature of 70 ^{o}F.

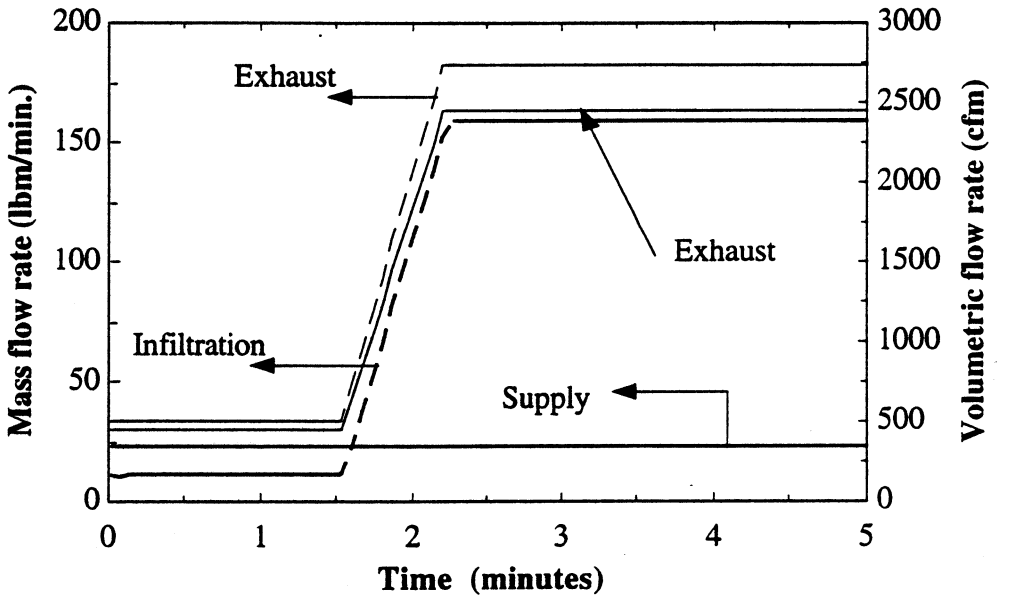

Figure 3.7: Validation of room model: Effect of increase in exhaust flow

The next example (Figures 3.8 and 3.9) shows the effect on room variables, temperature and pressure, due to an increase in the supply flow rate. All

parameters are unchanged from example 1 except the exhaust flow rate, $\dot{v}_{ex}$, which is kept constant at 450 cfm. The supply flow rate is quickly increased from 297 cfm to 2297 cfm. With the sudden increase in the supply flow rate, the room pressure rises and makes the room positively pressurized with respect to the adjacent pressure (i.e. $\Delta P < 0$). The room pressure then remains positive as the supply flow rate reaches steady value. The room temperature drops sharply for a short period as the supply flow rate increases momentarily and then continues to drop until it reaches a steady state value. The decrease in room temperature is expected as the supply air at 55 ^{o}F provides substantial cooling to the room. The final temperature and room pressure found to be consistent with steady state solutions for given boundary conditions and the rate of heat generation.

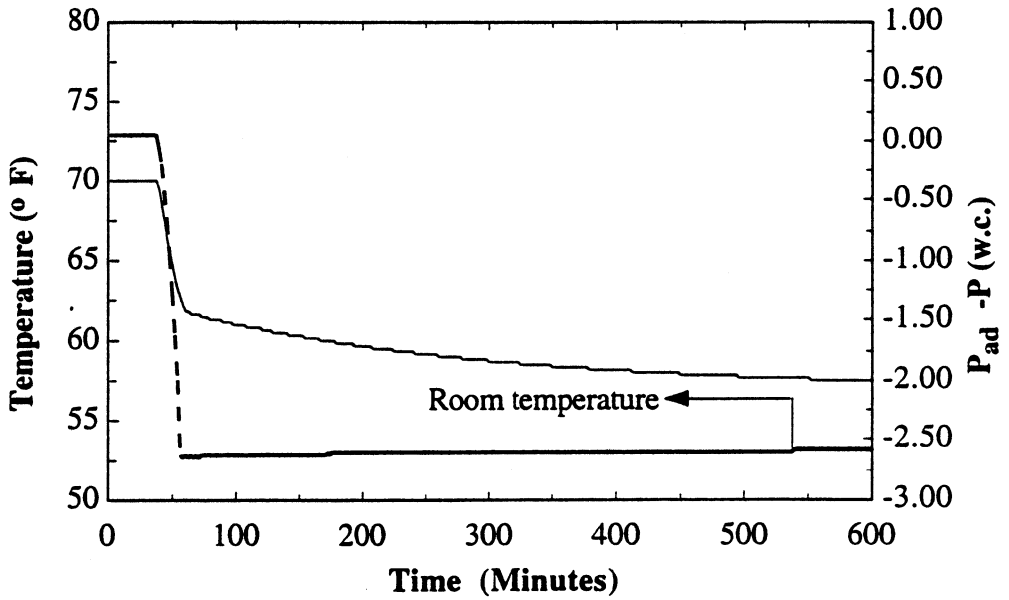

Figure 3.8: Validation of room model: Effect of increase in supply flow

The last example (Figures 3.10 and 3.11) demonstrates the effect of sudden change in the rate of internal heat generation as shown in Figure 3.11. The

sudden increase in the heat generation takes place due to the operation of lab equipment i.e. autoclave, oven, sterilizer etc. The internal generation rises to 82.50 Btu/ min. at 10 minutes from an initial value of zero, remains steady for another 10 minutes and then returns to the initial value. The room air temperature profile follows the heat load trend, the exponential rise and decay due to the storage in the envelope. The profile of room gauge pressure, however, is counter- intuitive. The increase in the internal load initially increases the room pressure, causing the ΔP (P_{ad} -P) value to drop. The infiltration rate also decreases momentarily, and the room pressure, P decreases due to reduced inflow and constant exhaust flow rate. Then with the sudden decrease in the internal load, the pattern of room pressure follows the same trend but in the opposite direction.

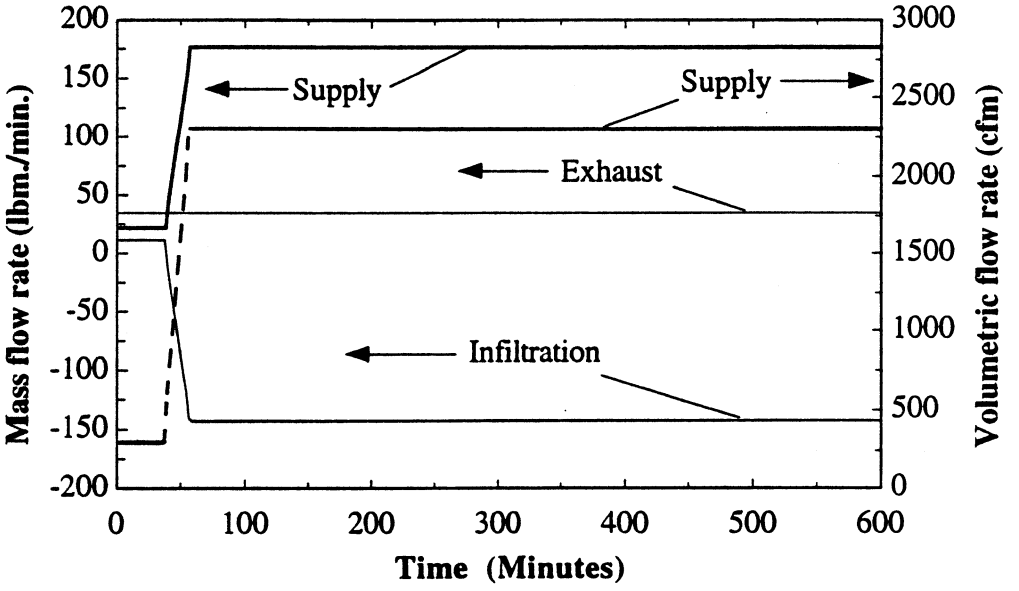

Figure 3.9 Validation of room model: Effect of increase in supply flow

The range of change in the room gauge pressure ΔP is extremely small; it is between 0.0052 to 0.0058 w.c. which is about 10% of the setpoint of .05

w.c. Nevertheless, such a change may contribute to a significant error in critical laboratory applications such as labs containing radiation or bio hazards where a tight range of ΔP is to be maintained (Hitchings 1994).

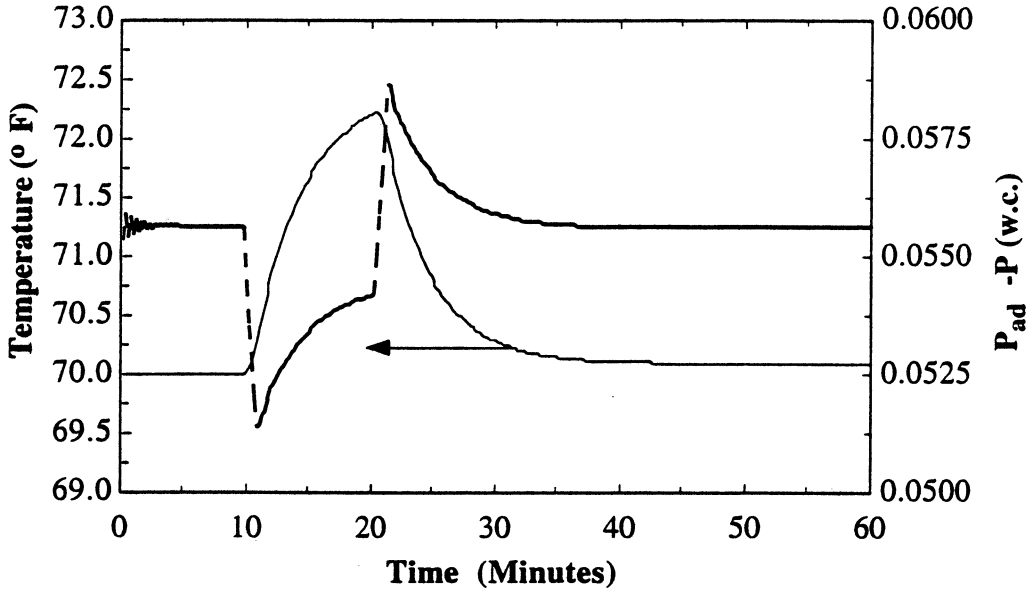

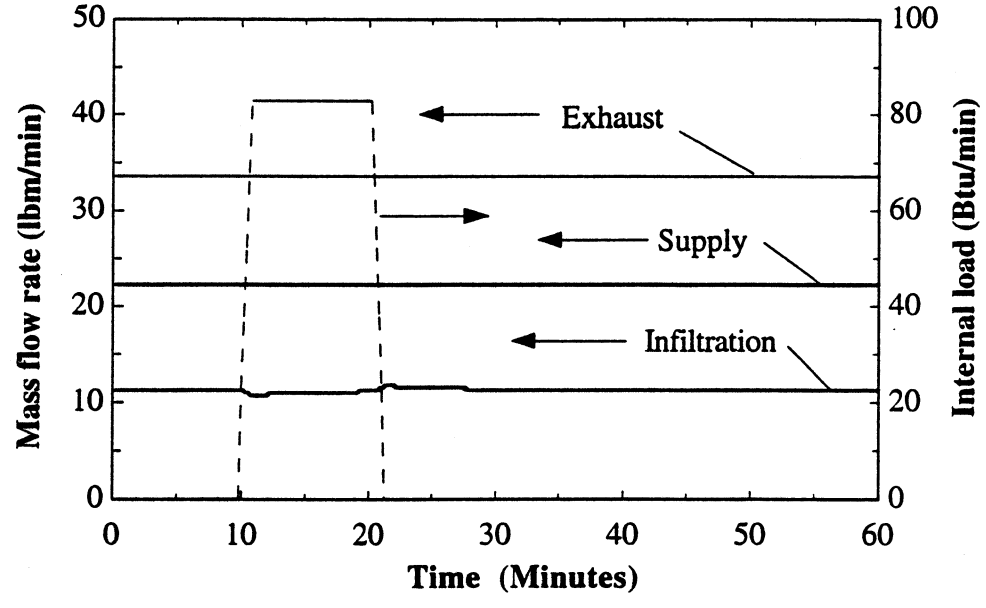

Figures 3.10 and 3.11 Validation of room model: Effect of change in heat load

3.6 Heating coil

The objective here is to determine a simple heating coil model to incorporate in the emulator yet one which will provide reasonable accuracy in emulating coil characteristics. The effectiveness model (Braun et al. 1987) is selected to achieve the desired objective. The schematic of a coil along with the effectiveness plot is shown in Figure 3.12.

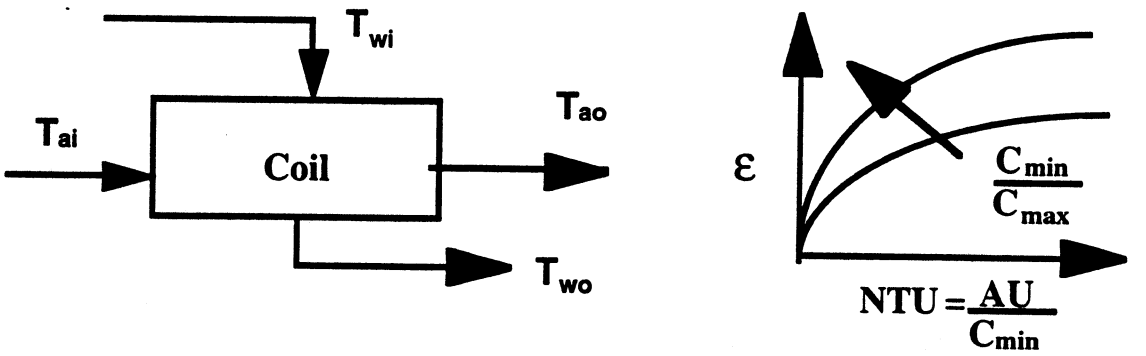

Figure 3.12: Coil schematics and effectiveness plot

The assumptions for the heating coil model are as follows:

- Negligible heat loss from the heat exchanger to the surroundings.
- Negligible kinetic and potential energy changes of air and water flow
- Constant fluid properties
- Negligible fouling factors

The basic coil heat transfer equation is the heat flow to the air:

$$\dot{q} = C_a (T_{a,o} - T_{a,i}) \qquad (3.23)$$

The coil effectiveness ε is defined as the ratio between the actual and maximum heat transfer rates or

$$\varepsilon = \frac{\dot{q}}{\dot{q}_{max}} \tag{3.24}$$

The maximum rate of heat transfer occurs when the fluid with the minimum product of flow rate and specific heat changes temperature to the entering temperature of the other fluid. Hence, actual coil heat transfer rate, $\dot{q}$ can be rewritten as

$$\dot{q} = \varepsilon C_{min}(T_{f,i} - T_{a,i}) \tag{3.25}$$

Combining equations 3.23 and 3.24,

$$T_{a,o} = T_{a,i} + \varepsilon(\frac{C_{min}}{C_a})(T_{f,i} - T_{a,i}) \tag{3.26}$$

In order to calculate heating coil effectiveness , ε the following equation is used for a counter flow heat exchanger (Incropera & Dewitt 1985)

$$\varepsilon = 1 - e^{(-\frac{1}{C_r}(1-e^{-(C_r NTU)}))} \tag{3.27}$$

Where,

$$C_r = \frac{C_{max}}{C_{min}}, \quad NTU = \frac{hc_{coil}A_{coil}}{C_{min}}, \quad C_{min} = min(C_f, C_a)$$

and $C_{max} = max(C_f, C_a)$

The coil number of transfer units, NTU is estimated based on design values of C_{min} and assumed value of ε. The coil NTU is determined from published coil data to develop a functional relationship between coil NTU, ε

and the ratio of C_{min} and C_{max} (Kays and London 1964). Once coil NTU is determined, it is appeared to change insignificantly with the flow rate. However, coil effectiveness ε will change with the variation in coil capacitance C_{min} and C_{max}. The use of design parameters is a simple yet effective way of selecting coil parameters. The other methods require extensive knowledge of coil physical properties and dimensions and use complicated equations.

The coil dynamics is represented assuming first order system (U.S. Dept. of Commerce 1984; Pearson 1974) as follows:

$$\tau_{coil} \frac{dT_{ao}}{dt} + T_{ao} = T_{ao|sp,\ (t-t_O)} \qquad (3.28)$$

The above equation indicates that $T_{a,o}$ will approach the setpoint exponentially. The rate of approaching the setpoint is determined by the coil time constant, τ_{coil}. Sample coil responses are shown in Figures 3.13 and 3.14. In Figure 3.13, the coil flow rate is changed instantaneously from an initial condition to 3.5 gpm and held constant. The coil flow rate is changed linearly for 100 seconds to reach 3.5 gpm and then held constant afterwards in Figure 3.14. The discharge air temperature is then calculated and plotted for various coil time constants. In both plots, sufficient simulation time is allowed to ensure that each run produces the steady state temperature at the end of the simulation period. The simulation parameters chosen are based on coil design conditions and are listed in Table 3.2.

Table 3.2

List of simulation parameters

Description	Symbol	Equation used	Values
Max. supply air temp	$T_{a,o\,l}$		72 °F
Max. supply air flow[1,2]	$\dot{v}_{s\,l\,max}$		2000 cfm
Coil entering air temp.[3]	$T_{a,i}$		55 °F
Max. design coil heat transfer	$\dot{q}_{max}$	$\dot{q}_{max} = 1.08\ \dot{v}_{s\,l\,max}\ \Delta T_{a,max}$ $\Delta T_{a,max} = (T_{a,o\,l\,max} - T_{a,i})$	36,000 Btu/hr
Max. coil water flow rate	$\dot{v}_{f\,l\,max}$	$\dot{v}_{f\,l\,max} = \frac{\dot{q}_{max}}{500\,\Delta T_f}$	3.5 gpm
Design water side temp. drop[4]	ΔT_f		20 °F
Air mass- capacitance	C_a	$C_a = \dot{v}_{s\,l\,max} \rho_a C_{p,a}$	36 $\frac{Btu}{min-^o F}$
Water mass- capacitance	C_f	$C_f = \dot{v}_{f\,l\,max} \rho_f C_{p,f}$	28 $\frac{Btu}{min-^o F}$
Ratio of fluid heat capacity	C_r	$C_r = \frac{C_{min}}{C_{max}} = \frac{C_w}{C_a}$	0.777
Effectiveness[5]	ε		0.70
Overall coil heat transfer coefficient[6]	UA	$\varepsilon = f(NTU, \frac{C_{min}}{C_{max}})$	70 $\frac{Btu}{min-^o F}$

1. Sufficient value at max. ventilation

2. Based on maximum fume hood exhaust

3. Design condition

4. Good design value (Bell & Gossett 1977)

5. Assumed value

6. Using ε plot

The coil response presented in Figure 3.14 is realistic since the water flow rate through the coil will vary depending upon the valve characteristics. A linear flow profile is chosen here for the sake of simplicity. However, as shown in damper/valve section, different profiles can be created by choosing suitable damper/ valve parameters. The plot in Figure 3.13 is performed to illustrate that the coil responds faster with the lower coil time constant τ_{coil}

.

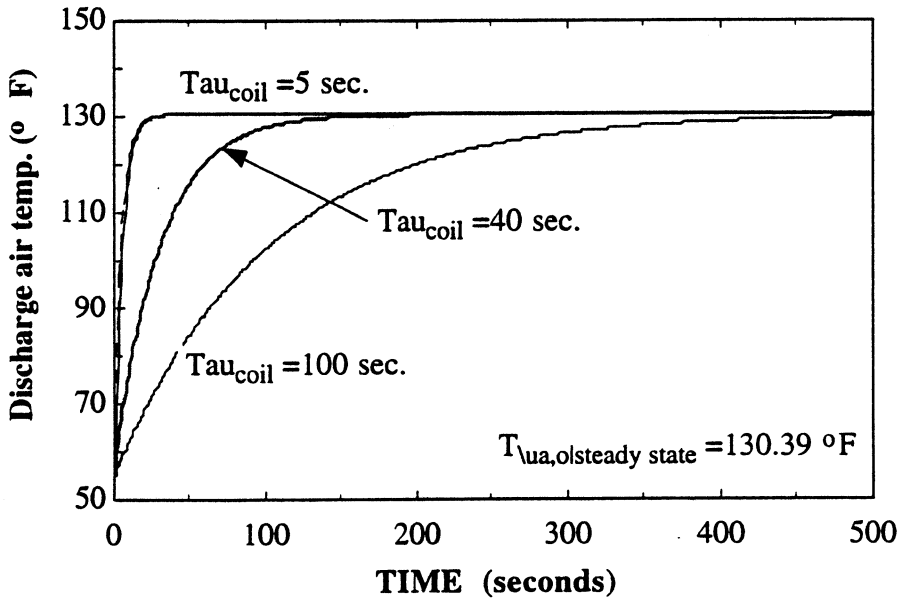

Figure 3.13 Coil response for fixed water flow rate

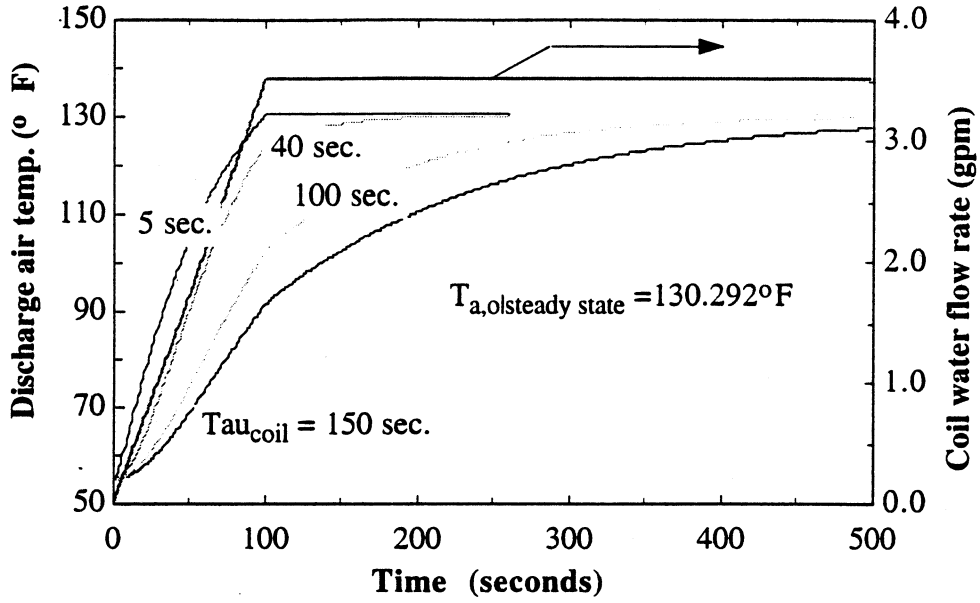

Figure 3.14 Coil response for variable water flow.

3.7 Damper/ Valve

A damper or valve is essentially a variable fluid resistance device. They exhibit the same fluid characteristics and their performances are expressed in terms of identical variables. The valves and dampers are, therefore, represented by the same models. As indicated in the literature survey, the models represented here are used in HVACSIM$^+$ simulation program (U.S. Dept. of Commerce 1984). The models are capable of representing both linear or non-linear behavior in terms of inherent characteristics. For clarity, only the term damper will be used although the models are also valid for valves.

The models consist of a damper, a duct section upstream and a duct downstream of the damper. In the case of a valve, the duct sections will be

replaced by pipes. A schematic of the damper/ valve model is shown in Figure 3.15.

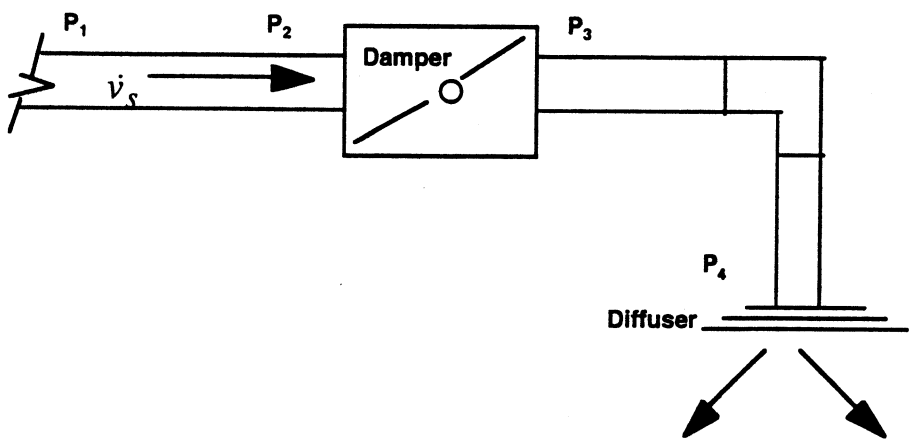

Figure 3.15: Damper schematics

For fixed upstream and downstream pressures, the model computes the flow rates by knowing the damper position. The damper position is linked to the actuator's position which is commanded by the controller. The models shown below assume,

- Density changes are negligible.
- Both inlet and outlet pressures P_1 and P_4 are known and fixed.
- Heat transfer from duct is neglected.
- Frictional coefficient in the flow range under consideration remains constant.
- Flow is fully developed.

The pressure- flow equations assume that the pressure difference is proportional to the square of the flow rate.

$$P_1 - P_2 = K_{12}(\dot{v}_s)^2 \tag{3.29}$$

$$P_2 - P_3 = K_{23}(\dot{v}_s)^2 \tag{3.30}$$

$$P_3 - P_4 = K_{34}(\dot{v}_s)^2 \tag{3.31}$$

Equations 3.29 to 3.31 will be also valid for valves except that the volumetric water flow rate through the damper, $\dot{v}_f$ will be replaced by the water flow rate through the valve. K_{12} and K_{34} are evaluated based on design conditions and standard HVAC design procedures. K_{23} is expressed as (U.S. Dept. of Commerce 1984),

$$K_{23} = \frac{W_f K_o}{[(1-\lambda)r + \lambda]^{2.0}} + (1 - W_f) K_o \lambda^{(2r-2)} \tag{3.32}$$

In equation 3.32 the parameter, W_f determines the non-linearity of the valve/ damper. W_f of 0 indicates a linear damper whereas 1.0 means truly exponential damper. The term λ indicates a leakage constant since most dampers leak. This constant prevents infinite an flow resistance when the damper is fully closed. The damper flow resistance coefficient at fully open position is denoted by K_o whereas r represents the normalized (0 -1) commanded position by the controller.

The flow through the damper can be also predicted by assuming installed characteristics denoted by authority, a. The installed authority dictates the ultimate performance of a damper in a system. For example, an inherently linear damper will exhibit non-linear performance as the authority becomes smaller. Therefore, by using system authority as a simulation variable it is possible to duplicate the installed performance of a damper. The system

authority can be defined as the ratio between the pressure drop across the damper and the total pressure drop when the damper is fully open. Mathematically,

$$a = \frac{(P_2 - P_3)|_{dfo}}{(P_1 - P_4)|_{dfo}} \tag{3.33}$$

By fixing the value of a, essentially K_{12} can be a variable. Solutions of equations 3.29 to 3.33 will determine the value of K_{12} based on the fixed authority and compute the flow rate. The values of K_{12} for various a are listed in Table 3.3 along with other parameters considered in simulating damper characteristics.

Table 3.3

Damper Simulation Parameters

λ = 1.0e(-6); W_f = 1.0; K_{34}= 5.00 e(-9); K_0= .042;

Authority	K_{12} (" w.g/(lb/sec)^2.0)	Maximum $\dot{v}_s$ (cfm)
1.00	-5.00e(-9)	2297
.70	2.75e(-7)	1924
.50	6.48e(-7)	1626
.20	2.61e(-6)	1028
.10	5.87e(-6)	727
.05	1.24e(-5)	514
.01	6.46e(-5)	230

The simulated characteristics of a linear damper/valve are shown in Figure 3.16. The plot shows the effects of authority on damper characteristics. A damper shows linear relationship between the % flow and % control signal for an authority of 1.00. Referring to equation 3.33, an authority of 1.00 indicates that the pressure loss across the damper equals the total pressure loss. This is possible when the damper is the only significant fluid resistance device in the circuit. However, in a typical HVAC distribution system where many dampers are connected to a manifold, individual circuit pressure is dictated by the main duct pressure drop instead of the individual damper pressure drop.

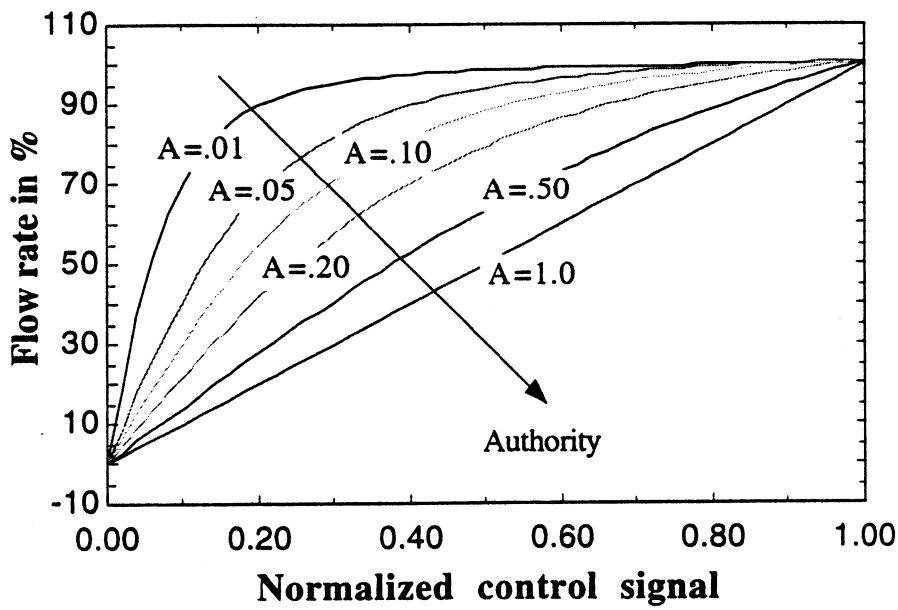

Figure 3.16 Simulated characteristics of a linear damper/ valve

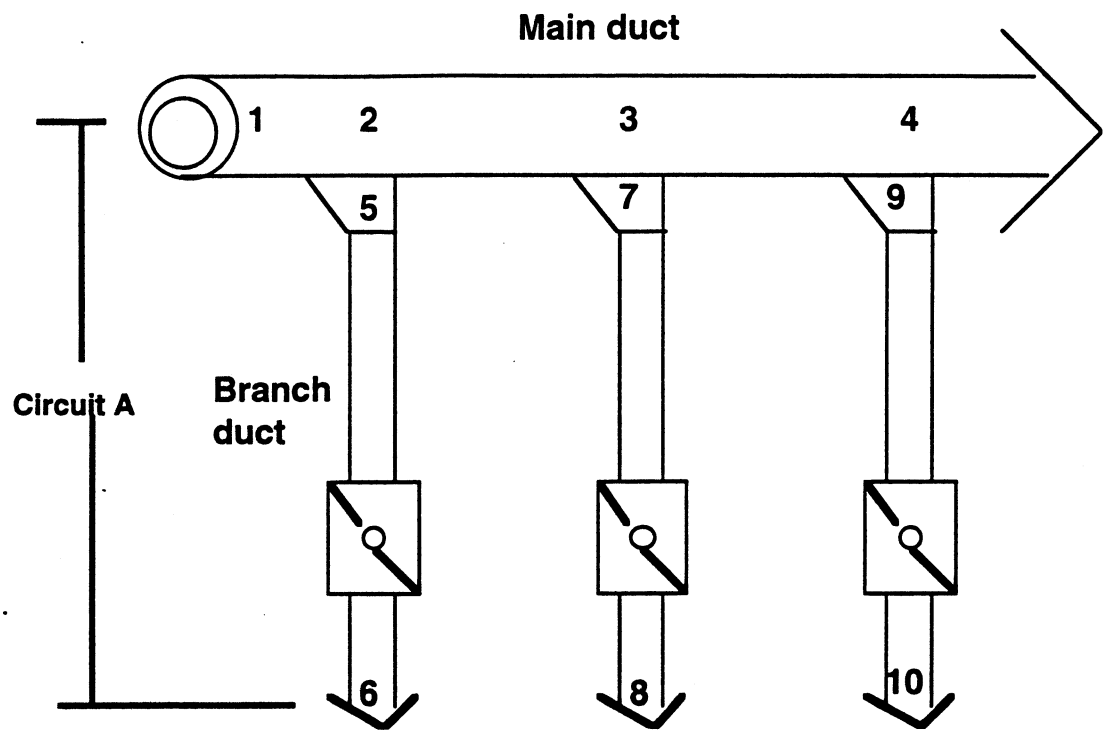

Figure 3.17 Manifold HVAC duct distribution system

For example, in Figure 3.17, the total pressure drop in circuit A may be dictated by the loss between section 1 and 2 just at the fan outlet as in that section the duct velocity may be significantly higher than in the section 5 to 6 and due to the fan discharge losses. In a VAV system, the authority is a time dependent variable as the flow in each circuit changes causing the authority to change for each circuit. Finally, the % flow scale in Figure 3.16 is based on the maximum flow rate obtainable for each authority. The maximum flow rate will decrease as the authority decreases. Hence, as the authority decreases, the absolute value of the flow rate will decrease for the same % flow rate. The concept of damper/ valve characteristics is important to capture since it shows the operating behavior of a linear damper shifts from linear to being non- linear.

3.8 Actuators

A simple first order linear model with a dead time was assumed for the actuator (U.S. Dept. of Commerce 1984). The dead time implies that at any instant t, the normalized position of the actuator, r_{ac}, is affected by the value of commanded position, r_{sp}, at t_o units of time earlier.

$$\tau_{act} \frac{dr_{ac}}{dt} + r_{ac} = r_{sp,(t-t_o)} \tag{3.34}$$

By choosing a different actuator time constant, τ_{act} and dead time t_o it is possible to simulate different actuator response profiles. Figure 3.18 shows a sample plot of the actuator response for various combinations of t_o and τ_{act} for a linear commanded positions.

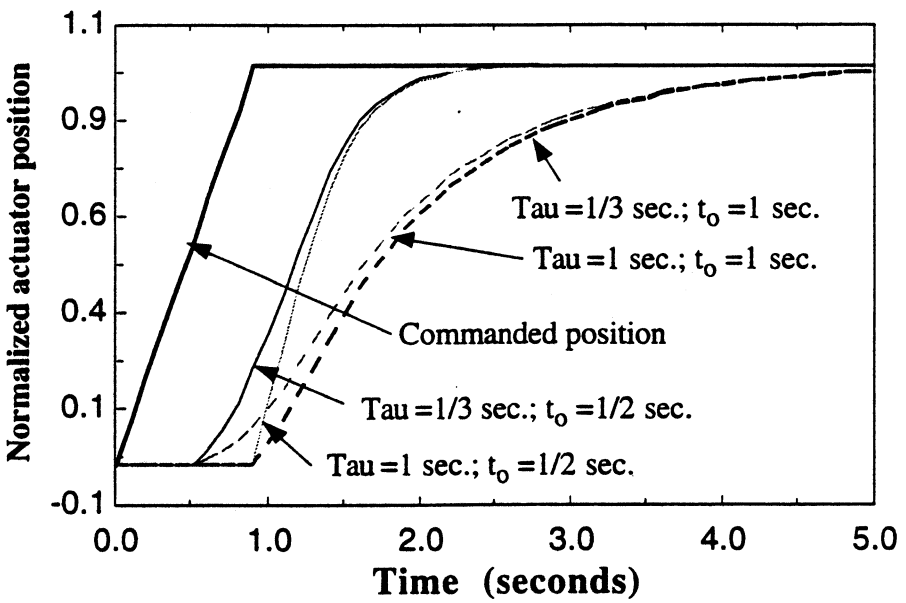

Figure: 3.18: Simulated actuator response

3.9 Thermostat

The development of a room thermostat model is described in detail in Chapter 4. The thermostat model is developed and verified using experimental results.

Chapter 4
Experimental Validation

4.1 Overview

All of the components of the lab emulator described in chapter 3, except for the room models, are taken from the published literature. From an user's perspective the thermal model selected should be easy to use and the parameters needed to model the room should be readily available from design information or by simple inspection. Both the room pressure and thermal models constitute a significant portion of the lab emulator and, hence, need some type of validation.

In order to validate both room pressure and thermal models, a series of experimental results were used. The results were obtained as a part of the commissioning of a product testing lab at Landis & Gyr Powers facility, Buffalo Grove, IL. Both pressure and thermal models are tested against the actual results and the agreement between the simulated and actual response is good considering the fact that the actual data were collected using commercial grade sensors and building automation system. The commercial sensors lack the accuracy of industrial grade and the building automation system is designed for control and not for data acquisition. Both factors contributed to the inaccuracy in the results. The next section describes the details of the test laboratory configuration and system. The simulation process to validate the models against the test results is included in section 4.3. The following sections 4.4 to 4.6 discuss the test sequences and compare

the results between actual and simulated values. The last section 4.7 summarizes the chapter findings. At the end of the chapter, an analysis of sensor bias error is included.

4.2 Test set-up

Two fume hoods, each capable of exhausting air from 250 to 2000 cfm are the main sources of the test lab exhaust. One of the fume hoods has a single vertical sash and the other is a combination hood having multiple sashes that can travel both in horizontal and vertical directions.

An additional general exhaust is available to duplicate the general exhaust control of a real laboratory. The lab supply system consists of an air handling unit with a variable speed fan and both cooling and heating coils that can modulate both supply air flow rate and discharge temperature.

The laboratory schematic in Figure 4.1 shows different streams of air in and out of the lab along with sensor locations. Basically, temperature and flow of each air stream are measured along with the room temperature, radiant wall temperature and the differential pressure sensor across the room.

The lab envelope consists of three panel walls and a radiant wall. The purpose of the radiant wall is to impose a cooling load in the laboratory. Figure 4.2 shows sections of lab envelope. The panel walls consist of a pre-fabricated metal wall having two metal sheets and 6 inches of insulation sandwiched between them. The radiant wall section is made of a radiant

panel, 3/4 inch of air gap, a layer of 4 inches thick Fiberglas insulation and a panel wall section. The lab metal floor is carpeted and the lab roof is made of a panel wall section, 1.5 feet of air space and acoustical tiles. The lab is 21' by 25' and floor to ceiling height is about 10'.

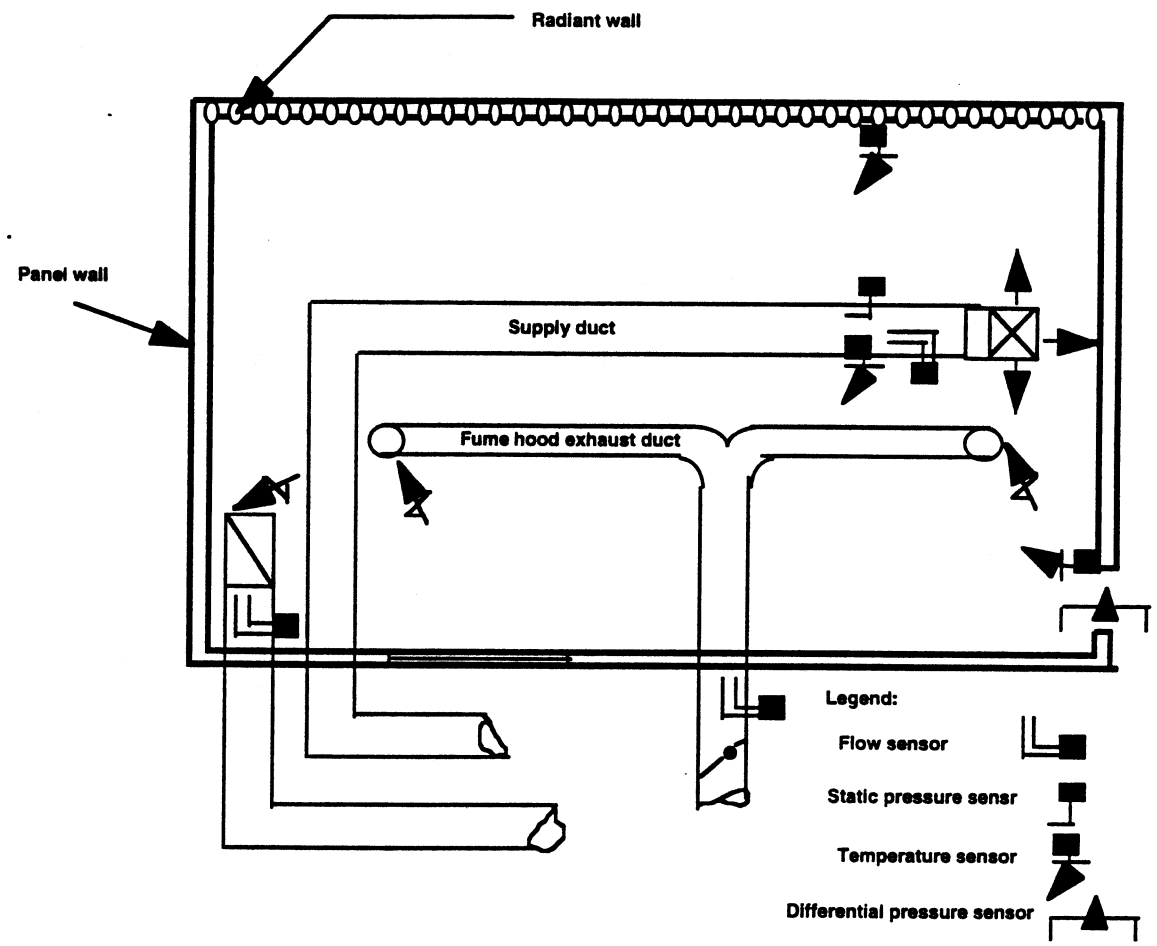

Figure 4.1 Schematic of test laboratory

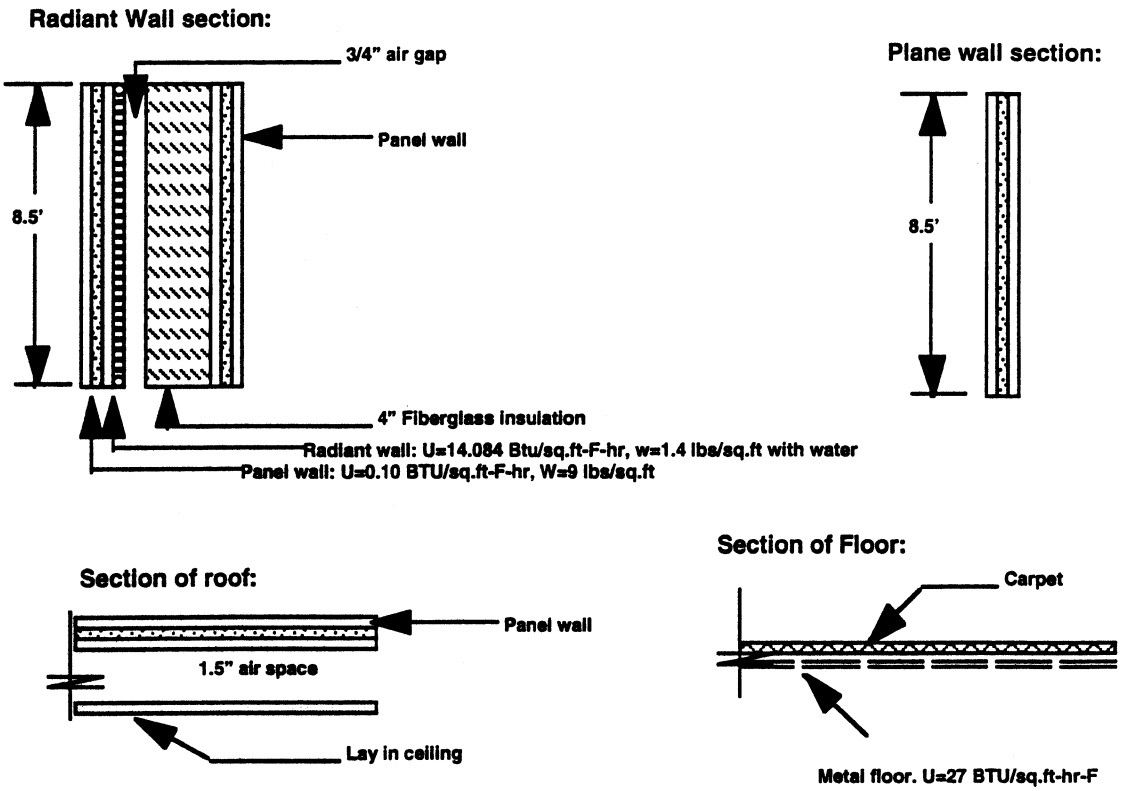

Figure 4.2: Test Lab Wall Sections

4.3 Validation process

For the purpose of validating the room models, the actual time-variant data from the test lab were fed into the room emulator. Then the predicted room temperature and differential pressure across the lab envelope were compared with the measured room temperature and the differential pressure. The overall process is shown in Figure 4.3.

The emulator used for validation of test results includes the transient mass balance (equation 3.6), energy balance (equation 3.11) and equations 3.12

and 3.13 to account for heat transfer between room air and walls, floor and ceiling. The envelope transient equations for each envelope are represented by the lumped-capacitance model shown in equations 3.18 and 3.19.

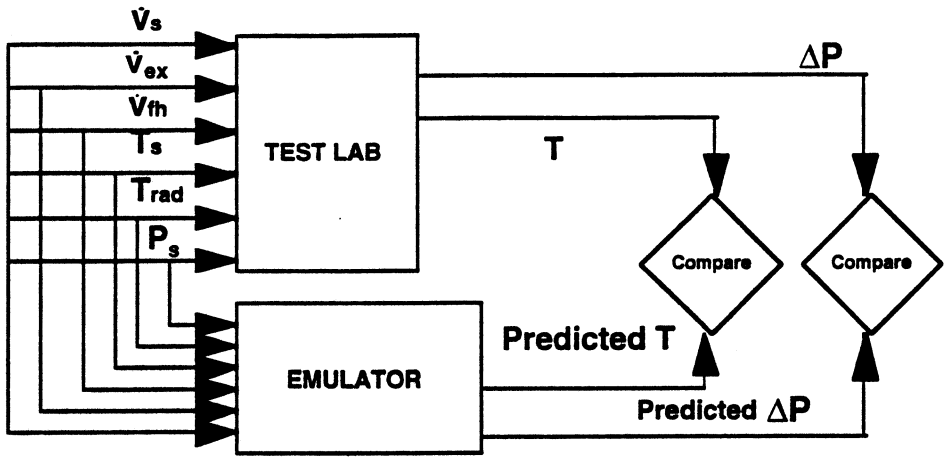

Figure 4.3: Overall validation process

The room air temperature was measured using a thermostat installed on the panel wall next to the entrance door. The thermostat does not provide a direct measure of the actual room air temperature. Hence, a model is needed to represent a thermostat, which essentially exchanges heat with the room air and the panel wall, in order to determine the air temperature.

A simple lumped capacitance model is used as follows to calculate the thermostat temperature. The simulated thermostat temperature is then compared with the measured thermostat temperature.

$$\frac{dT_{st}}{dt} = C1_{st}(T_{pw} - T_{st}) - C2_{st}(T_{st} - T) \qquad (4.1)$$

$C1_{st}$ is a coefficient denoting the ratio of conduction heat transfer coefficient between the panel wall and thermostat and thermostat thermal capacitance. $C2_{st}$ is a similar coefficient except the conduction coefficient is replaced by a convection coefficient. Equation 4.1 is a simple expression of the complicated dynamic thermostat heat transfer and storage process. The objective here is to determine the coefficients using measured values of thermostat temperature so that a simple equation can represent thermostat model. The process of determining thermostat coefficients, $C1_{st}$ and $C2_{st}$, using the measured response is described in section 4.5.3.

4.3.1 Determination of envelope leakage coefficients:

In addition to thermostat coefficients, the lab leakage coefficient, K_l, and flow exponent need to be determined in order to use the infiltration equation 3.22. A series of tests were done to measure Δp for various infiltration/exfiltration flow rates, $\dot{v}_{ad}$. The infiltration/exfiltration flows are obtained by varying the difference between the measured values of total lab supply and exhaust flow rates. The measured values are then fit to equation 3.22 in order to obtain K_l and flow exponent, n. The plots of exfiltration flow rates against the corresponding measured Δp are shown in Figure 4.4.

By curve fitting the results in the plot in Figure 4.4 to the leakage model, $\dot{v}_{ad} = k_l (\Delta p)^n$, a flow exponent, n of 1.150 and K_l of 1919.80 cfm/(w.g.)^n are obtained. Previous studies (Shah 1980; Homma 1975) have indicated that usually n varies between 0.5 and 1.0 where 0.5 indicates a

fully turbulent model whereas 1.0 indicates a plug flow. Most commonly, an n of 0.65 (Konrad 1978) is found for buildings. Furthermore, careful analysis reveals that the data in Figure 4.4 when extrapolated to zero flow rate yields a Δp of -0.32 w.g. This is similar to an offset commonly found in a transducer type device. The pressure transducer used to measure the pressure differential across the envelope is a bi-directional type. In other words, it is sensitive to the directional flow. However, often the transducers are calibrated to determine the zero and span by measuring the pressure differential considering flow of air in one direction. Since typically a lab application requires infiltration i.e. the lab pressure is kept lower than the reference pressure, the transducer used in the measurement is calibrated for infiltration conditions.

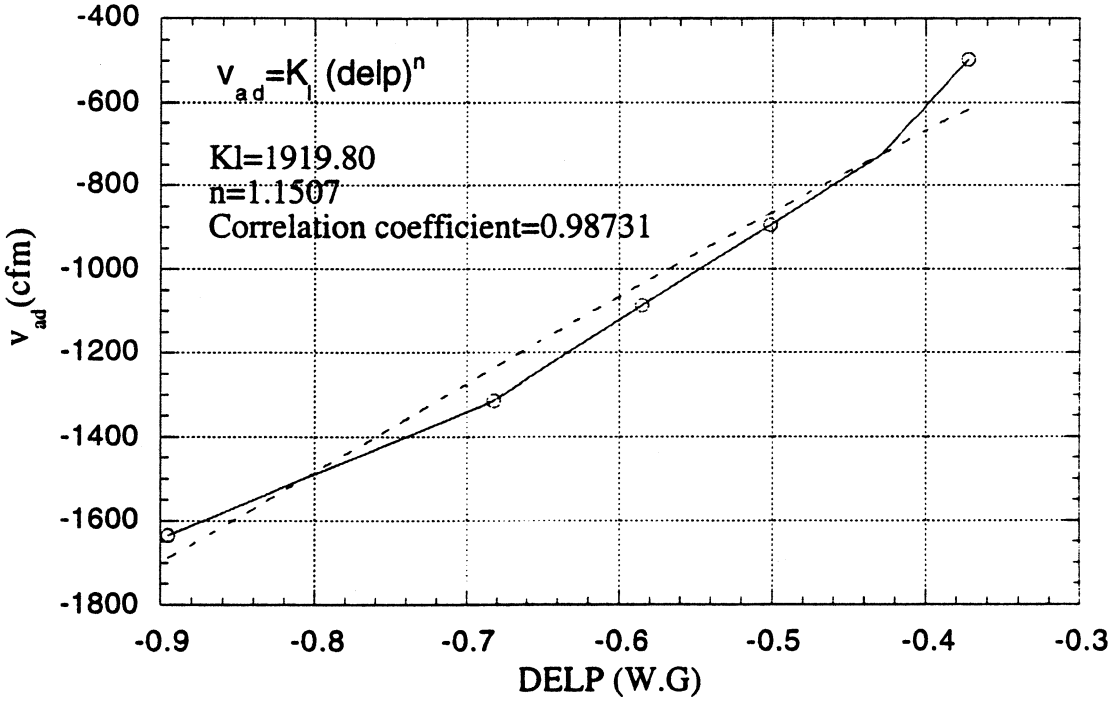

Figure 4.4: Exfiltration leakage characteristics before adding a constant offset.

Based on above observations and physical reasoning, a constant offset of -0.32 w.g. is subtracted from all measured values of Δp. The resultant plot along with the fit to the leakage model is shown in Figure 4.5.

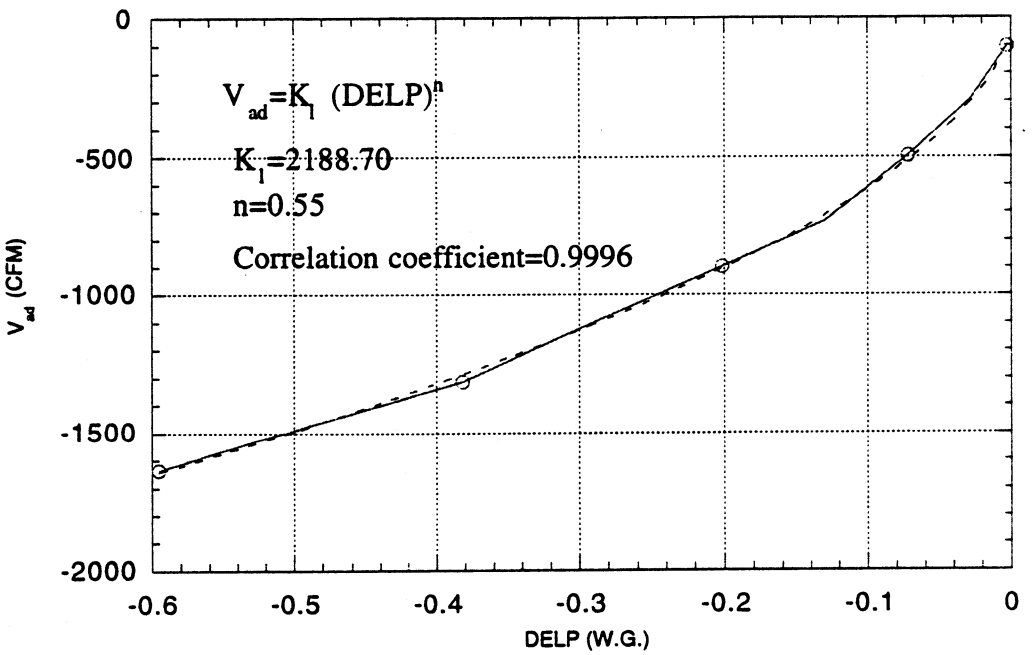

Figure 4.5: Exfiltration leakage characteristics after adding a constant offset.

The new flow exponent is found to be 0.55 and K1 is 2188 cfm/(w.g.)^n. The infiltration leakage characteristic is shown in Figure 4.6. The infiltration data fits very well to the leakage model resulting in flow exponent of 0.6341 and leakage constant, K1 of 2951 cfm/(w.g.)^n. The curve also passes through

the origin as expected. The values of K_l between 2000-3000 signify a tight envelope as high Δps in the range of -0.6 to 0.5 " w.g. were measured. The infiltration and exfiltration equations are easily incorporated into the overall room model.

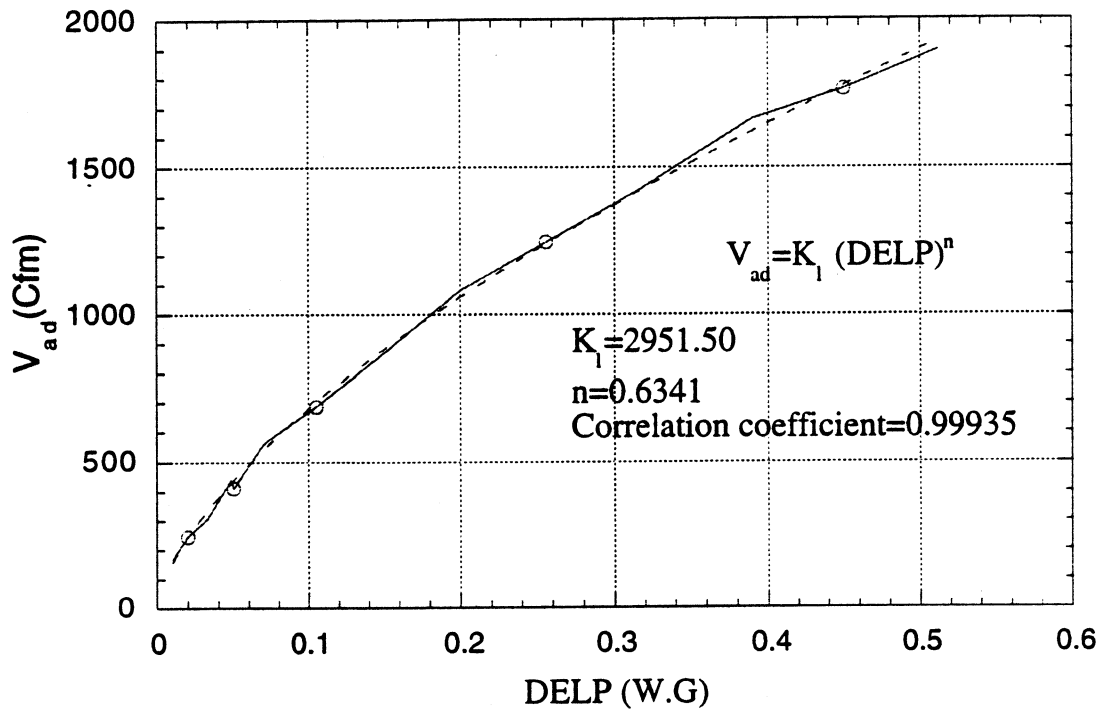

Figure 4.6: Infiltration leakage characteristics.

The overall leakage curve combining both infiltration and exfiltration is shown in Figure 4.7. Figure 4.7 shows all the leakage flow rates which are obtained by repeating measurements three times for each differential pressure across the envelope. The excellent fit of measured data with the assumed model justifies the selection of the leakage model shown as $\dot{v}_{ad} = k_l (\Delta p)^n$.

4.4 Test sequence:

Several test sequences were created to test the room pressure and thermal models. The first two sequences were to test the room pressure models and, therefore, all temperatures are kept at 70° F. The test sequences were meant to create the maximum positive and negative pressure differentials across the envelope by creating the maximum exhaust flow rate from the lab while keeping the supply minimum and then reversing the flow magnitudes respectively. Since the room pressure responds rapidly, the data were collected every second, which is the fastest rate with which the data can be collected using Landis & Gyr building automation system (1990).

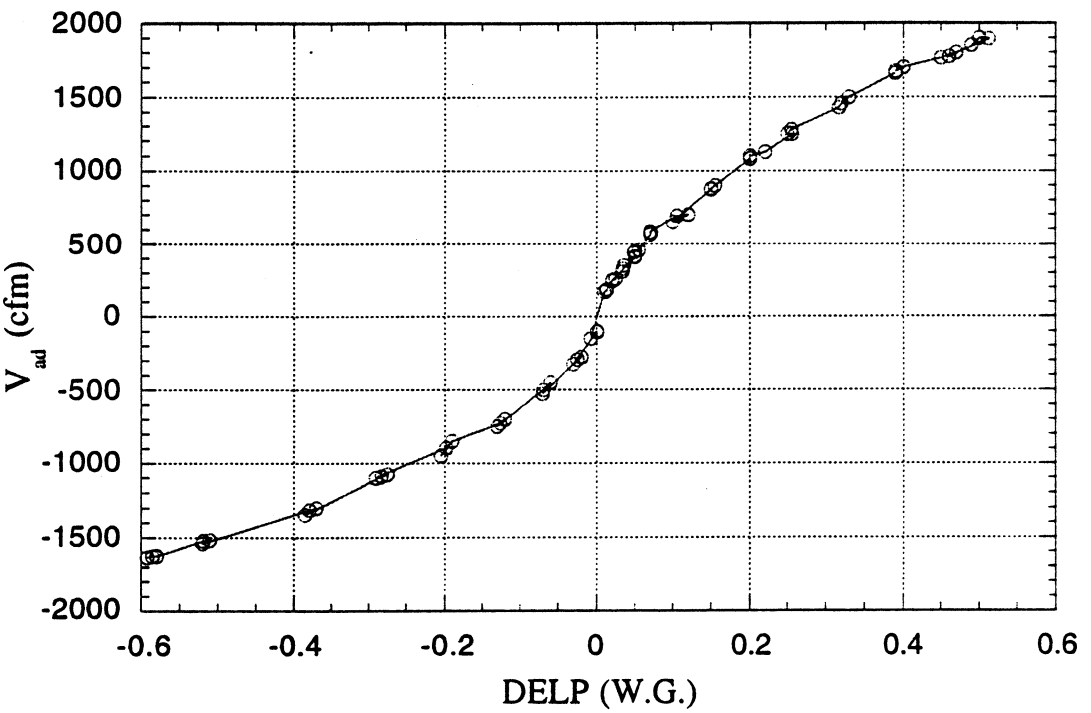

Figure 4.7: Overall leakage characteristics.

The next five sequences were designed to provide room thermal characteristics. In sequence A3, the objective is to lower the space temperature as much as possible in order to determine the maximum heating

load for the room control. The goal is provide heat to bring the space temperature from the coldest to the normal operating temperature at 70° F. Test sequence A4 operates the lab under normal cooling condition by keeping the boundary temperatures at 70° F and the lab supply air at 55° F. Similarly, test sequence A5 maintains the supply air temperature at 90° F in order to determine the lab normal heating operating condition. The objective in test sequence A6 is to observe the thermal response to sudden heat generation in the lab. The heat is generated by using a space heater that heats at a constant rate and by setting the radiant wall panel temperature at 140° F. Finally, the test sequence A7 is used to observe the dynamic lab thermal response due to a sudden increase in the supply temperature from an initial setting of 55° F to the final value of 90° F. This is a common sequence in a VAV lab as result of a sudden increase in total lab exhaust due to the opening of fume hoods. Under such conditions, the supply air, which is usually discharged from the central air handler at 55° F, is reheated to prevent lab undercooling. Since the thermal response is slow, data are collected during all thermal tests at an interval of 1 minute in order to avoid massive data storage and handling problem. The summary of the test sequences along with the tables showing the control and observed variables values at the different times follow.

TEST A1 and A2

1. Set discharge air temperature 70 °F
2. Recirculate water at 70 °F or shut- off the water circulation
3. Set fume hood and general exhaust to full flow and lab supply to minimum flow
4. Observe pressure differentials
5. Set fume hood and general exhaust to minimum flow and lab supply to maximum flow

6. Observe pressure differentials

Objective: Determine dynamic room pressure response

Table 4.1

Test Seq.	Time (min)	Measured Variables							
		$\dot{v}_{fh}$ (cfm)	$\dot{v}_{ex}$ (cfm)	$\dot{v}_{s}$ (cfm)	T_s (°F)	T_{rad} (°F)	P_s (w.c)	T_{st} (°F)	ΔP (w.c)
A1	0	1000	1260	400	70	70	0.23	70	0.52
A2	1.0	200	0	1700	70	70	0.80	70	-.36

The control variables are shown in boldface.

TEST A3

1. Set discharge air temperature 55 °F
2. Recirculate water at 45 °F
3. Set fume hood, general exhaust and supply to full flows
4. Observe room temperature

Objective: Determine maximum space cooling i.e. maximum heating load and observe room thermal response.

Table 4.2

Test Seq.	Time (min)	Measured Variables							
		$\dot{v}_{fh}$ (cfm)	$\dot{v}_{ex}$ (cfm)	$\dot{v}_{s}$ (cfm)	T_s (°F)	T_{rad} (°F)	P_s (w.c)	T_{st} (°F)	ΔP (w.c)
A3	0	150	1200	1200	70	64	0.37	69	-
A3	29	1050	2000	2900	64	51	0.85	65	-
A3	155	1050	2000	2900	53	47	0.87	58	-
A3	222	1100	2000	3000	53	47	0.87	57	-

The control variables are shown in boldface.

TEST A4

1. Set discharge air temperature to 70 °F
2. Recirculate water at 70 °F or shut- off the water circulation
3. Set fume hood, supply and general exhaust to minimum flows
4. Set discharge air temperature at 55 °F
5. Set fume hood and general exhaust to maximum flows

Objective: Determine dynamic room thermal response under normal cooling mode.

Table 4.3

Test Seq.	Time (min)	Measured Variables							
		$\dot{v}_{fh}$ (cfm)	$\dot{v}_{ex}$ (cfm)	$\dot{v}_s$ (cfm)	T_s (°F)	T_{rad} (°F)	P_s (w.c)	T_{st} (°F)	ΔP (w.c)
A4	0	1100	1200	2900	70	70	0.85	71	
A4	59	1100	1200	2900	52	66	0.85	71	-
A4	160	1100	1200	2900	50	53	0.85	59	
A4	184	1100	1200	337	50	53	0.23	59	
A4	300	1000	1200	275	53	65	0.25	67	

The control variables are shown in boldface.

TEST A5

1. Set discharge air temperature to 70 °F
2. Recirculate water at 70 °F or shut- off the water circulation
3. Set fume hood, supply and general exhaust to minimum flows
4. Set discharge air temperature at 90 °F
5. Set supply flow at maximum

Objective: Determine dynamic room thermal response under normal heating mode

Table 4.4

Test Seq.	Time (min)	Measured Variables							
		$\dot{v}_{fh}$ (cfm)	$\dot{v}_{ex}$ (cfm)	$\dot{v}_{s}$ (cfm)	T_s (°F)	T_{rad} (°F)	P_s (w.c)	T_{st} (°F)	ΔP (w.c)
A5	0	150	1650	2000	70	73	0.62	73	
A5	17	150	0	0	72	73	0.28	73	-
A5	78	150	0	1756	81	73	0.80	73	
A5	95	150	0	1756	101	80	0.88	79	
A5	256	150	248	1700	100	91	0.29	88	

TEST A6

1. Set discharge air temperature to 70 °F
2. Recirculate water at 70 °F or shut- off the water circulation
3. Set fume hood, supply and gen. exhaust to minimum flows
4. Set discharge air temperature at 55 °F
5. Set supply at maximum flow
6. Turn on room space heaters (2000 W)
7. Reset water temp at 140 through the radiant panel

Objective: Determine dynamic room thermal response due to sudden generation of internal load.

Table 4.5

Test Seq.	Time (min)	Measured Variables							
		$\dot{v}_{fh}$ (cfm)	$\dot{v}_{ex}$ (cfm)	$\dot{v}_{s}$ (cfm)	T_s (°F)	T_{rad} (°F)	P_s (w.c)	T_{st} (°F)	ΔP (w.c)
A6	0	200	0	0	73	71	0.27	73	
A6	16	52	0	1664	73	71	0.86	73	-
A6	213	1091	1942	2877	88	140	0.85	89	
A6	423	1100	2000	2857	72	127	0.86	77	

TEST A7

1. Set discharge air temperature to 70 °F
2. Recirculate water at 70 °F or shut- off the water circulation
3. Set fume hood, supply and general exhaust to maximum flows
4. Set discharge air temperature at 55 °F
5. Set supply to minimum flow
6. Set water temperature at 45 °F
7. Set discharge air temperature at 90 °F

Objective: Determine dynamic room thermal response due to sudden increase in room supply air temperature.

4.5 Test results

The results are presented in three different sub-sections. First, the steady state simulated results are compared with the experimental values. The next

sub-section compares the simulated and measured lab pressure responses obtained in test sequence A1. The final sub-section discusses the results obtained from test sequences A2 to A6, the corresponding simulated results, and includes discussion of the calibration of constants for thermostat model as described in section 4.3.

TABLE 4.6

Test Seq.	Time (min)	Measured Variables							
		$\dot{v}_{fh}$ (cfm)	$\dot{v}_{ex}$ (cfm)	$\dot{v}_s$ (cfm)	T_s (°F)	T_{rad} (°F)	P_s (w.c)	T_{st} (°F)	ΔP (w.c)
A7	0	2432	1279	1184	70	71	0.23	71	
A7	99	2432	2252	3044	68	70	0.81	71	-
A7	328	1082	2023	2931	51	63	0.87	59	
A7	337	1082	418	438	49	52	0.23	59	
A7	638	1245	2258	2254	82	52	0.94	66	
A7	761	1245	1106	1184	75	67	0.25		

4.5.1 Comparison of steady state results:

As a part of the validation process, the results obtained from the dynamic tests are compared with the simulated values under steady state conditions to ensure that the dynamic tests are sufficiently long to achieve steady state conditions. The steady state simulated results are obtained by ignoring the

time derivative terms in the models as well as by running the simulation for the same amount of time as the tests are conducted. The comparison of results are shown in Table 4.7.

Table 4.7

Validation of Steady State Conditions

Test seq.	v_{fh} (cfm)	v_s (cfm)	v_{gex} (cfm)	P_s**	T_s (°F)	T_w (°F)	*Delp* (*w.g*)	***Delp*** (***w.g***)	*T* (*°F*)	**T** (**°F**)
D1	1000	394	1300	0.23	70	70	*0.52*	0.50	72	70
D1	200	1767	0	0.84	70	70	*-0.36*	-0.368	71	70
B.1	1100	3000	2000	0.87	53	47	*.01*	.004	57	54.1
D.11	1000	300	1300	0.23	53	65	*0.55*	0.54	67	67
D.21	150	1700	238	0.89	100	92	*-.42*	-0.446	89	98
E.1	1100	2850	2000	0.86	72	126	*0.0*	.00166	76	76
E.13	1100	3000	2000	0.87	50	52	*0.0*	.00370	57	52

P_{ad}=408.0 inches of water

T_{ad}=70 Deg. F

** P_s is in gauge values with respect to P_{ad} (inches of water).

The boldface columns represent simulated values while the rest of the table are measured values. The measured steady state conditions are fed into the steady state room emulator models to determine the simulated values of room temperature, T, and pressure differential, Δp. The results indicate good agreement between simulated and measured steady state pressure differential,P_{ad}-P, and temperature,T, except for the temperature values for test sequence A5. This may be caused by the fact that sufficient time was not allowed during the experiment for steady state to be achieved. This is clear from Figure 4.20 which shows that the radiant wall temperature was still

increasing when the experiment was terminated. Such truncation can lead to a large error since the radiant wall heating effect to the room air may have a large thermal lag. Failure to deduce the correct steady state condition from the experimental results may also explain the discrepancy in temperature for test sequence A7.

The pressure values match very well under all test sequences. Any kind of time lag in the case of the pressure is absent due to the fast dynamics of the room pressure.

4.5.2 Comparison of dynamic lab pressure response.

Figure 4.8 presents the profiles of the flow rates of the different lab air streams used to obtain the dynamic lab pressure response. Initially, the lab general exhaust and fume hoods are kept open to achieve maximum lab exhaust flow while the supply flow is kept at a minimum. This condition will lower the lab pressure which means maximum positive pressure differential across the lab envelope since by definition, $\Delta p = P_{ad} - p$. Careful observation reveals that the measured values show a step trend as the digital control system digitizes the analog signals from the flow sensors and the pressure transducers. This creates a small error in the value of the measured results.

Figure 4.9 shows that the measured and simulated pressure differential agree remarkably well. The simulated values not only agrees well with the measured values but also tracks the change in the sign of Δp in going from positive to negative. The agreement further validates the selection of the

leakage model using power law. The time domain for dynamic pressure experiment usually takes only few minutes since the steady state is reached quickly due the fast dynamics of room pressure.

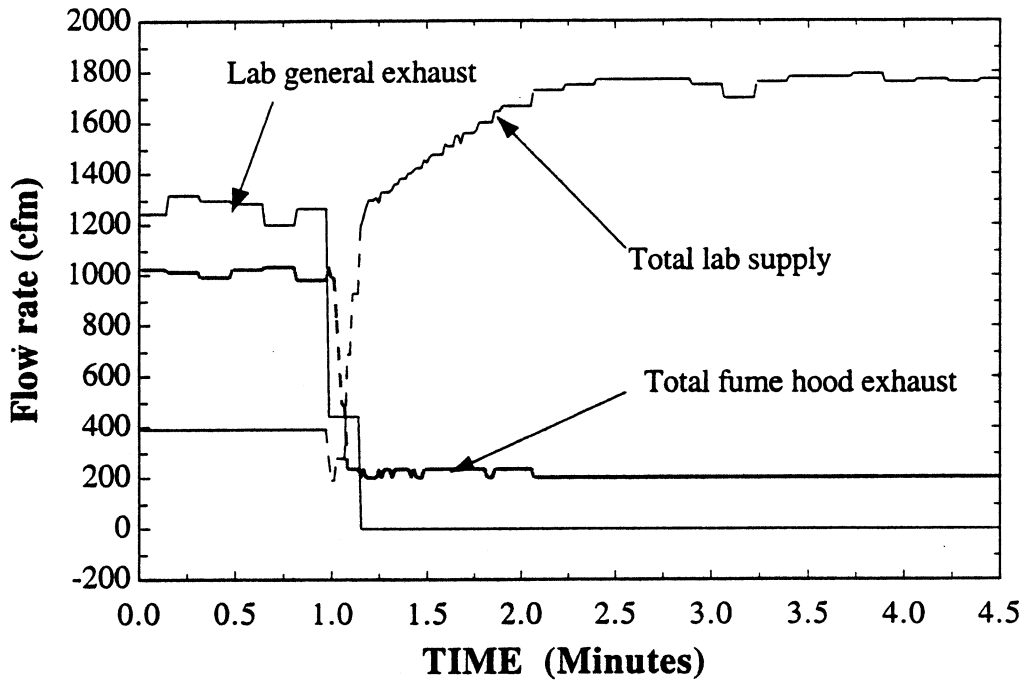

Figure 4.8: Profiles of lab flow rates for pressure response

4.5.3 Determination of thermostat constants:

The room temperatures during the experiments were measured by a thermostat mounted on a panel wall. However, the simulation model calculates the room temperature assuming that the room air is well mixed. Therefore, a model was necessary to represent a thermostat and compare the simulated thermostat temperature with the measured values.

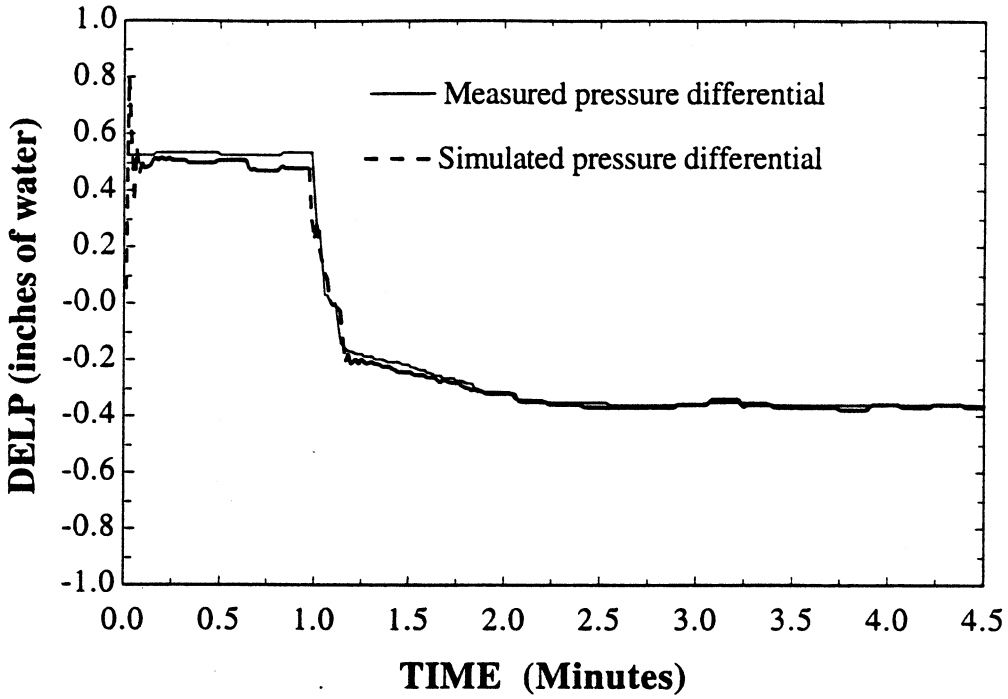

Figure 4.9: Response of room pressure differential

A simple lumped capacitance model coupling the thermostat with the panel wall and the room air temperatures was selected as shown in equation 4.1 and repeated below. The thermostat constants $C1_{st}$ and $C2_{st}$ are determined using measured temperatures in the test sequence, A5. The absolute error between the measured and simulated thermostat temperature using the complete room model and the thermostat model was minimized.

$$\frac{dT_{st}}{dt} = C1_{st}(T_{pw} - T_{st}) - C2_{st}(T_{st} - T) \qquad (4.1)$$

The total error, which is the sum of errors from each sample, is minimized by varying $C1_{st}$ and $C2_{st}$. Once the optimum values are obtained, neighborhood values are used to calculate the errors and compared with the

minimum error to ensure that the global optimum is achieved. The optimum values of $C1_{st}$ and $C2_{st}$ are then used in the other test sequences to verify that those values also yield close to minimum total errors for all test sequences. The results are shown in Table 4.2. For each test sequence a variety of values were chosen. The best values are shown in boldface. An average error of 2.0 ^{o}F between the simulated and measured thermostat temperatures for a $C1_{st}$ of 0.1 $(\frac{^{o}F}{min})$ and $C2_{st}$ of 0.12 $(\frac{^{o}F}{min})$, is encouraging.

Assuming that $C1_{st}$ and $C2_{st}$ are equal with experimental error, Equation 4.1 can be re-written as,

$$\tau_{st}\frac{dT_{st}}{dt} = (T_{pw} - T_{st}) - (T_{st} - T) \qquad (4.2)$$

The term τ_{st} is referred as a time constant of a first order linear system in control theory. Since τ_{st} is the reciprocal of $C1_{st}$, a range of 0.1-0.12 means a time constant of about 10 minutes. The time constant depends on many factors including air flow rate around the thermostat, radiation effects and the local shielding around the thermostat enclosure. Therefore, the range of thermostat time constant vary widely and typically within 5-15 minutes (Henderson 1992; Landis & Gyr Powers 1995).

The test sequence A5 is selected based on the test conditions of both high and low lab flow rates and maximum radiant wall temperature. The test ran for a long time, almost 7 hours. It is believed that under such test conditions

covering a wide range, the calibration of thermostat coefficients will yield good yet robust results.

Table 4.8

Calibration of thermostat constants

Test sequences	Coefficients		Sum of Abs. error	Average of Abs. error
	Cst1	***Cst2***		
A5/E1	0.004	0.12	836	1.978
A5/E1	0.02	0.12	792	1.873
A5/E1	**0.1**	**0.12**	**668.58**	**1.581**
A5/E1	0.2	0.12	753.137	1.78
A5/E1	0.004	0.0833	818.939	1.936
A5/E1	0.1	0.2	726.075	1.716
A5/E1	0.1	0.1	683.33	1.615
A5/E1	0.12	0.12	670	1.586
A2/B1	0.004	0.0833	172.726	0.754
A2/B1	**0.1**	**0.12**	**171.098**	**0.747**
A3/D11	0.004	0.0833	931.02	3.013
A3/D11	**0.1**	**0.12**	**679.342**	**2.257**
A4/D21	0.004	0.0833	1236.108	4.847
A4/D21	**0.1**	**0.12**	**808.771**	**3.172**
A6/E13	0.004	0.0833	1943.434	2.554
A6/E13	**0.1**	**0.12**	**1297.539**	**1.705**

4.5.4 Validation of thermal test results:

In order to compare the measured room thermal response with the simulated results, simplifications are made in the simulation model by ignoring the pressure derivative terms with respect to the temperature derivative terms. As a result, equations 3.6 and 3.11 representing the mass and energy conservation terms are re-written as follows:

Conservation of mass:

$$\frac{P_S \dot{v}_S}{RT_S} + \frac{P_{ad} \dot{v}_{ad}}{RT_{ad}} - \frac{P \dot{v}_e}{R} = -\frac{VP}{T^2}\frac{dT}{dt} \tag{4.3}$$

Conservation of energy:

$$\frac{P_S \dot{v}_S}{R} c_p + \frac{P_{ad} \dot{v}_{ad}}{R} c_p - \frac{P \dot{v}_e}{R} c_p + \dot{q}_{gen} + \dot{q}_{tr} = 0 \tag{4.4}$$

The simplifications essentially decouple the pressure changes from the temperature relations. The decoupling is justified since the pressure response is much faster than the temperature response and therefore, with a sample time of 1 minute, the pressure change will have no impact on the temperature response. However, actual pressure values are used in both equations 4.3 and 4.4 to predict the temperature by considering the effect of pressure on the temperature by treating the pressure response to be a steady state value within a minute. This simplification enhances the solution process and helps reduce computation time. The solution diverges when the pressure dynamics are considered over a large transient time (e.g. 1 minute) whereas the room pressure, in reality, changes every second. For test sequence A1 and A2, a sample time of 1 second is used to capture pressure dynamics.

The decoupling has virtually no impact on the overall goal of investigating temperature control strategies for different control sequences since the actual control system has separate loops to respond to pressure and thermal sequences. For example, the supply flow rate always responds to the room pressure loop, the reheat valve modulates to meet heating needs, and the general exhaust flow rate varies to meet the cooling requirement.

For each test sequence as described in section 4.4, four categories of plots are shown to compare the simulated results with the measured values. The first category shows the profiles of different lab flows measured during the test. The flow rates can be considered as the major process variables whose setpoints are changed from one value to another. The room temperatures are then trended as a result of such change.

The second plot category shows the simulated surface temperature of various lab envelope components and the room air temperature. The simulation is performed using the actual measured flow rates and other measured boundary conditions i.e. supply air temperature, radiant wall temperature, rate of internal heat generation and supply duct static pressure as input to the simulation model. The simulation model assumes the adjacent space temperature to be 70 ^{o}F and the pressure to be atmospheric. Measured temperatures are shown in the third category of plots which also includes the simulated thermostat temperature. Finally, normalized measured and simulated thermostat temperatures responses are shown in the fourth plot category. The normalized temperatures are computed as follows:

$$NT_{st} = \frac{T_{st} - Ti_{st}}{T\,max_{st} - T\,min_{st}} \tag{4.5}$$

Essentially, the normalized thermostat temperature, NT_{st}, is the difference between the thermostat temperature and initial value divided by range (difference between the maximum and minimum values). The normalized plot is a better comparison of the dynamic trend between the measured and the simulated values. These trends are a true indicator of how well the simulation model agrees with the measured data as opposed to the specific values as shown in the third category of plots. The effects of measurement uncertainty, modeling errors and assumptions, and the thermostat calibration constants influence the specific values. The normalization process minimizes such effects and captures the average dynamic behavior of the process variables i.e. thermostat temperature.

The following is a summary of observed results for each test sequence. The sequences described here were carried out to calibrate and determine the operating range of the newly built building control system testing laboratory. Therefore, the sequences are unique and may not represent the normal HVAC system operation. On the other hand, the test data are appropriate to validate the models considering the wide operating ranges and the variety of the sequences.

Test sequence A3:

The objective in this test sequence is to cool the space as much as possible in order to determine the maximum space heating load. With this objective, both the fume hoods and the general exhaust dampers are fully opened while

the maximum supply air is introduced to the space at 55 ^{o}F. The radiant wall temperature is kept at minimum of around 50 ^{o}F. As a result, the measured room thermostat temperature falls below 60 ^{o}F as shown in Figure 4.12. Although, the lab flow rates increase at around 25 minutes (Figure 4.10), the lab supply air temperature does not fall to about 55 ^{o}F until about 135 minutes, as shown in Figure 4.12. The cause of such delay is found to be an error with the AHU cooling coil water inlet temperature setpoint which was erroneously set to be 60 ^{o}F instead of the desired temperature of 45 ^{o}F. This same plot shows that the radiant wall temperature reduces to about 50 ^{o}F at about 45 minutes.

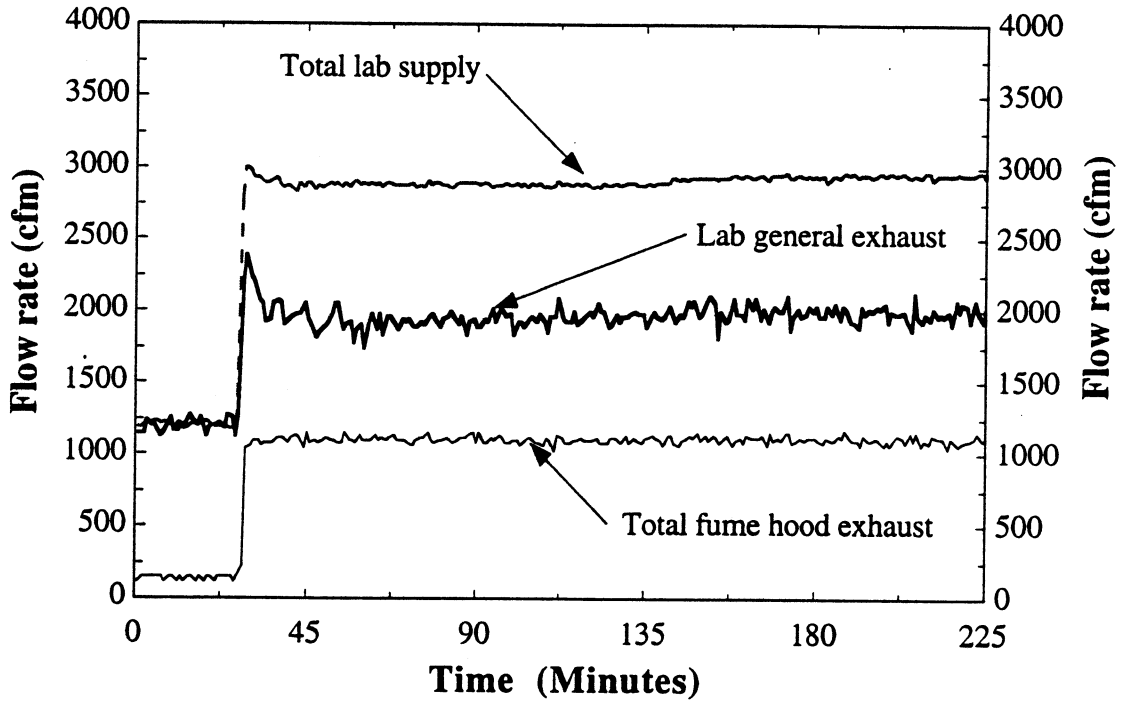

Figure 4.10: Profiles of lab flows: Test sequence: A3

The room thermostat temperatures, both measured and simulated, fall gradually until 135 minutes when the supply air temperature drops to about

55 ^{o}F (Figure 4.12). This clearly indicates that the effect of radiant wall temperature on the measured temperature is slow while the supply air temperature quickly impacts the measured temperature, especially when the room air flow rate is very high. The room thermostat may have responded even quicker as the convective heat flow increases with the higher room air flow.

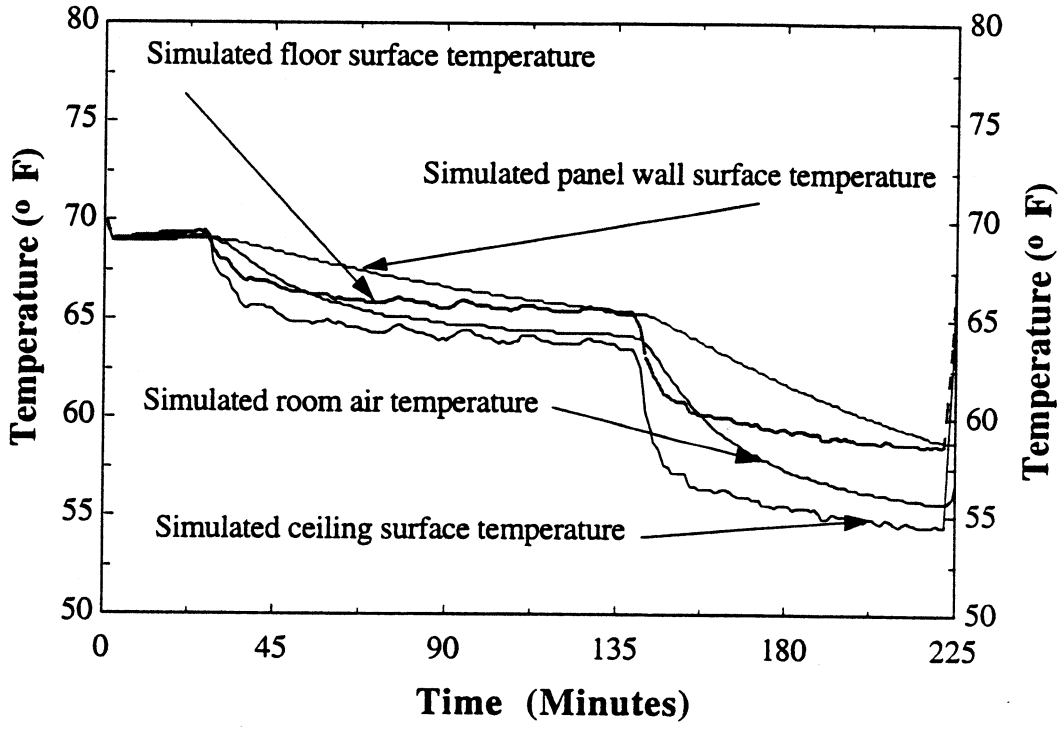

Figure 4.11: Simulated temperatures: Test sequence: A3

The simulated profiles in Figure 4.11 show the same trend as explained above and the simulated room air temperature is found to be nicely bounded by the envelope temperatures. The normalized plots in Figure 4.13 show a remarkable similarity in trends between the measured and simulated thermostat temperature. Since the thermostat maximum and minimum temperatures also happen to be the initial and the final values in this test

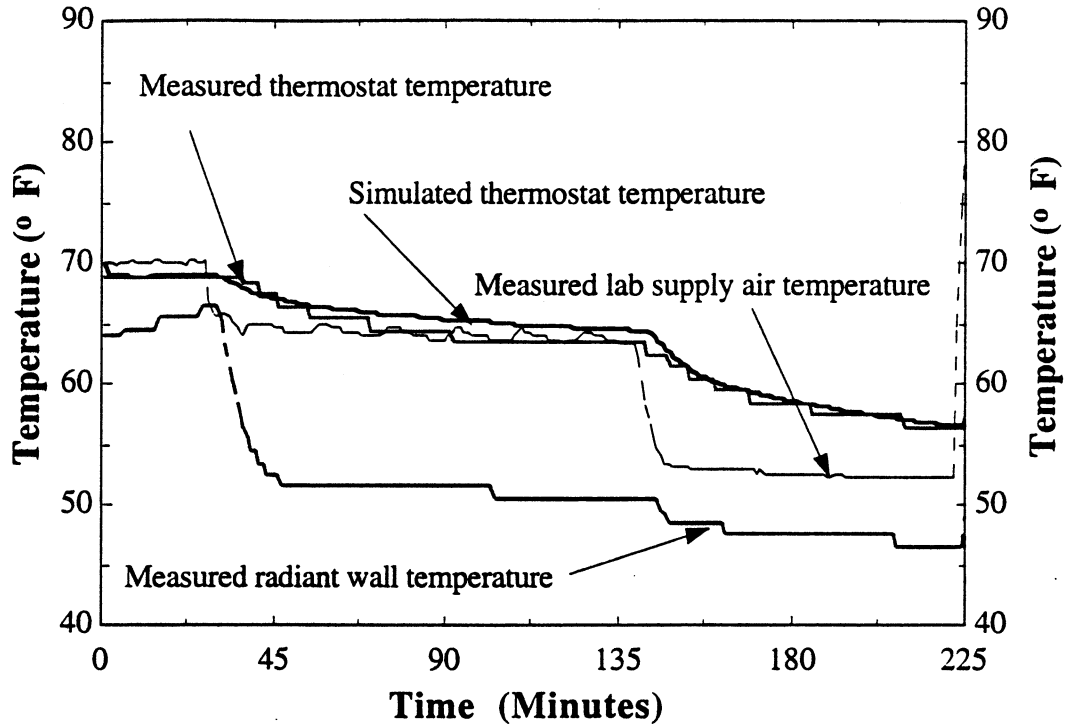

Figure 4.12: Measured temperatures: Test sequence: A3

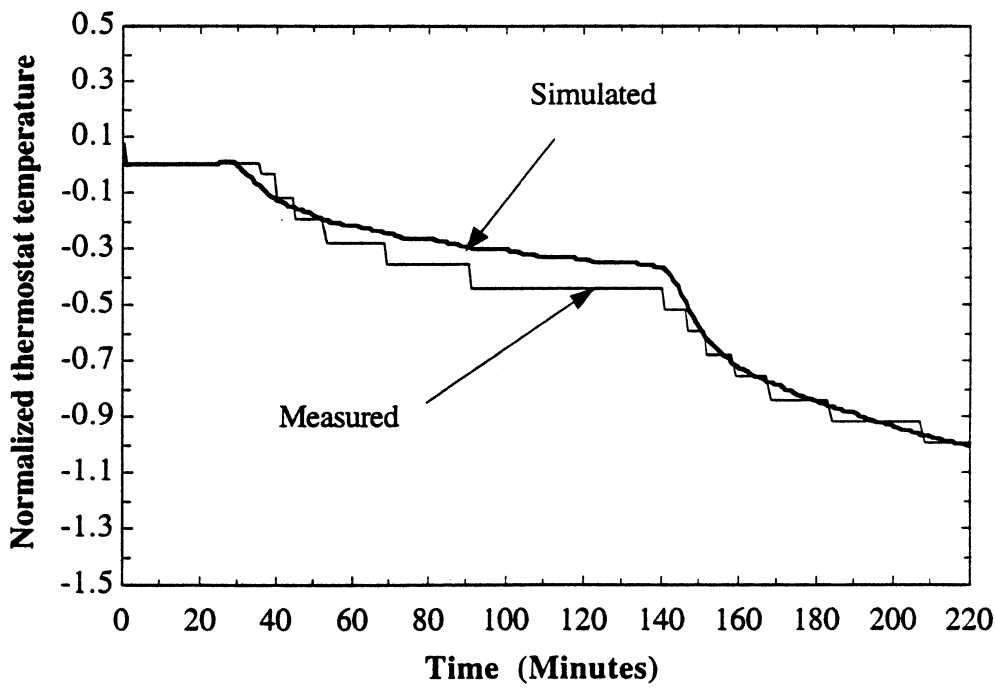

Figure 4.13: Normalized temperatures: Test sequence: A3

sequence, the normalized simulated and measured values agree with each other at both ends of the sequence. Most important, the shape of the simulated and measured temperature responses with time agree. This establishes that the room and thermostat dynamics are adequately captured by the models.

Test sequence A4:

In this test sequence, the supply and exhaust flows are initially maintained at a maximum rate followed by decreasing the supply flow rate to minimum at about 180 minutes while the general and fume hood exhaust remain unchanged. The flow profiles are shown in Figure 4.14. The supply air temperature is dropped from 70 ^{o}F to 50 ^{o}F at about 65 minutes.

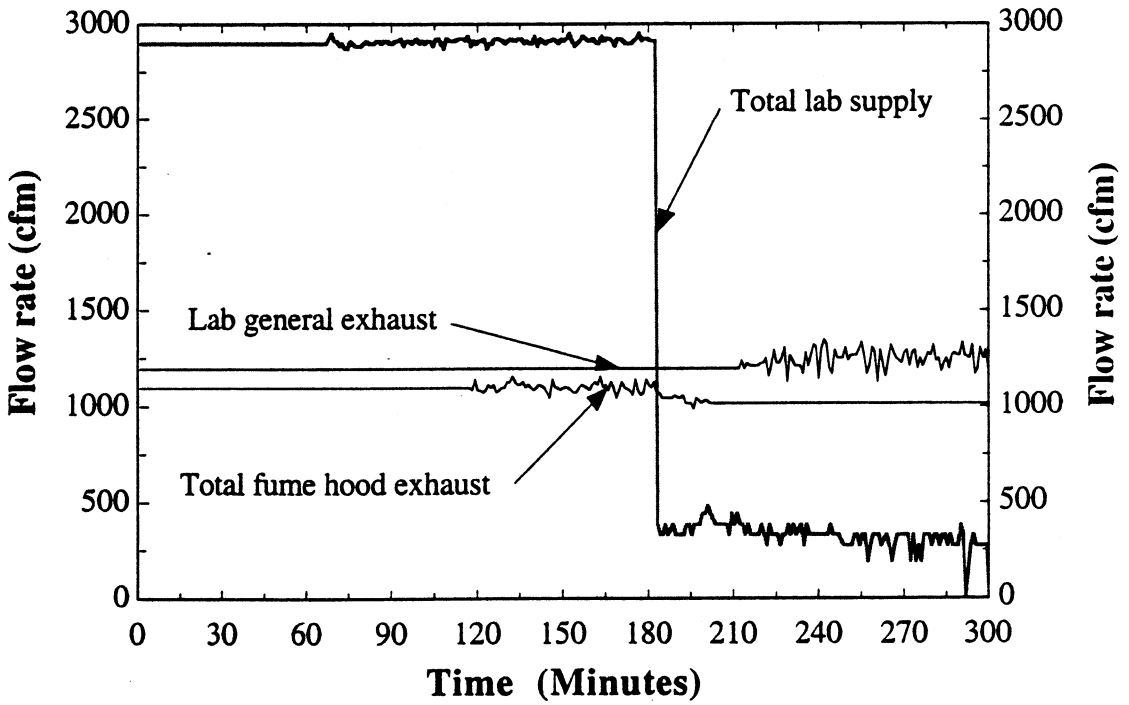

Figure 4.14: Profiles of lab flows: Test sequence: A4

Although the supply air temperature setpoint is kept at 55 ^{o}F, the actual temperature undershoots to about 50 ^{o}F around 65 minutes and gradually comes back to the setpoint (Figure 4.15). The undershoot was most likely caused by poor tuning of the control loop. The radiant wall temperature gradually falls to about 55 ^{o}F from an initial temperature of 70 ^{o}F and then slowly backs up again to the initial temperature. The measured temperature profiles are shown in Figure 4.16.

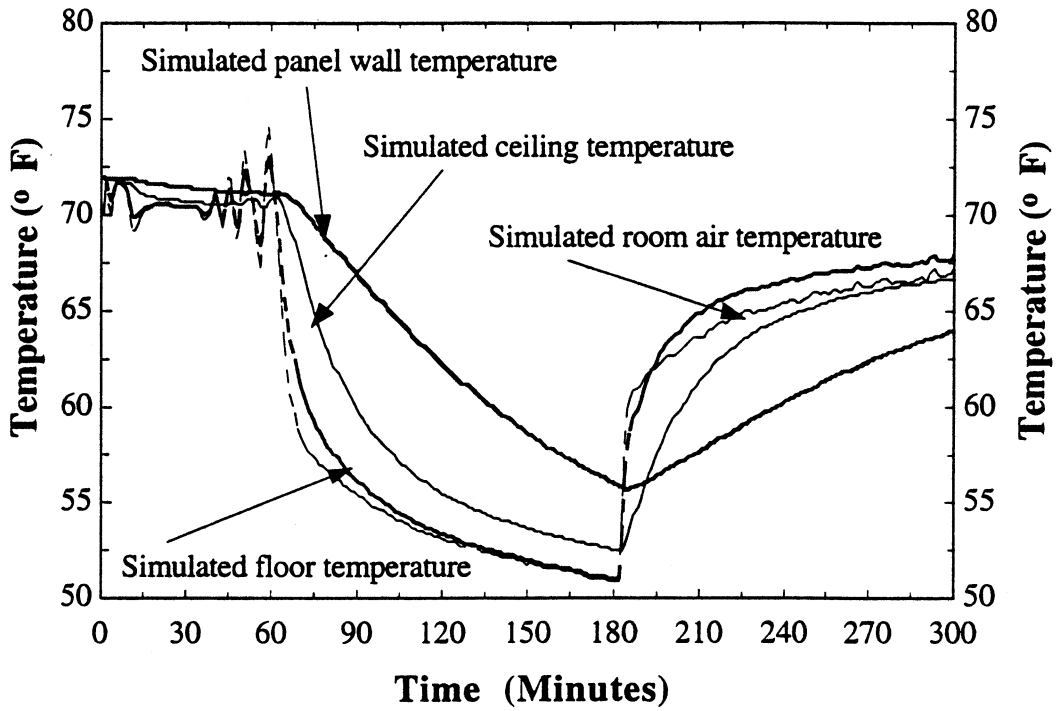

Figure 4.15: Simulated temperatures: Test sequence: A4

The goal in this test sequence is to cycle the flows and the measured temperatures within the cooling operating range of 55 to 70 ^{o}F and then evaluate the measured response of the room thermostat with simulated values. The simulated temperature profiles of various components of lab envelope and the room air temperature are shown in Figure 4.15. The room air temperature is bounded by the envelope temperatures and follows the

cycle of lab supply flow rate and the air temperature. Initially, the room temperature falls due to the decrease in the supply air temperature and higher flow rate and then increases due to the reduced supply air flow rate and the increased supply temperature.

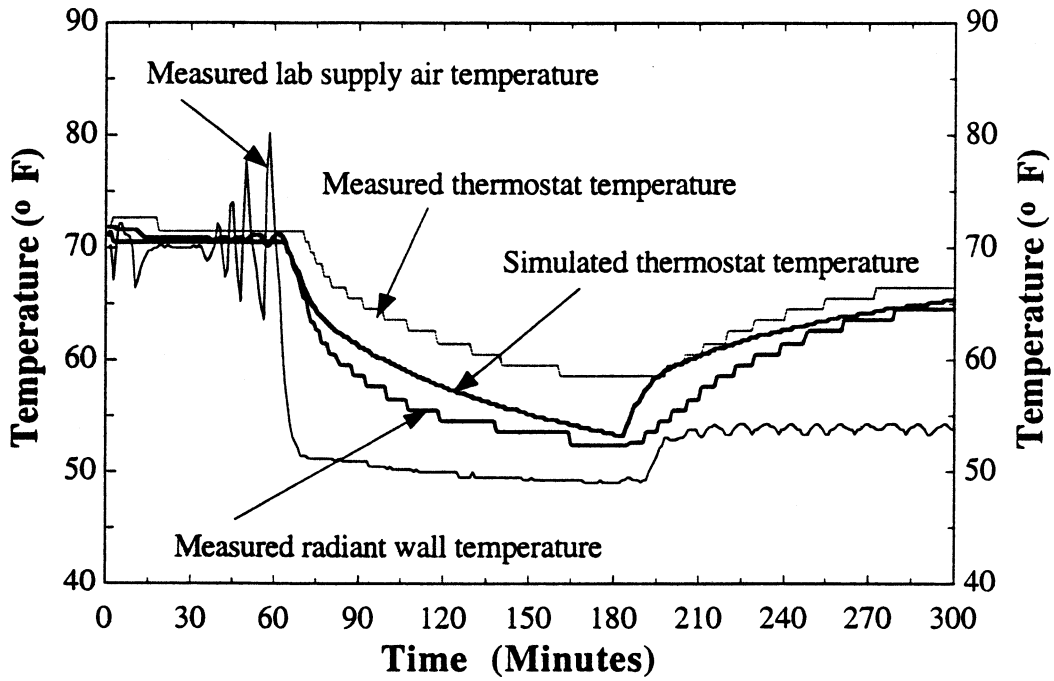

Figure 4.16: Measured temperatures: Test sequence: A4

The simulated panel wall temperature shows more thermal lag compared to the ceiling and floor due to its relatively heavy mass. The simulated thermostat temperature closely follows to the measured thermostat as shown in Figure 4.16. The normalized temperature plots again capture the agreement between the simulated and measured thermostat as illustrated in Figure 4.17.

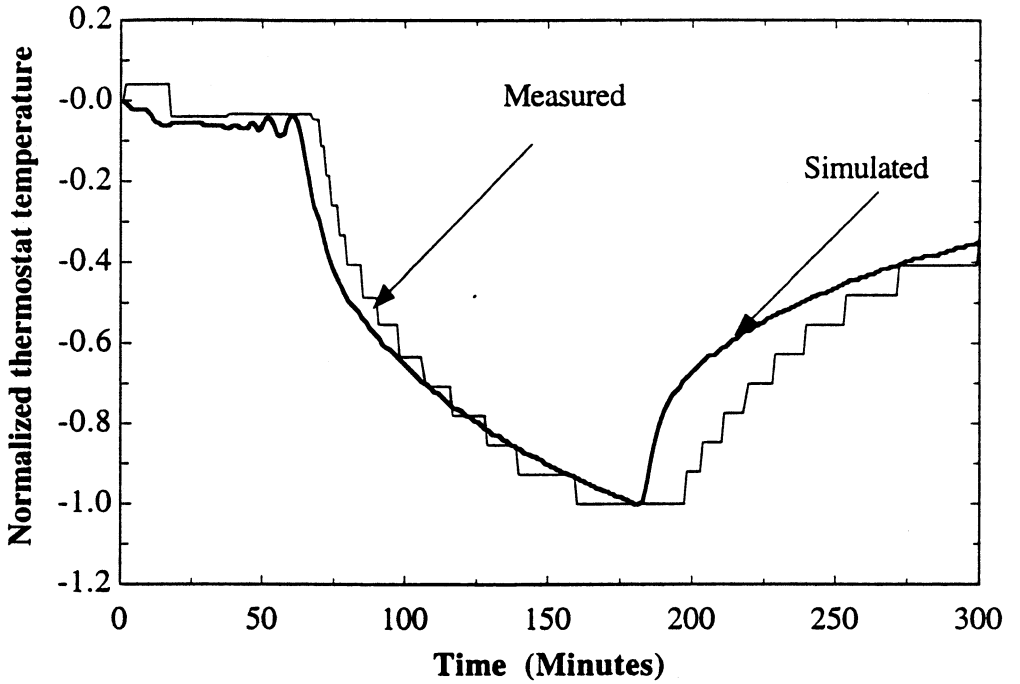

Figure 4.17: Measured temperatures: Test sequence: A4

Test sequence A5:

The objective here is just the opposite of test sequence A3. Instead of a heating load, the focus is to determine the maximum space cooling load. The supply flow rate in this sequence is maintained at maximum and both the general and fume hood flows are at minimum levels as indicated in Figure 4.18. The erratic plot of fume hood exhaust flow is a result of overall inaccuracy in measuring low flow rate. The supply air temperature is maintained at a maximum value of 100 ^{o}F while the radiant panel temperature is slowly increased starting at 75 minutes to 90 ^{o}F as shown in Figure 4.20.

The plots in Figure 4.19 show that the simulated room air and floor temperatures are almost identical, the ceiling temperature lags a little, and the panel wall temperature lags considerably.

The initial oscillation in supply air temperature, as shown in Figure 4.20 is due to poor tuning of the supply air temperature control loop. However, after necessary correction at 75 minutes, the control loop provided stable control. Comparing the simulated and measured thermostat temperatures in Figure 4.20, a divergence between the absolute values can be noted.

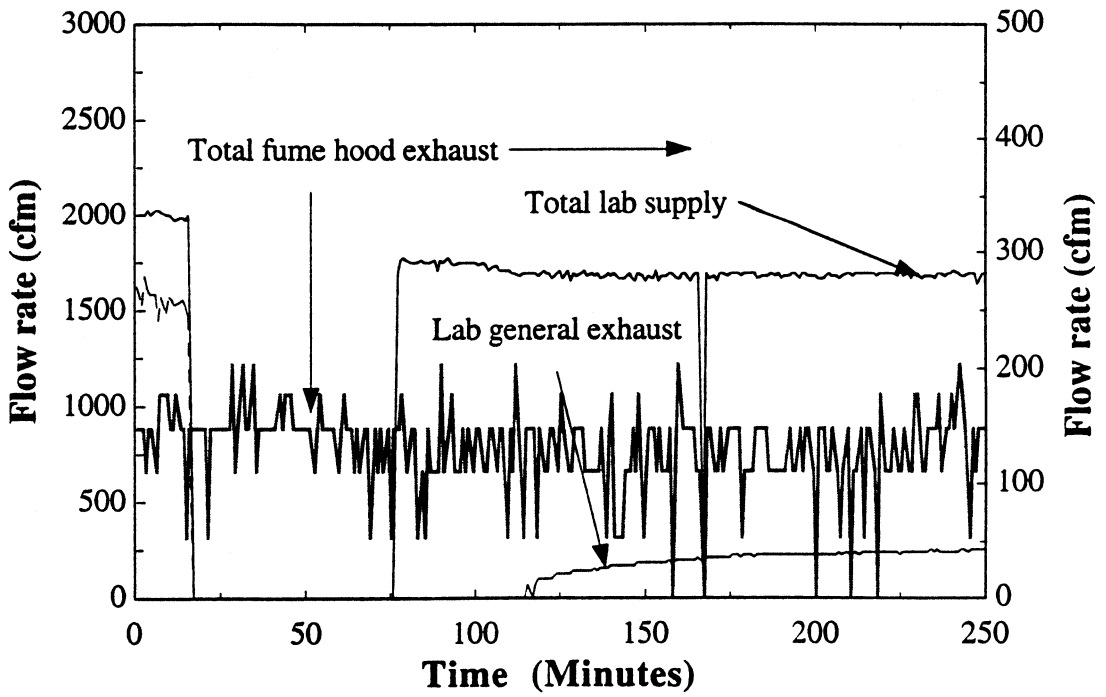

Figure 4.18: Profiles of lab flows. Test sequence: A5

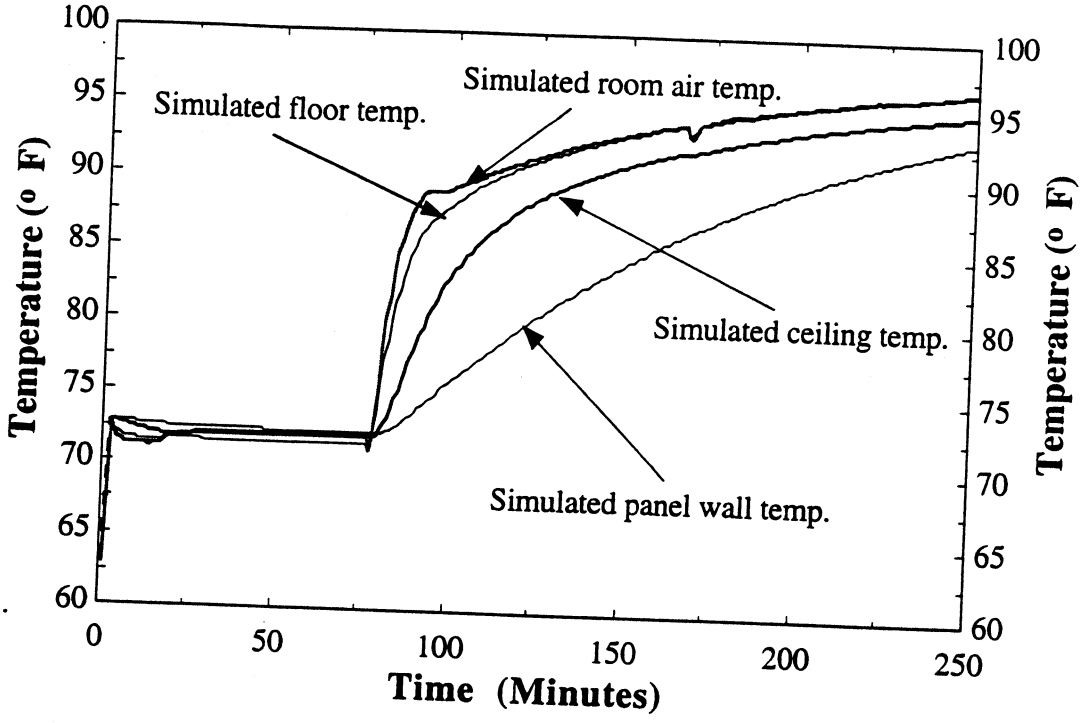

Figure 4.19: Simulated temperatures. Test sequence: A5

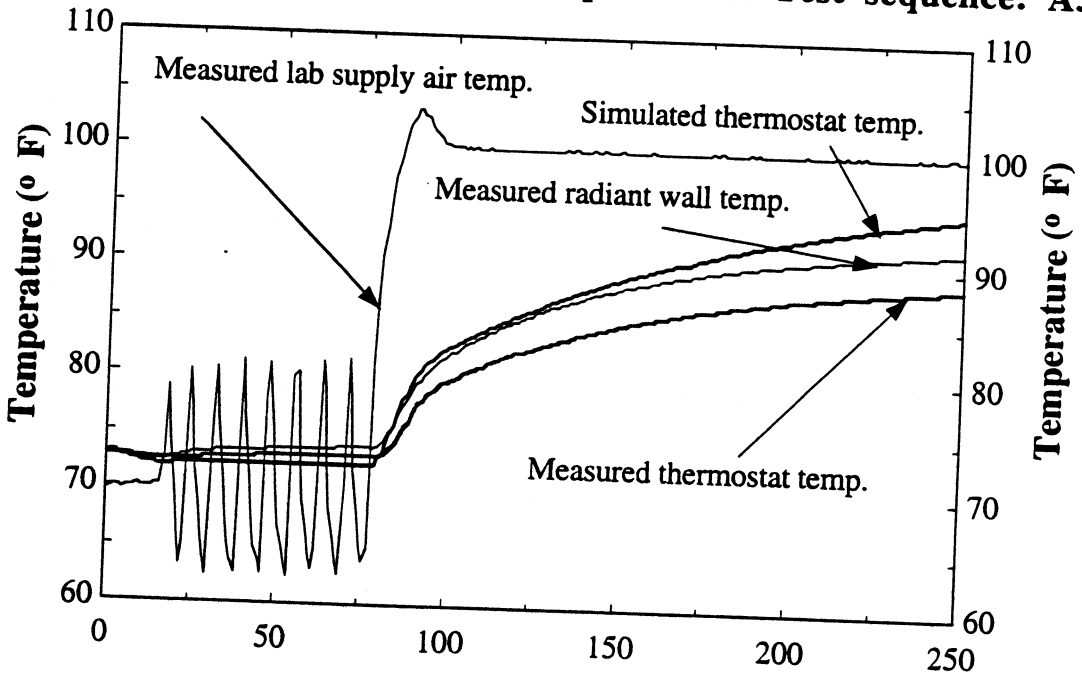

Figure 4.20: Measured temperatures. Test sequence: A5

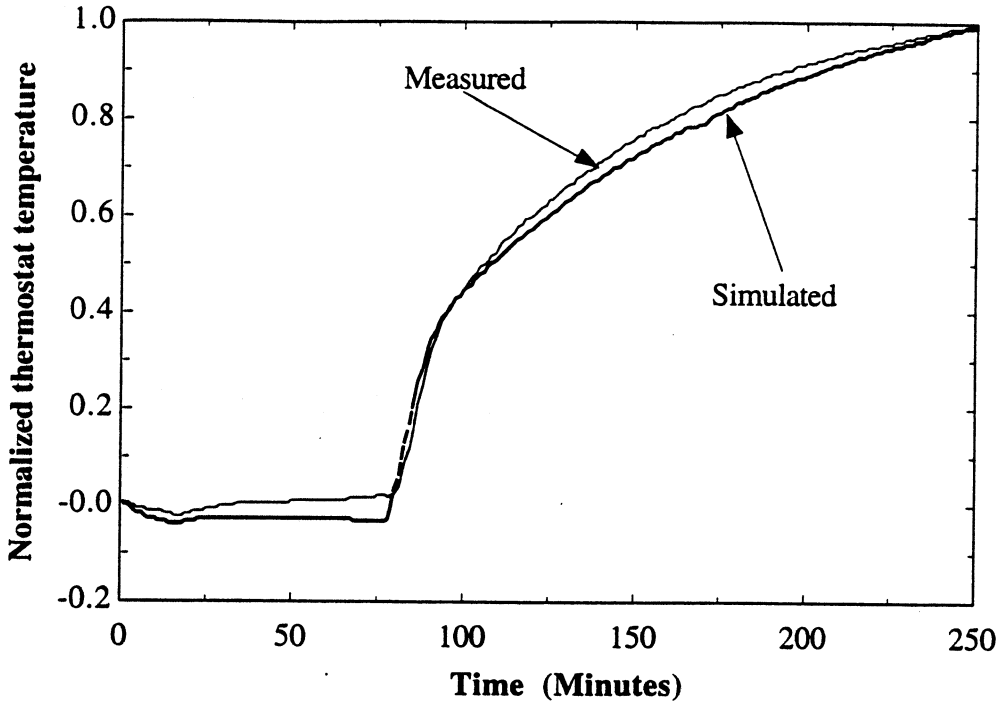

Figure 4.21: Normalized temperatures. Test sequence: A5

However, as shown in Figure 4.21, excellent agreement is obtained between the normalized simulated and the measured thermostat temperatures. These are essentially similar dynamic trends.

Test sequence: A6

The sequence here is the opposite of the test sequence A4. Figure 4.22 shows that the supply flow is increased to maximum at 215 minutes from initial condition while the exhaust, both fume hoods and the general, are increased from minimum to the maximum rate. The supply air temperature is cycled in the heating mode between 70 ^{o}F and 87 ^{o}F while the radiant wall temperature is maintained at the maximum setting of 140 ^{o}F and then decreased to 130 ^{o}F as indicated in Figure 4.24.

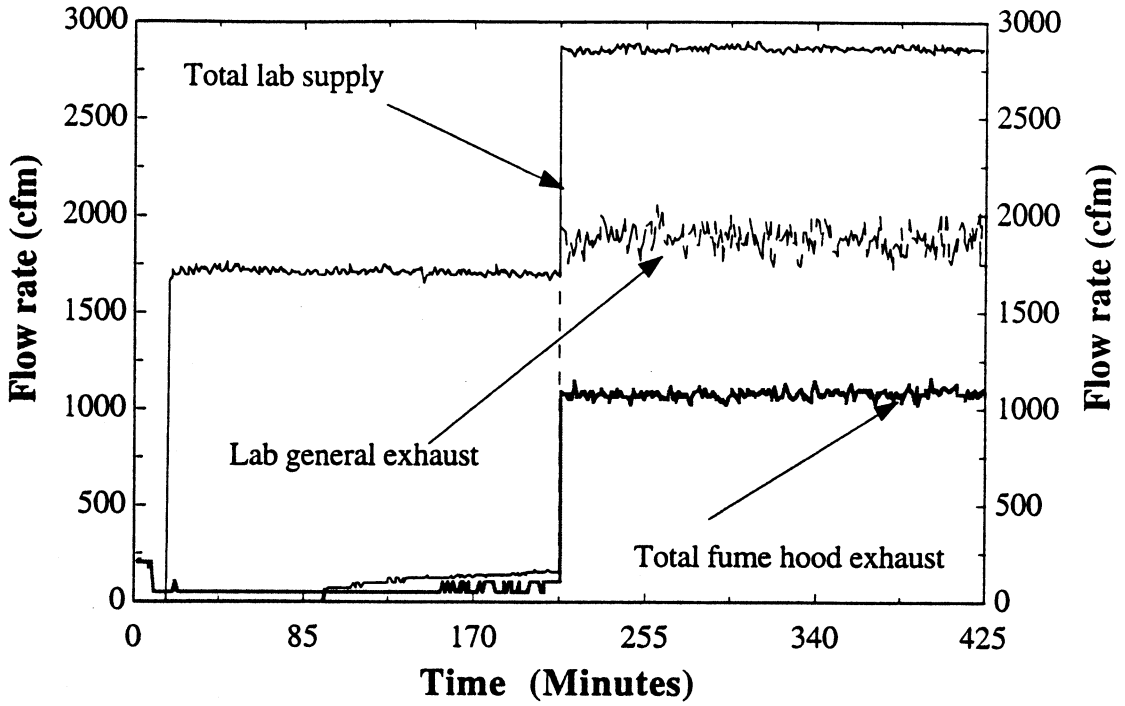

Figure 4.22: Profiles of lab flows: Test sequence: A6

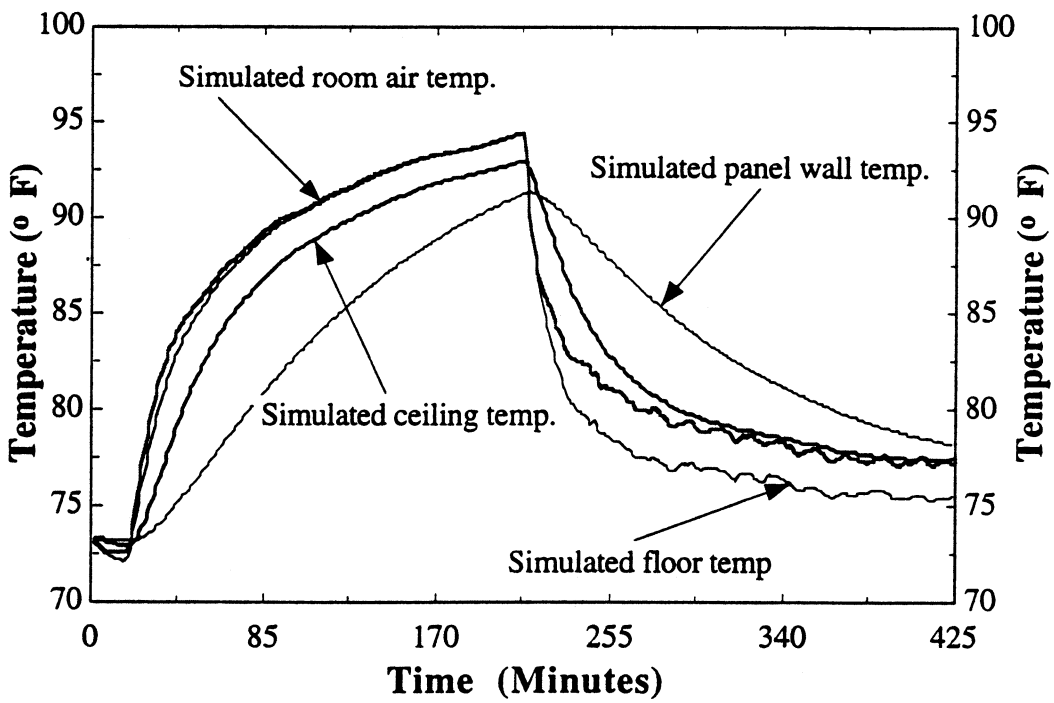

Figure 4.23: Simulated temperatures: Test sequence: A6

The simulated temperature profiles are shown in Figure 4.23. The lag characteristics of the panel wall are clear as compared to the other lab envelope components i.e. ceiling and floor. Both floor and ceiling temperatures follow the room air temperature closely as the room is heated while the floor temperature reduces rapidly following the measured supply air decrease. This behavior is expected since the metal floor with carpeting does not have significant thermal storage.

Comparison between the measured and simulated thermostat temperatures shows good agreement in terms of both absolute and normalized values in Figures 4.24 and 4.25 respectively. In Figure 4.24, the simulated temperature overshoots the measured values but tracks very well in the normalized plot in Figure 4.25.

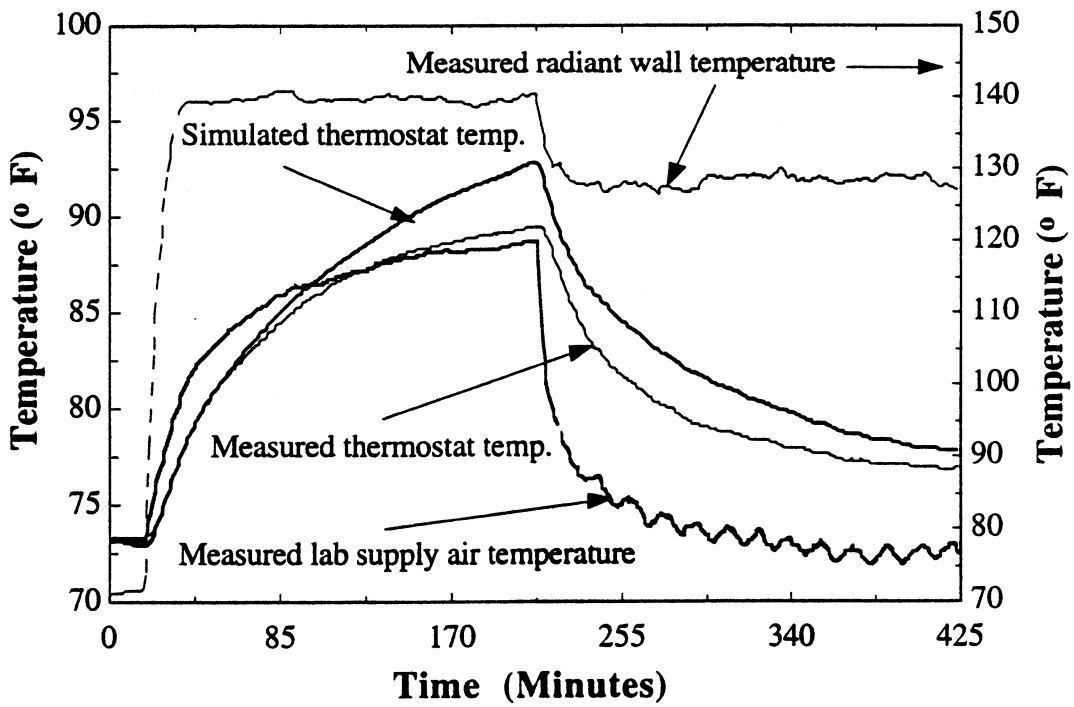

Figure 4.24: Measured temperatures: Test sequence: A6

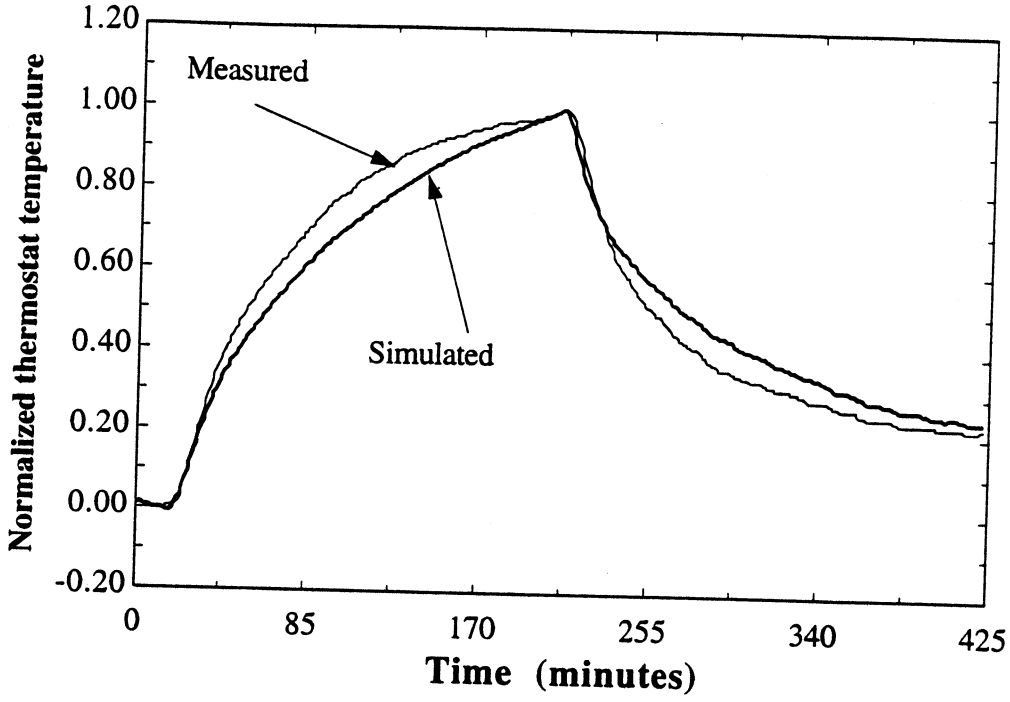

Figure 4.25: Normalized temperatures: Test sequence: A6

The measured temperature plots in Figure 4.24 also show that the measured thermostat tracks the supply very well in the room heating mode but lags considerably in the cooling mode although the supply air flow rate remains high. As the room and the envelopes heat up, it takes longer to cool the space due to the storage effects of walls and ceiling.

Test sequence A7:

A total of more than twelve hours of test data are collected in this sequence to capture the long term dynamics of room response due to the cycling of lab flows and supply air temperature. The flow rates are cycled from maximum to minimum to the maximum conditions as shown in Figure 4.26. The supply air temperature is decreased from an initial value of 70 ^{o}F to around 55 ^{o}F

at 225 minutes and then suddenly increased to about 100 ^{o}F at 640 minutes. The other process variable, the radiant panel temperature, is cycled from 70 ^{o}F to 55 ^{o}F to 70 ^{o}F. The objective in this sequence is to see how well the simulation can capture the long term dynamics.

The plots of flow are shown in Figure 4.26 while the plots of temperature are shown in Figure 4.28. The smooth plots signify that the controller was well tuned before the test started and maintained all the measured variables, i.e. flows and the temperatures, within a close range of the respective setpoints.

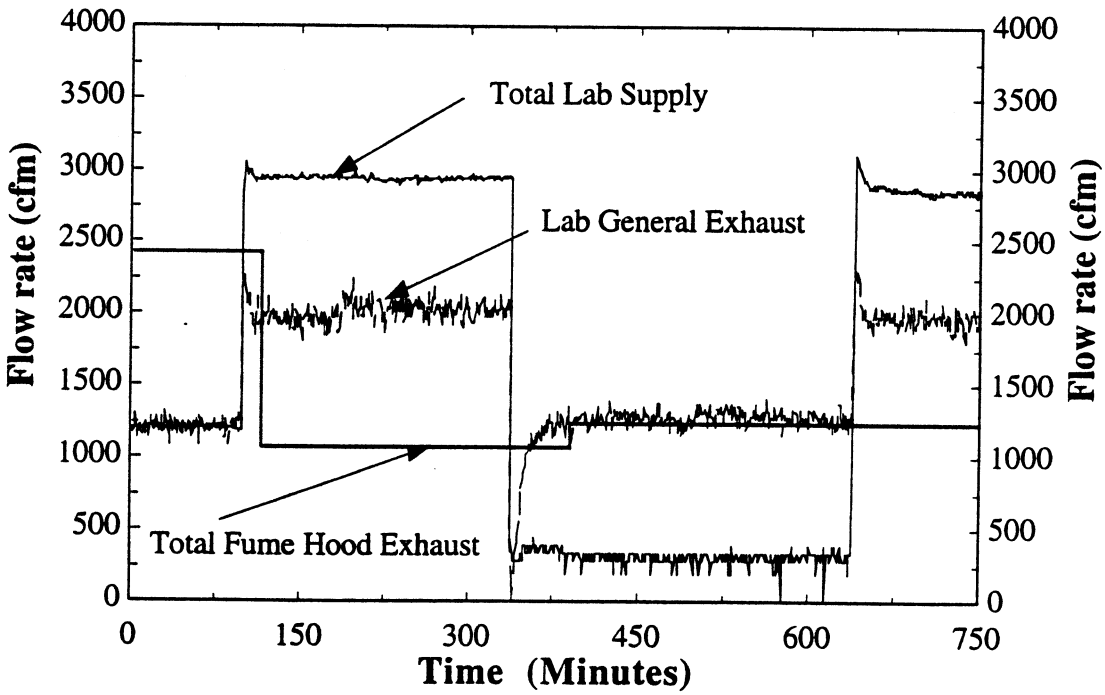

Figure 4.26: Profiles of lab flows. Test sequence: A7

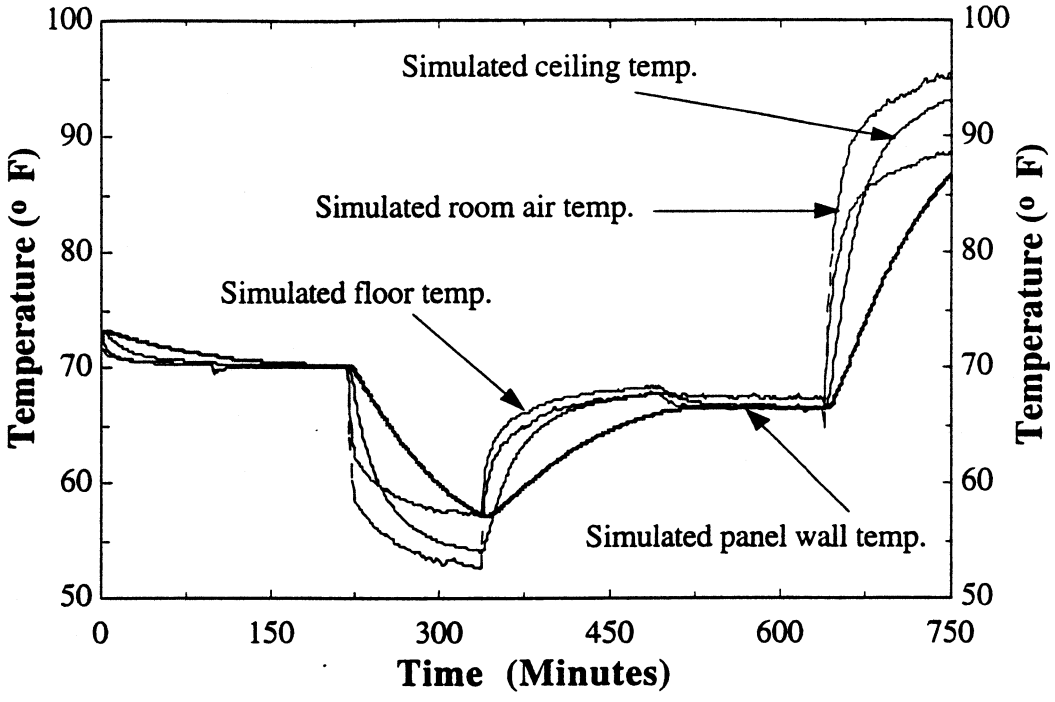

Figure 4.27: Simulated temperatures. Test sequence: A7

The simulated temperature plots in Figure 4.27 show similar characteristics as noticed in the earlier tests in terms of trends and lag. The panel wall exhibit a maximum lag followed by the ceiling and floor with respect to the room temperature.

Figure 4.28 compares the simulated and measured thermostat temperatures while Figure 4.29 presents the normalized plot. The agreement in terms of both the absolute and the normalized values is good. The close agreement between the measured and the simulated temperature in terms of absolute values over a long range is expected due to a well tuned controller. This test partly verifies the accuracy of the models as an emulator.

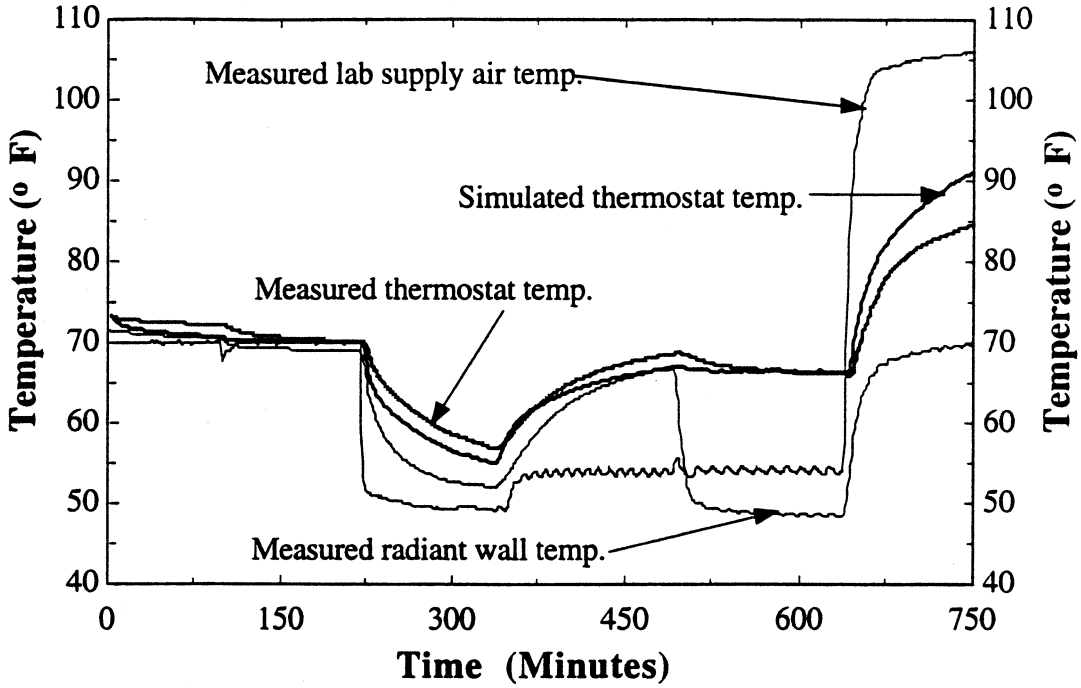

Figure 4.28: Measured temperatures. Test sequence: A7

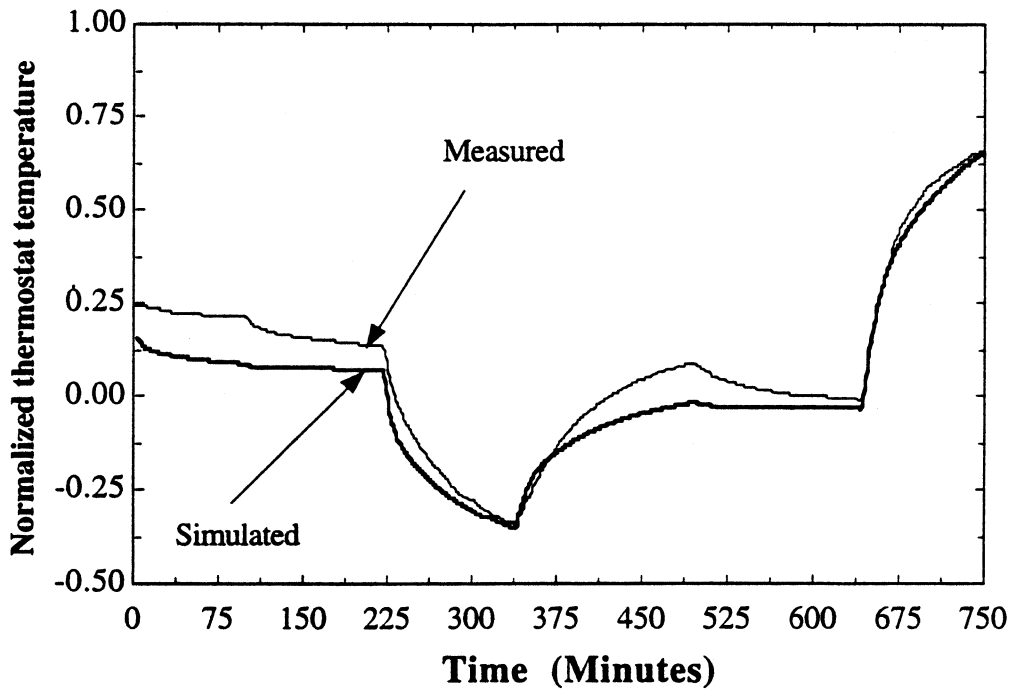

Figure 4.29: Normalized temperatures. Test sequence: A7

4.7: Summary

A series of test sequences performed over short term for room pressurization and long term for thermal response have been presented in this chapter. The simulated and actual test results in terms of room pressure and thermal responses have been compared. Considering the measurement uncertainties, use of Building Automation System for data acquisition, and inaccuracies with the simple models, the agreement is excellent. Most encouraging is the ability of the models to capture both short and long term trends. This is useful if the room emulator has to duplicate the actual system response within allowable limits. The goal of the emulator is not to generate accurate absolute values, but to exhibit similar trends so that different control strategies can be emulated and compared using the room emulator to model an actual laboratory.

Chapter 5

Development of Proposed Control Strategy

5.1 Overview:

At the end of the literature survey in Chapter 2, reasons were given to support using a combined feedforward and feedback control method for laboratory HVAC systems. Although labs are specifically focused on, the proposed control topology and results will be valid for cleanroom applications where pressure is kept higher than the adjacent space to prevent any contaminants flow from outside. In order to reduce complexity, the lab humidity control is not considered. The choice of a combined approach is based on performance, ease of implementation, cost-effectiveness and added customer value criteria. This chapter expands and elaborates on the concept of a combined approach. The feedback control block is discussed first, and followed by a discussion of the feedforward and combined approaches.

For feedback control, the Proportional-Integral-Derivative (PID) method is selected as it is currently used as a standard in both process control and the HVAC industry. Hence, an elaborate discussion on PID is not required, but a brief explanation is given in section 5.2. Section 5.3 discusses development of feedforward approach in detail. Finally, the combination of feedforward and feedback is discussed in section 5.4, followed by the chapter summary.

In the first step of the feedforward control, physical models are used to determine the setpoints for control variables; i.e. supply air flow rate and temperature and general exhaust damper. The selection of a particular

control variable is based on the application. An application is defined as a sequence of events initiated by a disturbance in a process variable; i.e. lab pressure and temperature which requires the controller to respond in order to change the state of a control variable. For example, if the lab total exhaust suddenly increases due to the hood sash opening, the room pressure will decrease. Hence, the supply flow rate has to be increased in order to keep the room pressure at its setpoint. In this example either the total lab exhaust flow or differential pressure across the lab is a process variable, depending upon which one is measured, whereas the supply flow rate is the control variable.

The second step of a feedforward controller involves generating control signals based on the setpoint determined in the first step and the HVAC equipment characteristics. In a VAV lab HVAC system, two types of control equipment are commonly found. There would typically be a valve or a damper which restricts the flow of water or air followed by a water-to-air coil which heats up the lab supply air. The characteristics for each component correlate input variables to the output as a control signal. The identification process of capturing characteristics for each component is described in section 5.3.3.

Finally, in section 5.4 the options of combining the feedforward and feedback controls are discussed. A simple pressure control sequence is used to simulate and compare the performance of each option. The selected option is then further used to simulate other control sequences and compared with both feedback and feedforward controllers in Chapter 6.

5.2 Feedback control:

The feedback controller uses the error between the setpoint and the measured variable as input. The outputs from the feedforward and feedback blocks are used to control the HVAC system as shown in Figure 5.1. The controller would typically use PID control to return the process variable to the set point.

A simple digital version for the control signal $C_{s,m}$ from a PID can be developed starting with a discrete expression for PID at m^{th} sample time as follows (Mollenkamp 1981):

$$C_{s,m} = \overline{C} + P_g e_m + I_g S_t \sum_{i=0}^{m} e_i + \frac{D_g}{S_t}(e_m - e_{m-1}) \qquad (5.1)$$

The first term on the right hand side of the equation represents a constant offset. The second term is proportional, the third term is integral and the last term is derivative.

A similar expression can be written for m-1^{th} sample as,

$$C_{s,m-1} = \overline{C} + P_g e_{m-1} + I_g S_t \sum_{i=0}^{m-1} e_i + \frac{D_g}{S_t}(e_{m-1} - e_{m-2}) \qquad (5.2)$$

Now, by subtracting equation 5.2 from equation 5.1 the following equation can be obtained which is easy to implement in a digital controller.

$$C_{s,m} = C_{s,m-1} + P_g(e_m - e_{m-1}) + I_g S_t e_m + \frac{D_g}{S_t}(e_m - 2e_{m-1} + e_{m-2}) \quad (5.3)$$

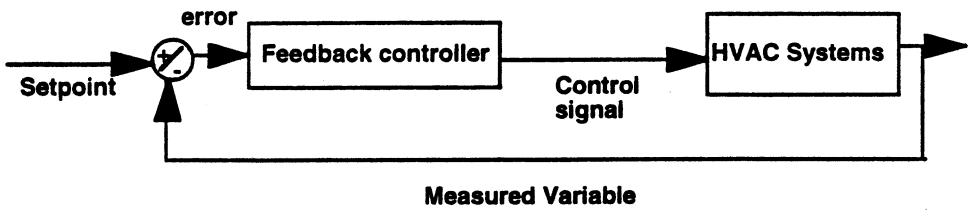

Figure 5.1: Schematic of a Feedback control

5.3 Feedforward block for a VAV laboratory HVAC system :

5.3.1 Method of control

The feedforward controller has both an identification and a control block as illustrated in Figure 5.2. The identification block captures and updates the process characteristics based on the process input control signals and the measured variables. The identification block passes the updated characteristics periodically to the control block for control action.

In this context, feedforward control does have a feedback mechanism to compensate as the system characteristics change. However, this is different from a feedback control where the measured process variable is compared with its setpoint to generate the error signal and the output signal is essentially a function of this error signal. In the feedforward identification process, the process variable and, if it is cost effective and feasible, the system disturbance are measured. The feedforward control block acts upon

receiving a setpoint signal and provides a control signal based on the identified characteristics of the process. The essence of a feedforward control is to generate the control output in response to a change in the setpoint of a process or measured variable. Since the feedforward control does not need an error to generate the control signal, it responds faster than the feedback control.

The identification process captures the system characteristics over the entire operating range which makes the controller robust. If the identification scheme were able to capture the system characteristics perfectly, there would be no need for the feedback controller. However, perfection can not be achieved without incurring a major cost due to errors, noise, and accuracy in the data. Thus, feedback is required to compensate for the steady state error or offset.

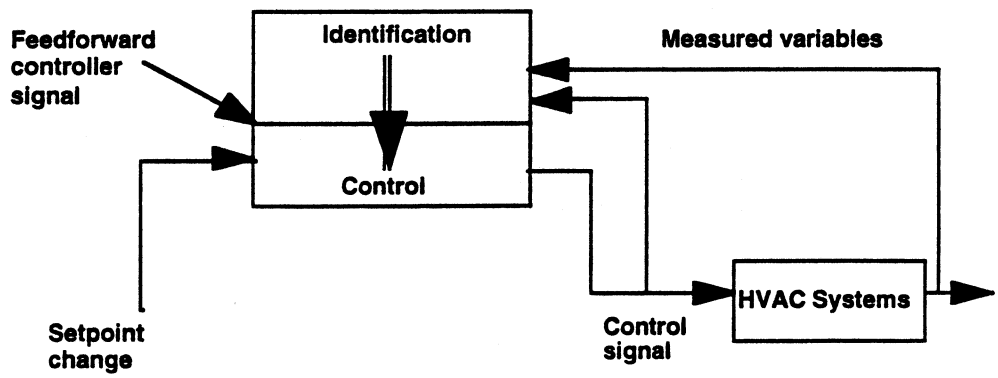

Figure 5.2: Schematics of feedforward control

For each piece of control equipment in a VAV lab HVAC system, the feedforward controller is capable of generating a control signal in response to a setpoint change of a process variable. The physical process associated

with each component is needed in order to understand how the control signal can be generated.

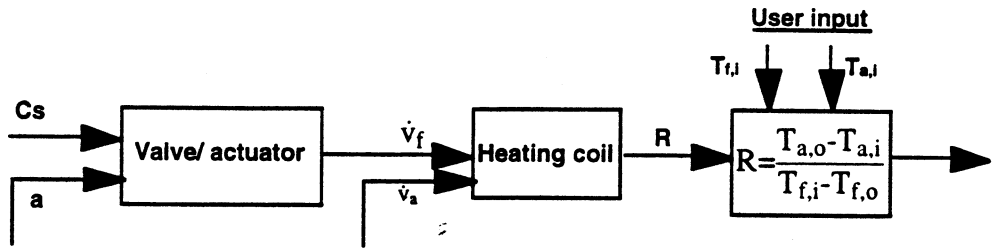

Figure 5.3: Physical process of water-to-air heating coil

The physical process of heating a zone is shown in Figure 5.3, and involves two components: a valve/actuator assembly and the heating coil. Referring to Figure 3.1, a VAV laboratory will commonly have a heating coil, a valve/ actuator and damper actuators in order to satisfy both pressure and temperature requirements in the laboratory. The valve/actuator characteristics are similar to those of a damper/actuator used to modulate air flow rate in a HVAC air distribution system. Therefore, the process described here for the valve is equally applicable to dampers and actuators. By choosing an example of a heating process, the identification of all HVAC components in a VAV laboratory can be illustrated.

The water flow rate through the valve will depend on the valve open area and the authority, a. The authority is defined as the ratio of pressure drop across the valve to the overall circuit pressure drop when the valve is fully open, or for each valve,

$$a = \left(\frac{\Delta P_{valve}}{\Delta P_{circuit}} \right)_{valve\ is\ fully\ open} \tag{5.4}$$

Expressing the valve characteristics in terms of authority, percent valve open and percent maximum flow rate is typical (ASHRAE 1992).

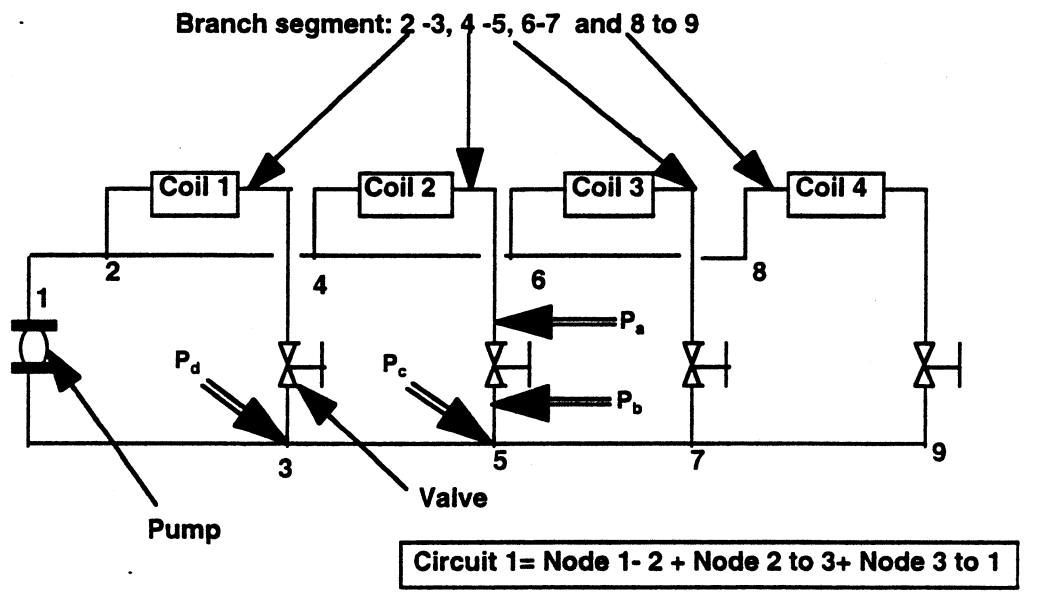

Figure 5.4: Water distribution system for HVAC applications

For a single circuit system, in practice, the circuit pressure drop will be small compared to the valve which will cause a to be close to 1.0. However, for a system with multiple circuits as shown in Figure 5.4, the pressure loss in the main segment becomes significant compared to the branch segment as

the distance between the pump and the coil increases. As a result, the value of authority varies depending upon the ratio of pressure losses as indicated in equation 5.4. The authority of any circuit is time dependent because the flow in each circuit varies with the time. The valve authority can be calculated either using the basic relations between design pressure drop and flow rate or by measuring static pressures at the pump outlet and valve inlet at the design flow conditions and calculating authority at any time.

As shown in Figure 5.3, a control signal, Cs is generated based on the heating demand and is sent to the valve/actuator to open or close the valve. The heating coil has physical inputs of water and air flow rates and inlet air and water temperatures. The coil outputs are water and air outlet temperatures. Since water outlet temperature is not directly linked to the control of supply air thermal energy, it is not considered in the identification. Instead, R is used as a non-dimensional variable combining the water inlet temperature, Tf,i, and air inlet and outlet temperatures, $T_{a,i}$ and $T_{a,o}$ respectively. Both Tf,i and $T_{a,i}$ are either known constants for a given system as user input parameters or are measured and input to the controller. The dimensionless variable R, which can also be viewed as coil effectiveness, is a measure of the heating supplied. R can be expressed as,

$$R = \frac{T_{a,o} - T_{a,i}}{T_{f,i} - T_{a,i}} \tag{5.5}$$

The physical process described above relates the system process variables as a function of the control input. The process needs to be inverted when used

in a feedforward controller to produce the desired control signals that set the valve at the desired position in response to the water flow rate setpoint.

This control scheme can be explained using Figure 5.5. The entire control scheme is divided into feedforward and feedback blocks.

The order of the physical heating process of heating as shown in Figure 5.3 is reversed in the feedforward block shown in Figure 5.5. The feedforward block is activated upon receiving a signal of coil outlet air temperature setpoint, $Ta,olsp$. The on-line identification normalizes and inverts the characteristics to produce the desired signal. The coil characteristic is utilized first in the control process to yield the desired water flow rate, $\dot{v}_f$ for the desired coil outlet air temperature setpoint, $Ta,olsp$ and for given supply air flow rate, $\dot{v}_a$. Knowing the water flow requirement and the authority, a, the identified valve characteristic then generates a control signal, Cs.

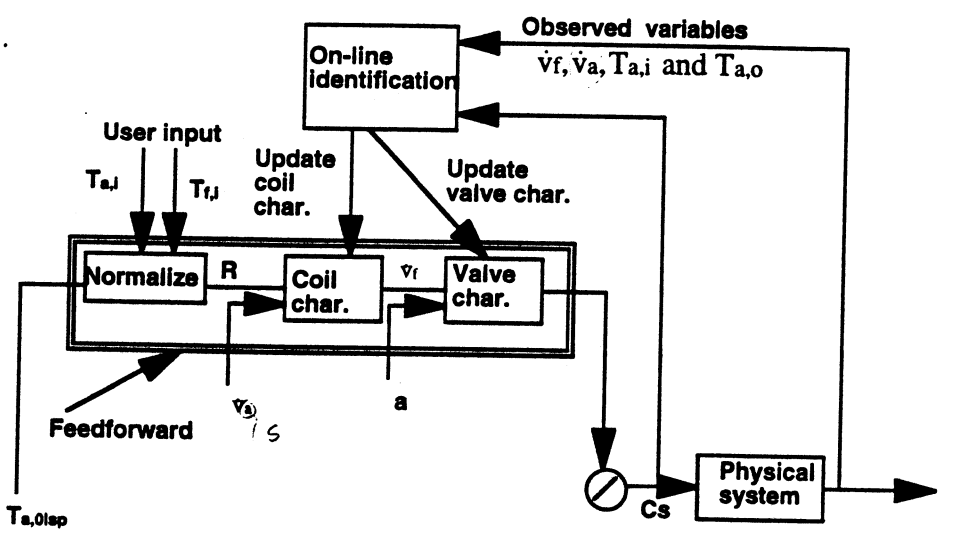

Figure 5.5: Feedforward control of heating coil

The observed variables from the system along with the control signal, *Cs*, may be periodically collected and used to update the coil and valve characteristics by a separate identification scheme that is indicated as an on-line adaptive identification in Figure 5.5. The observed variables will include $T_{a,o}$, $T_{a,i}$, $\dot{v}_a$, and $\dot{v}_f$. Instead of an expensive means of measuring water flow rate, the coil outlet water temperature, $T_{f,o}$ can be measured and $\dot{v}_f$ can be calculated using the following energy balance.

$$\dot{v}_f = k\frac{\dot{v}_s(T_{a,o} - T_{a,i})}{(T_{f,i} - T_{f,o})} \tag{5.6}$$

where k is a constant that is determined empirically and expressed as a ratio of the products of the mass- capacitance of air and water or,

$$K = \frac{\rho_a c_a}{\rho_f c_f} \tag{5.7}$$

Equation 5.6 is proposed as a way to calculate the water flow rate through the local heating coil considering cost and practicality as opposed to measuring flow directly. The HVAC control system usually trends the air flow rate through the coil as well as the discharge air temperature for control purposes. The values are updated every second or more. The values for coil air and water inlet temperatures are also available from the central air handling unit and chiller plant. Thus, by adding a water temperature sensor, the coil water flow rate can be estimated using equation 5.6. This is a cost effective proposition since flow sensor costs more than a temperature

sensor and such cost difference becomes significant considering the large number of local heating coils present in a building. Also, in a retrofit application, a strap-on temperature sensor can be installed outside the pipe to avoid costly job interruption. On the other hand, most types of flow sensor needs to be inserted inside the existing pipe which interrupts the system operation.

A few additional factors favor the use of temperature sensor. First, equation 5.6 will be only used for identification purposes. Hence, dynamic data are not needed to solve for water flow rate from equation 5.6. Instead, only periodic steady state data are needed. The steady state data should not be difficult to obtain given the sample rates of 1 or higher per second.

Secondly, the governing relationships between the water flow rate and air flow rate and air and water side differential temperature across the coil are important in estimating the coil water flow rate. The absolute accuracy of each measurement, hence, is not critical. Finally, the purpose of the feedback controller in a combined feedforward and feedback approach is to compensate for inaccuracies with the identification process which include measurement error. Hence, accurate measurement for identification is not required.

Figure 5.5 clearly demonstrates the need for estimating the coil outlet temperature setpoint $Ta,o|sp$ before the feedforward block can produce any control signal to the valve. In fact, the inverse of heating coil characteristics will generate a setpoint for water flow rate through the valve. By knowing

the valve authority and water flow rate setpoint, the controller will then be able to generate a control signal to the valve.

The process described for a valve is similar to that for a damper. In the case of a damper, the signal will be generated in response to the demand for air flow rate. The air flow rate setpoint is determined first which along with the damper authority is used by the feedforward block to generate the control signal. The schematic of a damper feedforward control is illustrated in Figure 5.6.

5.3.2 Determination of setpoints and prediction of room load for feedforward control.

As explained in section 5.2, a method is needed to determine the setpoints for supply air flow rate and temperature and general exhaust flow rate. The supply air flow rate setpoint is coupled to the pressure loop for lab safety. The supply air temperature setpoint is determined when the room temperature falls below the setpoint and heating is needed. The general exhaust is opened when the room becomes hot and the temperature exceeds the setpoint. In all cases, physical models are used to calculate the setpoints as follows:

Determination of supply flow setpoint:

The steady state mass balance and infiltration equations can be used to solve for the supply flow setpoint. The steady state mass balance (from equation 3.6) written in terms of setpoints is

$$\frac{P_s|_{sp}\,\dot{v}_s|_{sp}}{T_s|_{sp}} + \frac{P_{ad}|_{sp}\,\dot{v}_{ad}|_{sp}}{T_{ad}|_{sp}} - \frac{P|_{sp}\,\dot{v}_e|_{sp}}{T|_{sp}} = 0 \qquad (5.8)$$

The infiltration relation (from equation 3.21) is

$$\dot{v}_{ad}\,|_{sp} = K_l\,(\Delta P\,|_{sp}\,)^n \tag{5.9}$$

The lab pressure differential, $\Delta P\,|_{sp}$, is defined as a differential as follows:

$$\Delta p\,|_{sp} = P_{ref}\,|_{sp} - P\,|_{sp} \tag{5.10}$$

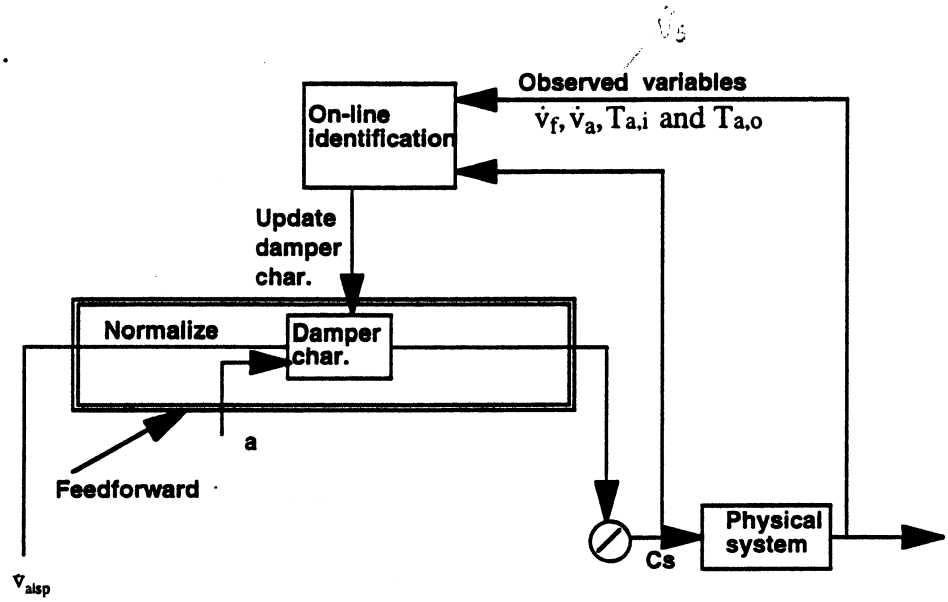

Figure 5.6: Schematics of damper feedforward control

There are nine variables in equation 5.8 comprising the temperature, flow rate and pressure of three air streams: supply, infiltration and lab exhaust. The room setpoints for temperature and pressure infiltration are known. The volumetric flow rate of infiltrating air at the setpoint, $\dot{v}_{ad}\,|_{sp}$, is also known from equations 5.9 and 5.10. Similarly the supply air pressure, $P_s\,|_{sp}$, room

pressure, $P|_{sp}$, and temperature, $T|_{sp}$, setpoints are given from design data. There are three unknowns: lab supply air flow rate, $\dot{v}_s|_{sp}$; total lab exhaust setpoint, $\dot{v}_e|_{sp}$; and supply air discharge temperature setpoint, $T_s|_{sp}$. The total lab exhaust is a sum of general exhaust and exhaust from fume hoods and given by:

$$\dot{v}_e|_{sp} = \dot{v}_{fh}|_{sp} + \dot{v}_{ex}|_{sp} \tag{5.11}$$

In a VAV lab, the fume hood exhaust setpoint is a known quantity for each position of the fume hood sash. Hence, by determining the setpoint for total lab exhaust, the general exhaust setpoint will be known.

Determination of supply air temperature and general exhaust flow rate setpoints:

In order to solve for either supply air discharge temperature or general exhaust setpoint, the steady state energy equation 5.12 is used in addition to the equations 5.8 to 5.11. This is the same equation derived in Chapter 3 (equation 3.11) but the time derivative term is set to zero and the steady state solution is used.

$$\frac{P_s|_{sp}\dot{v}_s|_{sp}}{R}c_p + \frac{P_{ad}|_{sp}\dot{v}_{ad}|_{sp}}{R}c_p - \frac{P|_{sp}\dot{v}_e|_{sp}}{R}c_p + c_f\,\dot{q}_{load} = 0 \tag{5.12}$$

where,

c_f is a unit conversion factor

When the supply air discharge temperature setpoint is to be determined then the general exhaust is usually a known quantity and vice versa. The need for determining the desired supply air discharge temperature arises when the fume hood exhaust suddenly increases as the sashes are opened. The increase in exhaust means more supply air is required to maintain the room pressure differential. However, the room will be overcooled if the quantity of supply air at 55 ^{o}F exceeds the amount required to offset the cooling load in order to maintain room temperature at 70 ^{o}F. To prevent room overcooling, the supply air must be heated and the heating coil valve controlled in order to achieve a desired supply air temperature setpoint.

The general exhaust is needed when fume hoods are closed and the rate of internal heat generation is increased due to process or equipment operation. The room, under such situations, needs more cooling. However, just additional cooling by means of an increase in volumetric flow rate of 55 ^{o}F supply air will upset the room pressure equilibrium. As a result, the general exhaust damper is opened to allow more supply air to provide added cooling. The controller has to determine and control the general exhaust flow rate and supply air flow rate in order to maintain the room pressure and temperature setpoints. In this case, of course, the supply air temperature at 55 ^{o}F is fixed. When heating is required the general exhaust damper is usually closed which means that $\dot{v}_{ex}\,|_{sp}=0$.

Hence, the use of equations 5.8 to 5.12 will yield a setpoint solution for a combination of supply air flow rate and temperature or supply and general exhaust flow rates depending upon the control sequence.

In equation 5.12, the space thermal load, $\dot{q}_{load}$, needs to be determined in order to obtain the setpoints. The transient room load is approximated as proportional to the first order derivative of room temperature with respect to time. This is the internal energy storage term assuming the mass of air in the lab remains constant.

$$\dot{q}_{load}\,|_{tr} = \rho c_v \frac{dT}{dt} \tag{5.13}$$

The room temperature, T, can be measured directly by placing the temperature sensor in the room exhaust duct instead following usual practice of mounting a wall room thermostat. In most labs, the exhaust from the fume hoods and the lab are ducted together and the common intersection between the two exhaust streams provides a good location for a duct temperature sensor. Due to the high ventilation requirement, the air in a laboratory space is well mixed and therefore, exhaust air temperature is a good representation of the room temperature, T. In certain situations, however, it is not feasible to install a duct temperature sensor due to the fear that the electrical voltage supplied to the sensor may react with the volatile fumes. Under those situations, the room wall thermostat sensor can be still used and the room temperature can be estimated by simplifying the equation 4.1 (shown again as equation 5.14 for convenience) and using a temporary room air temperature sensor as explained below.

$$\frac{dT_{st}}{dt} = C1_{st}(T_{pw} - T_{st}) - C2_{st}(T_{st} - T) \tag{5.14}$$

Equation 5.14 couples both the panel wall and the room air temperature to the thermostat temperature, T_{st}. The coupling between the panel wall and the thermostat temperature was necessary to validate the experimental results described in Chapter 4 since the radiant wall heats and cools the panel wall on which the thermostat is mounted. In actual labs, however, the wall temperatures will be very close to the space temperature since both lab and the lab adjacent spaces are usually interior zones and are maintained at the same temperature. As a result, equation 5.14 can be simplified as

$$\frac{dT_{st}}{dt} = -C2_{st}(T_{st} - T) \qquad (5.15)$$

The only thermostat calibration constant, $C2_{st}$, can be easily found during commissioning process by locating a temperature sensor in the exhaust duct temporary or at a good location within the room, changing the room temperature setpoint, trending both thermostat temperature, T_{st}, and room air temperature, T, from a temporary location and fitting trended data to the equation 5.15 to determine $C2_{st}$. Once the thermostat constant is calibrated, the temperature sensor can be removed from the temporary location. As an alternative, if feasible, the sensor to measure the room air temperature can be located in the general exhaust duct for the lab air only. The sensor in the general exhaust duct can not be used continuously in lieu of the thermostat since often the general exhaust damper may be closed completely and the sensor will not be exposed to the room air flow. On the other hand, by having a sensor in the general exhaust, the calibration process can be automated to update the value of the calibration constant, $C2_{st}$, routinely by

using the trended sensor and the thermostat values in equation 5.15 when the general exhaust flow is significant.

When the room temperature is steady, the total cooling load can be determined by using energy equation 5.16, which relates the load to the total lab exhaust flow rate, room temperature and the supply flow rate at the preceding time step, t-1. The air density is assumed to be constant and identical for supply, exhaust and infiltration air.

$$\dot{q}_{load}|_{ss} = \dot{v}_{e,(t-1)}\rho c_p T_{(t-1)} - \dot{v}_{s,(t-1)}\rho c_p T_s - \dot{v}_{ad}|_{sp}\rho c_p T_{ad} \tag{5.16}$$

The total lab exhaust is expressed as a sum of general exhaust and fume hood exhaust flows,

$$\dot{v}_e = \dot{v}_{s,(t-1)} + \dot{v}_{ad}|_{sp} \tag{5.17}$$

In both equations 5.16 and 5.17 the infiltration flow rate setpoint, $\dot{v}_{ad}|_{sp}$, is used instead of actual infiltration flow rate, $\dot{v}_{ad}$ to avoid an oscillation in the room load prediction. The transients in ΔP will introduce oscillation in both infiltration flow rate, $\dot{v}_{ad}$, and room temperature, T. As a result, the calculated room cooling load will oscillate.

In order to see the effects of transient ΔP and $\dot{v}_{ad}$ on the calculated load, a simulation is performed by selecting a simple control strategy. The room pressure and temperature responses are obtained by increasing the room internal heat generation rate from a steady value of 82.50 Btu/min to 412.50

Btu/min. As the room temperature increases due to the higher rate of internal generation, the room calls for more cooling.

Additional cooling can be only provided by increasing the flow rate of supply air at 55 ^{o}F. However, before the supply air flow rate is increased, the total lab exhaust has to be increased to maintain the room pressure differential, which in turn requires the general exhaust to be increased. The lab flow responses are illustrated in Figure 5.7 while the room pressure and temperature responses are shown in Figure 5.8.

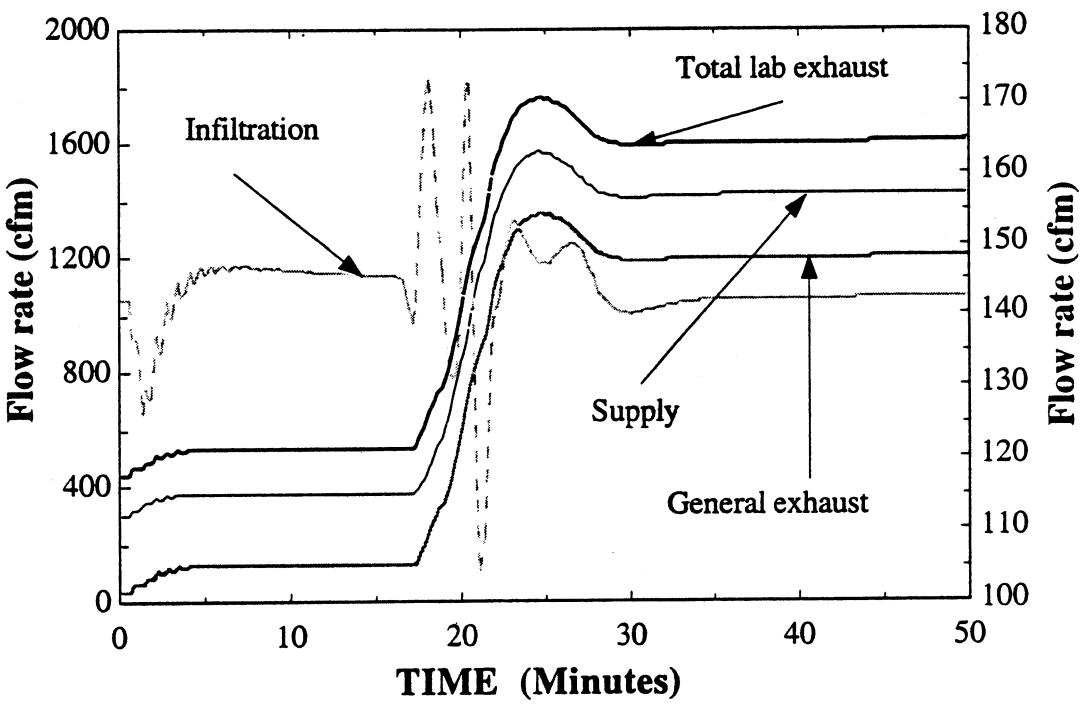

Figure 5.7 : Lab flow responses due to increase in rate of heat generation

The transient shapes of both supply and general exhaust flow rates are the results of assuming first order linear supply and general exhaust damper/ actuator as indicated in equation 3.34. The open loop controller used for this simulation does not have any delay and uses a feedforward strategy using a neural network as explained in section 5.3.

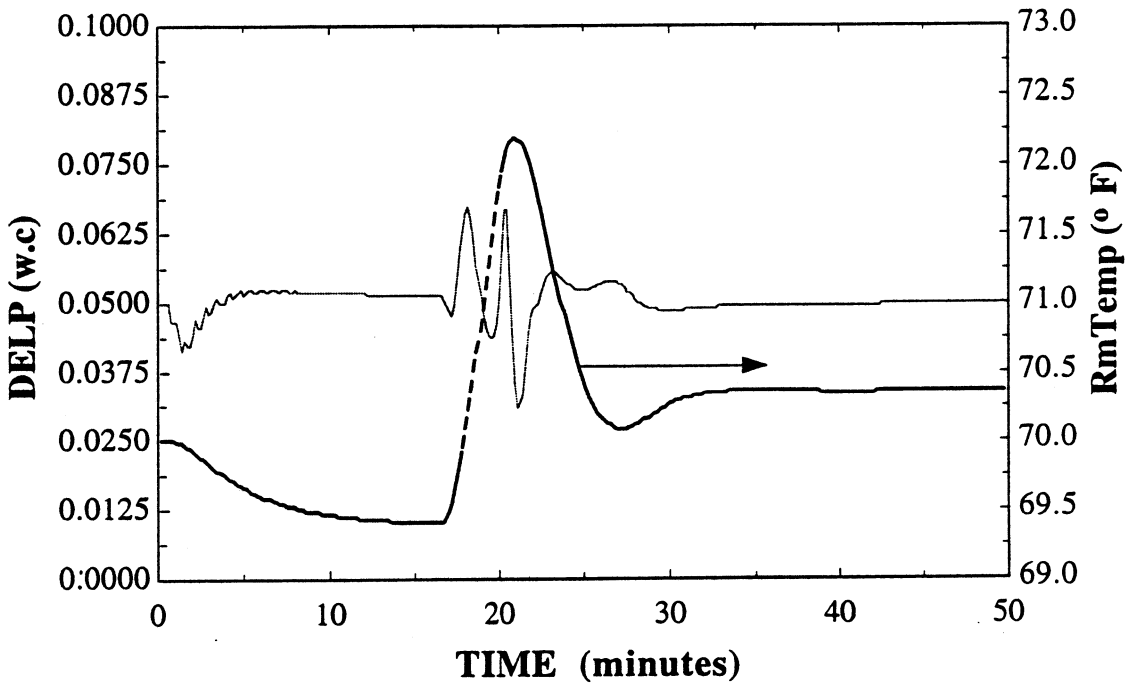

Figure 5.8: Room temperature and pressure response due to an increase in the rate of heat generation

The effect will be further amplified when setpoints are calculated using predicted loads. The use of the infiltration flow rate setpoint in predicting the load is found to work since the objective here is determine the required supply air flow rate, temperature or general exhaust flow rate in order to

achieve room pressure differential and temperature setpoints. Essentially, the controller drives the supply and general exhaust dampers to maintain the room pressure differential of .05 w.c. and room temperature of 70 ^{o}F. The controller first calculates the set points for supply and general exhaust flows at the steady state conditions before and after the increase in the rate of internal heat generation takes place.

Based on the flow setpoints, the controller determines the damper positions using the identified relationship between flow rate through the damper and the damper position. The purpose of using a simple simulation is to illustrate that the pressure and temperature transients cause, in turn, transient behavior in infiltration flow rate as shown in Figure 5.8. The resultant effect is that the predicted load will follow the transient changes in infiltration flow rate and ΔP which are oscillatory. The instantaneous load response is demonstrated in Figure 5.9. The load using a simulated pressure difference reaches a high value and does not even agree at the steady state. The instantaneous load under steady state condition is determined applying equation 5.16 which uses the actual total lab exhaust, $\dot{v}_{ex}$. In contrast, the predicted steady state load, $\dot{q}_{load}\,|_{ss}$ using the setpoint follows the actual load very closely during the transient, and agrees with the simulated load which includes both steady state heat generation and the wall effect. The $\dot{q}_{load}\,|_{ss}$ at steady state uses equation 5.16 which calculates $\dot{v}_{ex}$ assuming a setpoint for ΔP. As a result, the setpoint for $\dot{v}_{ad}\,|_{sp}$ corresponding to ΔP setpoint of .05 " w.c. is used in equation 5.17. For the selected control sequence, the difference in actual $\dot{v}_{ex}$ and as determined by equation 5.17 is

found to be about 41 cfm which translates into a difference of about 43 Btu/min between the instantaneous load and $\dot{q}_{load}|_{ss}$ under the steady state.

Based on the observations, the predicted steady state load is selected for use in simulation instead of the instantaneous load. The controller also does not need to follow the actual instantaneous room load as that will cause the dampers to oscillate. The use of the predicted load based on setpoints will provide a stable control state.

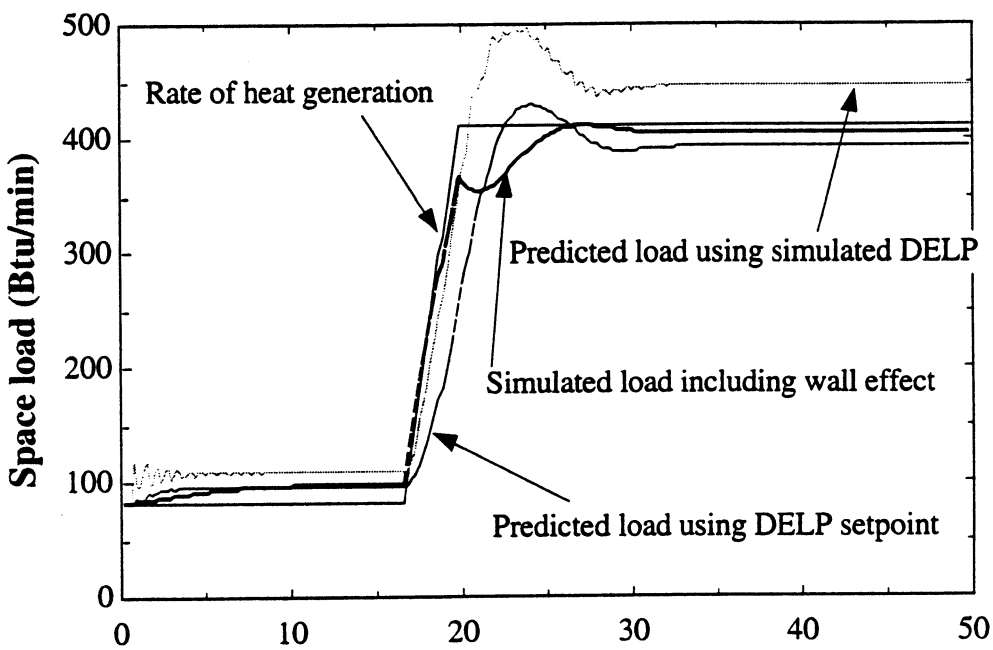

Figure 5.9: Predicted load using various techniques

When the room needs cooling, both the storage and steady state load terms are added to compute the load, $\dot{q}_{load}|_{ss}$ in order to determine the general exhaust and supply flow rate setpoints. In the case of heating only, however, the storage term is neglected to compute $\dot{q}_{load}|_{ss}$ in calculating the supply air temperature setpoint.

5.3.3 Identification of component characteristics:

A suitable process is needed that will produce component outputs based on input, output and information related to other variables using the identified component characteristics. There are two types of components which need to be identified: a heating coil and a valve/ damper. However, since the physical characteristics will be inverted in the control process as explained in section 5.21, the identification process should capture the relationship between the inputs and outputs of the inverted physical processes. For example, referring to Figure 5.3, for a heating coil, the inputs are a non- dimensional variable, R and fixed variables Ta,i, coil inlet air temperature and fluid inlet temperature, Tf,i. The coil output will be the water flow rate through the coil, $\dot{v}_f$.

Similarly, referring to Figure 5.5, the identification of an inverted physical process for a damper or valve involves flow rate and authority as two inputs and control signal as an output. A damper or a valve is essentially a variable fluid resistance device. Both exhibit similar fluid characteristics and their performance is expressed in terms of identical variables and, hence, can be represented by the same models.

The General Regression Neural Network (GRNN) is chosen to identify the coil and valve characteristics due to its simplicity, robustness and excellent capability in system identification (Specht 1991). Unlike a conventional neural network, it requires minimal computational time to effectively capture the system characteristics. The following is only brief account of GRNN to illustrate its implementation in identification of the components. The theory behind GRNN is discussed in detail in literature survey, Chapter 2.

The input to a GRNN is a series of data that can be in multiple dimensions. For sample values of X_i and Y_i of input vector X and the scalar output Y, an estimate for the desired mean value of Y at any given value of X is found using all of the sample values in the following relations:

$$\hat{Y}(X) = \frac{\sum_{i=1}^{n} Y_i \exp(-\frac{D_i^2}{2\sigma^2})}{\sum_{i=1}^{n} \exp(-\frac{D_i^2}{2\sigma^2})} \qquad (5.18)$$

where the scalar function D_i^2, representing the Euclidean distance from the given value to the known points, is given by

$$D_i^2 = (X - X_i)^T (X - X_i) \qquad (5.19)$$

and σ is the single smoothing parameter of the GRNN. Equations 5.18 and 5.19 are the essence of the GRNN method. For a small value of the

smoothing parameter, σ, the estimated density assumes non- Gaussian shapes but with the chance that the estimate may vary widely between the known irregular points. When σ is large, a very smooth regression surface is achieved. The Holdout method (Specht 1990) is used to calculate the value of smoothing parameter, σ.

The implementation of GRNN to the characteristics of a heating coil or valve/ damper also offers advantages over the conventional methods of identification. In a traditional regression method for identification, the operator has to input *a priori* knowledge of the equation type or has to search for the best fit equation exhaustively. The code requirement for a non-linear regression is intensive and may be prohibitive for effective on-line use. In contrast, the GRNN does not require any user input for the functional form of the characteristics and uses a strikingly simple code. Moreover, the GRNN algorithm can be imbedded into a neural hardware processor, thereby eliminating software development process to a large extent since software coding during field installation is not necessary.

For a heating coil, the input vector X contains dimensionless variable R and $\dot{v}_{a|sp}$ while the output, Y, is water flow rate through the coil, $\dot{v}_{f|sp}$. Using valve authority, a and $\dot{v}_{f|sp}$ as input, the valve GRNN then produces an output of required valve control signal, *Cs*. For a damper/ actuator for flow control, the input and output variables are the same as that for a valve.

5.3.4 Simulation and identification of coil and valve characteristics

Coil and valve characteristics were generated using the models described above, and subsequently used in the GRNN to identify the characteristics. The physical variables are first normalized. Besides R and authority, a, whose range is 0 to 1, other normalized variables used are

$$nC_s = \frac{C_s}{C_{s\,max}};\quad n\dot{v}_s = \frac{\dot{v}_s}{\dot{v}_{s\,max}} \text{ and } n\dot{v}_f = \frac{\dot{v}_f}{\dot{v}_{f\,max}} \tag{5.20}$$

In this example, the values of $C_{s\,max}$, $\dot{v}_{f\,max}$ *and* $\dot{v}_{s\,max}$ are 1.0, 2500 cfm (1180 L/s) and 1.0 gpm (.0631 L/s), respectively. Using the value of R required to meet the load and a given value of $n\dot{v}_s$, a value of $n\dot{v}_f$ can be determined which can be subsequently used in a valve model along with the given authority to generate a control signal, *nCs,* as indicated in Figure 5.10. The coil and valve characteristics data in Table 5.1 are generated using normalized variables and the models described above.

The GRNN method can be best explained by using an example of regressing valve data for a constant authority. For example, choosing a to be 0.1, a non-linear relation, shown in Figure 5.10, is established between the normalized control signal and normalized flow. For a constant authority, there is only one input and the vector X in equation 5.19 becomes a scalar series of normalized flow rate, $n\dot{v}_f$. In equation 5.19, the scalar function, D_i^2 can be computed where X_i is the ith sample in the $n\dot{v}_f$ series. Equation 5.18 can then be solved using D_i^2 and corresponding Y_i as the ith sample of nC_S in the identification data.

Table 5.1

Valve Simulation Parameters

λ = .00001; W_f = 1; K_{cd} = .08641(64.89); K_0 = .042 (31.54);

Authority	K_{ab} $\frac{Inches\ of\ H_2O}{(gpm)^2}$ $\left(\frac{kPa}{(L/s)^2}\right)$		Maximum $\dot{v}_f$ gpm (L/s)	
1.00	-.086	(-64.58)	3.00	(0.1893)
.70	-.034	(-25.53)	2.50	(0.1577)
.50	.037	(27.78)	2.12	(0.1337)
.20	.407	(305.63)	1.34	(0.0845)
.10	1.02	(765.97)	0.95	(0.0599)
.05	2.25	(1689.64)	0.67	(.0423)
.01	12.13	(9109.02)	0.30	(.0189)

The simulation of coil and valve characteristics as well as GRNN is performed using the Engineering Equation Solver (Klein and Alvarado 1994). The simulated data in Figure 5.9 are shown by the solid line while the points are generated by using GRNN equation 5.18 for various smoothing parameter (σ) values. Although smaller values of σ seem to represent the data better, overfitting by choosing a very small σ should be avoided . The simulated data contain fourteen samples obtained by varying nCs from 0.0 to 1.0 in increments 0.1 and nCs of .05, 0.15, 0.25.

The Holdout method (Chapter 2, Section 2.5) is used to calculate the optimum value for sigma, σ, and it is found to be .01. The effect of choosing a higher value of σ is apparent in Figure 5.10. With the larger value of σ of 0.5, a smooth nearly linear trend is found that differs significantly from the input while with smaller values, the GRNN attempts to approximate all samples and is not smooth between points. For σ=0.01, the average error between the predicted and simulated signals is found to be 2.62% while the maximum error of 14% is observed for the lowest value of control signal that is not included in the identification data (nC_S of .35). A slight error is also observed at the higher value of $n\dot{v}_f$ since the control signals becomes highly sensitive to the normalized flow rate.

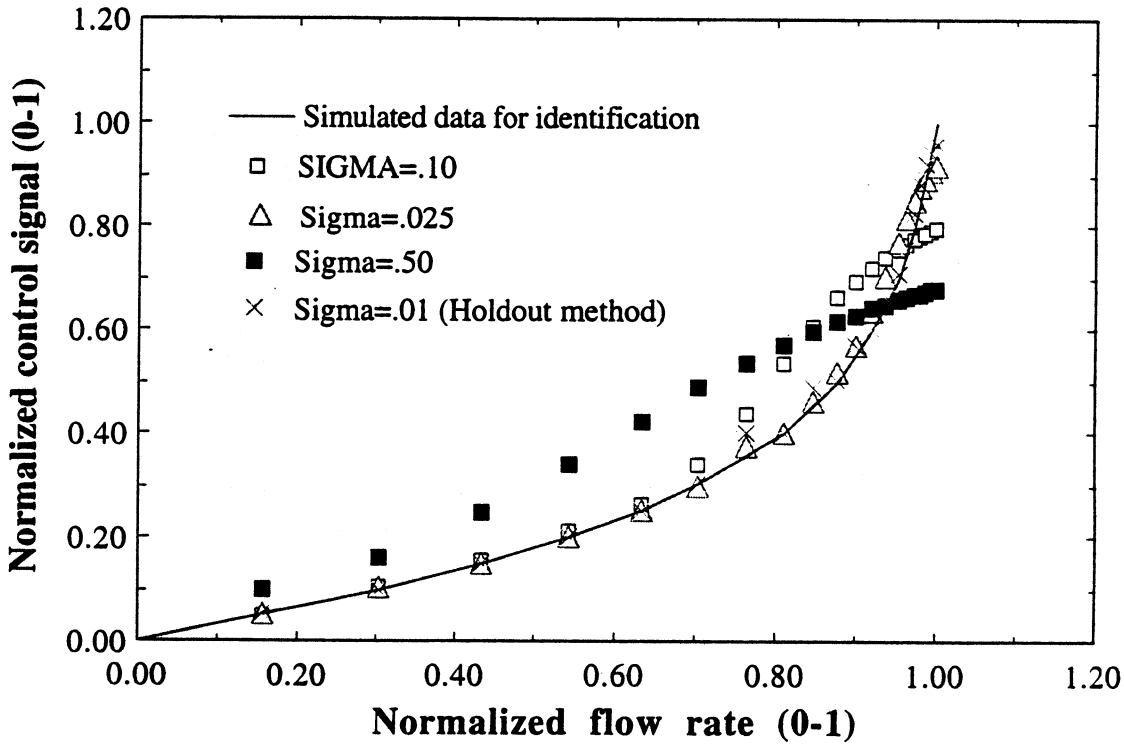

Figure 5.10: Simulated valve data (a=0.1) for identification and to predict using GRNN

However, the relative error at the higher end of the valve curve is much smaller compared to the lower end due to the higher absolute value of control signal at this end. The sample size and the choice of samples, therefore, are important variables along with the smoothing parameter, σ. In fact, by including the sample of nC_S=0.35 in the identification data, the error between the simulated and the predicted control signal for that specific sample can be decreased from 14% to less than 1% while the average error can be dropped from 2.62% to 1.31%. In order to identify damper/ valve characteristics, only 200 samples at most will be required to cover the entire range of operation. This is based on the assumption that the authorities can be varied between .001, .01, .05 and .1 to 1 in increments of 0.10 while the control signal can be varied between .05, .075, .01, .15, .20, .25, .30, .35 and 0.40 to 1.0 in increments of 0.1. Any state-of-the-art local controller will be able to process the 200 sample values with ease and speed. In reality, however, the total number of points to cover the actual operating range will be much less, i.e. less than 100.

Next a range of valve authority between 0.5 and 0.1 is chosen to test the GRNN method. Again, the Holdout method is used to determine the optimum smoothing parameter, σ which is now .05, and which produces a sum of square error of 0.189 over a identification data size of 30 samples. The identification data set includes values of authority of 0.10,0.30 and 0.50 and nCs between 0.10 to 1.0 equally spaced. The test data set varies nCs from .05 to 0.95 in increments of 0.10 and also includes intermediate authorities of 0.20 and 0.40. The average error of about 3.0% is low compared to the

range of the data set. Some errors higher than the average are found for higher values of control signal where the curve becomes very steep with the normalized flow rate, $n\dot{v}_f$.

The operating range for the valve or damper is typical of these control applications. Hence, the method of using GRNN to represent characteristics using a small data set is promising and implementable in a real controller on an on-line basis. In a real application, operating characteristics over the entire operating range can be developed during commissioning by varying the damper open area. Once captured, the operating characteristic will be stored in the feedforward controller and control signal will be generated based the stored data using GRNN. The time and effort required to tune the feedback loop will decrease as the error signal for the feedback loop will always have a low value. Reduction of commissioning cost and time and enhancement of system performance are the two major factors in favoring combined feedforward and feedback controller for a building HVAC distribution system.

The measured data obtained during the commissioning process will be used only to initialize the identification process. As the system operates and more operating data are collected, the identification will be updated accordingly. The essence of combined feedforward and feedback is to generate a rough estimate of the control signal with the feedforward block while the refinement is made with the feedback. In fact, the feedforward block also has a feedback mechanism that updates the identification. However, the

identification process is kept separate from the control process for ease of implementation and cost effectiveness.

Another method for implementing GRNN in a real controller is to generate the characteristics using the simulated data. The characteristics can be stored and updated as the real data become available and replaces the simulated data.

Figure 5.11 shows both the identification and the test data covering the entire operating range of a valve. These were obtained by simulating control signals that varied between 0.1 to 1.0 for each authority in the identification set over which the authorities vary from .01 to 1.0. Also, additional samples are duplicated from the test set to the identification set at low values of authority and control signal. In total, 160 samples are used in the identification set while 150 samples are included in the test set. The Holdout method using a smaller data set with authorities of .01, 0.10, 0.25, 0.50, and 1.0 is used to optimize the value of σ. A smaller data set having sparse values still yields a good choice of σ of 0.01 for the data set shown in Figure 5.11.

The plot comparing simulated and predicted control signals is shown in Figure 5.12. Again, higher than average errors occurs for large control signals as well as for low authorities. The large error for a specific sample can be vastly decreased by including that sample in the identification set. This can be easily achieved in a real controller by comparing the control signal sent to the valve and the damper and the control signal generated by

the feedforward control signal (Figure 5.2). If the difference between the feedforward and the total control signal increases more than a pre- fixed threshold value, the control signal and corresponding normalized flow rate, $n\dot{v}_f$ and the authority can be put back into the identification set.

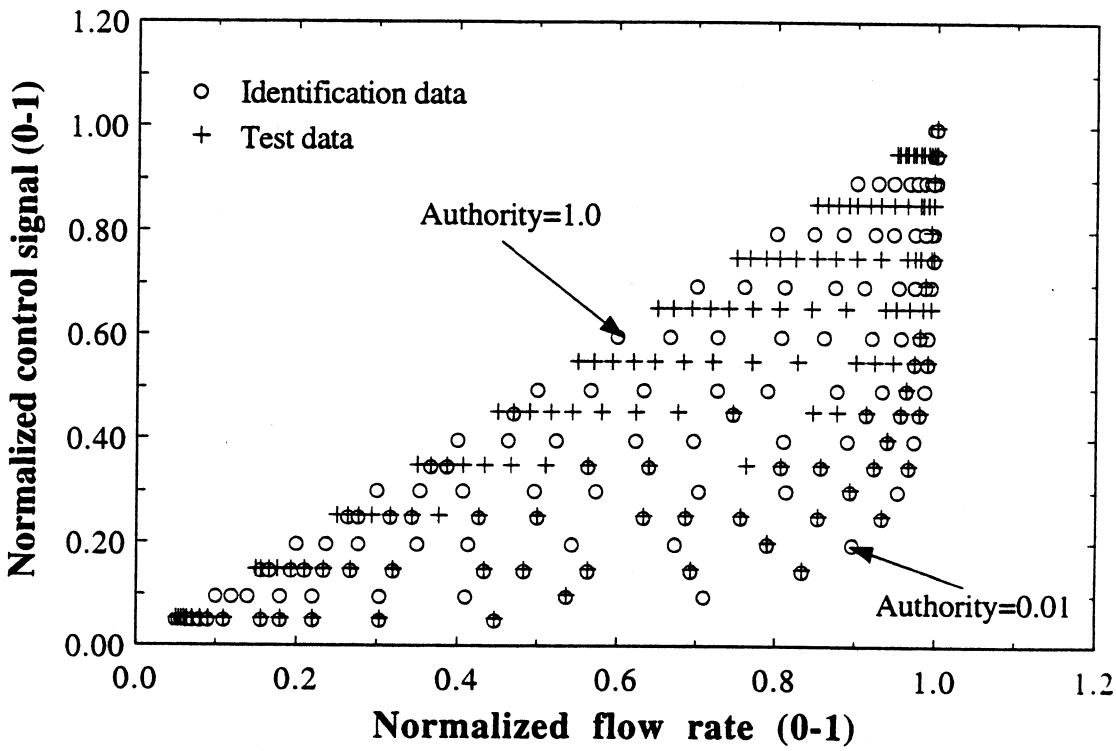

Figure 5.11: Simulated valve data (1>a>0.01) for identification and to predict using GRNN

Finally, the GRNN is used to identify the characteristics of a heating coil. Referring to Figure 5.5, the GRNN needs to predict the required water flow rate through the coil for given R and air flow rate. For randomly selected values of normalized supply air flow rate $n\dot{v}_s$ and R, the normalized flow rates, $n\dot{v}_f$ are calculated using equations 5.6, 5.7 and 5.20. A portion of the simulated data is used for identification purpose while the rest is set aside to

test the GRNN algorithm. The test samples are purposely chosen as to cover the entire operating range. Figure 5.13 shows both the identification and the test data.

An average error of 2.6% between the predicted and simulated normalized flow rates is found. Unlike the valve in which a definite pattern is evident, the coil plot in Figure 5.13 appears random. Even with such sparse and random distribution of input data, the GRNN is able to predict the coil flow rates with good accuracy.

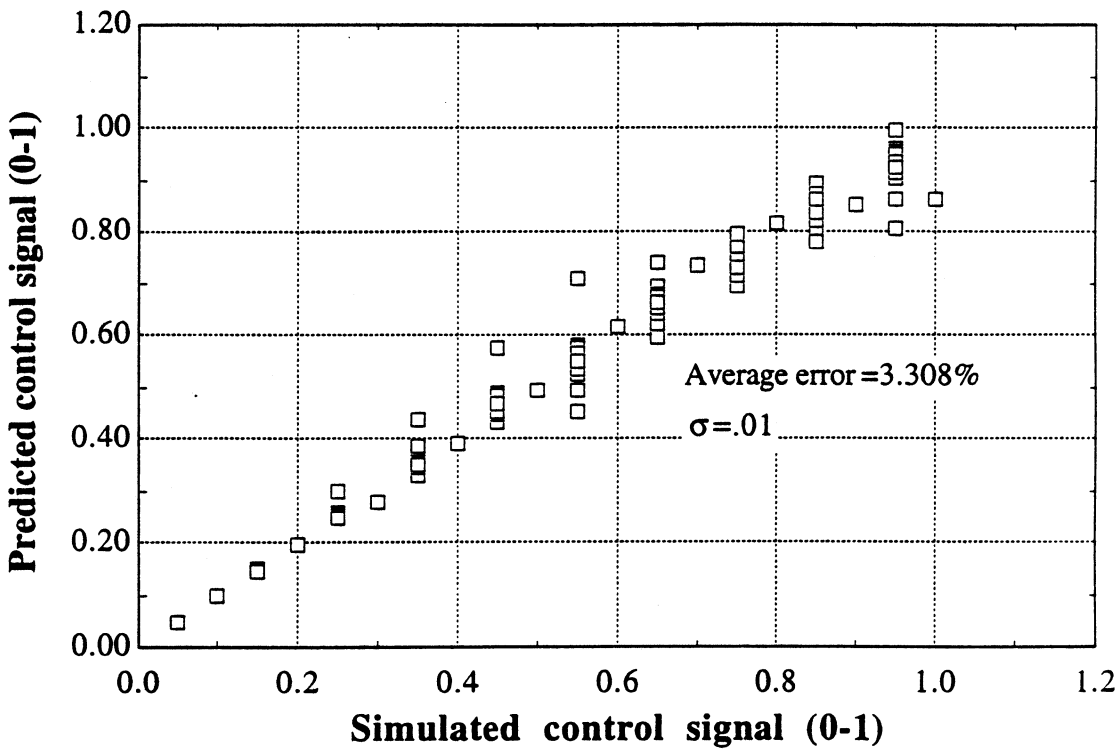

Figure 5.12: Comparison between simulated and predicted control signals using GRNN for a valve (1>a>0.01)

5.3.5 Identification of damper characteristics using measured data:

In addition to the simulated data, measured damper characteristics are also used to test GRNN. Two sources were used to obtain the measured values: 1) Test data taken to calibrate damper performance and 2) Active damper performance at a job site using a building automation system (BAS). In the first case, damper curves are experimentally generated for three damper authorities as shown in Figure 5.14.

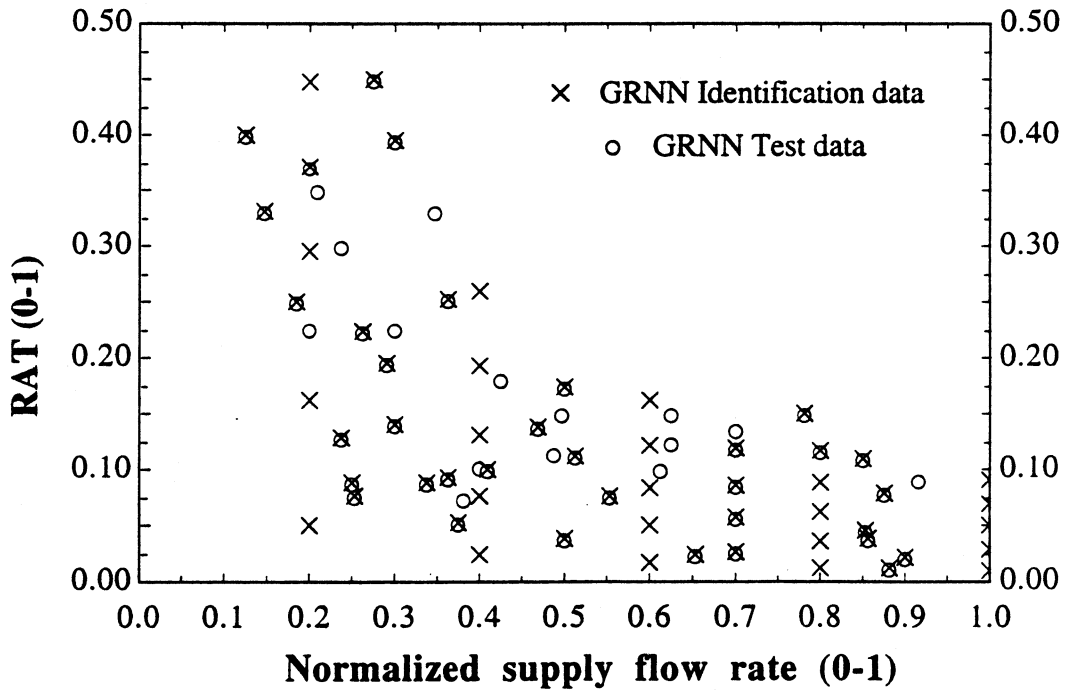

Figure 5.13: Simulated coil data for identification and to predict using GRNN

The test sensors used to obtain data are similar to those used in commercial building control systems. For a given control signal, the flow rate through the damper is noted and normalized using equation 5.20. The GRNN is identified using the measured values of the control signals, flow rate and authorities while intermediate points on the authority curves are used to test the GRNN as shown in Figure 5.14.

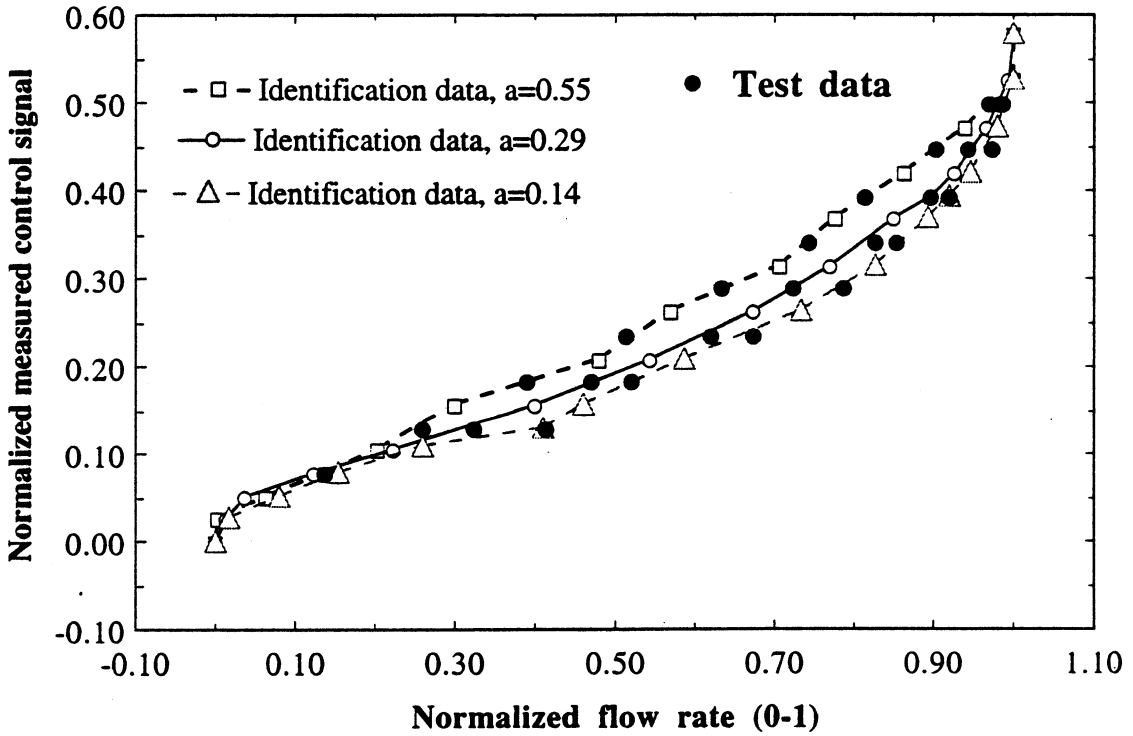

Figure 5.14: Damper test data for identification and prediction by GRNN

Compared to the simulated data, the measured curves in Figure 5.14 exhibit more randomness as expected. At low flow rates, the three authority curves converge into a single one indicating the difficulty of measuring flow rate when the damper is barely open. At high flow rates and low values of

authority, increasing the control signal will not increase the flow. The GRNN predicts the measured values with an average accuracy of 4.30% which is encouraging considering the error associated with the measurement and data collection system. The Holdout method is used to determine the optimum smoothing parameter, σ of .066. The error increases with the higher flow rate as the authority curves become highly sensitive as can be noticed from Figure 5.14. The range of the test data for GRNN chosen in the normal operating range of the damper between 10 to 100% of flow rate.

For the damper at the job site, the authority remained unchanged at 7% during the data collection. Figure 5.15 shows this damper characteristics.

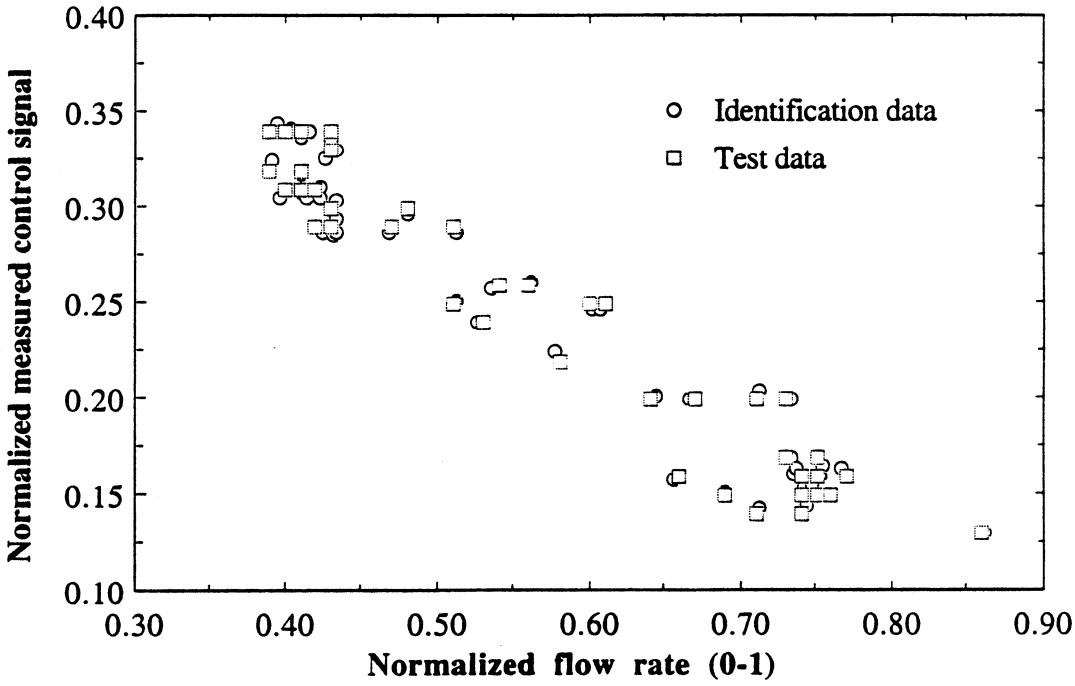

Figure 5.15: Data from BAS for identification and for prediction using GRNN.

The plot indicates more randomness than for the test damper, as expected. For the same flow rate, the damper control signal varied over a wide range at both high and low flow rates. The GRNN output is tested for each sample observation that has been used in the identification data. Pre-processing of the raw measured values is not used before the data are fed to the GRNN for identification. A pre-processing filter could be used on measured values to reduce the uncertainty with the measured values. The purpose here is to test the GRNN most conservatively considering all sample values.

Figure 5.16 shows that the accuracy of GRNN in predicting control signals is within 6%. A linear regression of valve characteristics was also used for the data shown in Figure 5.15, and yielded an average error of 7%.

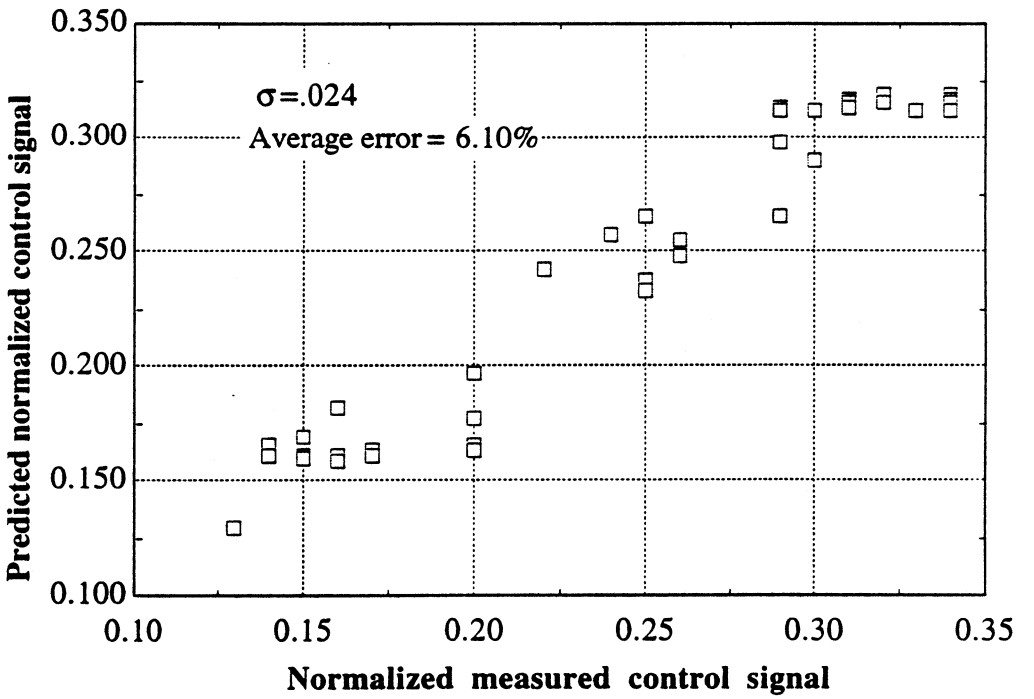

Figure 5.16: Comparison between measured data from BAS and predicted by GRNN

The essence of GRNN is the capability of predicting both non- linear as well as linear characteristics without any user input for a fixed smoothing parameters. In the case of a regression tool, significant user input to specify the form the regression is required which often limits the actual on- line implementation of regression analysis for identification. Therefore, the results demonstrating that the performance of GRNN exceeds that of linear regression is encouraging.

5.4 Combination of feedforward and feedback control:

The aim of the feedforward-feedback combination topology is to generate the majority of the control signal from the feedforward block such that the feedback block only deals with a small steady state error and thus requires little tuning. Unlike the feedback loop, the feedforward loop acts only upon the setpoint value and does not require the measured values of the variables.

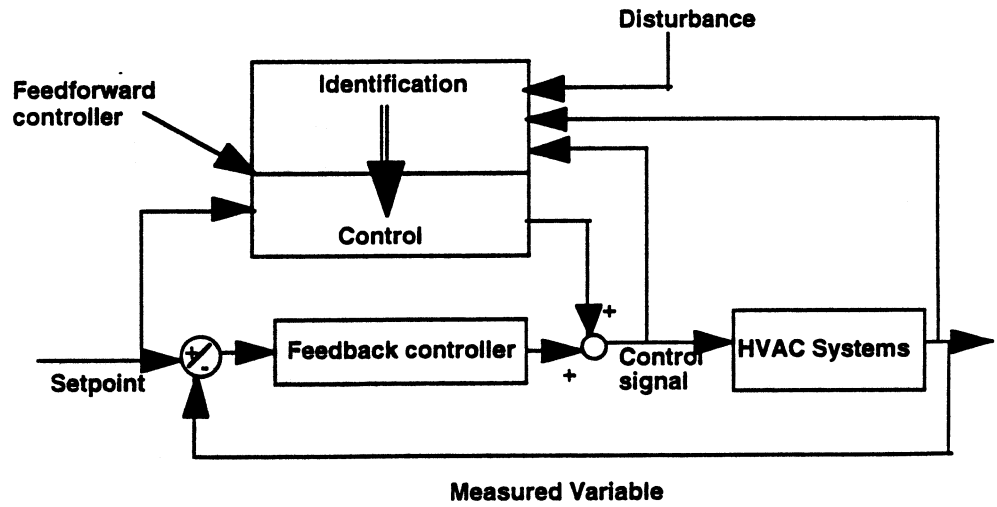

Figure 5.17: Combined Feedforward and Feedback Control Topology

As a result, the feedforward signal can enhance control speed in tracking the setpoint change. The most common method of employing feedback is the traditional approach of Proportional-Derivative-Integral (PID) algorithm, and is appropriate for the combined approach.

The specific control topology shown in Figure 5.17 is particularly suitable for identifying and controlling room or zone level processes and is often referred to as a local HVAC controller. This local controller uses valves and dampers to modulate the flow of water and air respectively with heating coils used to provide local heating. Both valve and damper are flow restricting devices and by capturing the characteristics of the valve or damper and of the heating coil, a feedforward block can be suitably developed for local HVAC control process.

Local controllers are found in large numbers in mid-size to large buildings and must have limited memory and processing capability to remain cost effective. Hence, a control scheme is needed that is simple, easy to implement, inexpensive, and that provides substantial enhancement in performance by coupling feedforward and feedback algorithms. This provides an improvement over the PID controller that react to a control affected by the dynamic response of the coil and valve signal. In the feedforward block explained in detail in section 5.3.1, static characteristics of these devices are stored and updated.

Two options are considered for combining feedforward and feedback blocks. As a first option, a simple switch is used to set the control signal from the PID algorithm to zero whenever a setpoint change is noticed. This first approach, hereinafter identified as model 1, is shown in Figure 5.18. Only the feedforward block produces a control signal when the setpoint is changed. The PID output is only added when the setpoint does not change, which indicates that the system is under steady state. This combination approach is based on the fact that feedback is only responsible for the steady state error that will not be detected by the open feedforward block. It is reasonable to expect a relatively small steady state error due to the uncertainties introduced with the identification scheme, measurement and controller.

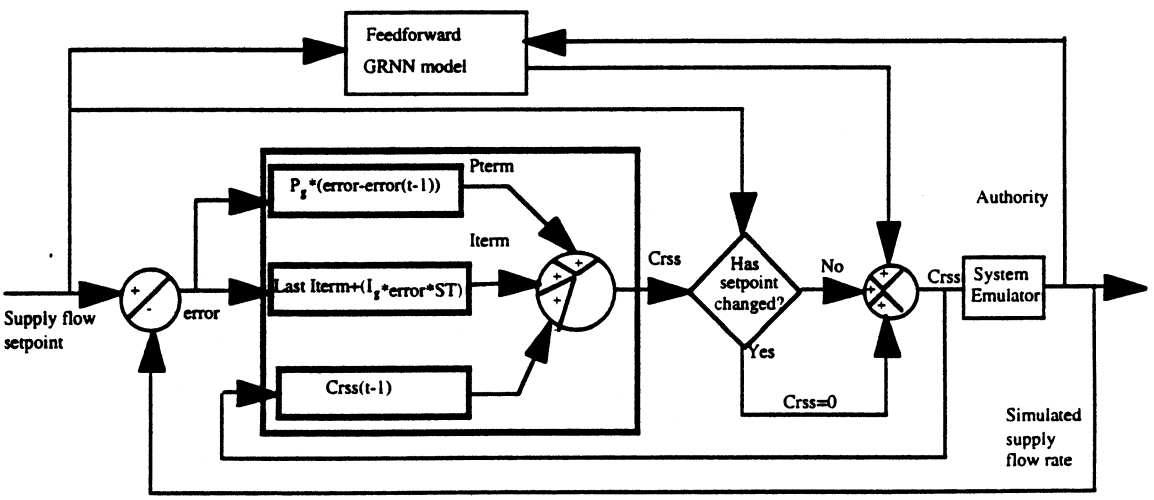

Figure 5.18: Feedforward and feedback combination model 1

In the second approach, termed model 2 and shown in Figure 5.19, the net controller output is the result of addition of the feedforward output, the

integral and derivative portions of the PID output and the subtraction of the proportional part of the PID output. The logic employed here is that by subtracting the proportional output, the feedback will remain inactive to any change in the setpoint. The feedback will only provide the integral and the derivative actions allowing the controller to respond to the setpoint change by means of feedforward block.

Both combination models are simulated and compared to each other using a simple sequence of pressure control to illustrate the responses. A detailed comparison is presented in Chapter 6. In this sequence, the only disturbing force is the total room exhaust flow. The room, supply air and the adjacent space are at same temperature of 70° F. As the exhaust flow rate from the lab changes due to the opening of the fume hood sash, the supply side reacts to maintain a constant Δp across the lab envelope. The change in flow rates along with the response of Δp are shown in Figure 5.19.

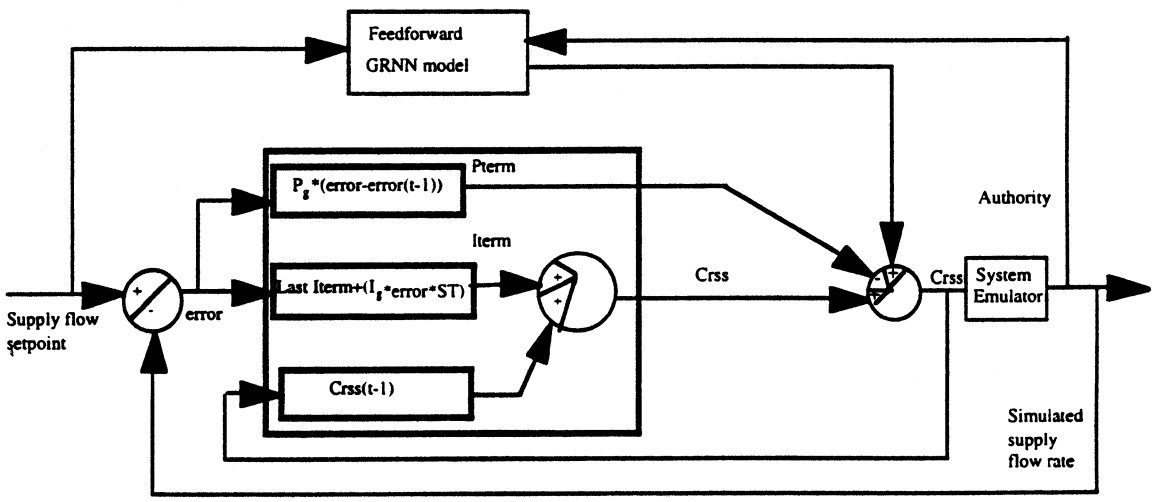

Figure 5.19: Feedforward and feedback combination model 2

The feedback loop in both models are tuned using the Bekker et al. (1991) method of PI control and setting the derivative term to be zero. The tuning procedure is discussed in Chapter 6 in detail. The plots in Figure 5.20 show that both models perform well although model 1 performs slightly better compared to model 2 in terms of both undershoot and response time.

Model 1 is further explored by varying the sample time from 1/5 sec. to 1/40 sec. The performance of model 1 for various sample times and for a decrease in exhaust flow from a high exhaust is shown in Figure 5.21.

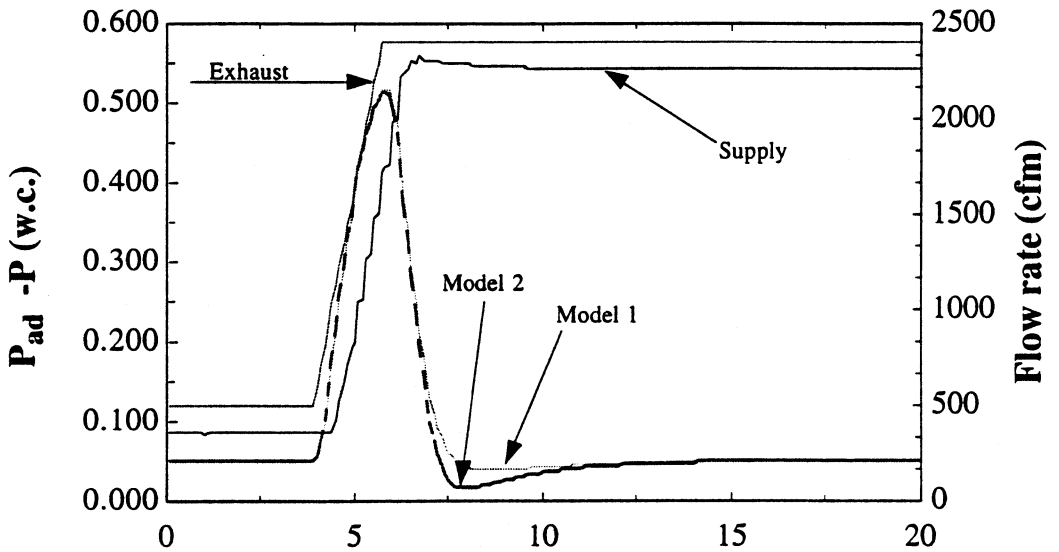

Figure 5.20: Room differential pressure response to compare the performance of Models 1 and 2.

For decreasing flow, the trend is exactly opposite to that for increasing flow. It is clear from these plots that the performance of the controller improves significantly with shorter sample times. The sample time is function of controller processing and communication speed and often dictated by the

cost. Based on competitive, available HVAC local controllers on the market, a sample time of 1/10 sec. or 10 samples per second is a logical choice. In simulating Model 1 for different control sequences (Chapter 6), sufficient time was allowed before the feedback controller was activated to ensure that the steady state has been reached.

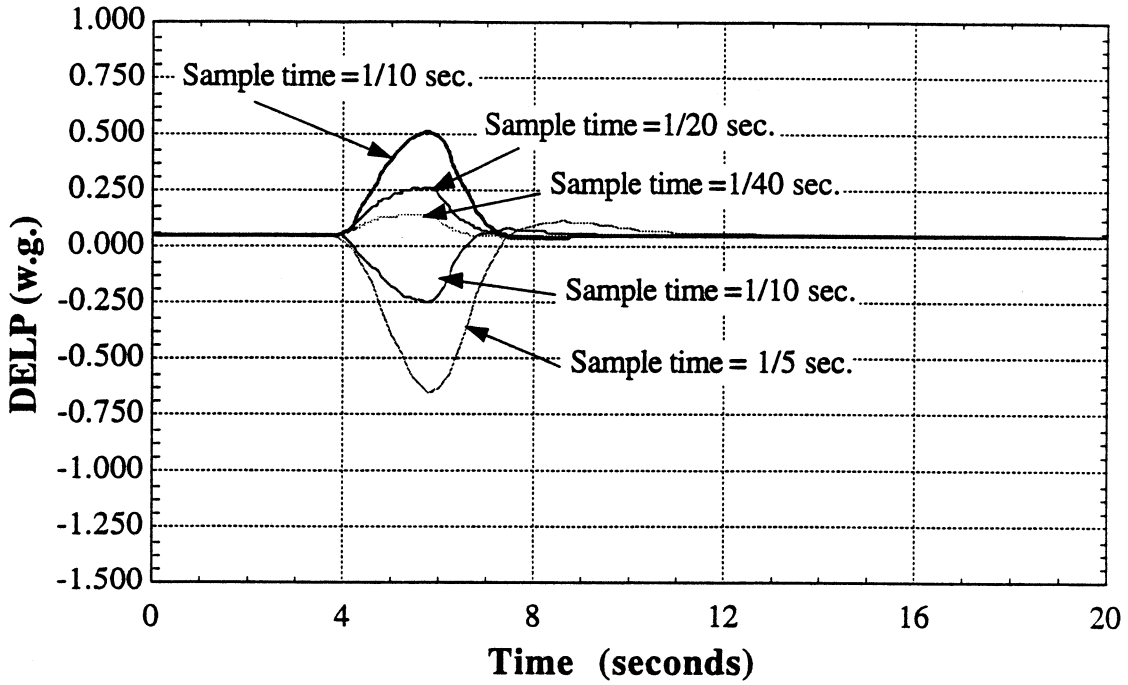

Figure 5.21: Room differential pressure response using Model 1 for various sample times.

5.5 Summary:

The method of General Regression Neural Network (GRNN) holds promise to effectively identify characteristics of HVAC components for subsequent use in controls. The strength of the GRNN is apparent as it has demonstrated its ability to adapt to both linear and non- linear relations using both simulated and measured sample observations. Unlike a traditional regression equation, however, *a priori* knowledge of the relationship in terms of an

equation is not necessary for implementing the GRNN. The nature of the GRNN algorithm allows the method to be imbedded in a neural network architecture which makes hardware implementation possible. The smoothing parameter is the only variable that needs to be selected and it can be determined using the Holdout or other methods.

Since a small data set is needed for local HVAC control component, i.e. valves, dampers and heating coils characteristics, the GRNN provides a promising means of characterizing static performance of HVAC components for use in a feedforward block coupled with the feedback controller. Although the output Y is treated in this paper as a scalar, multiple outputs can be also handled by GRNN (Specht 1991).

Based on the results using measured data, a conservative estimate of a 6% error in identifying coil and valve characteristics with the GRNN method is reasonable. Hence, a control signal can be generated with an average accuracy of 8.8% based on a simple quadrature formula and individual valve and coil errors $(\sqrt{(6.0^2 + 6.0^2)} = 8.8)$ The average error of 8.80% is quite encouraging using the GRNN in a feedforward controller. The feedback controller will be adequate to generate a control signal in order to eliminate a residual error of less than 10%. Additionally, the feedback controller will require minimum tuning since the error range is anticipated to be in a fixed low range.

The use of combined feedforward and feedback controller enhances performance while reducing commissioning cost. For a large data set, the

performance of GRNN may be degraded because for each sample the estimating algorithm will use a large number of stored identification data. However, for such applications, a clustering technique (Specht 1991) is suggested to reduce the size of the identification data set.

The combined model 1 which uses the PID controller under steady state only demonstrated better performance for simple room pressure control compared to Model 2. Model 1 showed improved performance in terms of response time, oscillation and stability when compared to the other model considered here. The combined feedback and feedforward is further investigated and compared with the PID and feedforward control only are included in Chapter 6. The comparison is made for room pressure and temperature control, considering both cooling and heating sequences.

Chapter 6
Comparisons of control methods

6.0 Overview:

This chapter begins with a general overview of control methods followed by a brief description of each, their sequence of operations, and a discussion of the results. Simulation is used to evaluate the performance of the different control strategies. The proposed strategy of a combination of feedforward and feedback control strategy is compared with the conventional feedback control method. In addition, simulated results of exclusive control is also included to illustrate its features and limitations for pressure control sequences. The individual results of feedback and feedforward control methods also demonstrates the necessity of combining the two approaches. Although the three control methods were discussed in detail in Chapter 5, a summary of each method is included in this chapter for the sake of continuity. The three control methods considered are: feedback; feedforward only and a combination of feedback and feedforward methods.

The next section describes the three control sequences which are used to test the performance of each control method. The sequences are common to a laboratory VAV control system and cover the normal modes of operation. The sequences are: pressure control; temperature control due to heating and the temperature control due to cooling. The final three sections cover the simulation results pertinent to each control method. For the sake of simplicity, the three control methods are initially tuned and the performance

is analyzed assuming that the valves and the dampers have linear characteristics having an authority, $a=1.0$. For the rest of the analyses, which include different authorities, operating points and non-linearity, the tuning values are then held constant. The objective of such an analysis is to illustrate the limitation of the feedback method to cope with system characteristics different from the linear characteristics assumed for tuning. The combination of feedback and feedforward, on the other hand, provides superior performance by capturing the operating characteristics over the entire range. This is a significant advantage in terms of enhancing performance of the lab environment while reducing operating and maintenance cost by avoiding downtime due to poor control. Since the feedforward algorithm is expected to provide the majority of the control signal needed, the feedback loop will only see a small steady state error. Hence, tuning will be simplified which will reduce commissioning cost. A closure at the end of the chapter summarizes the major findings.

6.1.1 Feedforward control:

The controller has an identification and a control block as shown in Figure 5.2. The identification block captures and updates the process characteristics based on the process input control signals and the measured variables. The identification block passes the updated characteristics periodically to the control block for control action. In this context feedforward control does have a feedback mechanism to compensate for the system change. The main difference between feedback and feedforward control, is that in feedback control the control output is entirely dependent on the error while in a feedforward controller the feedback mechanism only influences the

identification process. The disturbance is often measured and used in the identification process if it is cost effective and feasible to do so.

6.1.2 Feedback control:

The feedback controller uses the error between the setpoint and the measured variable as input. The most common approach of employing feedback is the traditional linear Proportional-Derivative-Integral (PID) algorithm. In a PID controller, the tuning parameters are derived for a specific operating range. Feedback control is simple to implement and performs well as long as the operating range and the setpoints do not vary significantly. The linear PID controller does not perform well for non-linear systems. In most HVAC applications, however, derivative control adds unneeded complexity and tuning difficulty (Haines and Hittle 1983). A well tuned PI can achieve the desired response without the needed derivative control action. The PI algorithm is selected for simulation and comparison with combined algorithm for the sake of simplicity.

6.1.3 Combination of feedforward and feedback control:

The aim of the feedforward-feedback combination topology is to generate the majority of the control signal from the feedforward block so that the feedback block only deals with a small steady state error and thus requires little tuning. Unlike feedback, the loop acts only upon the setpoint value and does not require the measured value of the variable. As a result, the signal can enhance control speed in tracking the setpoint change.

6.2 Control sequences:

The three control sequences used to test the different approaches cover the entire domain of normal operation in a VAV laboratory systems. The pressure control sequence analyzes the pressure loop without considering the temperature consequences. The coupled pressure and temperature loop for heating represents the situations when the supply air has to be reheated locally to maintain both the room pressure and the temperature setpoints. The cooling sequence occurs when the rate of generation of internal heat dictates the quantity of supply air and the general exhaust damper is modulated. Each sequence is described with an aid of figures showing the cause of disturbance and the resultant effect due to the control actions.

6.2.1 Pressure control:

The room pressure is typically controlled in terms of a differential instead of an absolute value. The differential is defined as a difference between a reference space i.e. an adjacent corridor and the lab space. The goal in a lab is to keep the differential pressure positive within a range of .005 to .05 w.c.. This assures that the room pressure remains lower than the adjacent pressure under all operating conditions. By keeping the room pressure a bit lower than the adjacent space the leakage of lab air to adjacent spaces is prevented.

There are three common methods of room pressure control in use today: 1) direct pressure, 2) flow tracking and 3) cascaded control (as discussed in Chapter 1). However, each of the schemes essentially modulates the supply

flow in order to maintain the room differential pressure. Hence, a simple sequence is considered to assess the performance of different control methods for pressure control. A step change in the fume hood exhaust requires modulation of the supply air flow to maintain the differential pressure setpoint.

The thermal effect is decoupled from the pressure effect by assuming the temperatures of supply, exhaust and infiltration air are constant at 70 ^{o}F. The pressure control sequence is shown in Figure 6.1.

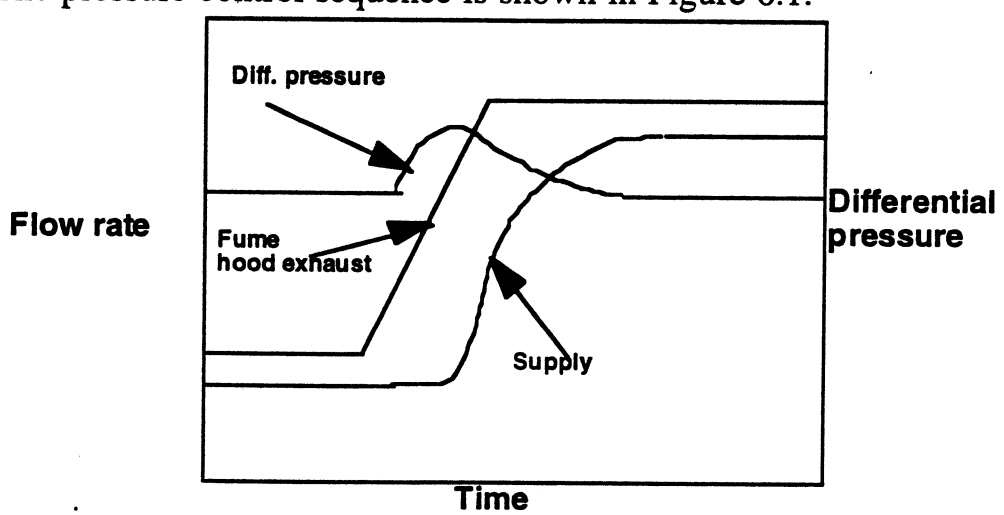

Figure 6.1: Pressure control sequence

From a steady state condition the fume hood exhaust jumps to a maximum value as the hood sash is opened. As a result, the lab pressure decreases which make the differential pressure go higher. The control senses the deviation between the actual differential pressure and the setpoint and opens the supply flow to return the setpoint.

6.2.2 Temperature control- heating:

The control sequence is shown in Figure 6.2. In most VAV applications, the supply air is discharged into the laboratory space at a constant temperature of 55 ^{o}F. Based on the normal design cooling load, the supply volumetric flow rate is selected to maintain the specified room temperature, usually a value between 70 and 75 ^{o}F.

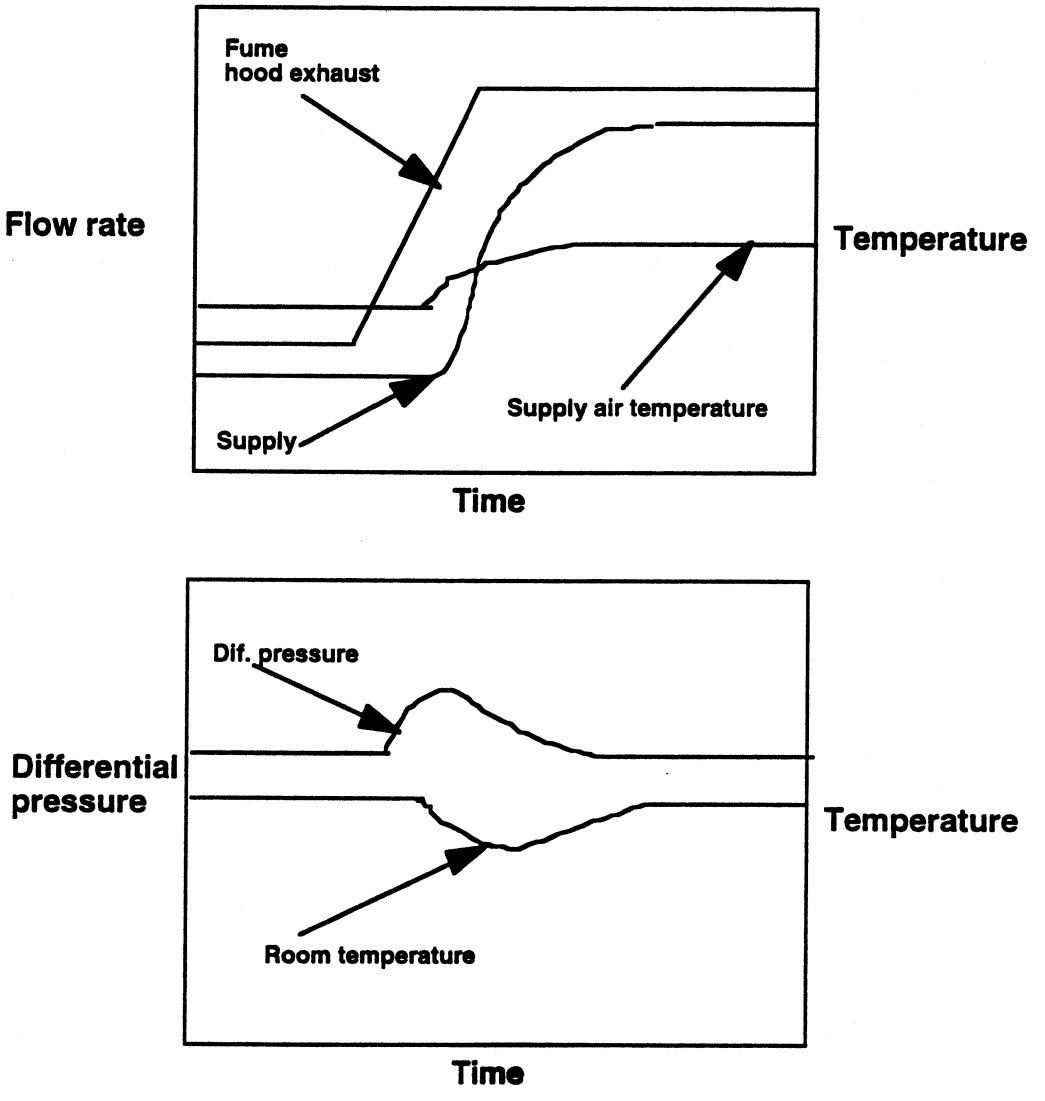

Figure 6.2: Temperature control- heating sequence

In order to maintain the differential pressure it is necessary that the minimum total lab exhaust exceed the supply flow rate due to the cooling demand. However, when the lab exhaust suddenly increases due to the fume hood sash opening, the supply flow rate also increases accordingly. The new supply flow rate at a constant 55 ^{o}F may exceed the requirement of the cooling demand. The room temperature, therefore, may drop below the setpoint. This sequence requires the local reheat valve to open and increase the supply air temperature to keep the room temperature setpoint. The coupling between room pressure and thermal constraints is complex.

6.2.3 Temperature control-cooling:

The final sequence represents temperature control as a result of cooling needs. The rate of internal heat generation is the primary disturbing force that activates this sequence. The internal rate of heat generation can increase by many fold due to other activities in a laboratory such as autoclaves, ovens and occupancy. When the internal generation suddenly increases, the room temperature rises. The only cooling source available is the supply air stream at 55 ^{o}F. However, the supply flow cannot be increased unless the exhaust flow is also increased in order to maintain the differential pressure constraint. But, the lab exhaust flow cannot be increased because that will upset the lab pressure. In order to circumvent this problem another source of the exhaust, i.e. general exhaust, is opened to allow an increased supply flow. By artificially increasing the total lab exhaust, both room temperature and the pressure setpoints are maintained. Figure 6.3 shows cooling sequence.

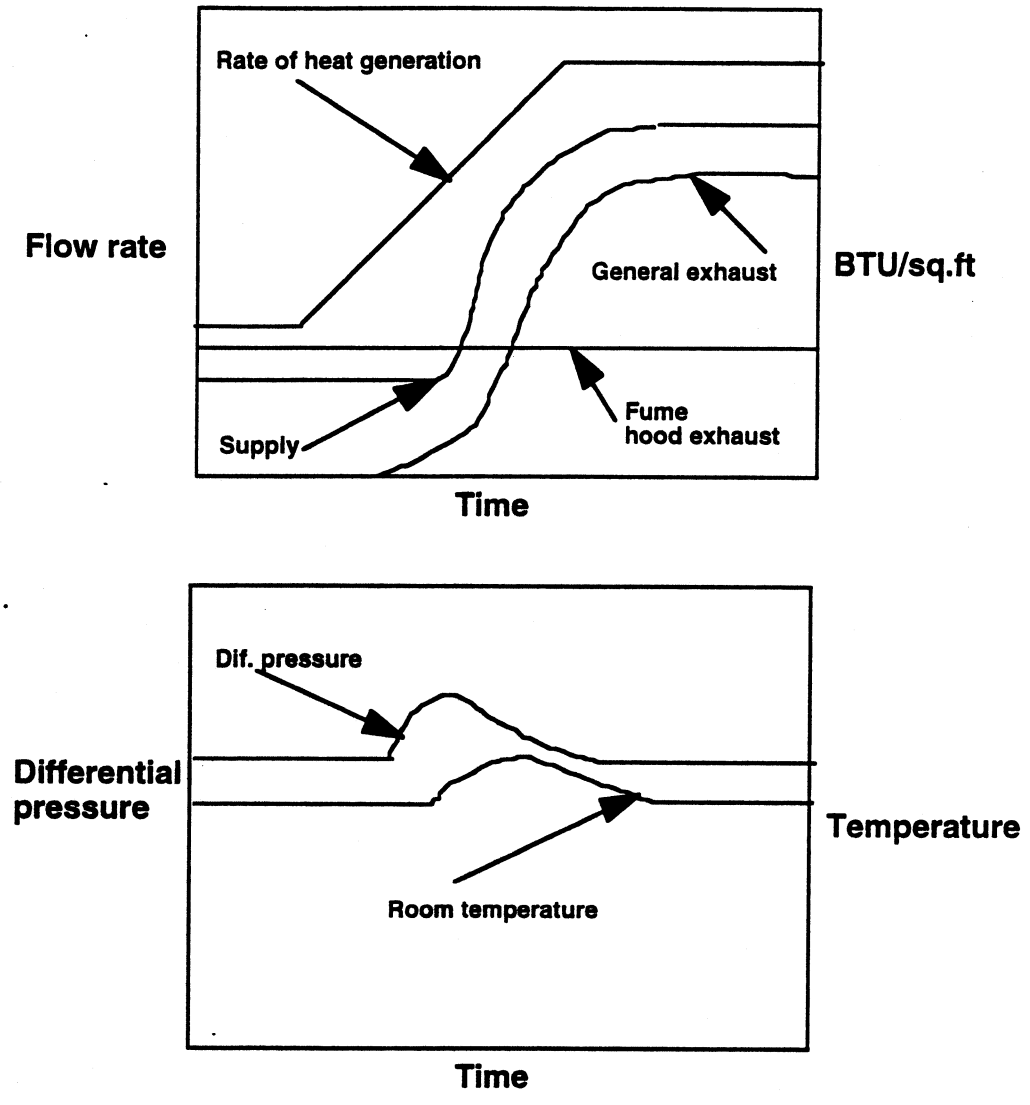

Figure 6.3: Temperature control- cooling sequence

6.3. Simulation and results - Pressure control sequence:

The proposed combination feedforward and feedback, referred to as FFPI hereinafter, is compared with feedback control method (i.e. PI control) for all of the control sequences described in section 6.2. For the sake of simplicity, a PI controller is chosen as a feedback method instead of PID. In

addition, open loop control, referred hereinafter as FF control, is also included for comparative analysis where appropriate.

Two forms of Proportional-integral control are considered here. One is a PI controller specifically suited for HVAC applications (Bekker et al. 1991) and the other one is based on a proprietary feedback controller (referred to as PPI hereinafter), typical of what being offered by the control vendors for HVAC applications. The Proportional-integral controller is selected since it was developed for HVAC processes that are commonly found in coils and valve/ damper actuators which are often modeled as first order linear system with delay. Such models are also assumed to represent coil and actuator dynamics as a part of the lab emulator described in Chapter 3 (Equations 3.27 and 3.34). The tuning of the PI control is based on the root-locus method. Using simulated results, the tuned PI controller is compared with the traditional tuning approaches of Ziegler-Nichols (1942) and Cohen-Coon (1953) methods. Based on the simulated results, the tuned PI controller based on root locus and pole cancellation methods performed better than the traditional methods of tuning.

The basic form of the PI controller is the same as Equation 5.3 less the derivative term and can be expressed as follows:

$$C_{s,m} = C_{s,m-1} + P_g(e_m - e_{m-1}) + I_g S_t e_m \qquad (6.1)$$

Where the gains P_g and P_i are tuned as per the following equations.

$$I_g = \frac{1}{d_t S_g} e^{-1} \tag{6.2}$$

and

$$P_g = \frac{\tau}{d_t S_g} e^{-1} \tag{6.3}$$

For a given first order system, the system gain, S_g, the delay time, d_t, and the time constant, τ can be found easily from the open loop response of the process. The pneumatic actuators which are used for lab environments usually respond within a couple of seconds from closed to fully open position (Landis & Gyr 1994). In order to achieve such response time, the dead time and time constant are adjusted and the resultant response curve is shown in Figure 6.4. Such a response curve is used to tune the PI controller (Mollenkamp 1981).

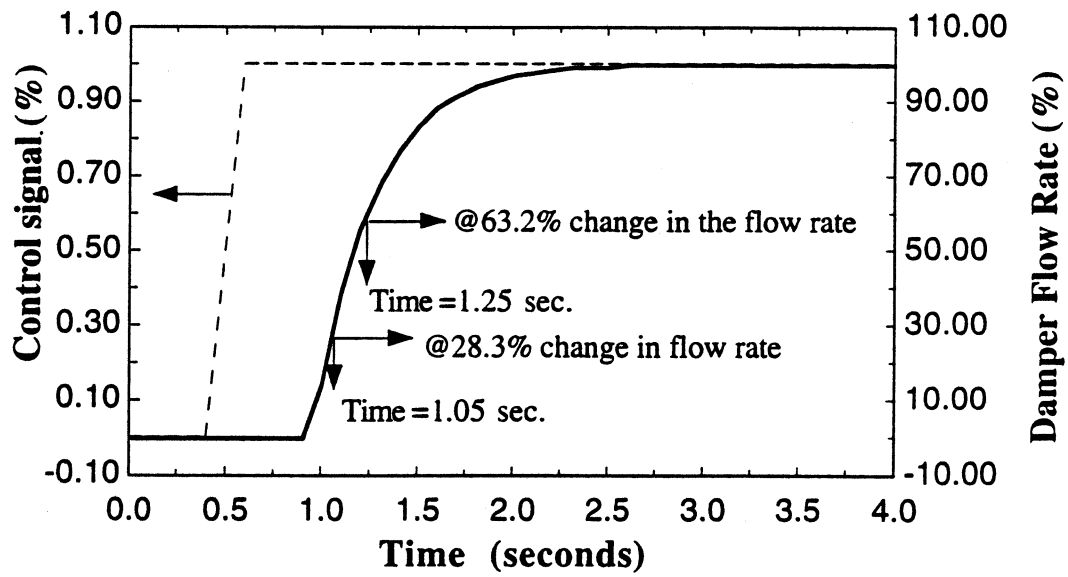

Figure 6.4: Open loop response of a linear damper/actuator

The system gain is defined as the ratio between the change in the output variable to the input variable. In Figure 6.4, the change in the input variable (i.e. control signal) is changed from 0% to 100% resulting in a change of 100%. The corresponding change in the output variable (i.e. flow rate) is the same for a linear damper. Hence, the system gain, S_g, is 1.0. The time constant, τ, is the time the output variable takes to reach 63.20% of the final value less the delay time. Hence, by definition and by noting the time to reach 63% change, from Figure 6.4, the sum of delay and time constant is,

$$\tau + d_t = 1.25 \; sec. \tag{6.4}$$

Similarly, another expression for 1/3 of time constant, can be written as time the output variable takes to achieve 28.3% of the total change excluding the delay time. Noting this time to be 1.05 seconds the relation is

$$\frac{1}{3}\tau + d_t = 1.05 \; sec. \tag{6.5}$$

Solving equations 6.4 and 6.5 yields, τ=0.3 seconds and d_t=0.95 seconds. Inserting these values along with S_g into equations 6.2 and 6.3, the controller gains are obtained as, P_g=0.116 and I_g=0.387.

Further fine tuning, by trial and error, was necessary to make the loop respond without undershoot or overshoot and to achieve good response performance comparable to the response obtained from FFPI controller. The final values of the tuning parameters are P_g=0.188 and I_g=0.617.

The simulation sample time is chosen to be 0.1 seconds based on the current state-of-the-art HVAC process controllers (Landis & Gyr 1994). Any faster processor for HVAC process may become cost prohibitive. The simulation sample time is adequate compared to the time constant of 0.3 seconds as usually 2-3 samples in a time constant is usually used for a digital controller (Dorf 1980). The simulation sample time of 0.1 second means about 17-18 samples during end-to-end damper stroke which is also adequate according to the published literature (Haines and Hittle 1983; Weaver 1983).

The PPI loop algorithm considered is a proprietary system offered by most of the control system vendors. The system operator are usually given a loop tuner to tune the control loop by providing information obtained from the open loop response. One such control loop is used here (Landis & Gyr 1988) as a black box and tuned using a loop tuner just as done in the field.

As in the case of FFPI, the flow setpoint is also determined by solving steady state mass conservation Equations 6.6 and infiltration equation 6.7 in both PI and PPI control loops. The supply flow setpoint can be calculated for a temperature setpoint of 70 ^{o}F and a room pressure of 407.95 w.c. or Δp (P_{ad}-P) of .05 w.c. The other variables in Equations 6.6 and 6.7 are known quantities.

$$\frac{P_S \dot{v}_S}{RT_S} + \frac{P_{ad}\dot{v}_{ad}}{RT_{ad}} - \frac{P\dot{v}_e}{RT} = 0 \qquad (6.6)$$

$$\dot{v}_{ad} = k(\Delta p)^n \qquad (6.7)$$

Once the supply flow rate setpoint, $\dot{v}_{s|sp}$, is known, then a conventional PI or PPI loop can be utilized to achieve the flow setpoint. This is a significant shift from the traditional approach in which the flow setpoint is determined by assuming a fixed difference between the lab exhaust and supply flow setpoint. Hence, by knowing the total lab exhaust setpoint, the supply flow setpoint can be easily calculated. The traditional method is known as volume tracking and has serious limitations as often the difference in flow is assumed based on experience as illustrated in the published literature (Ahmed 1993; Ahmed et al. 1993). The limitations include over or under pressurization of the lab space if the difference in flow is selected incorrectly. The FFPI and PI/PPI control strategy models, as used in the simulations, are shown in Figures 6.5 and 6.6.

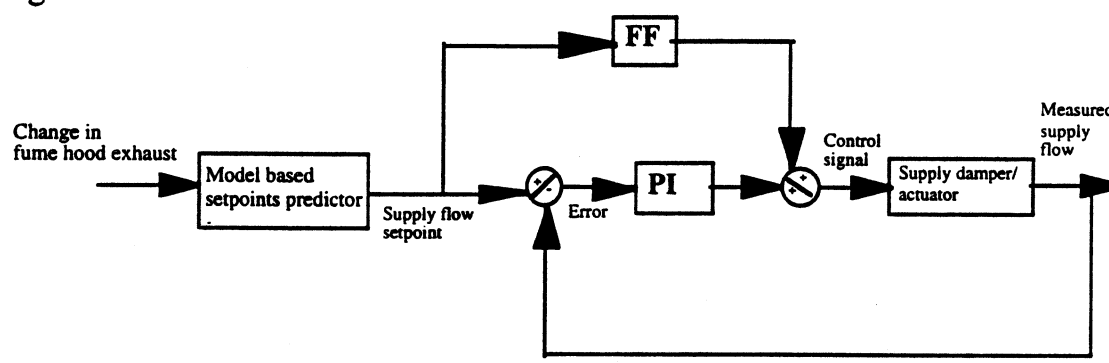

Figure 6.5: Schematic of FFPI for pressure control sequence

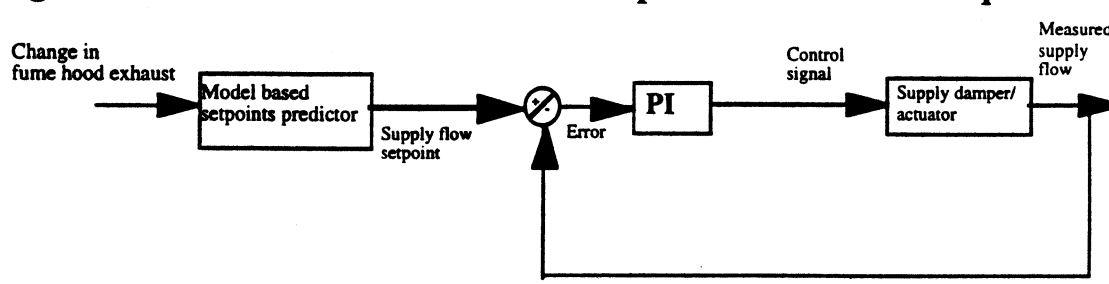

Figure 6.6: Schematic of PI and PPI for pressure control sequence

In the case of FFPI control, for a known supply flow rate setpoint, the identified damper characteristics are used to generate the required control signal. The combined FFPI approach uses a PI control loop in conjunction with the loop to eliminate the steady state error. The PI or PPI control loops only work with the error between the setpoint and the simulated flows.

6.4 Simulated results:

Control systems are judged on accuracy, robustness, stability and ease of implementation. The ease of implementation is important in for keeping the commissioning cost down, and is often a major factor for an owner in selecting a specific control method for a given application. A lab control system should be capable of keeping the lab environment under tight control under a wide range of operations. Failure to do so translates into significant cost to the owner as the lab needs to be shutdown and requires maintenance. This is specially true in a research or process lab where inadequate environment conditions may cause a loss in productivity.

The three control methods were simulated and compared considering six different damper characteristics and operating points. Three were for a linear damper with different authorities. Typically, a linear damper is installed in a job but it hardly stays as linear since the authority changes with varying system flows. The other cases are based on non- linear damper characteristics and under different operating conditions. In equation 3.32, the term W_f represents the linearity. A value of 1.0 for W_f indicates a linear

damper whereas 0.5 means a true exponential damper. A W_f of 0.5 is chosen for non-linear damper while the authority varied between 0.1 and .01. The five damper characteristics are shown in Figure 6.7.

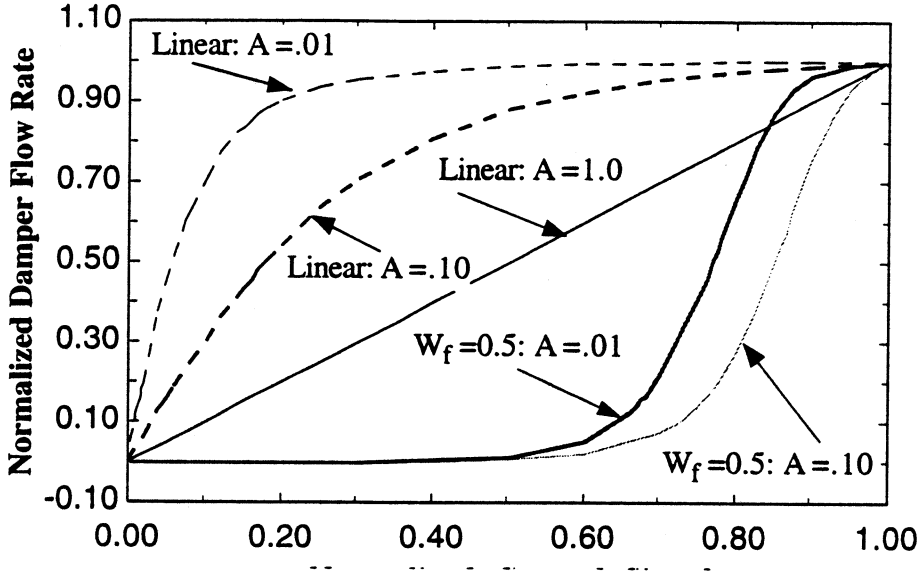

Figure 6.7: Damper/valve characteristics for simulation

In case of laboratory pressure control, the change in fume hood flows are considered to be the disturbance function. Two different disturbance sequences were considered for the simulations. First, the total lab fume hood exhaust flow is reduced from a maximum of 2400 cfm to 500 and then increased to 2400 cfm again. The corresponding supply flow rates to maintain a space temperature of 70 ^{o}F and Δp of .05 w.c are 2257 and 357 cfm.

After comparing results for this sequence and noticing that at the maximum flow the operating point is more or less same for different damper

characteristics, another operating point was selected as the mid- point between the minimum and maximum flows i.e. 1450 cfm. Both sequences are shown in Figure 6.8. The results are discussed for each simulation case.

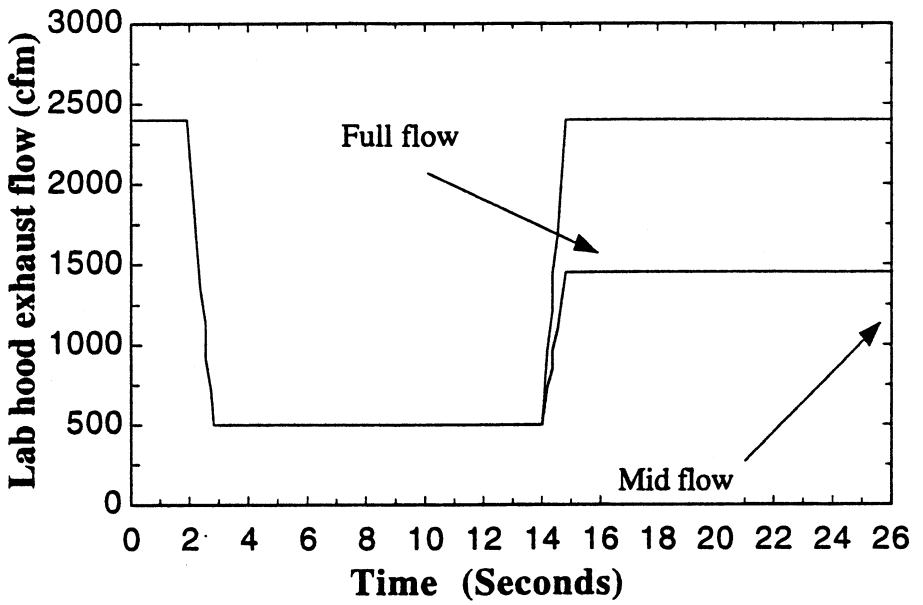

Figure 6.8: Disturbance in lab exhaust flow for pressure control

Case P1: Linear damper with an authority of 1.0

All of the different control loops are tuned for this case. This assumption is appropriate since HVAC control equipment manufacturers usually calibrate and supply the valves, dampers and actuators as linear. Also, during the commissioning process they are usually tuned at fully open positions. As a result the pressure drop across the control equipment is maximum and authority achieves a value close to unity. This is logical since during tuning each damper usually is fully opened and tuned one at a time. Hence, the system pressure loss is mostly due to the pressure loss in the branch which

has the damper to be tuned, resulting the authority close to 1.0. The combined approach, FFPI is also tuned for this case. The P and I gain are relatively very small for FFPI loop compared to the PI or PPI loops. Appendix A2 lists tuning parameters for different control loops for various sequences.

All of the control loops for case P1 perform exceedingly well. The responses of room differential pressure, Δp, are shown in Figure 6.9. The responses seem reasonable for the given disturbance in fume hood exhaust flow that was illustrated in Figure 6.8. As the fume exhaust flow suddenly decreases at the start of the sequence, the differential pressure ($\Delta p = P_{ad} - p$) momentarily becomes negative which means that the room remains at a higher pressure than the adjacent room until the supply flow reduces to match the exhaust flow for the correct differential. The reverse takes place when the fume hood exhaust is increased from a minimum flow. Both the PI and PPI have zero offset under steady state and the under and overshoots are very comparable to those for FF and FFPI approaches.

In case of open loop control (FF), considerable offsets are noted for both sequences when the room pressure becomes positive as a result of sudden decrease in the fume hood exhaust flow and vice versa. However, using the combined loop, FFPI, the offsets are eliminated while the response time and the under and over shoots remain the same.

Case P2: Linear damper with an authority of 0.1

The authority has been changed here from 1.0 to 0.1 while other simulation parameters remain the same. Figure 6.10 shows that the performance of PI controller remains unchanged with respect to the response time when compared to A=1.0 except that the undershoot has increased. The PPI fails to achieve the setpoint at the minimum flow condition. At the maximum flow condition, both the stability and the setpoint are achieved. The open loop response remains similar to that with an authority of 1.0 and shows both over and undershoots. The response of FFPI loop is good with zero offset and a quick response.

Case P3: Linear damper with an authority of 0.01

The responses of different control loops are shown in Figure 6.11. The results show that the PI controller in this case becomes unstable at the low end of the flow, as was the case for the PPI for A=0.1. The stability problem also occurs for the PPI control loop for this case. For both of these feedback loops, the controller seems to do much better when the flow is increased. As expected, the FF loop reacts rapidly but has offsets. The combined loop, FFPI, eliminates such offsets and responds very quickly.

In this case with the decrease in the flow setpoint from 2400 to 500 cfm, the Δp undershoots almost to -1.00 w.c. for both FF and FFPI loops compared to -0.75 w.c. in case of A=1.0 (Case P1). Such a significant undershoot can be explained. The damper is modeled as a linear first order differential

equation with time constant, τ_{act} and dead time t_o as shown in Chapter 3 (Equation 3.27) and repeated below for ease of understanding.

$$\tau_{act}\frac{dr_{ac}}{dt} + r_{ac} = r_{sp,(t-t_o)} \tag{6.7}$$

The solution for the above differential equation can be expressed as

$$r_{ac} = br_{ac,(t-t_o)} + (1-b)r_{sp,(t-t_o)} \tag{6.8}$$

Where,

$$b = e^{-(\frac{S_t}{\tau_{act}})} \tag{6.9}$$

The command signal, r_{ac}, to the actuator in Equation 6.8 is obtained by adding two terms: The first term is a product of a constant exponential term b and the command signal sample taken t_o time before the current sample time. The second term is a product of a constant exponential term 1-b and the command signal setpoint taken t_o time before the current sample time. Equation 6.8 clearly shows that for a given value of b, the actuator response will be slow if the difference between the actuator setpoint and the current command signal is large and vice versa.

As the flow setpoint reduces from 2257 to 357 cfm (i.e. 98% to 15%), the required control signal setpoint to produce 15% flow found to be about .016 for A=.01 whereas the value is 0.15 for A=1.0 (Figure 6.7). Hence, the difference between the current actuator command signal, r_{ac} and the setpoint, r_{sp} is larger for an authority of .01 than for the authority of

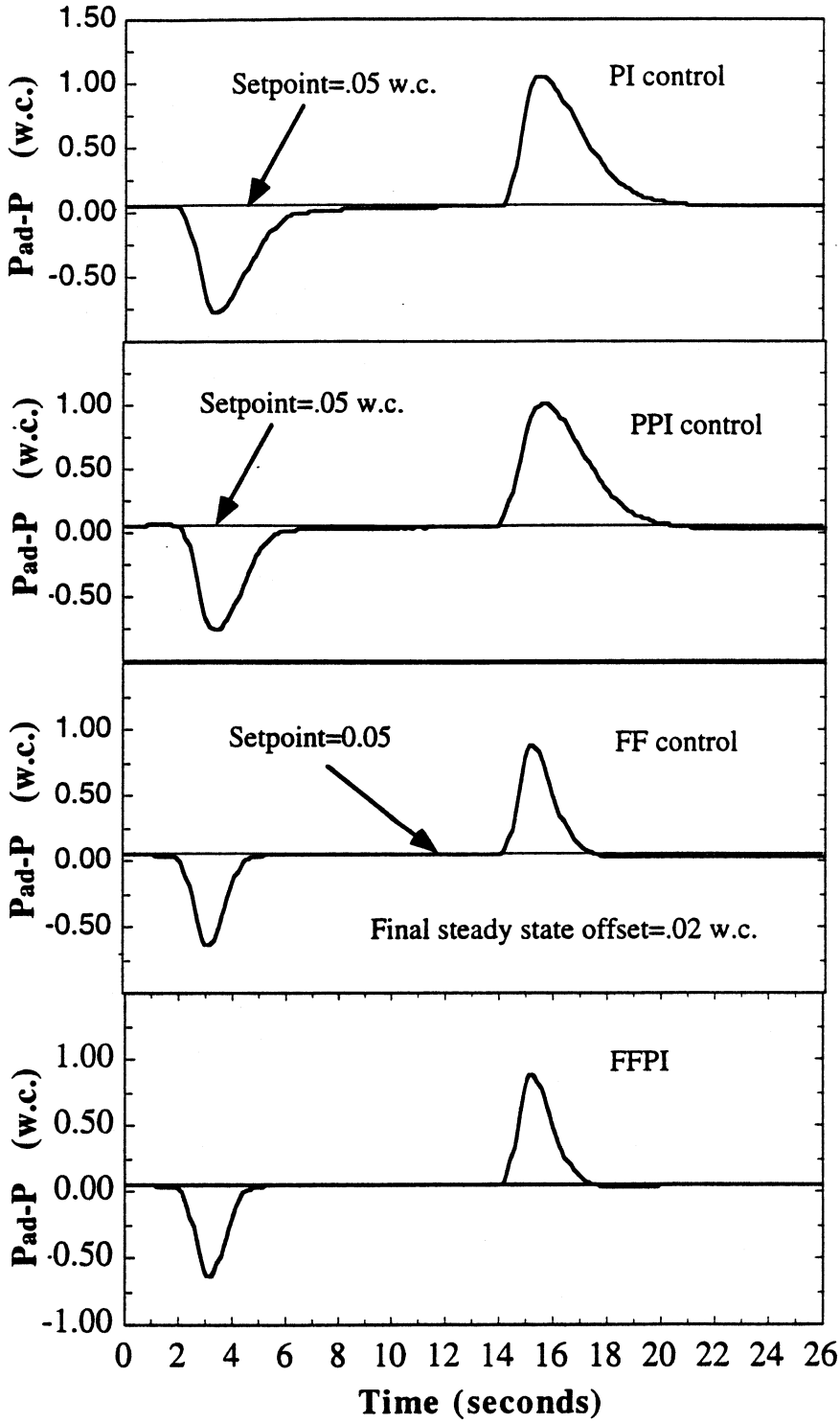

Figure 6.9: Dynamic pressure response for control sequence P1

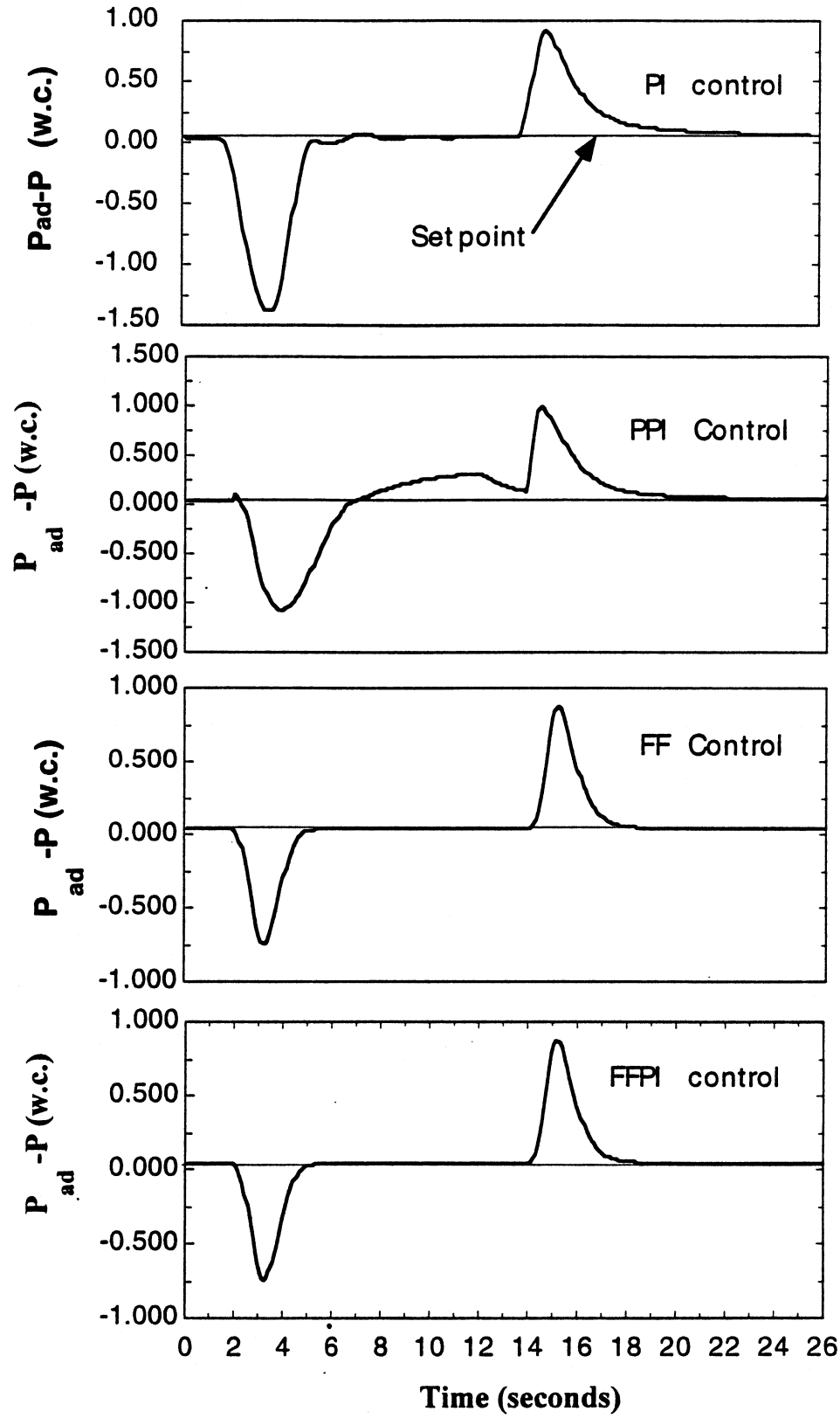

Figure 6.10: Dynamic pressure response for control sequence P2

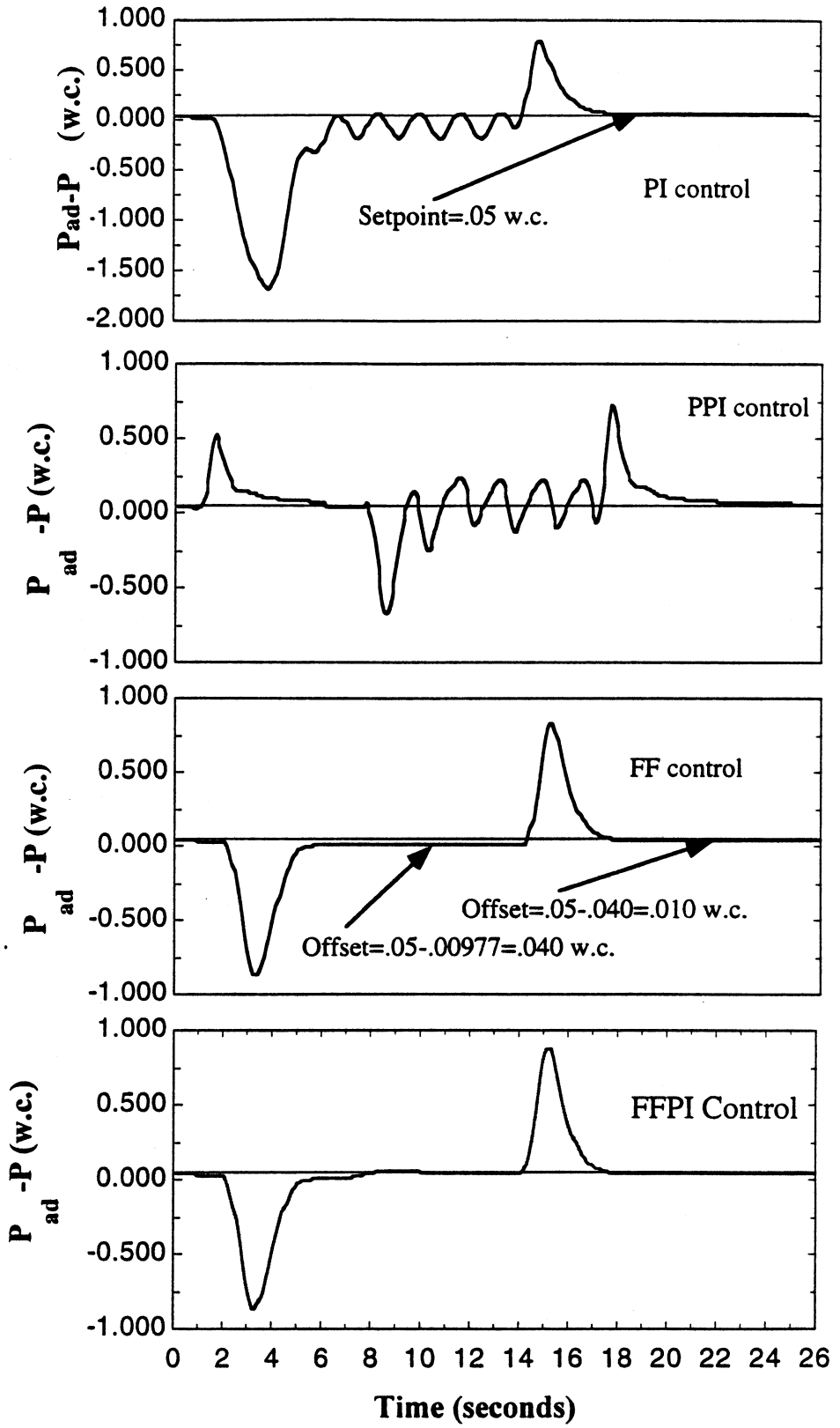

Figure 6.11: Dynamic Pressure Response for Control Sequence P3

A=1.0. The flow response, therefore, is slow for a damper having A=.01 when the flow setpoint is decreased. Due to the slow response, it takes a longer time for the damper/ actuator to reach the low flow position. As a result the lab becomes highly positively pressurized causing a larger undershoot in Δp. The slow response is shown in Figure 6.12.

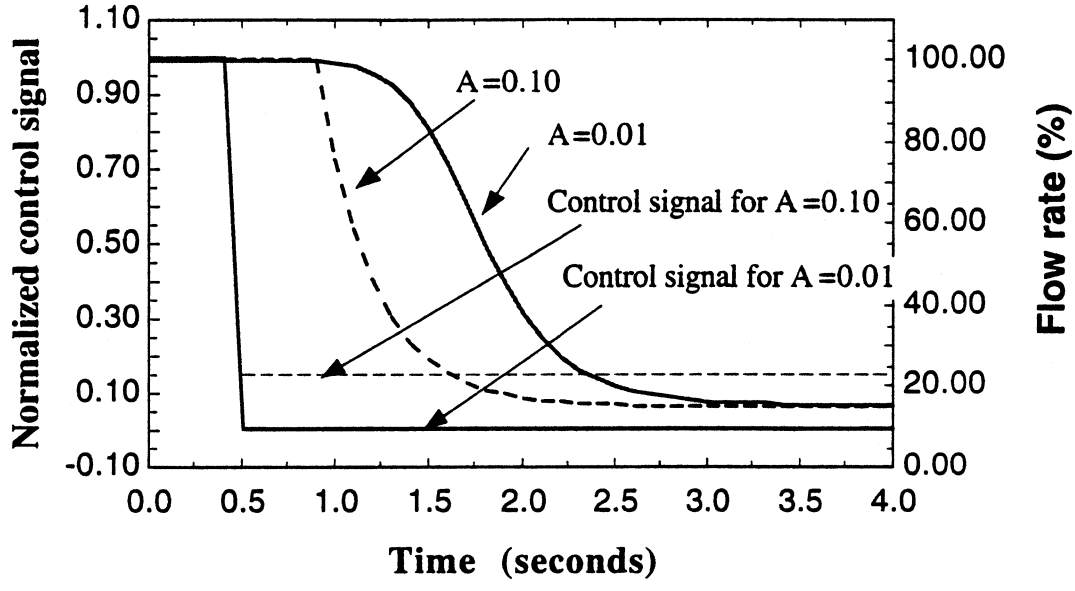

Figure 6.12: Response of supply flow for a linear damper

Case P4: Non-linear damper, W_f= 0.5, A=.1

In last three cases, P4, P5, and P6, a non-linear damper is considered instead of a linear damper. In Chapter 3, as a part of damper model, the damper non-linearity parameter appears in the expression for the damper flow-resistance coefficient (Equation 3.32) which is again shown in Equation 6.9.

$$K_{23} = \frac{W_f K_o}{[(1-\lambda)r+\lambda]^{2.0}} + (1-W_f)K_o\lambda^{(2r-2)} \qquad (6.10)$$

A value of Wf 1.0 represents a linear damper whereas a value of 0.0 indicates a true exponential damper. It is possible for a linear damper to exhibit the non- linear characteristics due to mechanical problems. For simulation purposes, a Wf of 0.5 is chosen.

Figure 6.13 shows the response curves for various control loops.The PI in this case shows stable control while PPI loop shows instability as the exhaust flow is decreased from 2400 to 500 cfm. In this case, the combined approach works well in providing good stability and eliminating the steady state offset observed for FF control loop.

Case P5: Non-linear damper, Wf= 0.5, A=.10, flow increased to 1450 cfm.

A test was performed to evaluate the performance when the flow was increased to a midrange value of 1450 cfm instead the full range of 2400 cfm. The objective here is to observe the controller performance for an operating point which lies on the non-linear portion of the damper curve for A=0.1 (Figure 6.7) and which deviates considerably from the corresponding point on a linear characteristics. For example, a flow of 1450 cfm is about 60% of maximum flow. Hence, for a linear damper/actuator, a control signal of 60% is required to achieve 1450 cfm. However, referring Figure 6.7, a control signal of about 22% is require to generate 1450 cfm for a damper with an authority of 0.10.

The results on Figure 6.14 show that the PI controller still performed well when the exhaust flow is decreased. In fact, the undershoot in Δp is considerably less compared to Case P2 under the same condition of decrease in the exhaust flow rate. As the exhaust flow increased in the mid-range, severe instability is observed with the PI loop as expected as the damper is operating within the non- linear portion of the damper curve (Figure 6.7). The PPI remains unstable throughout the entire sequence. The combination FFPI controller shows good trends while the PPI control loop remains unstable throughout the entire control sequence.

Case P6: Non-linear damper, Wf= 0.5, A=0.01, flow increased to 1450 cfm.

The last case is considered by assuming an authority of 0.01 for a non-linear damper. The resultant highly non- linear damper characteristics is shown in Figure 6.7. PI loop shows stability when the exhaust flow is decreased while instability is noted when the exhaust flow is increased from the minimum to the midrange. PPI control loops show significant stability problem throughout the simulation while the FFPI achieved same results as before providing stability, fast response, accuracy and zero offset error under steady state. The pressure response for different control loops are shown in Figure 6.15.

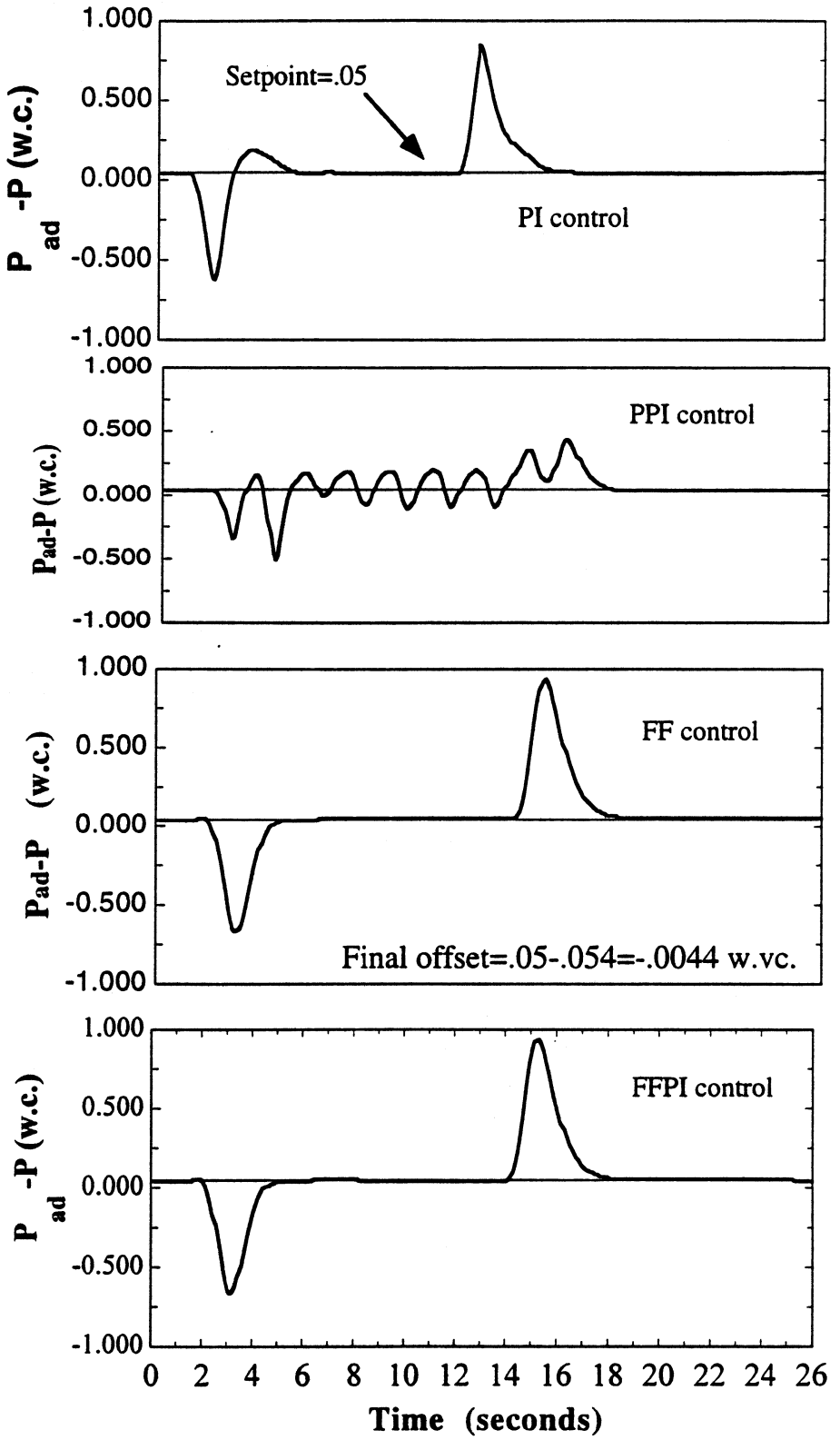

Figure 6.13: Dynamics Pressure Response for Control Sequence P4

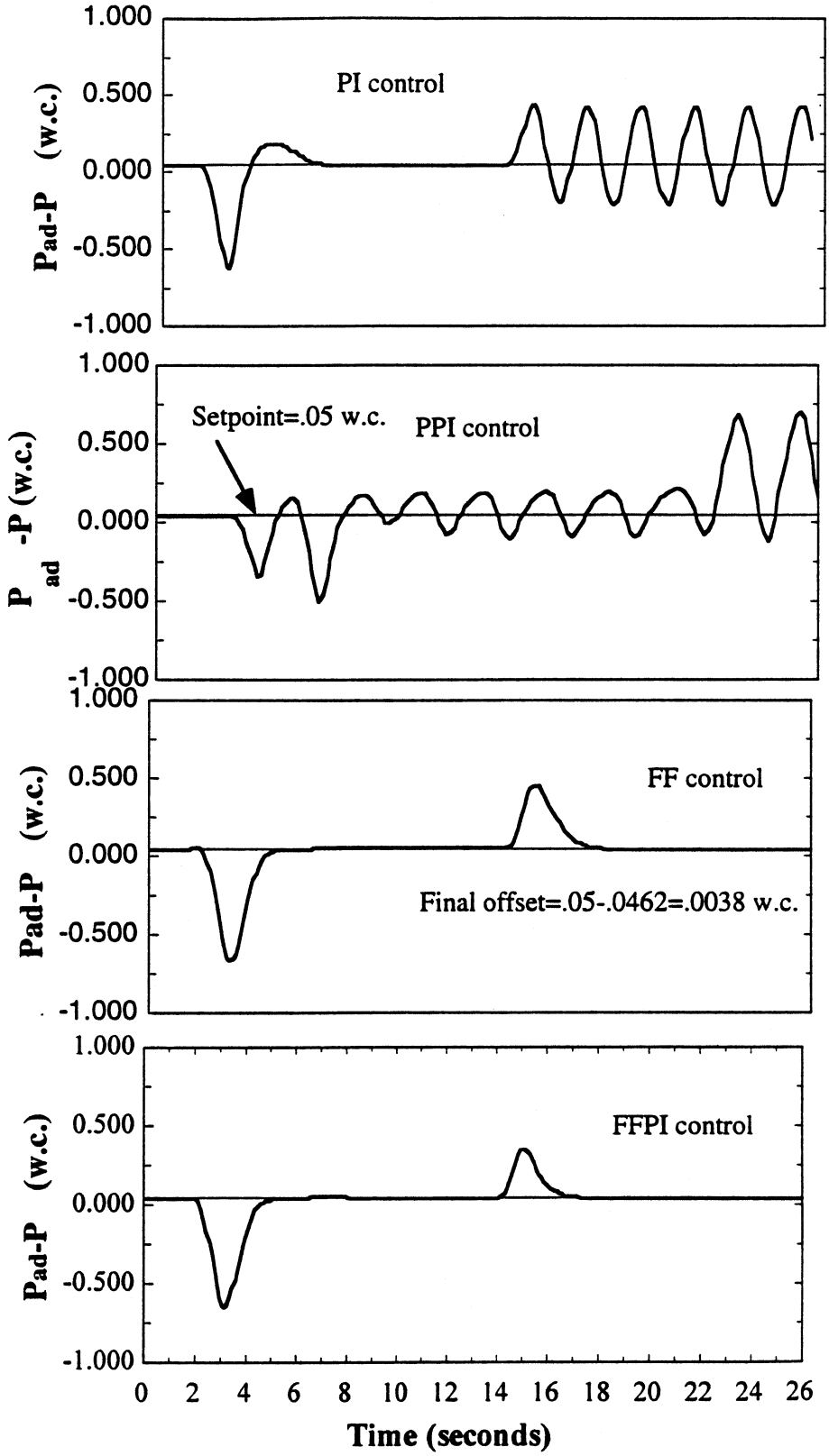

Figure 6.14: Dynamic pressure response for control sequence P5

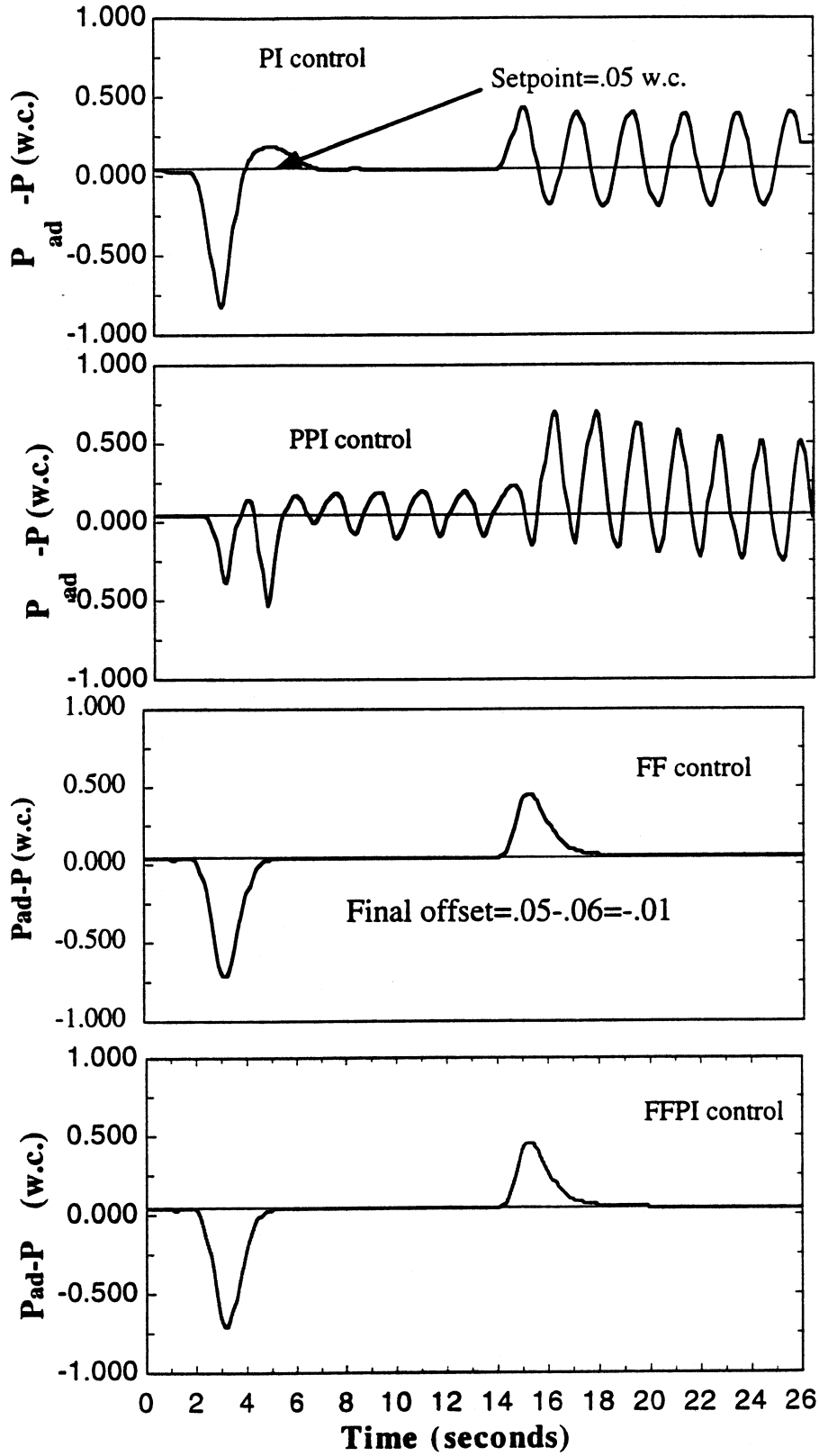

Figure 6.15: Dynamic Pressure Response for Control Sequence P6

6.4 Simulation and results - Temperature control: Cooling sequence.

Based on the observed results obtained from the pressure control sequence, the following changes were made for this sequence:

1. Only three damper curves are considered: linear; non-linear (W_f=0.5) with an authority of .01 and linear damper with an authority of .01. Along with the linear, two extreme damper characteristics (Figure 6.7) were thought to be sufficient enough to test the various control loops.
2. Only PI and FFPI control loops are considered since the PPI control loop failed to perform better than PI for all pressure control sequences. The response of FF control loop was very predictable in terms of having offset from setpoints and providing stability.

For the temperature control loops, the simulation sample time is selected to be 10 seconds instead of the 1/10 sec. considered for the pressure control loops since the room thermal time constant is found to be about 4 minutes instead of 1/3 of a second as for the flow loop. The room temperature response under an open loop test when supply flow rate at 55 ^{o}F is increased to maximum is shown in Figure 6.16. The room thermal time constant is determined from the open loop response in a similar way as described before in determining supply flow time constant (section 6.3). A sample time of 10 seconds means 24 samples in a ime constant which should be more than adequate for a digital controller. Any smaller sample time poses the problem of storing massive amount of data necessary for simulation considering the entire simulation period for temperature control which extends to more than

an hour. A long simulation period is necessary to ensure that the steady state is reached after a disturbance is introduced.

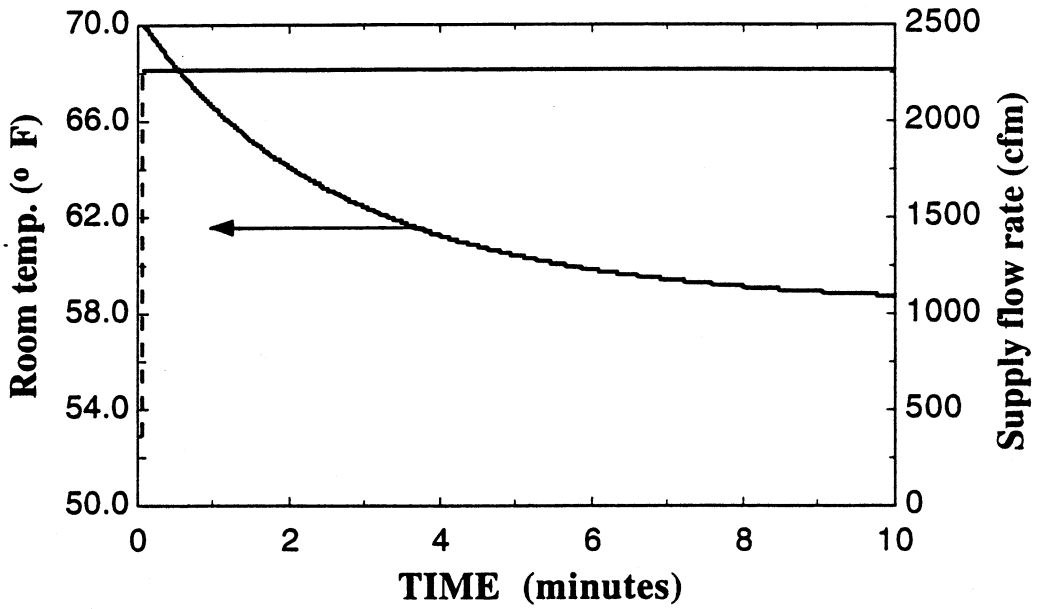

Figure 6.16: Open loop response of room temperature due to cooling

However, choosing a large sample time posed a problem with the pressure control loop. The time derivative of pressure became so large for a large sample time, that the simulation failed to converge. In order to resolve such problems, the time derivative of pressure was ignored and the transient energy and mass balance equations (i.e. Equations 3.6 and 3.11) are rewritten as

$$V\left[-\frac{P}{T^2}\frac{dT}{dt}\right]=\frac{P_S\dot{v}_S}{RT_S}+\frac{P_{ad}\dot{v}_{ad}}{RT_{ad}}-\frac{P\dot{v}_e}{RT} \qquad (6.11)$$

$$\frac{P_s \dot{v}_s}{R} c_p + \frac{P_{ad} \dot{v}_{ad}}{R} c_p - \frac{P \dot{v}_e}{R} c_p + \dot{q}_{gen} + \dot{q}_{tr} = 0 \qquad (6.12)$$

The assumption is justified from practical sense since in reality the fast flow loops will always achieve the setpoint before the next room temperature is sampled in a slow room thermal loop. To ensure that the flow loops will act much faster than the room thermal response, the ratio between the sample time and time constant in the exponential term, b in the solution for damper command signal (Equation 6.8 and 6.9) is chosen to be 3.30. As a result, the damper command signal in the next sample time will be almost equal to the damper command setpoint, r_{sp}.

The change in the rate of internal load is the main cause or disturbing function for cooling. Figure 6.17 shows two internal load curves used in the simulation.

In the first case, the generation has increased five fold from its initial value of 85.50 to 425.0 Btu/min while in the second case, the internal load is decreased by same proportion. The five fold change in the rate of internal heat generation within seconds is common in a lab environment as noted in Chapter 1 and 2.

The flow setpoints of general exhaust and consequently of supply are determined using steady state energy, mass and infiltration equations. The energy equation contains a room load term which is calculated based on the room air temperature and the supply flow rate at the preceding time step t-1.

The details of supply flow rate determination and the prediction of room load are discussed in Chapter 5.

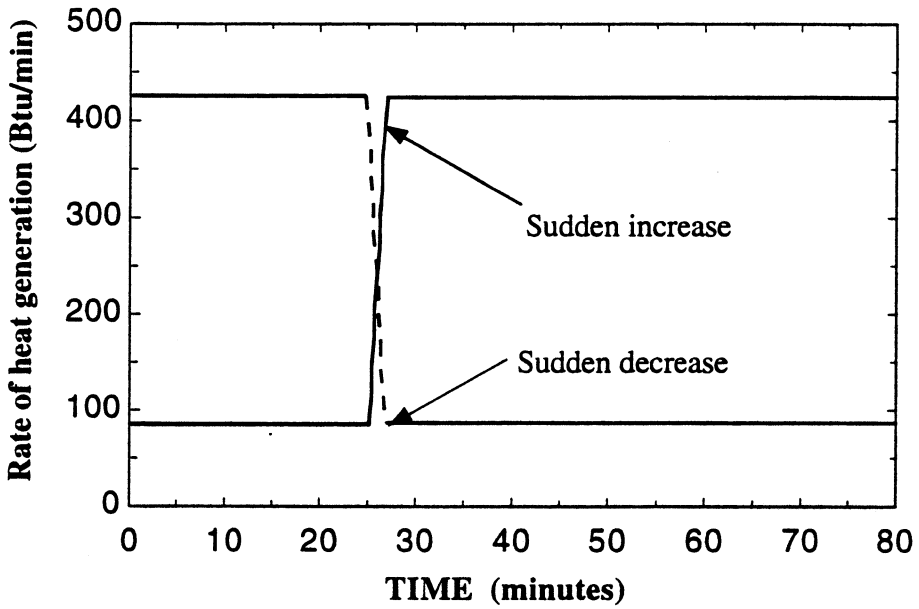

Figure 6.17: Disturbance in the rate of heat generation for cooling sequence

Once the setpoints are known, the FFPI control loop employs the combination of feedforward and feedback approaches to reach the setpoint whereas the PI control loop uses only the feedback approach. The schematics of both FFPI and PI control loops are shown in Figures 6.18 and 6.19 respectively.

The success of both methods largely depend upon the accuracy of load prediction. Since the predicted load is calculated based the previous samples of room temperature and flows, which then influences the flow setpoints for next sample, any significant deviation from the room conditions will be propagated faster via the predicted load.

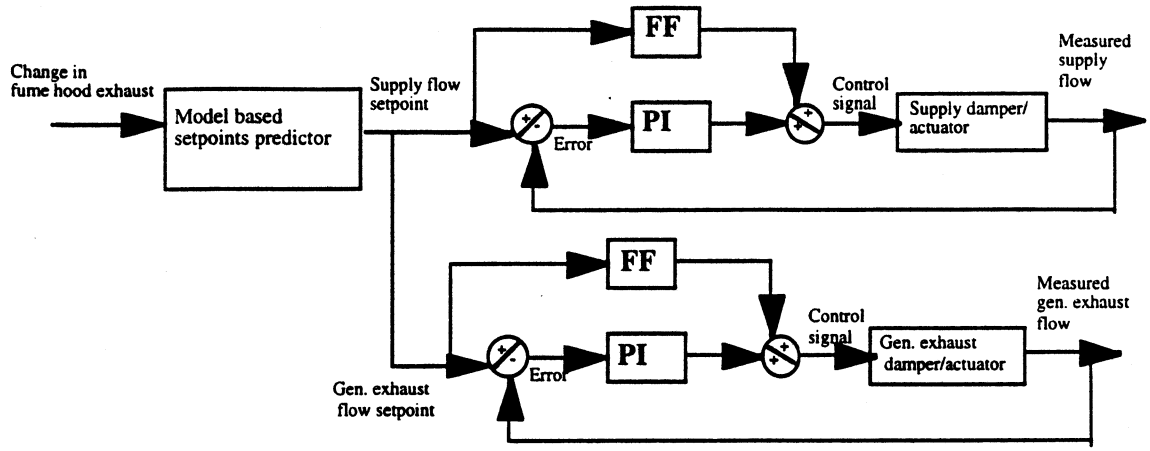

Figure 6.18: Schematics of FFPI for Temperature control- cooling sequence

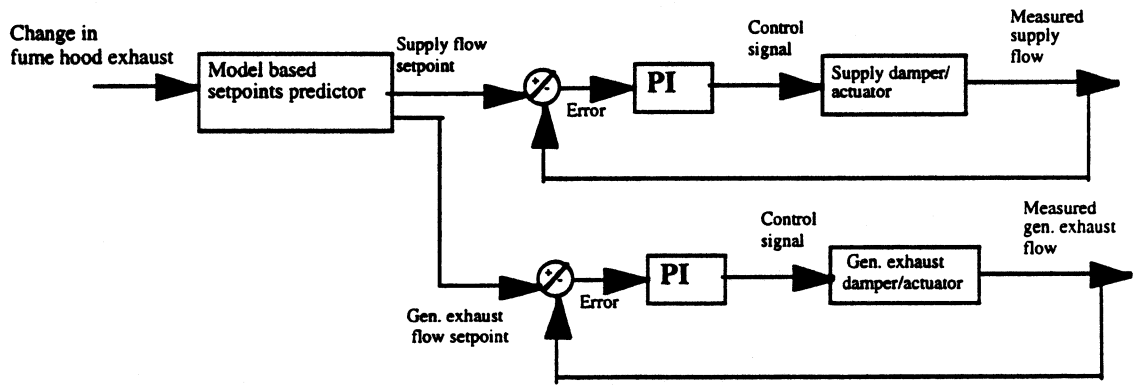

Figure 6.19: Schematics of PI for Temperature control- cooling sequence

Due to the presence of dual coupled control loops the operation of the control sequence is complicated compared to the pressure control. The tuning of two PI control loops also becomes complicated. In industry, instead of using the physical model, another PID is employed to determine the setpoint which further complicates the tuning process. To avoid such a complication, it was decided to use the model based setpoints for the PI loops as well for simulation. The PI and FFPI are then compared on the same basis

of controlling the dampers. At the end of this chapter a comparison is made between PI control loop using PID for setpoints with the FFPI approach.

CASE C1: Linear damper with an authority of 1.0

In cases C1, C2, and C3, a sudden increase in the rate of internal heat generation is imposed as a disturbance. Referring to Figure 6.17, it should be noted that at time t=0, there is a sudden increase in the load from 85 Btu/ min to 445 Btu/ min at time t= 25 minutes. Both PI and FFPI control loops are tuned for the linear damper/actuator characteristics. The tuning process was the same as explained before in discussing the pressure control sequence (section 6.3). The general exhaust damper flow loop was tuned first followed by the supply flow loop. The tuning of FFPI loop was relatively straightforward and simple with very small gains compared to the tuning of the PI control loop which was complex and time consuming. The supply and general exhaust characteristics are assumed to be the same in each case. Once tuned, the loop parameters are kept unchanged for other cases.

Figure 6.20 illustrates the temperature response for both PI and FFPI control loops. Also included are the simulated and predicted loads to indicate that the predicted load agreed extremely well with the simulated load. The simulated load is calculated by adding the known internal load term and the calculated wall heat transfer. A good load prediction is a precondition of achieving good control. Both PI and FFPI performed very well in terms of setpoint tracking accuracy and response time. While the PI control loop quickly settles to the desired setpoint of 70 ^{o}F, the settling is very gradual in

the case of FFPI. However, the FF part of the loop brings the room temperature within 0.5 ^{o}F very quickly, leaving only a small residual to be slowly handled by the PI component of the combination loop.

Case C2: Linear damper with an authority of .01

In this case the non- linear damper characteristic is assumed for both supply and general exhaust damper. The result for PI control is in Figure 6.21 and shows poor performance. The room temperature continues to fall when an initial load is imposed followed by an oscillations in the room temperature due to the sudden increase in the load. The room temperature initially falls due to an overshoot in general exhaust flow. As a result, the predicted load also overshoots which calls for more cooling and causes the room temperature to fall further. The FFPI control loop showed remarkable results in holding the temperature within a narrow range of 1 ^{o}F. The predicted load matched with the simulated load very well. For PI control, the predicted load is intentionally not shown as it demonstrates significant cycling. Cycling supply flow rate contributes to noise and equipment failure, a often observed effect of poor HVAC control (Blazier 1993; Cerami 1996).

C3: Non-linear damper with W_f=0.5 and an authority of 0.01

In this case the PI control is able to respond very well to the initial load but shows poor control as the load suddenly increased by five fold as shown in Figure 6.22. The FFPI control managed to control very well throughout the simulation period. The supply flow rate plots for both control loops are

shown in Figure 6.23 which clearly indicates that the supply flow essentially cycles between the maximum and minimum flows.

These types of situations will be completely unacceptable and demonstrate total failure of the control loop. In contrast, the supply flow response for FFPI loop is stable and tracks the desired setpoint very well.

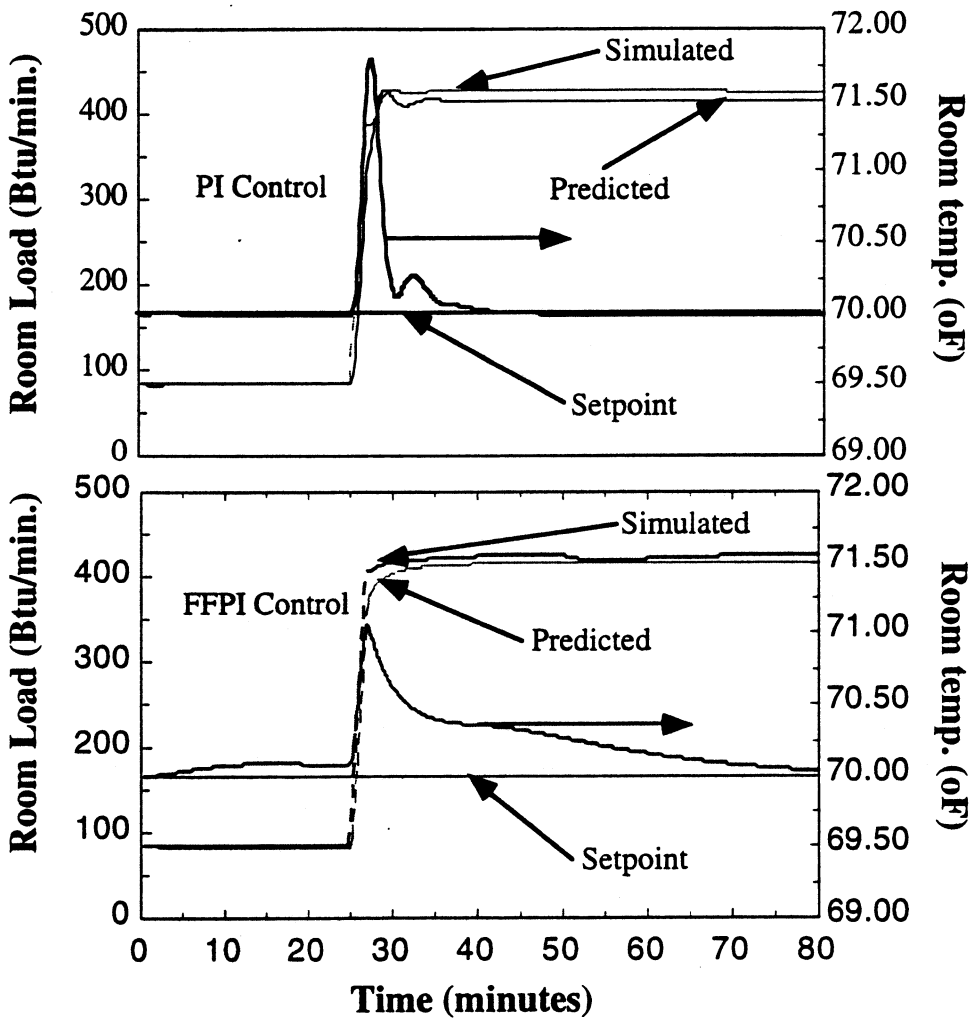

Figure 6.20: Dynamic response of room temp. and predicted load for control sequence C1

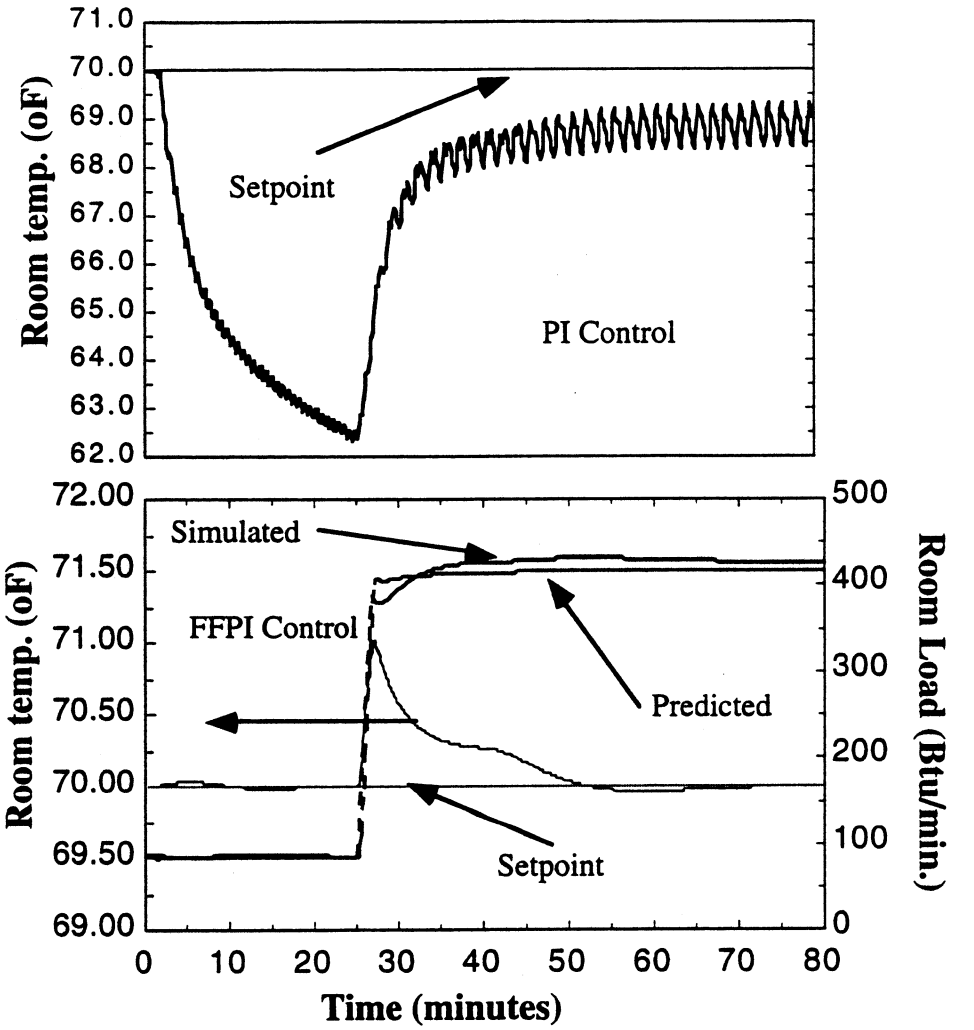

Figure 6.21: Dynamic response for room temperature and predicted load for control sequence C2

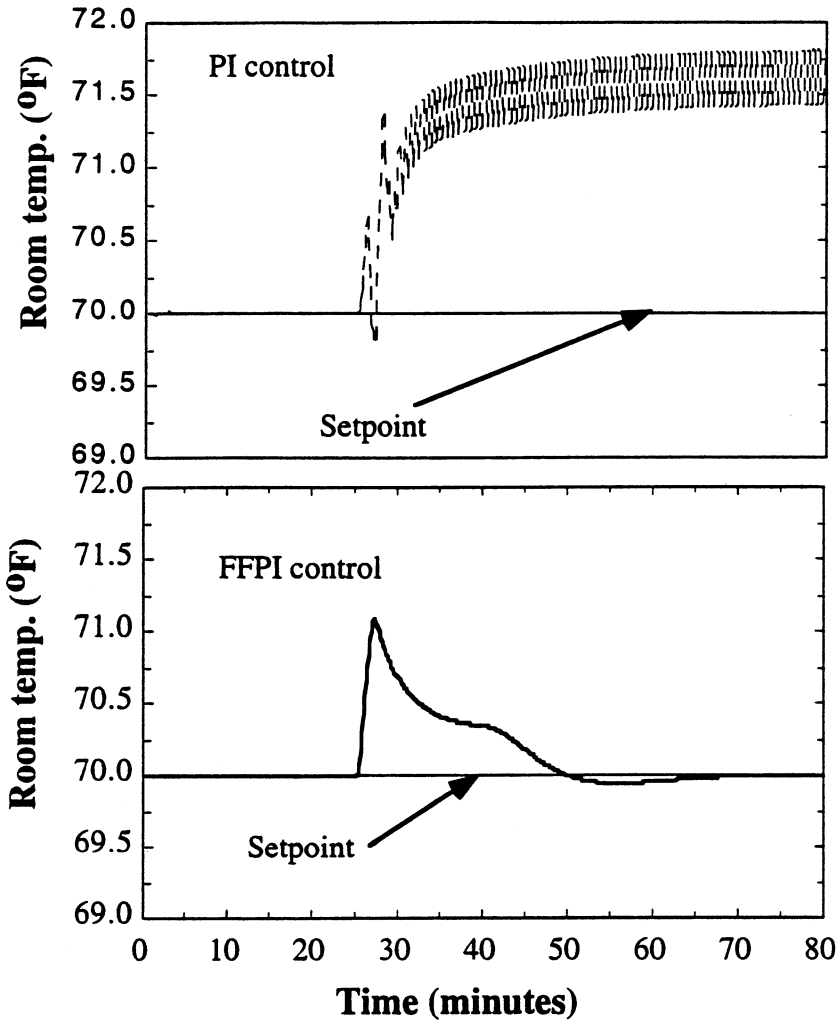

Figure 6.22: Dynamic response of room temperature response and predicted load for control sequence C3

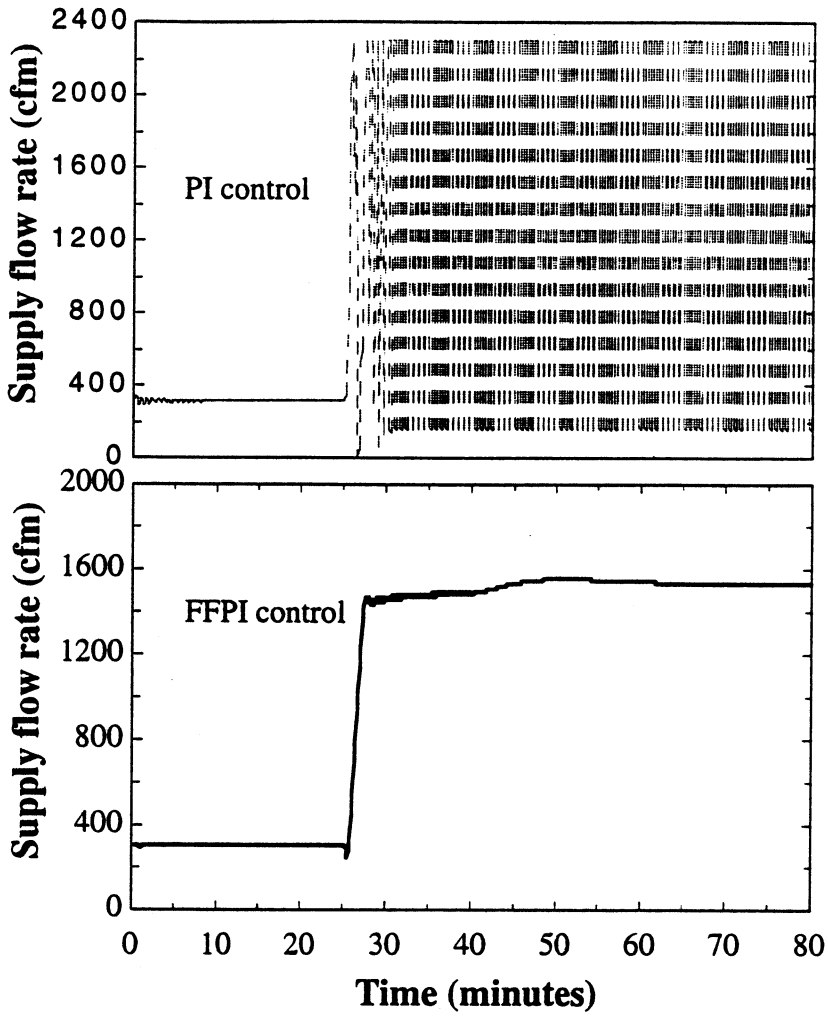

Figure 6.23: Supply flow response for control sequence C3

Cases C4, C5 and C6: Temperature control- cooling for decrease in room load

In cases C4, C5 and C6 the internal load is suddenly decreased by five fold from an initial steady value. These cases are just the opposite of the cases C1. C2 and C3.

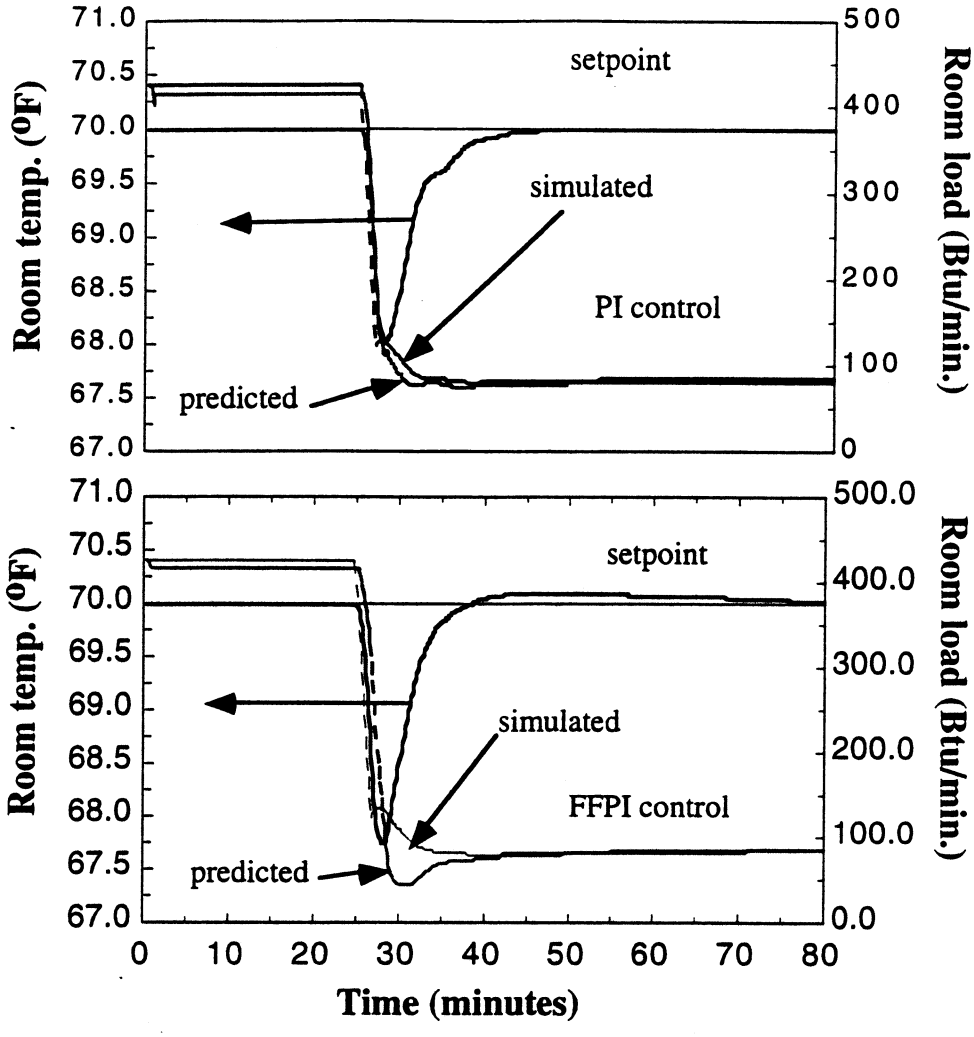

Figure 6.24: Dynamic response of room temp. and predicted load for control sequence C4

The results are quite similar but reverse the response compared to the cases C1, C2 and C3. In case C4, dhown in Figure 6.24 for linear damper with an authority of 1.0, the both PI and FFPI control loops work very well. For a linear damper with an authority of .01, the PI control performance deteriorates considerably as shown in Figure 6.25. For the last case C6 shown in Figure 6.26 for a non-linear damper with an authority of .01 again instability is observed at the high load and flow condition. However, when

the load is decreased, the PI seems to provide good control. For all cases, the FFPI provides accurate and stable control.

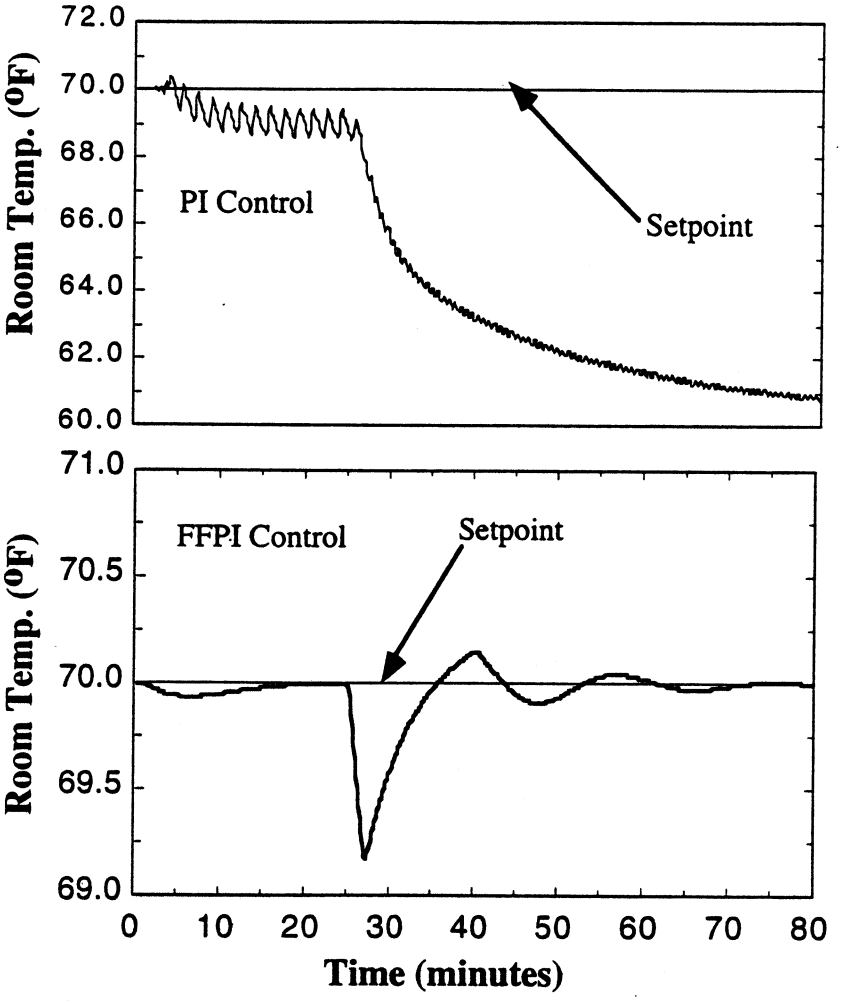

Figure 6.25: Dynamic response of room temperature control sequence C5

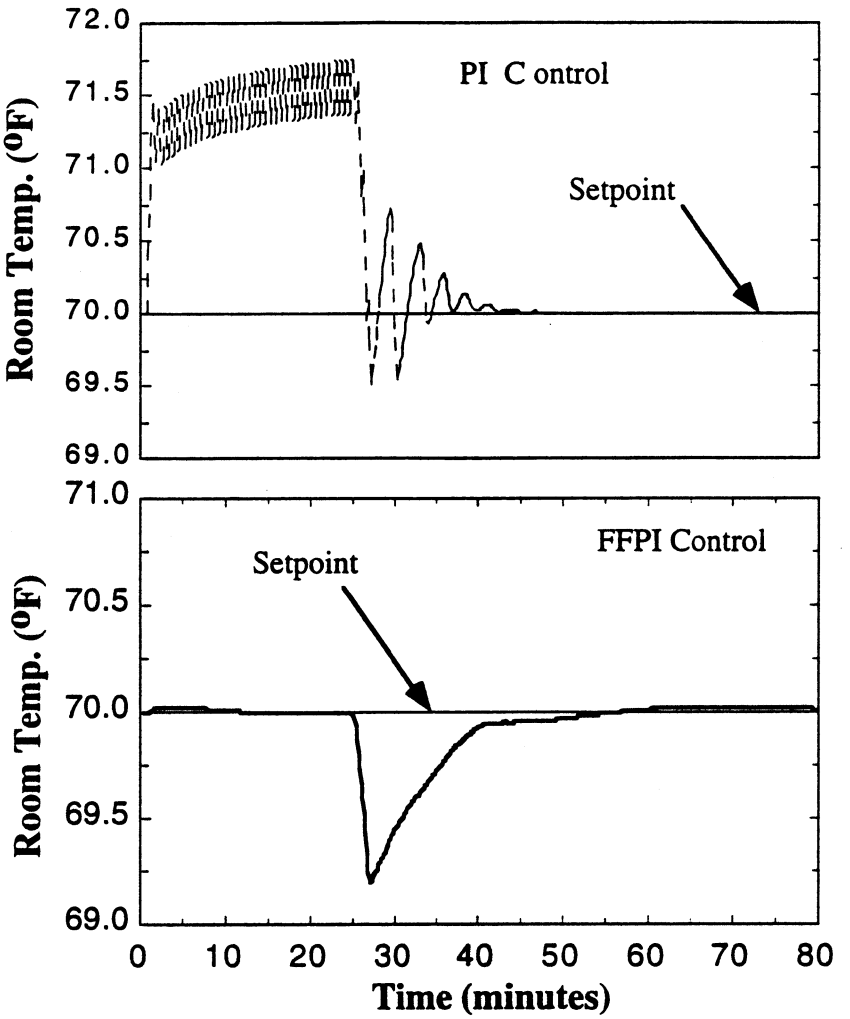

Figure 6.26: Dynamic response of room temperature control sequence C6

6.5 Simulation and results- Temperature control sequence-heating

For the heating sequence, the simulation sample time is chosen to be 2 seconds. This choice was based on considering the coil response shown in Figure 6.27. Published literature (Underwood 1989; Gartner and Harrison 1963; Pearson et al. 1974; Nesler and Stoecker 1984) reports that a heating coil responded within 10 seconds for a temperature increase of 30 °F and

within 40 seconds for a temperature increase of 5 ^{o}F across the coil. A coil response time of 20 seconds is needed to meet the rapid heating requirement in a lab environment.

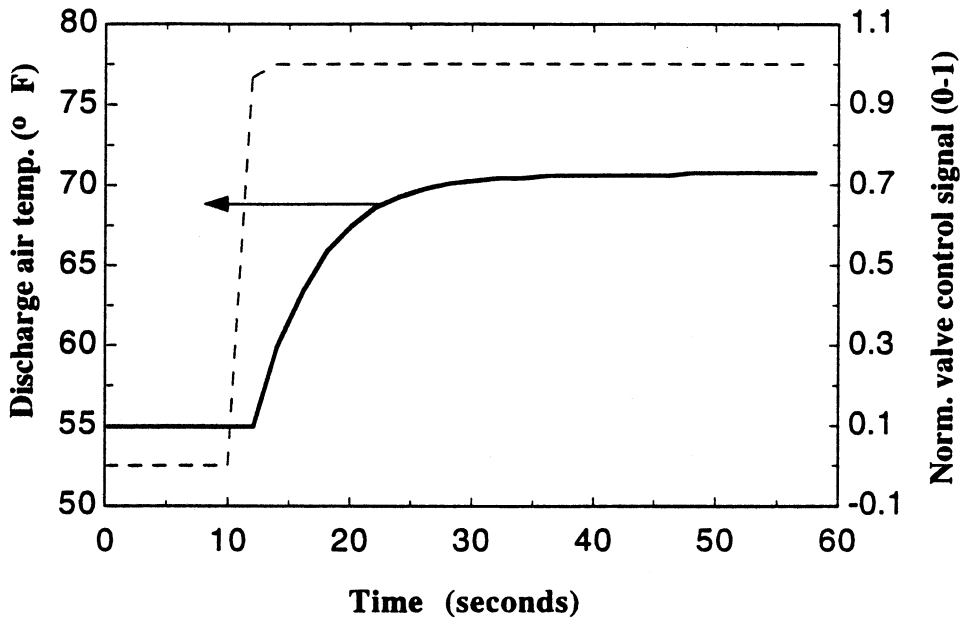

Figure 6.27: Open loop coil response

As discussed in Chapter 5, the coil is also modeled as a first order system with a dead time. Therefore, the expression for the coil response time will be the same as for an actuator as shown in Equation 6.8. For a given coil discharge air temperature setpoint, the response of discharge air temperature will vary with the ratio of sample time to coil time constant, $\frac{s_t}{\tau_{coil}}$. The ratio was varied and a value of 0.40 was chosen as reasonable in order to obtain the desired coil response for reaching the discharge air temperature setpoint at full flow. The coil time constant, τ_{coil} was determined from Figure 6.27 and found to be about 10 seconds. A sample time of 2 seconds,

therefore, means that about 5 samples per coil time constant, which is adequate as explained in sections 6.3 and 6.4. The choice of a smaller sample time by 5 fold compared to the sample time in the cooling sequence means that more samples are now available. However, the total time for simulation for the heating sequence is decreased to 20 minutes compared to 80 minutes for cooling sequence. A range of 20 minutes is adequate considering that there is only one disturbance (i.e. increase in lab exhaust) for heating as opposed to the two disturbances for cooling.

The tuning of the valves for the PI and FFPI controllers are done in the same way as described before with the pressure control sequence. The time derivative of pressure is also ignored in the simulation as was the case in cooling sequence.

Two separate disturbance sequences are considered for heating. In the first sequence, the disturbance is caused by the sudden increase in the fume hood exhaust due to the sash opening from minimum to full open position. The disturbance function (exhaust flow rate) is shown in Figure 6.28.

Since in this sequence the ventilation load will largely dictate how much heating is required, the supply air flow discharge air temperature setpoint is determined using the steady state mass, energy and infiltration equations. The internal thermal load remains constant and does not need to be predicted. The supply flow rate setpoint is also determined using the same set

of steady state equations in order to satisfy the room differential pressure requirement.

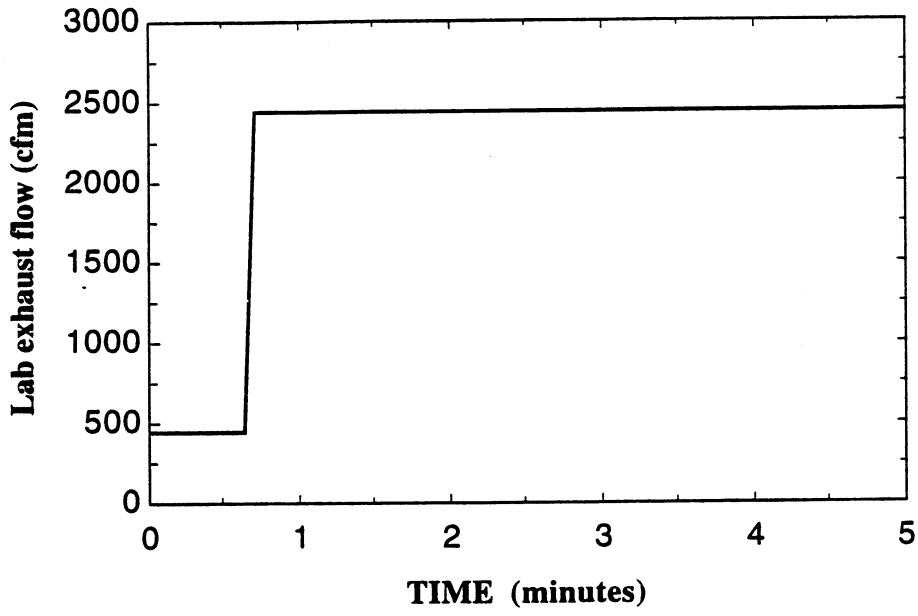

Figure 6.28: Disturbance for heating sequence due to ventilation

The control strategy for FFPI and PI approaches are shown in Figures 6.29 and 6.30 respectively. The control strategies are similar to that for the temperature control- cooling sequence. In Figure 6.29, the model based setpoints predictor determines the supply flow and discharge air temperature setpoint. The supply flow setpoint is fed into the FF loop for supply flow control while the coil loop receives the discharge air temperature setpoint information. The PI control loop for heating with a ventilation load only is similar to FFPI without the FF blocks.

The second control sequence considered for heating has a change in the space internal load. This sequence assumes that the lab initially has a maximum lab

exhaust flow and supply flow that maintain the room temperature and differential constraints at time t=0. Then the total lab exhaust is decreased and at the same time the internal load is generated. As a result, the space needs partial heating. The sequence is shown in Figure 6.31.

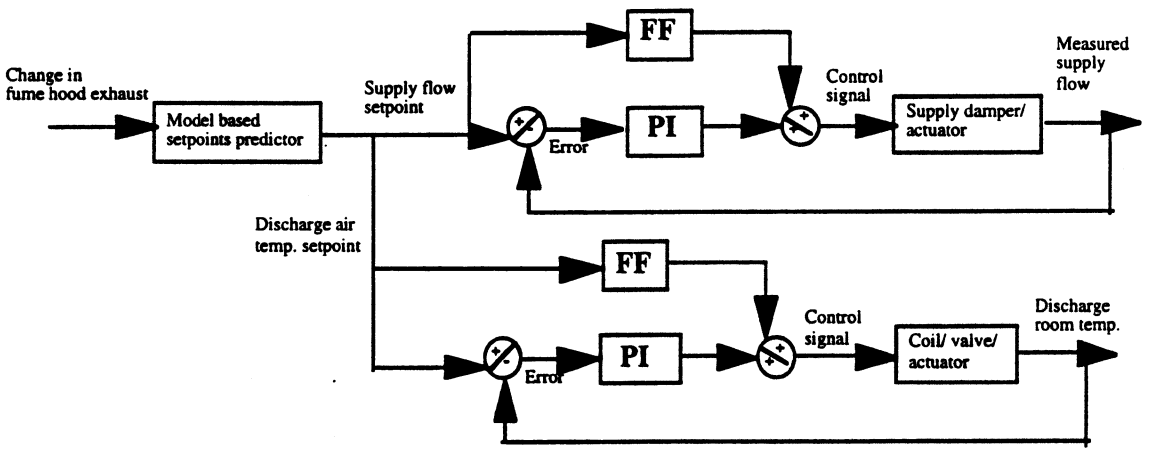

Figure 6.29: Schematics of FFPI controller for Temperature control- Heating sequence due to ventilation

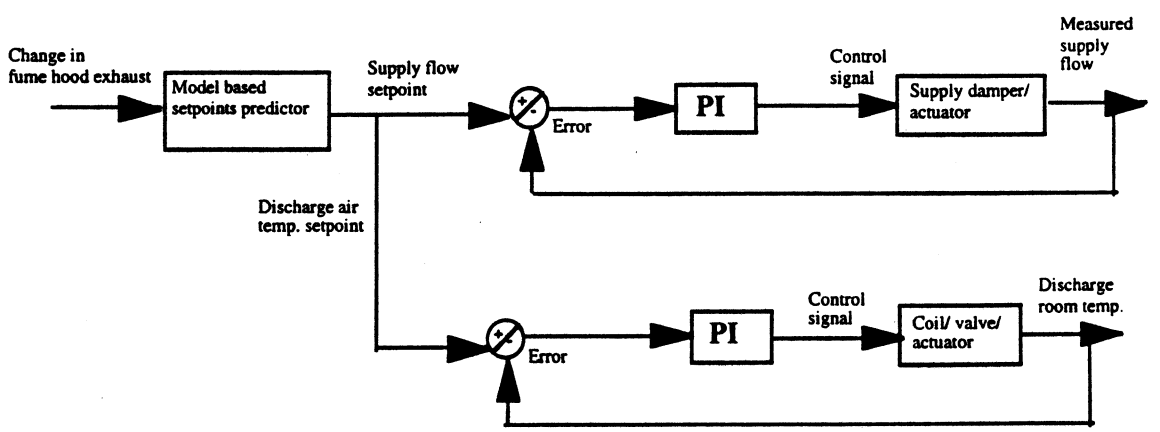

Figure 6.30: Schematics of PI controller for Temperature control- Heating sequence due to ventilation

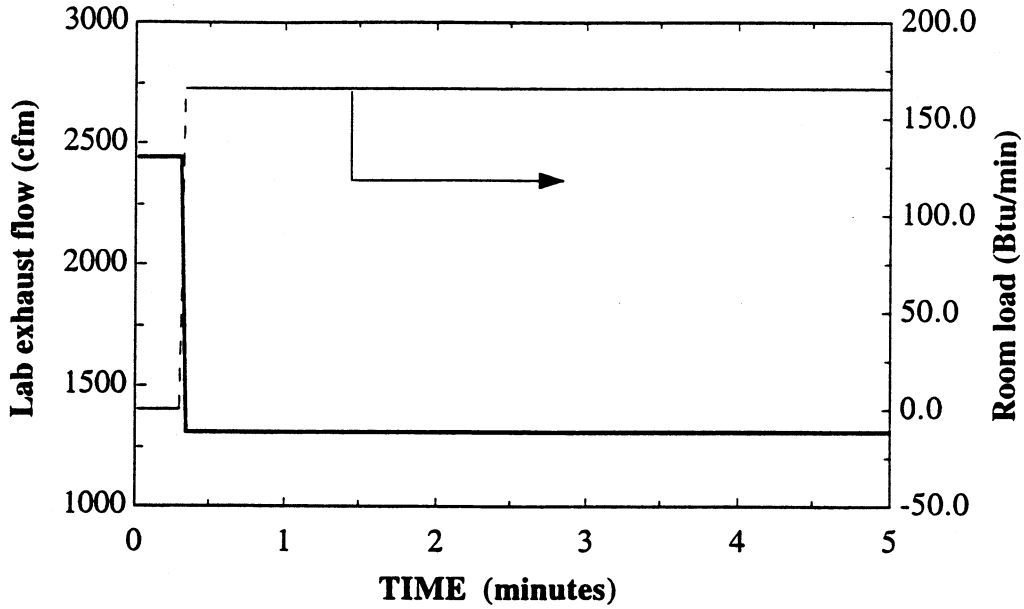

Figure 6.31: Disturbance in lab exhaust and room load for Temperature control- Heating sequence

The control strategy for the FFPI and PI controllers are shown in Figure 6.32 and 6.33, respectively, and are very similar to the previous sequence without the room load. However, the model based predictor now includes the predicted load in order to determine supply flow and temperature setpoints. Instead of using the discharge air temperature setpoint as in the ventilation disturbance, the room temperature setpoint is used in the feedback block for both FFPI and PI controllers.

If the predicted load is based on the discharge air temperature setpoint, any error associated with it propagates through the load calculation and make the error even larger for the discharge air temperature in the next sample time,

producing an unstable response. This instability was observed repeatedly during simulation, and it was decided to use a more direct control variable (i.e. the room temperature and its constant setpoint) in the control loop.

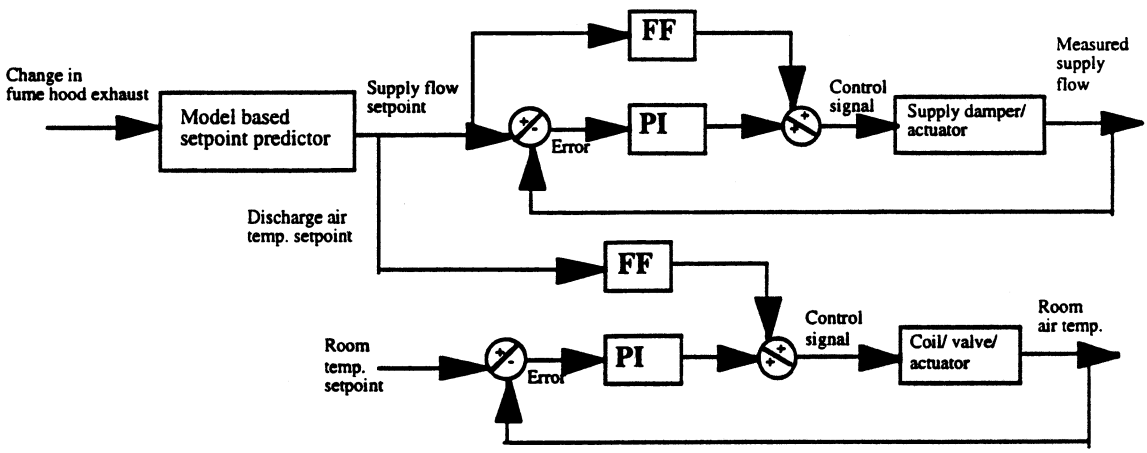

Figure 6.32: Schematics of FFPI controller for Temperature control- heating with room load.

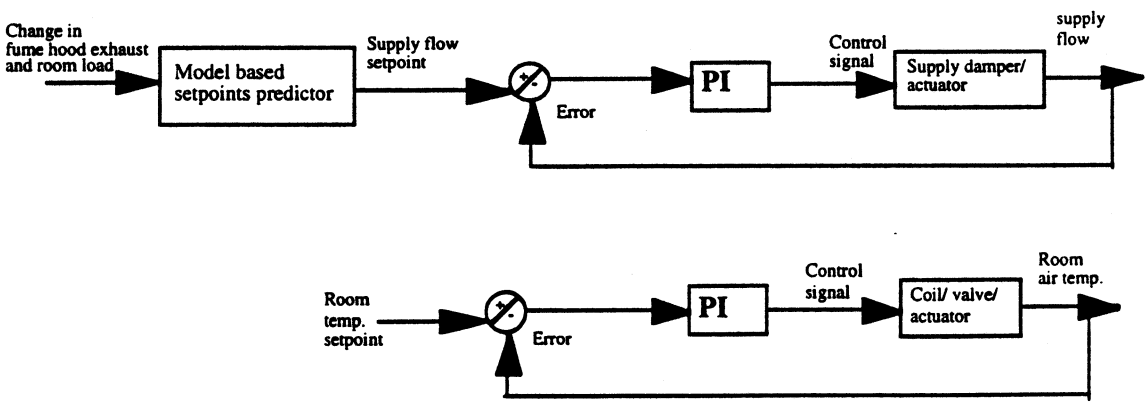

Figure 6.33: Schematics of PI controller for Temperature control- heating with room load.

The PI controller block shown in Figure 6.33 appears to have two uncoupled loops; one for pressure and the other for temperature. However, in reality they are coupled since the current samples of room temperature and the

discharge air temperature setpoints are used to determine the predicted load, which is then used to calculate the supply flow and temperature setpoints for next sample.

Cases H1, H2, H3: Ventilation only

As in the case of cooling three damper/ valve characteristics are considered for this sequence. Identical characteristics are chosen for the damper and valve for each sequence. The first case, H1, considers a linear damper/valve with an authority of 1.0. Case H2 illustrates results for a linear damper/ valve having an authority of .01 while the last case, H3, presents the results for a non-linear damper/ valve and an authority of .01.

The plots for cases H1, H2, and H3 are shown in Figures 6.34, 6.35 and 6.36 respectively. The time response of the room and discharge are temperature variables that are usually measured and are shown in the plots. In general, both PI and FFPI controllers work well for all control sequences. The good performance of the PI controller for all control sequences is expected since the operating condition requires the supply flow damper and the heating valve to open fully to meet the ventilation load caused by the increase in lab exhaust. The normalized control signals required to open dampers and valve are almost equal and close to unity irrespective of damper/ valve characteristics. The room temperature falls below the setpoint initially but quickly recovers and reaches the setpoint. The simulation was run for about 20 minutes to ensure that controller reaches the steady state without any oscillation or stability. The discharge air temperature quickly reaches the

setpoint as determined by the physics based steady state model as explained earlier. The method of determining setpoints using physical models proves to be viable as illustrated repeatedly in both pressure and temperature control sequences.

The initial undershoot in room temperature is expected as the sudden increase in room total exhaust causes the supply flow at 55 ^{o}F to increase. The increased supply flow rate is in excess of the required amount to offset the room thermal load. The room temperature, thus falls before the coil water valve is opened to provide heating and offset the sudden increase in room ventilation load driven by the lab exhaust. The initial undershoot in room temperature is less than 0.5 ^{o}F for both PI and FFPI controllers for cases H1 and H2. In Case H1 for a linear damper/valve, the room temperature falls below 69.5 ^{o}F for PI controller whereas the undershoot is about 0.25 ^{o}F for FFPI controller. The recovery in room temperature in Case H1 for both controllers is more gradual compared to Case H2 as expected since a quick opening damper/ valve (i.e. authority .01) is used. In the case of a FFPI controller, the temperature continues to fall until the PI is activated (about 5 minutes) which provides a residual control signal in addition to the FF signal to compensate only a small error of about 0.25 ^{o}F or less. This behavior demonstrates that the FF controller alone can provide a significant portion of the control signal that is required to achieve stability and accuracy.

In case H3, the PI controller produces a larger undershoot in room temperature compared to other two cases. The room temperature also shows

an overshoot in the case of the FFPI controller. The unusual trend is explained with the help of Figure 6.37 showing the response of temperatures for only first two minutes.

With a PI controller, the discharge air temperature produces an initial oscillation and there is a slow response in achieving the desired setpoint. Therefore, the room temperature takes longer and produces a larger undershoot before reaching the setpoint. The explanation for slow response is similar to what has been observed and explained before in case of pressure control sequence P3 which used identical linear damper/ valve with an authority of .01. As a result, the damper/valve opens quickly exhibiting non- linear characteristics (Figure 6.7).

The discharge air temperature overshoots considerably for a FFPI controller which causes the room temperature to increase. The overshoot is caused again by the slow response of the non- linear supply damper characteristics.

Since the supply flow responds slowly, the room does not receive sufficient heating. As a result, the discharge air temperature setpoint continues to increase to offset room's growing heating load. Finally, when the supply flow reaches its setpoint, the room is overheated due to the higher discharge air setpoint.

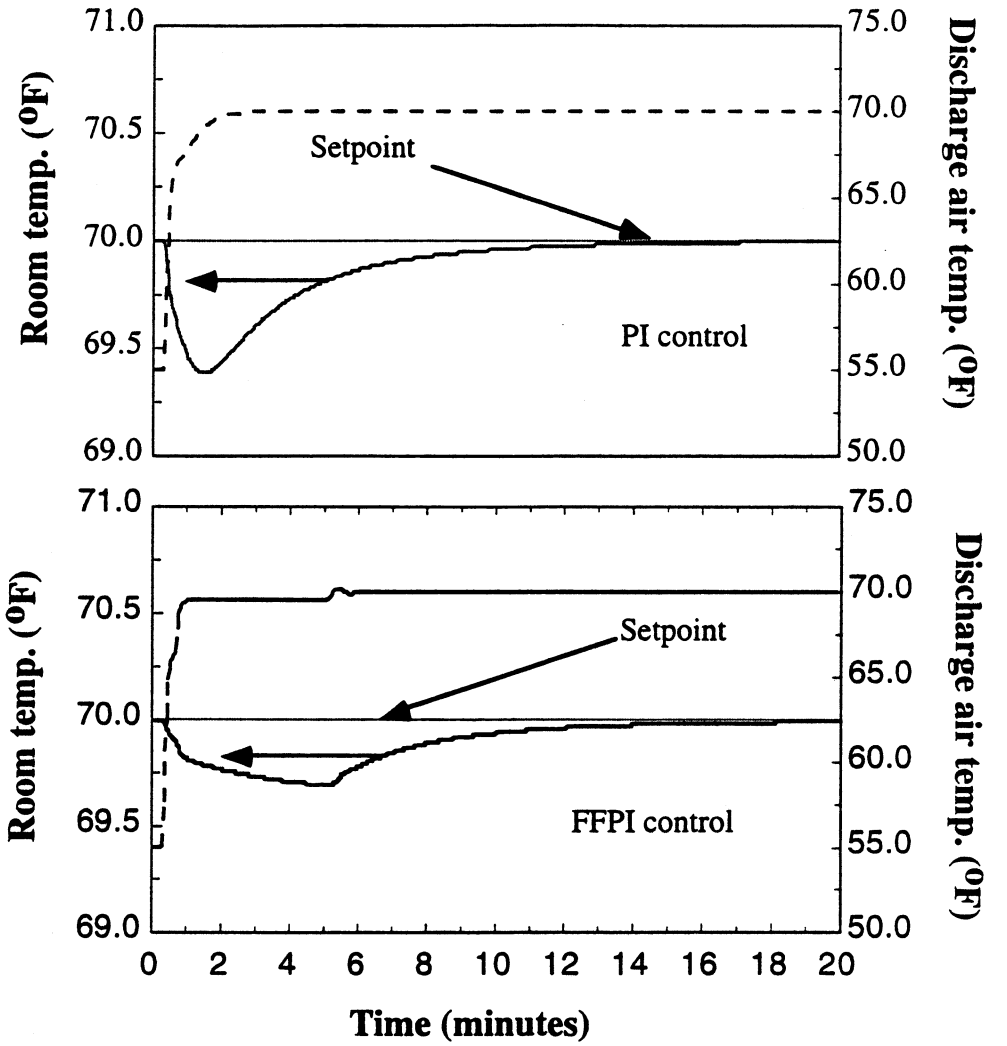

Figure 6.34: Dynamic response of room and discharge air temperature for control sequence H1.

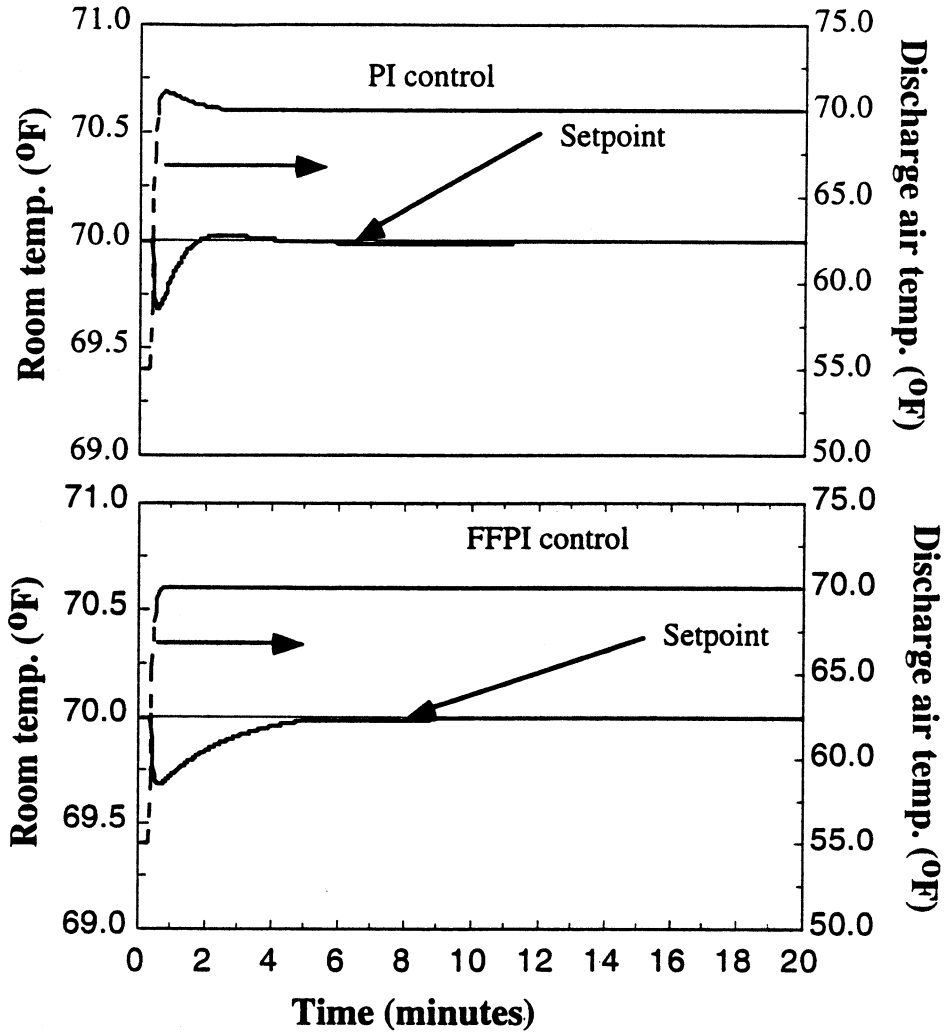

Figure 6.35: Dynamic response of room and discharge air temperature for control sequence H2.

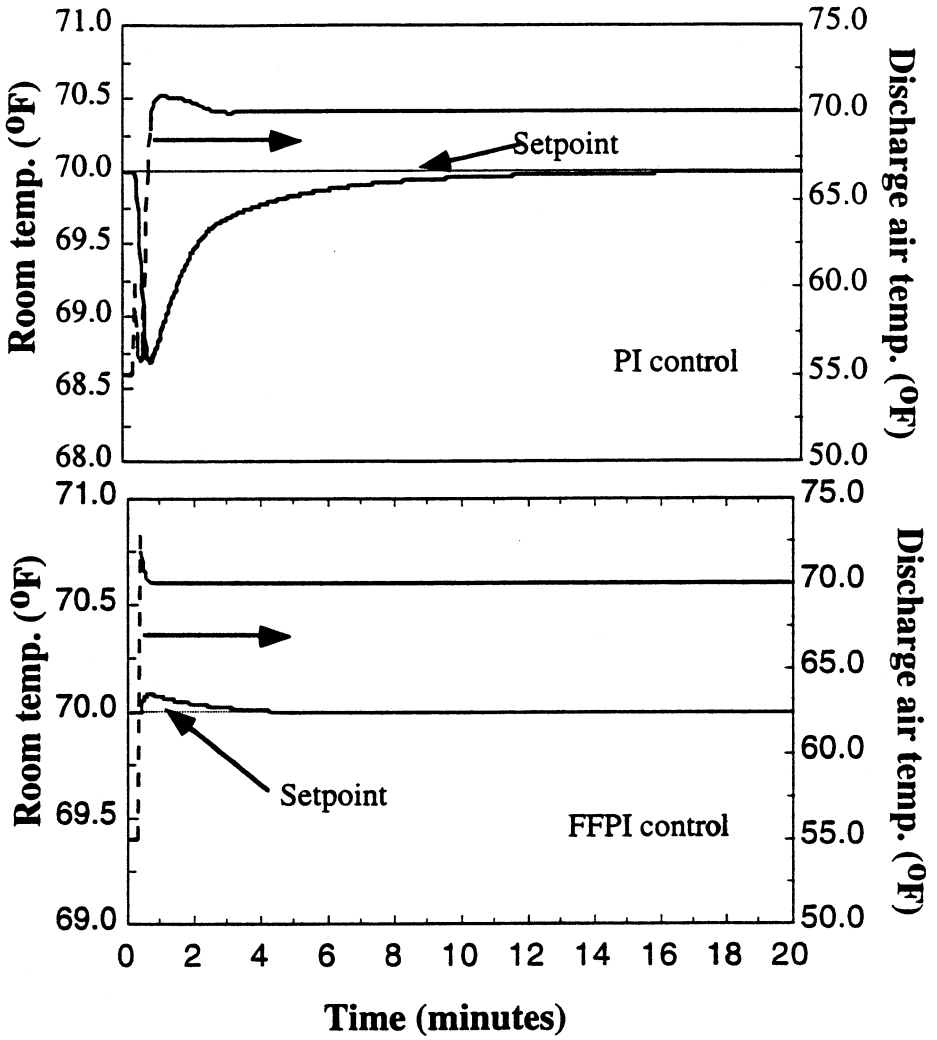

Figure 6.36: Dynamic response of room and discharge air temperature for control sequence H3.

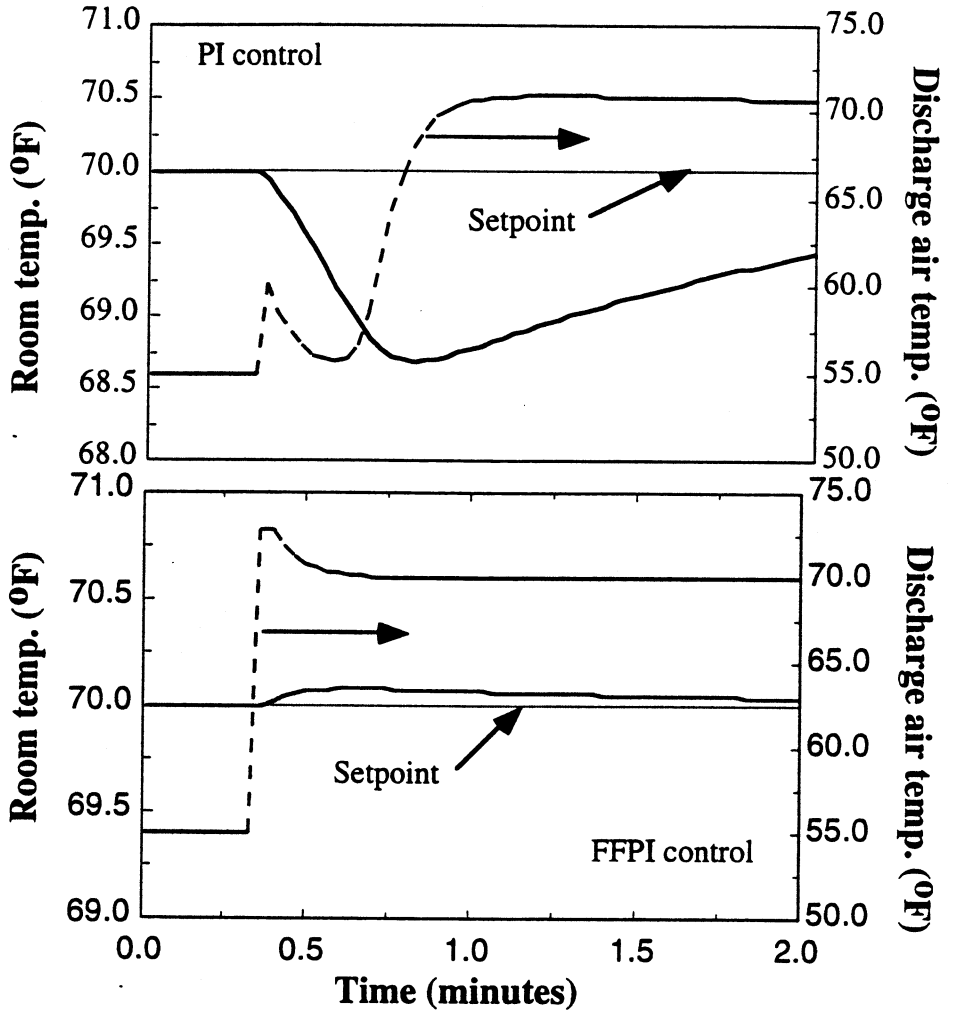

Figure 6.37: Initial response of room and discharge air temperature and predicted room load for control sequence H3.

Cases H4, H5 and H6: Ventilation with heat load

The last control sequence considers a sudden increase in heating load with the lab exhaust at midrange. Both the heating valve and supply damper operating points are in the middle of their respective end-to-end stroke. The PI controller under-performs for non-linear damper/valve characteristics

and mid-operating points. On the other hand, the FFPI controller provides stable and accurate control for all three cases.

Cases H4, H5 and H6 consider a linear valve, linear valve with an authority of .01 and non-linear valve with an authority of .01 respectively. The corresponding plots are shown in Figures 6.38, 6.40 and 6.41. Figure 6.39 shows the response for a shorter time interval for a linear damper/valve. The general trend is similar in all cases. As the sudden load is imposed, the room temperature increases before the physical model can determine that less heating is needed and signal the control system to close the valve. The discharge air temperature then settles to a new steady state value.

Figure 6.38 shows that both PI and FFPI controllers work very well for the linear damper/ valve. The response of the discharge air temperature and predicted load shown in Figure 6.39 for an initial time period of two minutes reveal some interesting transient behavior. The predicted load for both PI and FFPI controllers initially increases very rapidly followed by a dip and then gradual increase to reach the steady state value as shown in Figure 6.39. The steady state value of the predicted load is 167 and 169 Btu/ min. for PI and FFPI controllers, respectively, compared to the actual 165 Btu/min of generated load. The small difference between predicted and generated load is due to the heat transfer from the wall surface that is maintained at a slightly higher temperature than the room.

The initial sharp increase in the predicted load from zero is caused mainly by determining the steady state load using values of different variables at the sample time preceding time t=0. A sudden increase in heating load causes the discharge air temperature setpoint to jump which results in a decrease in load. As the initial disturbance becomes steady, the predicted load then continues to rise to reach the steady state.

The plots in Figures 6.40 and 6.41 demonstrate the deficiency, once again, of the PI controller as the operating points shift from the tuning point. The PI controller produces poor control. For case H5, the PI controller continues to operate the control valve in an oscillatory fashion. The room temperature then oscillates. In case H6, the oscillation amplitude continues to shrink from a large initial amplitude. A similar yet reverse trend may be noted when the response in C5 is compared to the H5 and the response of C6 is compared with the case H6. The similarity is expected as cases C5 and H5 use a linear damper with an authority of .01 while C6 and H6 use non-linear damper with an authority of .01. All of the cases use the predicted thermal load in a model based setpoints predictor but the load suddenly increases for C5 and C6 while the load decreases in the heating sequence. The FFPI controller for both cases H5 and H6 again show stable and accurate control.

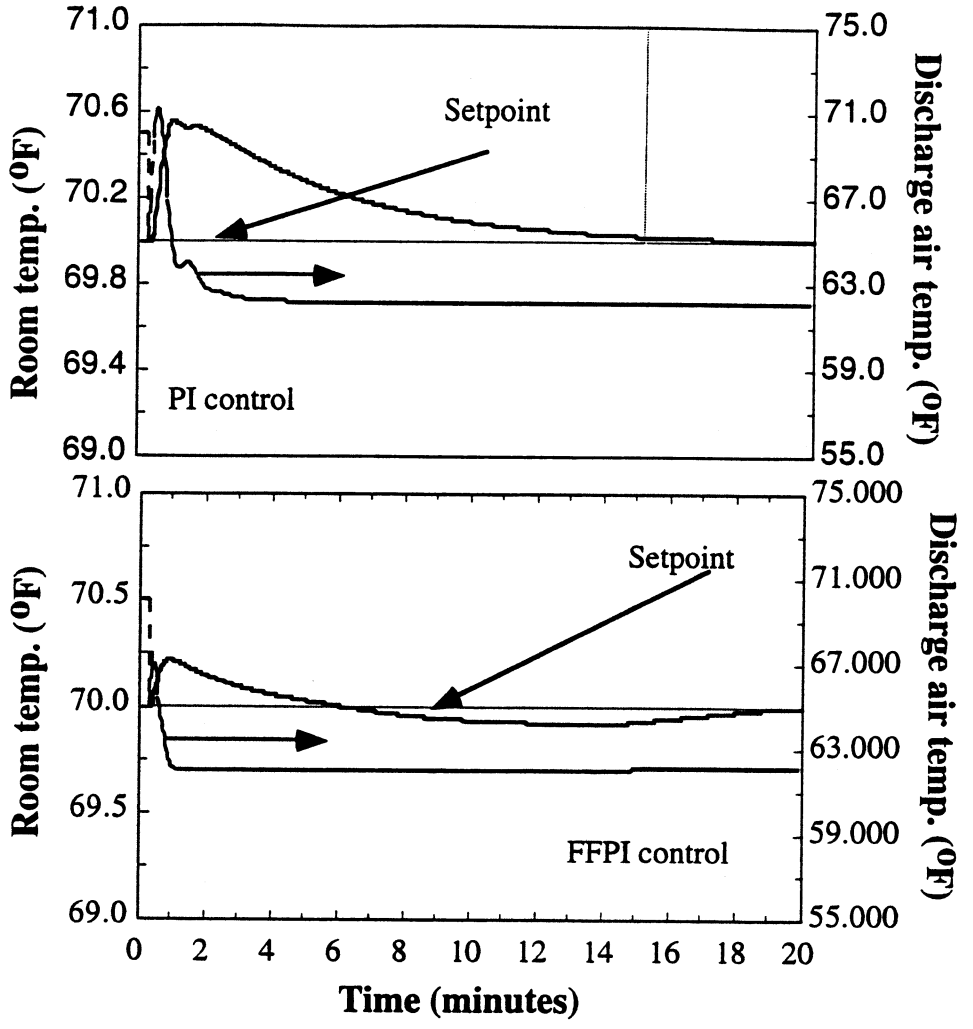

Figure 6.38: Dynamic response of room and discharge air temperature for control sequence H4

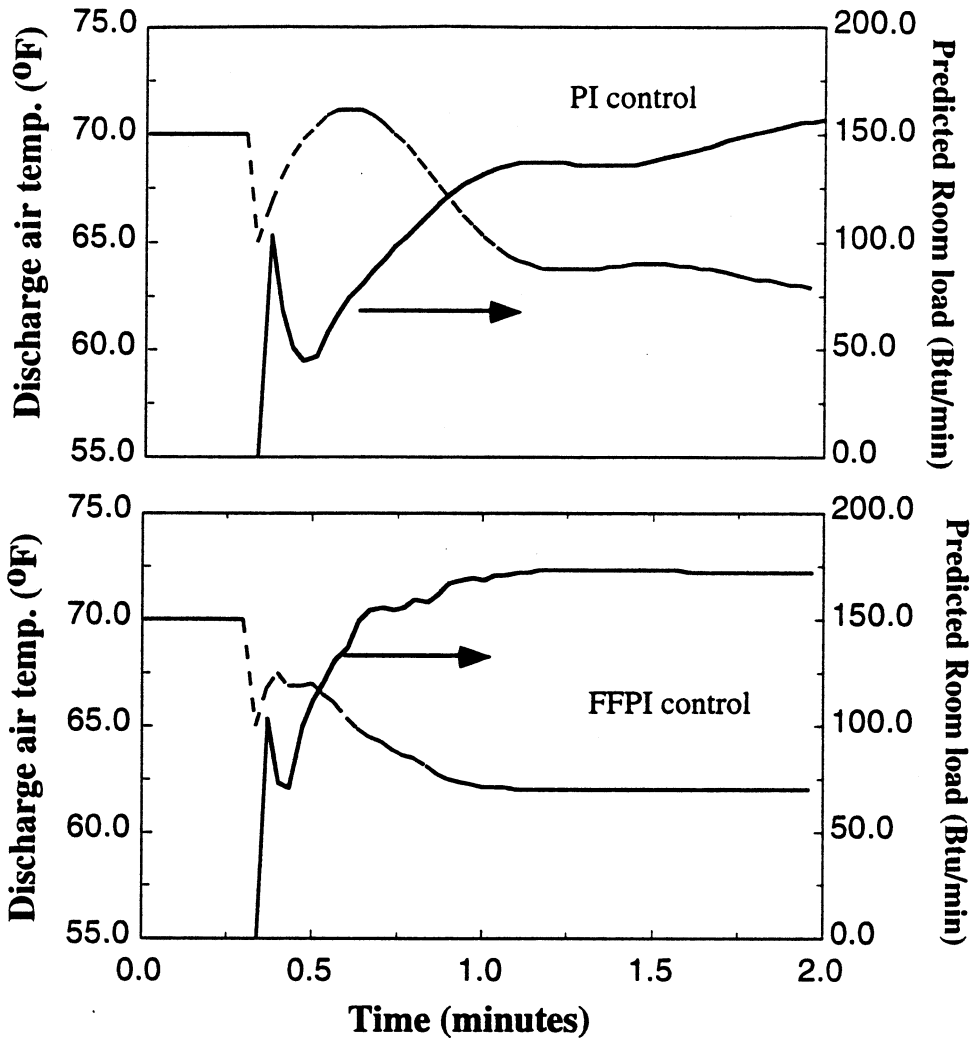

Figure 6.39: Initial response of discharge air temperature and predicted load for control sequence H4.

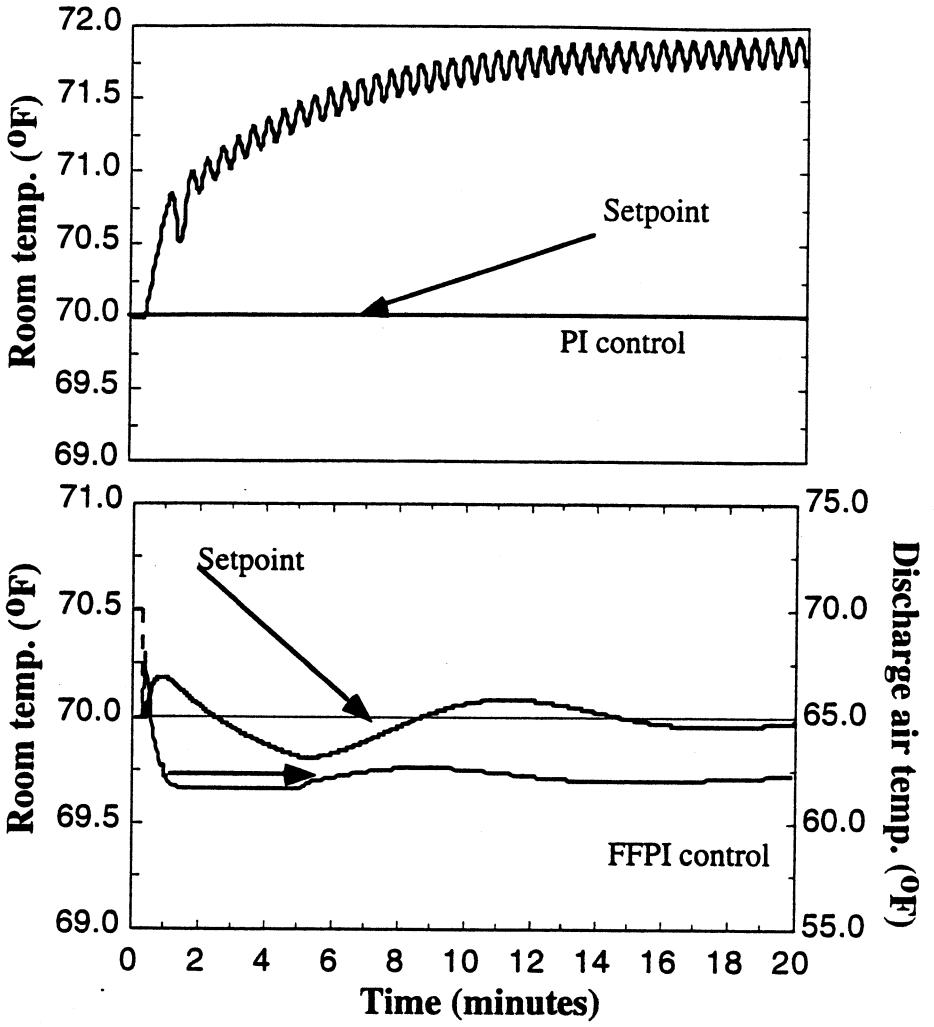

Figure 6.40: Dynamic response of room and discharge air temperature for control sequence H5.

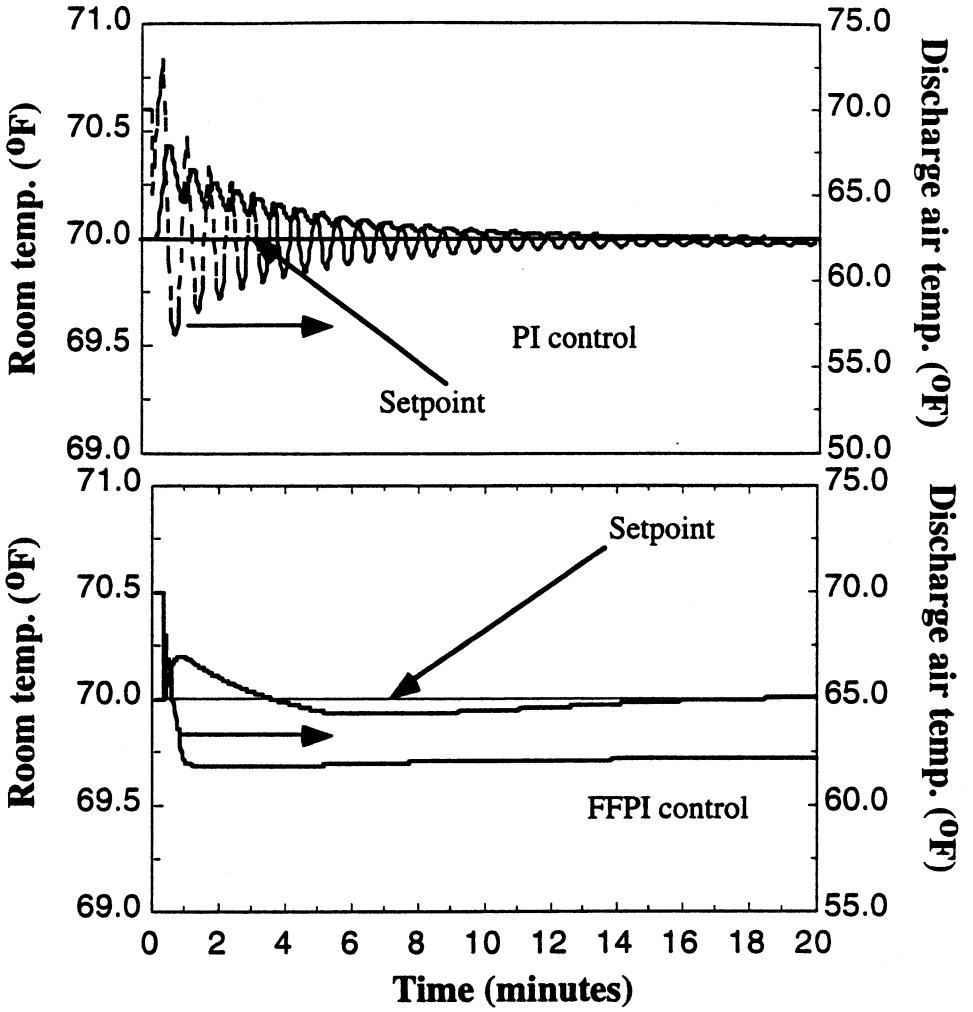

Figure 6.41: Dynamic response of room and discharge air temperature for control sequence H6.

6.6 Summary:

The cases for pressure and temperature control sequences are selected with an objective of evaluating controller performance under wide operating conditions and different equipment characteristics. The FFPI controller has performed well for each case by stable and accurate control. In contrast, the PI controller failed to perform adequately except at the peak operating

condition that was used in tuning. The FFPI is able to respond quickly to any setpoint change due to the presence of the feedforward element while the feedback loop provides stability and eliminates residual error between the setpoint and simulated values. As the damper characteristics shift from the assumed initial linear damper, the advantage of FFPI over the feedback loop becomes apparent. The FFPI controls rapidly and accurately over a wide range of operation and considering significant change in damper characteristics. The FFPI uses single tuning parameters for its feedback portion and thus control is robust.

In a FFPI controller a significant portion of the control signal is derived from the FF part while only a very small signal is needed from the PI part. The PI serves to improve the controller accuracy in reaching the desired setpoint and eliminates offset. As a result, the PI portion of the FFPI control loop only handles a small amount of error irrespective of the change in the system characteristics and operating conditions. This makes tuning of FFPI really simple and re-tuning is not necessary as is often the case with PI control loops.

The FF part requires only a single smoothing parameter to be estimated which can be held constant for most of the HVAC processes (i.e. dampers and valves) because the amount of data needed to identify the characteristics of such processes do not vary significantly. Finally, the FF portion of the combined approach can adapt to changes in system characteristics, a useful feature to provide correct control signal and diminish the role of feedback component.

A comparison between proposed FFPI and a state-of-the-art PID control system for VAV lab will highlight the advantage of FFPI from commissioning and operation point of view.

Figures 6.42 and 6.43 show the schematics a total integrated control system for VAV lab HVAC system using a conventional feedback and the proposed FFPI approaches. The feedback approach has a total of 5 coupled PID loops with a total number of 15 gains that have to be field tuned and adjusted. Even, if all PID controllers are considered to be PI only, there are still 10 tuning parameters. These coupled loops are difficult to tune and are usually tuned at a fixed operating condition. Re-tuning may be necessary if the operating condition shifts considerably, which is common in a lab environment. In general, the poor performance of the coupled feedback loops may prove to be costly for the lab owner.

In contrast, by shifting the burden of performance from PI to the FF component, the tuning may become an non-issue for the proposed FFPI controller. The ability of the FFPI to work over a wide range of operating conditions and component characteristics is very promising.

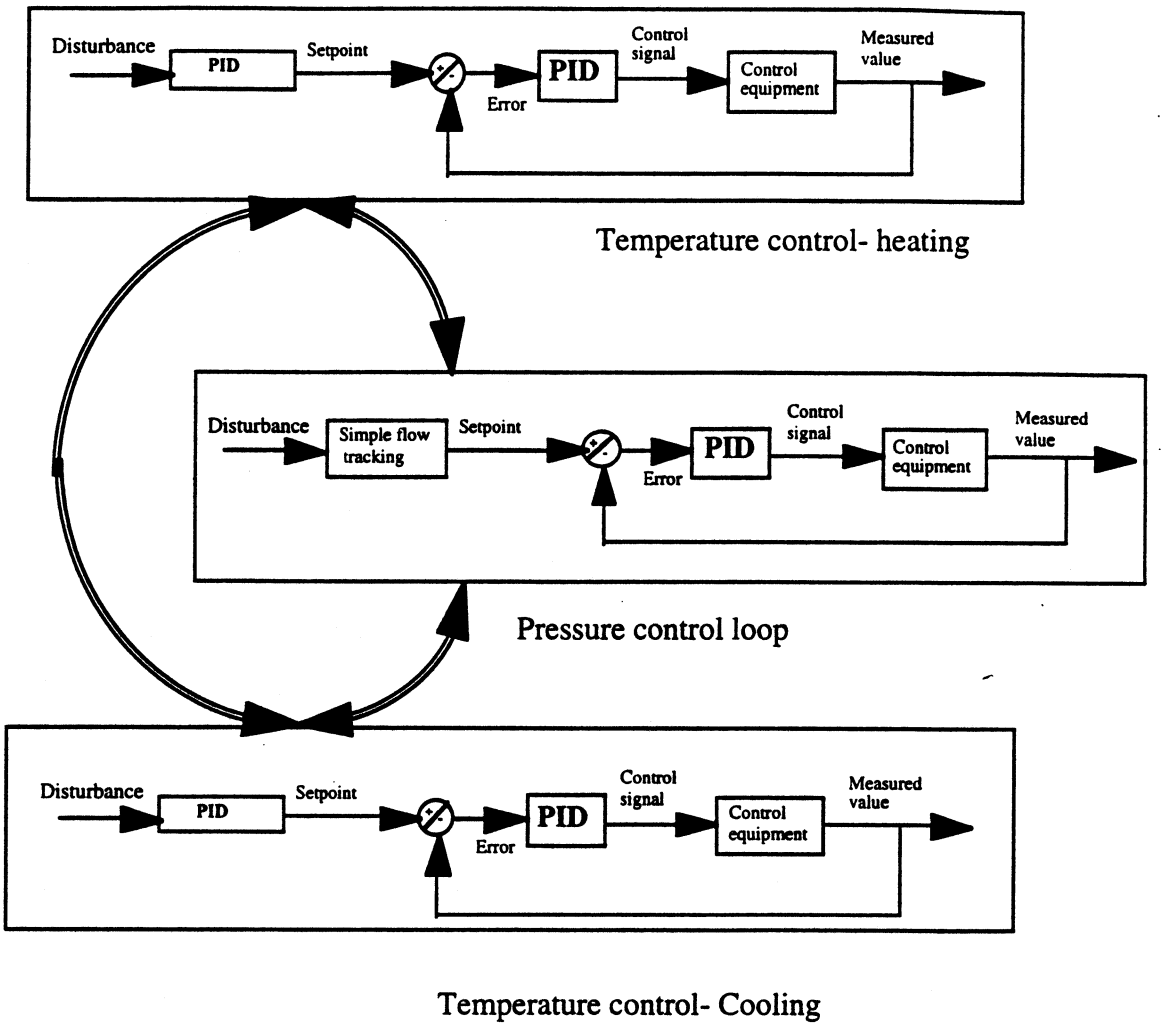

Figure 6.42: Schematic of PID control system for VAV lab.

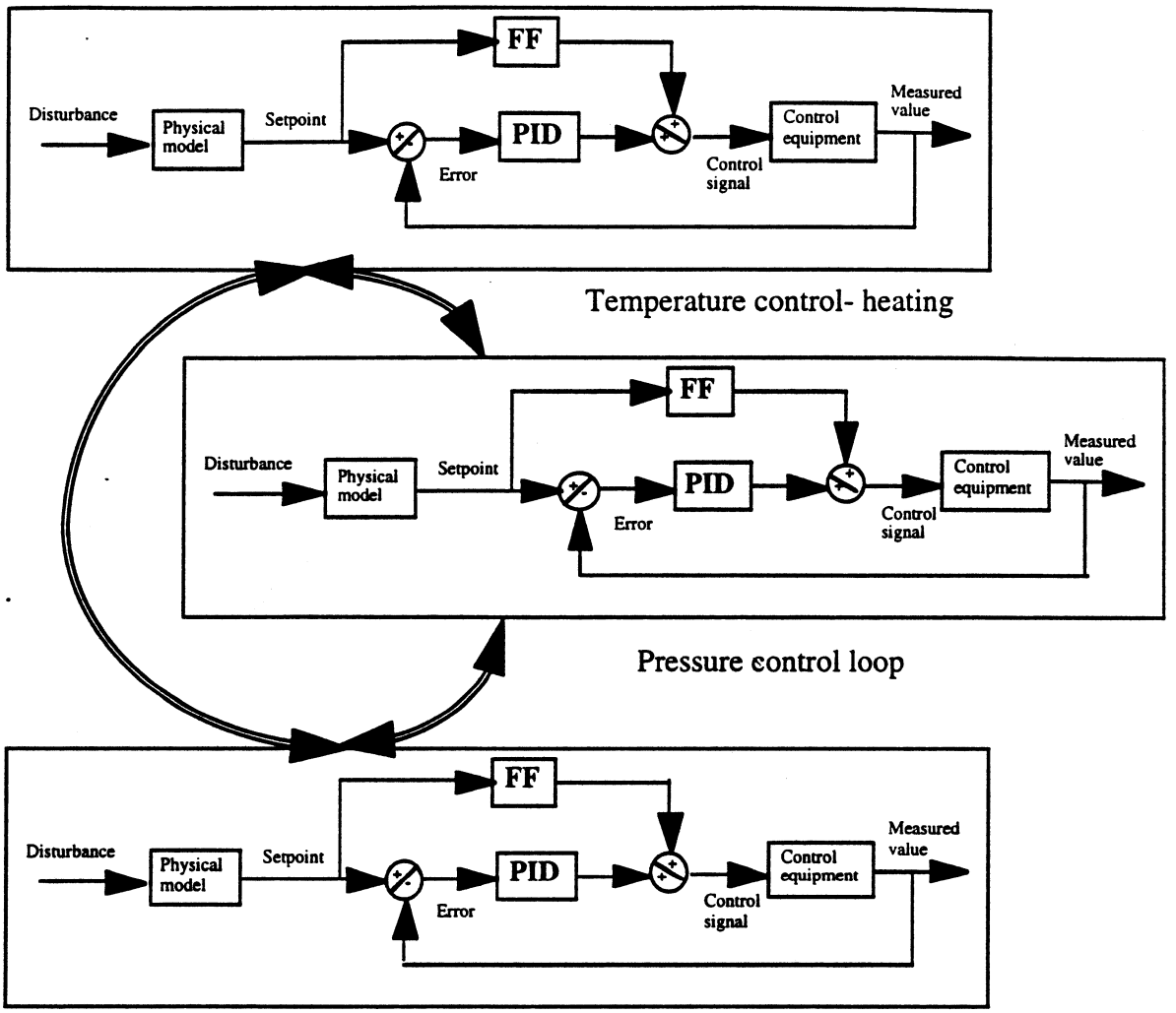

Figure 6.43: Schematics of proposed FFPI control system for VAV lab.

There is to no need for retuning to produce stable, robust and accurate control. The FFPI implementation in a real controller will translate into simple commissioning, better performance and as a result add value to the customer.

Furthermore, the FFPI controller does not need any additional sensors or added memory or processing capability. The sensors which are normally used in a current control system will be able to provide the required information for HVAC control equipment (i.e. valve and damper identification). The use of General Regression Neural Network and a model based setpoints predictor are simple algorithms and do not need significant controller memory. Therefore, the FFPI may be implemented without changing or adding any hardware/ sensor configuration. The only needed investment will be needed for algorithm development. The simplicity associated with the FFPI may translate into real cost benefit to the customer.

Chapter 7

Conclusions and Recommendations

Based on the current research and results in this thesis, the following conclusions can be drawn.

1. The laboratory environment is unique in terms of the comfort and safety requirements and the operation dynamics. The goals of the lab heating, ventilating and air conditioning (HVAC) and associated control systems are to maintain comfort and safety at all times. The lab safety constraint is aimed at effective control of possible contaminants that are generated within the fume hood and the lab space. By maintaining a proper fume hood exhaust flow, contaminants within the fume hood are captured and properly exhausted outside the lab building. At the same time, any leakage out of the lab into adjacent space is prevented by maintaining a lower lab pressure compared than the adjacent spaces and inducing infiltration into the lab.

2. The safety criteria preclude any recirculation of lab air. As a result, conditioning is achieved by 100% outside air that must be heated or cooled before it is supplied to the lab space. This process increases the lab operating cost by at least three to four fold as compared to the commercial space. In order to reduce operating costs, the concept of a lab variable air volume (VAV) HVAC system was introduced in late nineteen eighties. The VAV system reduces the supply air flow when the total lab exhaust decreases, and saves both heating/ cooling and fan energy. As a result, the operating

conditions in a lab VAV system vary widely which significantly challenges the control system. The traditional control methods of feedback often exhibit poor results in terms of stability and accuracy. Further, the feedback control requires extensive tuning since the lack of tuning may result in increasing operating cost and loss in comfort and productivity.

3. The lab comfort criteria is to maintain specified temperature and humidity, and this may conflict with safety constraints, which poses an additional challenge to the lab HVAC system. The conflicting nature of safety and comfort constraints coupled with the wide variation in operating conditions requires an innovative control system that will perform equally under all conditions and satisfy comfort and safety constraints.

4. A model based combined feedforward and feedback control strategy is proposed with an objective of enhancing performance of a lab variable air volume laboratory HVAC system while maintaining safety and comfort constraints. The implementation of such a method should be practical, simple and cost effective. The performance can be defined as providing stability, robustness, speed of response and accuracy under various operating conditions.

5. The feedforward controller explored in this thesis has identification and control algorithms. The identification algorithm captures and identifies the process characteristics and up-dates these characteristics on a regular interval. The control block uses the characteristics to generate the required control signal for given room conditions (i.e. space temperature and

pressure) and in response to any setpoint change. Any residual control signal needed under steady state condition will be provided by the feedback controller.

6. Identification of HVAC equipment (e.g. valve, damper and actuator) characteristics requires a small data set that consists of at most 200 samples. Hence, a memory based neural network may be appropriate for identification and control of HVAC equipment. Other methods of identification including back propagation and regression are difficult to implement. A back propagation method requires extensive training. Regression relations require *a priori* knowledge of the expected characteristics and the processing capability and user input needed for non-linear regression make real implementation extremely difficult.

7. A memory based General Regression Neural Network (GRNN) has been evaluated and found to hold promise for identification of HVAC equipment characteristics. It only requires that a single parameter be estimated and it does not require any training. The algorithm is simple and can be easily implemented for on-line control. The stored data in memory can be periodically updated, which makes the identification adaptive.

8. A lab HVAC emulator was developed and validated with measured data in order to compare the proposed system with the feedback only controller. The emulator has been excercised under various operating conditions to understand the physics of the lab HVAC system, especially the interaction between the safety and comfort constraints.

9. Comparisons were made between the proposed combined approach and the feedback controller for typical pressure, heating and cooling sequences under a wide range of operating conditions and extreme valve/damper characteristics. In all cases, the proposed combined feedforward and feedback system performed very well compared to the feedback only method in terms of providing stability, robust control and accuracy. The feedback control using a Proportional- Integral approach performed well only at the operating point selected for tuning and when the control equipment is fully open.

10. The benefits of the proposed system, besides performance, also includes a lower commissioning and operation cost as it needs less tuning and trouble shooting. The proposed system may provide significant customer value in terms of lowering energy cost, less tuning and maintenance, enhanced performance and maintenance of lab safety and comfort.

Based on the results of this study, the following recommendations can be made.

1. The present study completes a "Proof of Concept" phase. Verification of the actual implementation of combined feedforward and feedback loops in a laboratory VAV HVAC system will be the next step. The combined approach may be implemented using existing state-of-the-art hardware/software found in a building control system. The performance then needs to be compared with the current feedback approach. Besides control performance, the

tuning, trouble shooting, maintenance, ease of commissioning and operation will be key success factors.

2. The pressure and temperature control sequences used to test the controllers were considered separately in this research. In reality, however, the sequences will be coupled and overlapping. For example, while the increase in fume hood exhaust flow may require heating, the increase in the rate of internal heat generation may dictate more cooling. It will be necessary to test the controller with simultaneous demands.

3. In addition to the space temperature, space humidity might be included as an additional control variable. The humidity control is critical in the process and manufacturing labs but is seldom being controlled in a common research lab.

4. A supervisory controller is needed that will command and coordinate the actions of the supply flow, general exhaust flow and supply air temperature control loops. The focus of the supervisory controller will be to manage these different control loops in order to eliminate contradictions between them and to ensure a smooth transition between one control sequence to another.

5. The control signal from the feedback approach is added to the feedforward control signal after a certain time delay following the initial disturbance. The delay time was selected for each control sequence during tuning of the FFPI controller and was kept constant for all cases of a specific

control sequence. A scheme may be developed that combines the feedforward with feedback approach automatically. The method of combination may be based on the delay time, as was the case in this study, or on the achievement of steady state in terms of a process variable (e.g. flows, room temperature, pressure etc.). The combination method preferably should be a part of the commissioning process.

6. The success of any identification scheme, including GRNN, depends on gathering "quality" data from a real system. A data acquisition system with post-processing capability is required for this purpose. In addition a method needs to be adapted to update the current data stored and used by the GRNN. The adaptation is absolutely necessary in order to capture the effect of change in operating conditions on the characteristics. The ability to adapt is critical to reduce re-tuning effort, which in turn will require minimum troubleshooting and will increase operational efficiency.

7. Hysteresis with damper and valve actuator has been assumed negligible. A modification of the identification block may be suggested to include hysteresis with the HVAC control equipment. One approach may be to develop two separate GRNNs for each control equipment. One would identify the equipment characteristics when the control signal increases and the other one when the control signal decreases. A simple algorithm may select one GRNN over the other by noting the change in the direction of a setpoint change from the current value.

8. The initial conditions for the simulation of the different control sequence were steady and constant operation. The boundary conditions are the supply and general exhaust duct pressures, fume hood exhaust flow rate and pressure and temperature of the adjacent space. In reality, however, these conditions will have noisy data and fluctuate. Further simulation may be recommended to accommodate such noise and prove the control system's ability to handle noisy data.

9. The lab emulator may be developed to create a lab design software tool. Such a tool is greatly needed in the industry today in order to analyze both the steady and transient nature of lab environment; a key element for both efficient and safe lab operation. The lab emulator may include the models for room, thermal envelope, HVAC equipment, control equipment and controllers.

10. The lab emulator may be further extended to include the dynamics of supply, fume hood exhaust and general exhaust systems including diffusers, ductwork and fans and water piping and pumps serving heating coils. The ability to model and simulate the entire lab HVAC system will increase its scope and value in the lab HVAC industry.

11. Reliability of the identification block in the feedforward control has to be investigated. The risk of poor identification and its effect on control need to be assessed. Clustering and filtering of data for identification may be needed in order to increase accuracy of feedforward control signal.

References

Accatatta, A.S., "Energy Conservation for Pharmaceutical Manufacturing Facilities Using Recirculated Air," *ASHRAE Transactions,* Vol. 93, Pt. 1, 1987

Ahmed, O., "A Design Method for Laboratory Pressurization," *CLIMA 2000 conference*, London, U.K., 1993

Ahmed, O., and S.A.Bradley.,"An Approach to Determining the Required Response Time for a VAV Fume Hood Control System," *ASHRAE Transactions,* Vol. 96, Pt. 2, 1990

Ahmed, O., J.W. Mitchell., and S.A. Klein., "Dynamics of Laboratory Pressurization," *ASHRAE Transaction*, 1993

Ahmed, O., S.A.Bradley, S.Jacob, and S.Fritsche., " Apparatus for Controlling the Ventilation of Laboratory Fume Hoods," Patent number. 5,092,227, United States Patent and Trademark Office, Washington D.C., 1992

American Society of Heating, Refrigerating and Air Conditioning Engineers., " Chapter 13 on Laboratories: 1995 HVAC Applications Handbook, "*ASHRAE*, Atlanta, Ga, 1995

American Society of Heating, Refrigerating and Air Conditioning Engineers., "1993 Fundamentals Handbook," ASHRAE, Atlanta, Ga, 1993

American Society of Heating, Refrigerating and Air Conditioning Engineers., "Chapter 20: 1992 Systems and Equipment Handbook," ASHRAE, Atlanta, Ga, 1992

American Society of Heating, Refrigerating and Air- Conditioning Engineers., *ANSI/ASHRAE 110-1995 Standard: Method of Testing Performance of Laboratory Fume Hoods,* ASHRAE, Atlanta, GA,1995

Anderson, S.A.,"Control Techniques for Zoned Pressurization," *ASHRAE Transactions,* Vol. 93, Pt. 2, 1987

Antsaklis, P.J., "Neural Networks in Control Systems," *IEEE Control Systems Magazine,* Vol.15, No.2, 1992

Argüello-Serrano, B., and M. Vélez-Reyes., "Design of a Non-linear HVAC Control Systems with Thermal Load Estimation," *IEEE International Conference on Control Applications*, 1995

Äström, K.J., "Theory and Applications of Adaptive Control- A Survey," *Automatica,* Vol.19,No.5, 1983

Athienitis, A.K., M.Stylianou, and J.Shou., "A Methodology for Building Thermal Dynamics Studies and Control Applications," *ASHRAE Transactions,* 1990

Atkinson, G.V., and G.R. Martino.,"Control of Semiconductor Manufacturing Cleanrooms," *ASHRAE Transactions,* 1989

Baylie, C.L., and S.H. Schultz, "Manage Change: Planning for the Validation of HVAC Systems for a Clinical Trials Production Facility," *ASHRAE Transactions,* 1994

Bekker, J.E., Meckl, P.H., and Hittle, D.C., "A Tuning Method for First-Order Processes with PI Controllers," ASHRAE Transactions, 1991

Bell and Gossett, "Hydronic Systems Engineering Manual," *Bell & Gossett, ITT Fluid Handling Division*, Morton Grove, Illinois, 1964

Bentsen, L., "New VAV Controls for Fume Hoods," *Heating/Piping/Air-Conditioning,* February,1985

Bhat, N.V., P.A. Minderman, Jr., T. McAvoy, and N.S. Wang., "Modeling Chemical Process Systems via Neural Computation," *IEEE Control Systems Magazine,* 1990

Blazier, W.E., "Control of Low Frequency Noise in HVAC Air-Handling Equipment and Systems," *ASHRAE Transactions*, 1993

Borresen, B.A., "HVAC Control Process Simulation," *ASHRAE Transactions,* 1981

Bossart, K.A., and S.M.McGinley.,"Design Characteristics of Clinical Supply laboratories Relating to HVAC Systems," *ASHRAE Transactions,* 1994

Braun, J.E., J.W. Mitchell, S.A.Klein, and W.A.Beckman., "Performance and Control Characteristics of a Large Cooling System,"*ASHRAE Transactions,* Vol. 93, Pt.1, 1987

Bristol, E.H., "Pattern Recognition: An Alternative to Parameter Identification in Adaptive Control," Proceedings of the *sixth IFAC Congress on Control Technology,* Boston, MA, 1975

Brouwer, A.B., "Laboratory Renovation Vs. New Construction: How to decide- How much to Pay," *INFOBANK, 90.04*, Hamilton Industries, Two Rivers, WI, 1990.

Buchman, T.G., K.L. Kubos., A.J. Seidler., and M.J. Siegforth., "A Comparison of Statistical and Connectionist Models for the prediction of Chronocity in a Surgical Intensive care Unit," *Critical Care Medicine*, Williams and Wilkins, 1994

Caplan, K.J., and G.W.Knutson., "Laboratory Fume Hoods: A Performance Test," *ASHRAE Transactions,* Vol. 84, Part 1, 1978.

Caplan, K.J., and G.W.Knutson., "Laboratory Fume Hoods: Influence of Room Air Supply," *ASHRAE Transactions,* Vol.84, Part 1, 1984

Carnes, L., "Air-to-Air Heat Recovery Systems for Research Laboratories," *ASHRAE Transactions,* 1984

Carpenter, J.P., "Reliability of Systems and Duct Materials," Paper Presented at the *International Conference Publications Seminar*, Toronto, ICP, San Diego, CA, 1990

Cerami, V.J., "Controlling HVAC Equipment Noise," *Heating/Piping/Air-Conditioning*, 1996

Chapman, W.P., "Fundamentals of Linear Control Theory," *ASHRAE Journal,* April, 1964

Chen, C.T., "Linear Theory Systems and Design," *Holt, Rinehart and Winston*, New York, 1970

Chen, Y.H., and K.M.Lee." Adaptive Robust Control Scheme Applied to a Single- Zone HVAC System," *ASHRAE Transactions,* Vol.96, Pt.2., 1990

Clarke, D.W., and P.J. Gawthrop., "Implementation and Application of Microprocessor- Based Self-Tuners," *Proc. IFAC Symposium on Identification and System Parameter Estimation,* Darmstadt, Federal Republic of Germany, 1979

Cohen, G.H., and G.A. Coon., "Theoretical Consideration of Retarded Control," *ASME Transactions,* 1953

Coleman, H.W., and W.G. Steele., "Experimentation and Uncertainty Analysis," *McGraw-Hill*, New York, 1989

Corless, M., and G.Leitmann., "Adaptive Control for Uncertain Dynamical Systems," Balquiere, A., and G. Leitmann (eds.), Mathematical Theory of Dynamcial Systems and Microphysics: Control and Mechanics. New York: Academic Press, 1984.

Crane, J.T., "Biological Laboratory Ventilation and Architectural and Mechanical Implications of Biological Safety Cabinet Selection, Location, and Venting," *ASHRAE Transactions,* 1994

Crawford, R.R., R.G.Dykowski, and S.E. Czajkowski., "A Segmented Linear Least- Squares Modeling Procedure for Non-Linear HVAC Components," *ASHRAE Transactions,* Vol.97, Pt.2, 1991

Curtiss, P.S., "Experimental Results from a Network-Assisted PID Controller," *ASHRAE Transactions*, 1996

Curtiss, P.S., G. Shavit., and J.F. Kreider., "Neural Network Applied to Buildings- A Tutorial and Case Studies in Prediction and Adaptive Control," *ASHRAE Transactions*, 1996

Davis, S.J., and R.Benjamin., " VAV with Fume Hood Exhaust Systems," *Heating/Piping/Air Conditioning,* August, 1987

Dayhoff, J.E., "Neural Network Architecture," Van Nostrand Reinhold, New York, 1990

Department of Energy/ Energy Information Agency., "Commercial Building Characteristics," *Publication DOE/EIA-0246(89),* U.S. Government Printing Office, Washington D.C., 1991

Department of Energy/ Energy Information Agency., "Commercial Building Characteristics," *Publication DOE/EIA-0246(92),* U.S. Government Printing Office, Washington D.C., 1994

Dexter, A.L., and P.Haves., "A Robust Self- Tuning Predictive Controller for HVAC Applications," *ASHRAE Transactions,* Vol.95, Pt.2, 1989

Dexter, A.L., "Self-Tuning Control Algorithm for Single Chip Microcomputer Implementation," *Proceedings IEEE,* Vol.130, No.5, 1983

Ding, Y., and K.V. Wong., "Control of a Simulated Dual- Temperature Hydronic System Using a Neural Network Approach," *ASHRAE Transactions,* Vol.96, Pt.2, 1990

Dodge, F.W., "Total Laboratory Construction," *Dodge National Information Service*, Chicago, IL, 1995.

Dorf, R.C., "Modern Control Systems," *Addison-Wesley Publishing Company*, Reading, MA, 1980

Doyle, D.L., R.D. Benzuly, and J.M. O'Brien., "Variable-Air-Volume Retrofit of an Industrial Research Laboratory," *ASHRAE Transactions,* 1993

Esmond, J., "Research Laboratory Ventilation System," *Heating/Piping/Air Conditioning Magazine, February,* 1989

Farho, J.H., W.M. Goryl and S.A. Anderson., "Laboratory Fume Hood Control," *Heating/Piping/Air-Conditioning,* February,1984

Food and Drug administration. Part II: Department of Health, Education and Welfare. 1976., "Human Drugs. Current Good Practice in Manufacture, Processing, Packing or Holding of Large Volume of Parenterals," *Federal Register,* Rockville, MD, 1976

Gartner, J.R., and J.L. Harrison., "Dynamic Characteristics of Water-to-Air Crossflow Heat Exchangers," *ASHRAE Transactions,* 1963

Gawronski, W.K., and J.A. Mellstrom., "Antenna Servo Design for Tracking Low-Earth-Orbit Satellites," *Journal of Guidance, Control, and Dynamics*, 1994

Gawronski, W.K., C.S. Racho and J.A. Mellstrom., "Applications of the LQG and Feeforward Controllers to the Deep Space Network Antennas," *IEEE Transactions on Control Systems Technology*, December, 1995

Gerbig, F.T., "Clean Room Design for Microelectronics Manufacturing," *ASHRAE Transactions*, 1981

Goldschmidt, I., "DDC Software and Hardware," *ASHRAE Journal,* September, 1986

Green, W.L., D.R. Oglesby and C.F. Moore., "Preliminary Modeling for Applying Digital Control to a Dual Duct Air-Handling System," *ASHRAE Transactions*, 1977

Grother, P.J., and G.T. Candela., "Comparison of Handprinted Digit Classifiers," *National Institute of Standards and Technology*, U.S. Department of Commerce, Report NISTIR 5209, 1993

Guang, G., and G.M. Geary., "On Performance and Tuning of PID Controllers in HVAC Systems," *IEEE Conference on Control Applications*, September, 1993

Haines, R.W., and D.C. Hittle., "Control Systems for Heating, Ventilating, and Air-Conditioning," Van Nostrand Reinhold, New York, 1983

Henderson, H.I., "Simulating Combined Thermostat, Air Conditioner, and Building Performance in a House," *ASHRAE Transactions*, 1992

Hitchings, D.T. and R.S. Shull., "Measuring and Calculating Laboratory Exhaust Diversity- Three Case Studies," *ASHRAE Transactions,* 1993

Hitchings, D.T., "Laboratory Space Pressurization Control Systems," *ASHRAE Journal,* February, 1994

Homma, H., "Ventilation of Dwellings and Its Disturbances," *Faibo Grafiska*, Stockholm, 1975

Hrkman, L., "Lab Controls Lunch and Learn Presentation," *Landis & Gyr*, Buffalo Grove, IL, February, 1996

Huang, S.H., and R.M. Nelson., "Delay Time Determination Using an Artificial Neural Network," *ASHRAE Transactions*, 1994

Incropera, F.P., and D.P.Dewitt., "Introduction to Heat Transfer," *John Wiley & Sons.*, New York, 1985

Kamimura, K., A. Yamada.,T. Matsuba., A. Kimbara., S. Korosu., and M. Kasahara., "CAT (Computer-Aided Tuning) Software for PID Controllers," *ASHRAE Transactions*, 1994

Kays, W.M., and A.L. London., "Compact Heat Exchangers," *McGraw-Hill Book Company*, New York, 1964

Kelly, G., C.Park, D.R.Clark, and W.B.May., "HVACSIM+, A Dynamic Building-HVAC-Control Systems Simulation Program," Workshop on HVAC Controls, Modeling, and Simulation, Georgia Institute of Technology, Atlanta, 1984.

Klein, S.A., and F.L. Alvarado., "Engineering Equation Solver," *F-Chart Software*, Middleton, WI, 1994

Kleinman, A.L., "On an Iterative Technique for Riccati Equation Computations," *IEEE Transactions on Automatic Control*, Vol AC-13, 1968

Knutson, G.W., "Testing Containment of Laboratory Hoods: A Field Study," *ASHRAE Transactions,* 1987

Konrad, A., "ENCORE CANADA Computer Program," *Division of Building Research, National Research Council*, Ottawa, 1978

Koontz R.L., "Conventional Buildings for Reactor Containment," NAA-SR-10100, Office of Technical Services, Department of Commerce, Washington, D.C., 1965

Kraft, L.G., and D.P. Campagna., "A Comparison Between CMAC Neural Network Control and Two Traditional Adaptive Control Systems," *IEEE Control Systems Magazine,* 1990

Krakow, K.I., S. Lin.,and Z. Zeng., "Analytical Determination of PID Coefficients for Temperature and Humidity Control during Cooling and Humidifying by Compressor and Evaporator Fan Speed Variation," *ASHRAE Transactions*, 1995

Kurz, H., R. Isermann, and R. Schumann., "Experimental Comparison and Application of Various Parameter- Adaptive Control Algorithms," *Automatica,* Vol.16, 1980

Lacey, D.R., "Observed Performance of VAV Hood Controls," *ASHRAE Transactions,* 1989

Landis & Gyr Powers, "Laboratory Control and Safety Solutions Design Guide," *Landis & Gyr*, Buffalo Grove, IL,1994

Landis & Gyr Powers, "Powers Loop Tuner User Manual," *Landis & Gyr*, Buffalo Grove, IL, 1988

Landis & Gyr Powers., "Calibration of room thermostats (Internal document)," Landis & Gyr, Buffalo Grove, IL, 1995

Landis & Gyr Powers., "System 600 SCU User Reference Manual," Landis & Gyr, Buffalo Grove, IL, 1990

Li, X.M., and W.J.Wepfer., "Recursive Estimation Methods Applied to a Single-Zone HVAC System," *ASHRAE Transactions,* 1987

Lujan, P., "Variable Air Volume: Where Are We?," *ASHRAE Transactions,* 1977

MacArthur, J.W., E.W. Grald, and A.F. Konar., "An Effective Approach for Dynamically Compensated Adaptive Control," *ASHRAE Transaction,* Vol.95, Pt.2, 1989

Marsh C.W., " DDC Systems for Pressurization, Fume hood Face Velocity and Temperature Control in Variable Air Volume Laboratories," *ASHRAE Transactions,* Vol.94, Pt.2, 1988

McDiarmid, M.D., "Variable-Volume Fume Hoods: User Experience in a Chemistry Research Buildings," *ASHRAE Transactions,* 1990

Means R.S. Company Inc., "Means Mechanical Cost Data 1991," *R.S. Means Company Inc.,* Kingston, MA, 1991.

Mehta, D.P., "Dynamic Performance of PI Controllers: Experimental Validation," *ASHRAE Transactions,* 1987

Miller, J.M., and J.T. Williams., "The Laboratory Fume Hood: Safety Considerations," *American Laboratory,* June, 1988.

Mollenkamp, R.A., "Modern Digital and Automatic Process Control," *McGraw-Hill Chemical Engineering Seminar*, McGraw-Hill, New York, 1981

Mood, A.M., and F.A. Graybill., "Introduction to the Theory of Statistics," *Macmillan*, New York, 1962

Moyer, R.C., "Fume Hood Diversity for Reduced Energy Consumption," *ASHRAE Journal,* September, 1983.

Narendra, K.S., "Adaptive Control Using Neural Networks," Neural Network for Controls, Ed. by W.M. Miller III, R.S. Sutton, and P.J. Webros, The MIT press, 1992

Narendra, K.S., and S. Mukhopadhyay., "Intelligent Control Using Neural Networks," *IEEE Control Systems Magazine,* Vol.15, No.2, 1992

National Fire Protection Association., "National Fire Codes 1984 Standard on Fire Protection for Laboratories using Chemicals," *NFPA 45-1982,* pp. 45-1, 45-37, Vol.2, NFPA, Quincy, MA, 1984

Naughton, P., "HVAC Systems for Semiconductor Cleanrooms- Part I: System Components," *ASHRAE Transactions,* 1990

Naughton, P.J., "DCS Commissioning for a Microelectronics Factory," *ASHRAE Transactions,* 1992

Nelson, J.S., "Key Design Considerations for Mechanical and Electrical Building and Environmental Systems," Paper presented at the *1986 Tradeline Conference on the R & D Facility of the Future.* San Francisco, CA, 1986

Nesler, C.G., "Adaptive Control of Thermal Processes in Buildings," Paper presented at the *American Control Conference,* Boston, 1985

Nesler, C.G., and W.F. Stoecker., "Selecting the Proportional and Integral Constants in the Direct Digital Control of Discharge Air Temperature," *ASHRAE Transactions*, 1984

Neuman, V.A., and H.M.Guven., " Laboratory Building HVAC Systems Optimization," *ASHRAE Transactions,* Vol. 94., Pt. 2., 1988

Neuman, V.A., and W.H.Rousseau., "VAV for Laboratory Hoods- Design and Costs," *ASHRAE Transactions,* Vol. 92, Pt. 1A., 1986.

Neuman, V.A., "Design Considerations for Laboratory HVAC Systems Dynamics," *ASHRAE Transactions,* Vol.95, Pt.1., 1989.

Nguyen, D.H., and B.Widrow., "Neural Networks for Self-Learning Control Systems," *IEEE Control Systems Magazine, 1990*

Nordeen, H., "Fundamentals of Control from a Systems Perspective," *Heating/Piping/Air-Conditioning,* August, 1995

Norman, S.A., and S.P. Boyd., "Multivariable Feedback Control of Semiconductor Wafer Temperature," *American Control Conference*, 1992

Parker, J.A., O. Ahmed and K.A. Barker., "Application of Building Automation System (BAS) in Evaluating Diversity and Other Characteristics of a VAV Laboratory," *ASHRAE Transactions,* 1993

Parzen, E., "On Estimation of a Probability Density Function and Mode," *Annal of Mathematical Statistics*, 1962

Pearson, J.T., R.G. Leonard., and R.D. McCutchan., "Gain and time constant for finned serpentine crossflow heat exchangers," *ASHRAE Transactions,* Vol. 80, Pt.2,1974

Petersen, J., "Air Conditioning of Research and Test Facilities; Contamination Control," *ASHRAE Journal,* September, 1964

Phillip, D., "Direct Digital Control: Next Generation for Building Automation," *Specifying Engineer,* August, 1982

Psaltis, D., A. Sideris., and A.A. Yamamura., "A Multilayered Neural Network Controller," Paper presented at the *1987 IEEE International Conference on Neural Networks,* San Diego, California, 1987

Rabiah, T.M., and J.W. Welkenbach., "Determining Fume Hood Diversity Factors," *ASHRAE Transactions,* 1993

Rabiah, T.M., R.P. Garrison, and R.K. Sachdev., "Comparisons of Variable-Volume Fume Hood Controllers," *ASHRAE Transactions,* 1989

Rice, J.S., " Direct Digital Controls and Energy Management," *Air Conditioning, Heating and Refrigeration News,* November, 1987

Richardson, G., "Commissioning of VAV Laboratories and the Problems Encountered," *ASHRAE Transactions,* 1994

Rizzo, S.P., "Commissioning of Laboratories: A Case Study," *ASHRAE Transactions,* 1994

Rohrer, C.E., and W.F. Stoecker., "Z-Transforms as an Aid to DDC Systems Analysis," *ASHRAE Transactions*, 1986

Rumelhart, D.E., J.L. McClelland and the PDP Research Group., "Parallel Distributed Processing," The MIT Press, 1989.

Schei, T.S.,"Closed Loop Tuning of PID Controllers," *American Control Conference*, 1992

Schuyler, G., "Performance of Fume Hoods in Simulated Laboratory Conditions," *ASHRAE Transactions,* Vol. 96, Pt. 2, 1990

Scientific Apparatus Makers Association., *SAMA Standard LF-10-1980, SAMA*, Washington D.C.,1980

Shah, M.M., "Estimated Rate of Pressurization and Depressurization of Buildings," *ASHRAE Transactions,* Vol.86, Pt.1, 1980

Shavit, G., and S.G. Brandt., "The Dynamic Performance of a Discharge Air-Temperature System with a P-I Controller," *ASHRAE Transactions*, 1982

Shumaker, R.B., "User's Experiences with Variable-Volume Laboratory Fume Hood Exhaust Systems," *ASHRAE Transactions*, 1989

Simmons, C.G., and R. Davoodpour.,"Design Considerations for Laboratory Facilities Using Molecular Biology Techniques," *ASHRAE Transactions*, 1994

Specht, D.F., "A General Regression Neural Network," *IEEE Transactions on Neural Networks*, 1991

Specht, D.F., "Probabilistic Neural Network," *Neural Networks*, Vol. 3, 1990

Stoecker, W.F., "A Generalized Program for Steady- State System Simulation," *ASHRAE Transactions*, 1971

Streets, R.A., and B.S.V. Setty., "Energy Conservation in Institutional Laboratory and Fume Hood Systems," *ASHRAE Transactions*, 1983

Swiniarski. R.W., "Novel Neural Network Based Self- Tuning PID Controller Which Uses Pattern Recognition Technique," Paper presented at the *1991 American Control Conference.*

Tao, K.M., and M. Jurik., "Improved Back Propagation Algorithms- a Systems Control and Identification Approach," *Asilomar Conference on Signals, Systems & Computers*, 1989

U.S. Department of Commerce., "HVACSIM+ Building Systems and Equipment Simulation Program Reference Manual," *NBSIR 84-2996*, National Bureau of Standards, Washington, 1984

U.S. Dept. of Energy and U.S. Dept. of Housing and Urban Development,"Building Energy Performance Standards," DOE/HUD, Washington, D.C., 1990

Underwood., D.M., "Response of Self-Tuning Single-Loop Digital Controllers to a Computer-Simulated Heating Coil," *ASHRAE Transaction,* Vol.95,Pt.2,1989

Vance, H.J., "Laboratory Ventilation Design," Paper Presented at the *International Conference Publications Seminar*, Toronto, ICP, San Diego, CA, 1990

Varley, J.O., "Measuring Fume Hood Diversity in an Industrial Laboratory," *ASHRAE Transactions,* 1993

Viscovitch, M., "Enthalpy Recovery in Low- Humidity Pharmaceutical Clean Rooms," *ASHRAE Transactions,* Vol. 93, Pt. 1, 1987

Wasserman, P.D., "Neural Computing; Theory and Practice," Van Nostrand Reinhold, New York, 1989

Weaver, H.J., "Applications of discrete and Continuous Fourier Analysis," *John Wiley & Sons*, New York, 1983

Webros, P.J., "An Overview of Neural Networks for Control," Paper presented at the *1990 American Control Conference*, San Diego, CA., May, 1990

Wenz, R.G., "A Practical Laboratory Ventilation Control System," *ASHRAE Transactions,* 1989

West D.L., "Assessment of Risk in the Research Laboratory: A Basis for Facility Design," *ASHRAE Transactions,* 547-557, 1978.

Wiggins, M.E., and R.H. Morris., "Electronic Control for Fume Hoods," *Heating/Piping/Air-Conditioning,* February,1985

Willis, M.J., G.A. Montague, A.J. Morris, and M.T. Tham., "Artificial Neural Networks:- A Panacea to Modeling Problem ?," *American Control Conference,* 1991

Ziegler, J.G., and B. Nichols., "Optimal seting for Automatic Controllers," *ASME Transactions,* Vol. 64, 1942

Appendix A1
Uncertainty Analysis

The measurement uncertainty can be attributed to both the bias and the precision errors. The bias is a fixed error which is inherent with the sensor reading and usually published by the sensor manufacturers. The precision error, in contrast, is random in nature and can be determined by multiple of readings of the same value. The analysis in this section shows the logical steps to determine the measurement uncertainty using primarily bias error. The precision error is ignored as multiple readings during experimentation were not collected as they are difficult and costly to obtain. In addition to the bias error, the error due to the analog to digital (A/D) conversion is also added. The digital building automation system uses discrete values from continuous reading from analog sensors and therefore, introduces fixed error. The analysis below is based on method proposed by Coleman and Steele (1989).

The total experimental error, Y_r can be represented as a function of bias error, B_r, precision error, E_r, and A/D conversion error, D_r.

$$Y_r = (B_r^2 + E_r^2 + D_r^2)^{1/2} \qquad \text{(A.1)}$$

where, r is a function of several measured variables, X_1, X_2, X_3.....X_j. Hence,

$$r=r(X_1, X_2, X_3.....X_j) \qquad \text{(A.2)}$$

A simple example of r is duct flow rate which is a function of both duct velocity and the duct diameter. The duct diameter remains a constant. However, the duct velocity often varies and calculated by measuring the velocity pressure. Hence, duct flow, r, becomes a function of velocity pressure (X_1).

Referring to equation A.1 and ignoring precision error, Y_r reduces to

$$Y_r = (B_r^2 + D_r^2)^{1/2} \qquad \text{(A.3)}$$

However, uncertainty due to the bias error B_r when r is dependent on multiple variables can be found out as follows:

$$B_r = [(\frac{\partial r}{\partial X_1} B_1)^2 + (\frac{\partial r}{\partial X_2} B_2)^2 + ------ + (\frac{\partial r}{\partial X_j} B_j)^2 \qquad \text{(A.4)}$$

When r is directly measured, the uncertainty B_1, due to the bias error becomes equal to the error itself. The error analysis is done for direct measured variables i.e. temperature, T and room pressure differential, Δp, indirect measured variable, flow rate, $\dot{v}$ and dependent variable, density, ρ as follows.

Supply air temperature, T_S

Following equation 4.8, the error for supply air can be written as

$$Y_{T_S} = (B_{T_S}^2 + D_{T_S}^2)^{1/2} \qquad \text{(A.5)}$$

The bias error for supply temperature sensor is 0.7 ^oF while transmitter error is 0.2 ^oF. Hence,

$$B_{T_S} = (0.7^2 + 0.2^2)^{1/2} = 0.728\ ^oF \qquad (A.6)$$

The A/D conversion error for temperature sensor is based on a 16 bit controller and for a 0-10 volts sensor range where 10 volts corresponds to 100 ^{o}F. As a result, the error in volts due to the digitization is,

$$D_{volt} = \frac{1}{2}\left(\frac{10}{65536}\right) = .0076 V\ of\ Full\ Scale \qquad (A.7)$$

So, for a supply temperature of 55 ^{o}F, the A/D conversion error amounts to,

$$D_{T_S}\,|_{55\ ^oF} = .0076\left(\frac{100}{10}\right) = .076\ ^oF \qquad (A.8)$$

Finally, combining B_{T_S} and D_{T_S},

$$Y_{T_S} = \sqrt{(0.728^2 + .076^2} = 0.731\ ^oF \qquad (A.9)$$

Room thermostat, T

The bias error for supply temperature sensor at 70 ^{o}F is 0.7 ^{o}F while transmitter error is 0.2 ^{o}F. Hence,

$$B_T = (0.82^2 + 0.2^2)^{1/2} = 0.844\ \ ^oF \qquad (A.10)$$

The A/D conversion error for the thermostat remains the same as the supply air temperature. Hence,

$$Y_T = (0.844^2 + 0.076^2)^{1/2} = 0.847\ ^oF \qquad (A.11)$$

Radiant wall temperature, T_W

The bias error for radiant wall temperature sensor is 0.7 ^{o}F while transmitter error is 0.2 ^{o}F. Hence,

$$B_{T_W} = (1.5^2 + 0.2^2)^{1/2} = 1.513\ ^oF \qquad (A.12)$$

The A/D conversion error for the radiant wall temperature is changed since the range of this sensor is 150 ^{o}F. Therefore, following equation 4.13, the A/D conversion error for radiant wall temperature becomes

$$D_{T_w} = .0076\left(\frac{150}{10}\right) = .114\ ^{o}F \qquad \text{(A.13)}$$

Combining now B_{T_w} and D_{T_w}, the total error for radiant wall temperature is

$$Y_T = (1.513^2 + 0.114^2)^{1/2} = 1.517\ ^{o}F \qquad \text{(A.14)}$$

Room pressure differential sensor, Δp

The bias error for pressure sensor is .01 "w.g and the A/D conversion error can be found same way as before for the pressure sensor having a maximum range of 1 "w.g.,

$$D_{\Delta p} = .0076\left(\frac{1}{10}\right) = .00076\ "w.g. \qquad \text{(A.15)}$$

Hence, the total error for Δp is

$$Y_{\Delta p} = (.01^2 + 0.00076^2)^{1/2} = .01\ "w.g. \qquad \text{(A.16)}$$

Room static pressure sensor, P_S

The bias error for the pressure sensor remains same as .01 "w.g. However, the A/D conversion error will be doubled since the range is 2 "w.g.

Hence, the total error for P_S is

$$Y_{\Delta p} = (.01^2 + 0.00152^2)^{1/2} = .0101"w.g. \qquad \text{(A.17)}$$

Density, ρ

The expression for room air density assuming ideal gas law is

$$\rho = \frac{P}{RT}$$

Since the universal gas constant R is a constant, the density, ρ becomes a function of room pressure, P and temperature T only. Therefore, equation A.4 can be used to express the uncertainty, B_ρ as

$$B_\rho = [(\frac{1}{RT} B_p)^2 + (-\frac{P}{RT^2} B_T)^2]^{1/2} \qquad (A.18)$$

Dividing equation A.16 throughout by ρ yields

$$\frac{B_\rho}{\rho} = [(\frac{1}{RT}\frac{B_p}{\frac{P}{RT}})^2 + (-\frac{P}{RT^2}\frac{B_T}{\frac{P}{RT}})^2]^{1/2} \qquad (A.19)$$

Canceling similar terms in both numerator and denominator on the right hand side. of the equation results

$$\frac{B_\rho}{\rho} = [(\frac{B_p}{P})^2 + (-\frac{B_T}{T})^2]^{1/2} \qquad (A.20)$$

The room pressure in the above equation was not measured directly but estimated as

$$P = P_{ad} - \Delta P \qquad (A.21)$$

As a result the uncertainty in the room pressure, Bp can be calculated by using the propagation law shown in equation 4.9 as

$$B_p = [(B_{p_{ad}})^2 + (B_{\Delta p})^2]^{1/2} \qquad (A.22)$$

However, instead of the bias error, total uncertainty with the room pressure can be calculated using Y_r values which includes A/D conversion error. Assuming bias error with the barometer to measure the adjacent space pressure is 1% of the reading and $Y_{\Delta p}$ is .01" w.g.. Hence, the Y_p is

calculated to be 4.08" w.g. assuming that the adjacent pressure is atmospheric (408" w.g.).

$$Y_p = [(4.08)^2 + (.01)^2\ ]^{1/2} = 4.08" w.g. \qquad \text{(A.23)}$$

Now, inserting the values of Y_p and Y_T (from equation A.11) in equation A.18 for room pressure of 407.95" w.g. (for a differential pressure of .05" w.g.) and room temperature of 70 ^oF, the uncertainty with density, ρ is found to be within 1.5%.

$$\frac{Y_\rho}{\rho} = [(\frac{4.08}{407.95})^2 + (-\frac{0.847}{70})^2\ ]^{1/2} = .01549 \qquad \text{(A.24)}$$

Air flow rate, $\dot{v}$

The flow rate through the duct is calculated using equation A.25. In this equation, the measured velocity pressure of flowing air, Δp_{flow} is the difference between the total and static pressure.

$$\dot{v} = zA\sqrt{\frac{2\Delta p_{flow}}{\rho}} \qquad \text{(A.25)}$$

The uncertainty in the flow rate, $\dot{v}$, can be determined again using the theory of error progression represented by equation A.4 as follows.

$$B_{\dot{v}} = [(-\frac{zA}{\sqrt{2}}\frac{\Delta P_{flow}^{1/2}}{\rho^{3/2}}B_\rho)^2 + (-zA\frac{\Delta P_{flow}^{-1/2}}{\rho^{1/2}}B_{\Delta P_{flow}})^2\ ]^{1/2} \qquad \text{(A.26)}$$

Dividing A.26 by the expression for $\dot{v}$, equation A.25 is obtained

$$\frac{B_{\dot{v}}}{\dot{v}} = [(-\frac{zA}{\sqrt{2}}\frac{\Delta P_{flow}^{1/2}}{\rho^{3/2}}\frac{B_\rho}{zA\sqrt{\frac{2\Delta p_{flow}}{\rho}}})^2 + (-zA\frac{\Delta P_{flow}^{-1/2}}{\rho^{1/2}}\frac{B_{\Delta P_{flow}}}{zA\sqrt{\frac{2\Delta p_{flow}}{\rho}}})^2]^{1/2}$$

------ (A.27)

Canceling similar terms in numerator and denominator on the right hand side of the equation and simplifying yield equation A.28.

$$\frac{B_{\dot{v}}}{\dot{v}} = [(-\frac{B_\rho}{2\rho})^2 + (\frac{B_{\Delta P_{flow}}}{2\Delta P_{flow}})^2]^{1/2} \qquad \text{(A.28)}$$

Again, instead of using bias error only, the total uncertainty including conversion error can be easily calculated by replacing bias with total uncertainty, Y in equation A.28. Since the sensor used to measure the velocity pressure in the duct is similar to the one used to measure the room pressure differential, Δp, the value of $Y_{\Delta p}$ of 0.01" w.g. (from equation A.15) can be substituted for the value of $Y_{\Delta P_{flow}}$.

Now, for the range of flows in the ducts, the duct velocity varies between 2000 fpm to 200 fpm which corresponds to 0.707" w.g. to 0.223" w.g. Hence, using the standard room air density of 0.075 lbm./ cu. ft. with an uncertainty of .01549 from equation A.22, the uncertainty with the flow at the low end can be found out as

$$\frac{Y_{\dot{v}}}{\dot{v}} = [(-\frac{.01549}{2})^2 + (\frac{.01}{2\ 0.223})^2]^{1/2} = 0.023 \qquad \text{(A.29)}$$

while at the high end the uncertainty found to be

$$\frac{Y_{\dot{v}}}{\dot{v}} = [(-\frac{.01549}{2})^2 + (\frac{.01}{2\ 0.707})^2]^{1/2} = 0.01 \qquad \text{(A.30)}$$

Therefore, with an uncertainty of 2.3%, the error with the flow at the low end of 200 cfm will be 5 cfm while at the high end of 2000 cfm, the error in terms of absolute cfm will be 20 cfm.

Appendix A2

Table of Controller Gains

Control sequence	Control Equipment	FFPI Controller		PI Controller	
		P_g (Control signal/error)	IgS_t (Control signal/error)	P_g (Control signal/error)	IgS_t (Control signal/error)
Pressure	Supply damper	5.0 e(-6)	2.5 e(-5)	0.188*	.061*
Heating	Supply damper	3.0 e(-6)	2.5 e(-6)	.00018	6.1e(-5)
	General exhaust	3.0 e(-6)	2.5 e(-6)	.3675	.163
Cooling w/o load	Supply damper	3.0 e(-6)	2.5 e(-5)	.00018	6.1 e(-5)
	Coil valve	.03	.025	.00735	.00583
Cooling with load	Supply damper	3.0 e(-6)	4.9 e(-6)	3.0 e(-6)	2.5 e(-5)
	Coil valve	.00057	.00019	1.04	.00780

* Gains for PPI controller:
P_g=1.25
IgS_t=.075

Appendix A3

A sample listing of EES program

The following is a listing of a simulation program for only one control sequence. Copies of programs for other sequences will be available from Solar Energy Lab, University of Wisconsin- Madison.

```
This program listing correspond to control
sequence H4. Temperature control- Heating with sudden room load

Procedure load predicts room load as described in section 5.3.2. Note that room
temperature setpoint is assumed constant.

Procedure
LOAD(runno,ST,RMTEMP1,RMTEMP2,QDOTS1,qtx1,datsp,LOADP1:LOADP)

{
Input to the Procedure LOAD
Runno= Run number
ST= Number of samples
Rmtemp1=Room temperature at last sample time {deg.F}
Rmtemp2=Room temperature which precedes Rmtemp1 by a sample {deg.F}
Qdots1= Supply flow rate at last sample time {cfm}
qtx1=Lab total exhaust flow rate at last sample time {cfm}
DATSP= Discharge air temperature setpoint at last sample time {deg.F}. Setpoint, instead of
actual value, is used to avoid instability in predicted load
LoadP1= Predicted load at last sample time {Btu/min.}

Output from the Procedure LOAD
LOADP= Predicted room thermal load {Btu/min.}
}

{Load Prediction Fixed Variables}

V=7500 {room volume in cu.ft}
CV=0.172 {Constant volume specific heat: Btu/lbm.deg R}
Delpsp=.05 {Differential pressure setpoint: w.c.}
PREFS=408 {Adjacent space pressure: Inches of water}
PSP=PREFS-Delpsp {Room pressure setpoint}
RHOAIR=.075 {Air density: lbm/cu.ft}
QREFSP=142.669 {Infiltration air flow rate: CFM}
qdotsp=qtx1-QREFSP {Supply flow rate setpoint: cfm}
PSS=408 {Supply pressure: inches of water}
TREFs=530 {Adjacent space temp: Deg.F}
cpair=0.24 {Constant pressure specific heat: Btu/lbm.deg R}
TEMPSP=70 {Room temp. setpoint: deg. F}
```

```
{ Load prediction calculation}

Deltrm=RMTEMP1-RMTEMP2 {Difference in room temp.}
TERM1=qtx1*RHOAIR*cpair*RMTEMP2 {Energy leaving: Btu/min}
TERM2=qdotsp*RHOAIR*cpair*datsp {Energy in: Btu/min}
TERM3=QREFSP*RHOAIR*cpair*TEMPSP{Energy in: Btu/min}
Term4=(RHOAIR*V*CV*Deltrm/DELTIME) {Time derivative term}
LOADP=Term4+TERM1-TERM2-TERM3 {Enrgy balance to predict load: Btu/min}
If (ST>300) Then LOADP=LOADP1 {If time is greater than 10 minutes, assume load is
constant. Required to activate PI control and hold feedback control loop steady}
End;

{ Sflow procedure is PI controller for supply damper}

Procedure Sflow(runno,st,qdotsp,qdots1,qse1,qsi1:qsP,qskp,qski,qsI,qsOut,qse,CRSS)

{
Input to the Procedure SFLOW:
Runno= Run number
St=Number of samples
qdotsp= Supply flow rate setpoint {cfm}
qdots1= Supply flow rate at last sample time
qse1= Error between supply flow setpoint and simulated value at last sample time {cfm}
qsi1= Integral term at last sample time {control signal: 0-1}

Output from the loop:

qsP= Proportional control signal {0-1}
qskp=Proportional gain {Control signal/error}
qski=Integral gain {Control signal/error}
qsI= Integral control signal {0-1}
qsOut=Sum of proportional and integral term
qse=Error {cfm}
CRSS= Control signal {0-1}
}

{PI Controller calculations}

Stime=0.033 {minutes or 2 seconds}
qsfactor=0.05 {factor to change gains}
qse=(qdotsp-qdots1)
Kp=.00006 {Proportional gain} {Control signal/error}
KI=0.015 {Integral gain} {Control signal/error-min}
qskp=qsfactor*Kp
qski=qsfactor*KI*Stime
qsP=qskp*(qse-qse1)
qsI=qski*qse+qsi1
qsOut=qsP+qsI

{ If ST<300 or i.e. time< 10 minutes than do not activate PI Controller.
```

```
Also reset integral term, qsi=0.0}

If (ST<300.0) Then
CRSS=0.0;
qsI=0.0;
goto 80;
Else
CRSS=qsOut;
EndIf;
80:
END;

{ VALVE procedure is PI controller for coil valve}

Procedure Valve(runno,st,RMTEMP1,Ve1,Vi1:VP,Vkp,Vki,VI,VOut,Ve,CRSSV)
{
Input to the loop
runno= Run number
st= Number of samples
RMTEMP1= Room temperature at last sample time {deg.F}
Ve1= Error between room temperature and setpoint at last sample time {deg.F}
Vi1= Integral term at last sample time {control signal/error}

Output from the loop

VP=Proportional control signal {0-1}
Vkp=Proportional gain {control signal/error}
Vki=Integral gain {control signal/error}
VI=Integral control signal {0-1}
VOut= Sum of proportional and integral control signals {0-1}
Ve= Error between room temperature and setpoint {deg.F}
CRSSV= Control signal  {0-1}
}

{PI controller for heating valve}
Vtime=0.0333 {minutes} {sample time}
Vfactor=.05 {Factor to change gains}
Ve=(70-RMTEMP1)
KpV=.0114 {Proportional gain} {Control signal/error}
KIV=0.114 {Integral gain} {Control signal/error-min}

{PI Controller calculation for heating valve}

Vkp=Vfactor*KpV
Vki=Vfactor*KIV*Vtime
VKd=Vfactor*KDV

VP=Vkp*(Ve-Ve1)
VI=Vki*Ve+Vi1
VOut=VP+VI
```

```
{ If ST<300 or i.e. time< 10 minutes than do not activate PI Controller.
Also reset integral term, Vi=0.0}

If (ST<300.0) Then
CRSSV=0.0;
VI=0.0;
goto 80;
Else
CRSSV=VOut;
EndIf;
80:
END;

{Neural network to generate feedforward control signal for supply damper}

Procedure Snet (runno,Norm%,ST,CRSSL:CRSS1)

{
Input to the procedure Snet
Runno= Run number
Norm%= Normalized supply flow rate setpoint
ST=Number of samples

Output from the procedure SNET
CRSSL= FF controller output at last sample time
CRSS1= FF controller output using GRNN
}

{General regression neural network algorithm: Refer to equations 5.18 and 5.19}

SIGMA=.008 {smoothing parameter}
M=1
N=19
Duplicate j=M,N
D[J]=(Norm%-lookup(J,1))^2.0 {lookup table has observed normalized flows in the first
column}

E[J]=exp(-D[J]/(2.0*SIGMA*SIGMA))
F[J]=lookup(J,2)*E[J] {lookup table has observed control signals in the second column}
End
Outs=sum(F[J],J=M,N)/(sum(E[J],J=M,N)) {OUTS is GRNN output}

{If time is more than 10 minutes, the FF output remains unchanged}

If (ST>300) Then
CRSS1=CRSSL;
goto 10;
Else
CRSS1=Outs;
EndIf;
10:
```

```
End;

{Neural network to generate feedforward control signal for heating coil}

Procedure VCoil (runno,RAT:flowSP%)

{
Input to the procedure Vcoil
Runno= Run number
RAT=Normalized coil temperature {equation: 5.5}
Notice that norm%, another variable to the VCoil, remains constant in this example due to
fixed lab exhaust, Qtx

Output from the procedure Vcoil
flowsp%= Normalized coil water flow rate
}


SIGMACoil=.008 {smoothing parameter}

{Calculation for coil GRNN}

MM=1
NN=14
Duplicate jj=MM,NN
Dcoil[Jj]=(RAT-lookup('COILRAT',Jj,1))^2.0 {First column in Table 'COILRAT' has
observed RAT values}

ECoil[JJ]=exp(-Dcoil[Jj]/(2.0*SIGMACoil*SIGMACoil))
Fcoil[JJ]=lookup('coilrAT',Jj,2)*ECoil[JJ] {Second column in Table 'COILRAT' has
observed flow setpoints}

End
flowSP%=sum(Fcoil[JJ],JJ=MM,NN)/(sum(Ecoil[JJ],JJ=MM,NN)) {GRNN output}
END

{Neural network to generate feedforward control signal for valve actuator}


Procedure Vnet (runno,FlowSP%,ST,CRSSVL:CRSSV1)

{
Input to the procedure Vnet
Runno= Run number
flowsp%= Normalized coil water flow rate setpoint
ST=Number of samples

Output from the procedure SNET
CRSSVL= FF controller output at last sample time
CRSSV1= FF controller output using GRNN
}
```

```
SIGMAV=.008 {smoothing parameter}

{GRNN calculations}
MM=1
NN=19
Duplicate jj=MM,NN
DV[JJ]=(FlowSP%-lookup(JJ,1))^2.0 {First column in the lookup table has observed water
flow rate setpoints}

EV[JJ]=exp(-DV[JJ]/(2.0*SIGMAV*SIGMAV))
FV[JJ]=lookup(JJ,2)*EV[JJ] {Second column in lookup table has observed control signals}

End
OutV=sum(FV[JJ],JJ=MM,NN)/(sum(EV[JJ],JJ=MM,NN)) {OutV is GRNN output}

{ If time is more than 10 minutes than the FF controller signal remains unchanged}

If (ST>300) Then
CRSSV1=CRSSVL;
goto 20;
Else
CRSSV1=OutV;
EndIf;
20:
End;

{ Steady state equations to determine setpoints: refer to equations 5.8 and 5.12}

CFX=9.5227 {conversion factor}
Trmsp=460+70 {Room temperature setpoint. Deg R}
Delpsp=.05 {Room differential pressure setpoint. Inches of water column}
PSP=PREFS-Delpsp {Room pressure setpoin. Inches of water}
QREFSP=142.669 {CFM}
PREFS=408 {Adjacent space pressure. Inches of water}
PSS=408 {Supply static pressure. Incges of water}
TREFs=530 {Adjacnet space temperature. Deg. R}
CP=0.24 { Constant pressure specific heat. Btu/lbm-deg.R}


{Steady state energy equation}


CP*.09725*(PSS*QDOTSP+PREFS*QREFSP-PSP*QTX)+loadp=0

{Steady state conservation of mass equation}

QDOTSP=(TSSP/PSS)*((PSP*QTX/Trmsp)-(PREFS*QREFSP/TREFs))

{Normalization of flows}
```

```
norm%=QDOTSP/2297.0
DATSP=TSSP-460

{Transient energy equation}

{Fixed variables}

cpair=0.240 {Btu/lbm-deg.R}
HEATLOAD=0.220 {BTU/SQ.FT/MIN} Tempref=TREF-460 {deg.F}
RmTemp=TRM-460
Walltemp=Tw-460 {deg.F}

{PARAMETERS}

K=1000 {leakage constant}
PREF=408.0 {WC}
PS=408.0 {WC}
V=7500 {cu.ft}
CV=0.172 {Constant volume specific heat. Btu/lbm-deg.R}
QGEN=HEATLOAD*AREA {Btu/min}
AREA=750 {SQ.FT OF FLOOR AREA}
CF=.09725 {conversion factor}
Uwall=0.30 {Overall wall heat transfer coefficient. Btu/hr-sq.ft-deg.F}
CWALL=0.22 {Wall thermal capacitance. Btu/lbm-deg.R}
Tauw=5000 {Wall mass- thermal capacitance. Btu/deg.F: lightweight}
Awall=1100 {sq.ft}
ho=1.46 {Convective heat transfer coefficient between adjacent space and room exterior
wall. Btu/hr-sq.ft-deg.F}
hi=1.46 {Convective heat transfer coefficient between room air and interior wall surface.
Btu/hr-sq.ft-deg.F}

{Conservation of energy equation neglecting pressure derivative: Refer eqn: 6.12}

0=(PS*QDOTS*cpair)+(PREF*QDOTREF*cpair)-
(P*QTX*cpair)+(QGEN/CF)+hi*Awall*(Tw-TRM)/5.835

{Transient conservation of mass equation neglecting pressure derivative: refer eqn: 6.11}

-V*P*dtrmdt/(TRM*TRM)=(PS*QDOTS/TS)+(PREF*QDOTREF/TREF)-(P*QTX/TRM)

{leakage equation}

QDOTREF=(DELP/abs(DELP))*K*abs(DELP)^NF
P=PREF-DELP {P=Room pressure} {inches of water}
NF=0.65 {flow exponent}

{solution of integral equations}

TRM=TRMINIT+integral(dtrmdt,TIME)
Tw=T[1]+460 {Tw= wall surface temperature: deg.F}
Trminit= 530 {deg.R}
```

{Adjust the temperature if exfiltration takes place instead of infiltration}

TREF=if(QDOTREF,0,TRM,530,530)

{Calculation of mass flow rates}

RX=53.3 {ft-lbf/lbm-deg.R}
mdots=5.188*PS*QDOTS/(RX*TS)
mdotex=5.188*P*QTX/(RX*TRM)
mdotinf=5.188*PREF*QDOTREF/(RX*TREF)

{Finite Differencing Implicit Scheme: Refer equations: 3.15-3.17}

{Surface temperature equation}

T[1]*(1+2*FO+2*BI*FO)-2*FO*(BI*RmTemp+T[2])=tablevalue(runno-1,#T[1])

{Equations for intermediate nodes}

NMAX=6
MAX=5

{DUPLICATE J=2,NMAX
T[J]=1.0
END J}

Duplicate J=2,MAX
T[J]*(1+2.0*FO)-FO*(T[J-1]+T[J+1])=tablevalue(RUNNO-1,#T[j])
End J

{Equations for last node for convection condition}

(1+2.0*FO+2*FO*BI)*T[NMAX]-FO*2.0*(Tempref*BI+T[NMAX-1])=T[NMAX]

{PARAMETERS FOR 1/2 INCHES GYPSUM BOARD}

KT=.09 {BTU/HR-DEG.F-FT}
RHO=50 {LBM/CU.FT}
{CP=0.26 {BTU/LBM-DEG.F}}
L=0.5/12 {FT}
FO=.275 {Fourier number}
BI=.135 {Biot number}

{Damper/actuator simulation model:Refer equations 3.29-3.32}

{Static pressure calculations}

{Coefficients K12, K34, KO and P1 are arbitrarily chosen to get full flow of 2297 cfm when damper command Crss=1.0}

```
P1=3.5 {w.c. static pressure, fan static pressure}
P2=P1-K12*(QDOTS)^2.0 {inlet damper pressure}
P4=.05 {w.c static pressure at the outlet of the diffuser}
P3=P4+K34*(QDOTS)^2.0 {Damper outlet pressure}
{K23=.000000215}
a=(P2-P3)/(P1-P4)
K12=-5.0*10^(-9)
k23=.00001554*KF {.00001554 is conversion factor between metric [HVACSIM] to
British}
K34=.05*10^(-7)

{Damper equation}
P2-P3=k23*(QDOTS)^2.0

{Damper characteristics}
KO=.042
KF=(K1/K2)+K3
K1=WF*KO
K2=((1-LAMDA)*C+LAMDA)^2.0
K3=(1-WF)*KO*LAMDA^(2*C-2.0)
WF=1
LAMDA=.000001

{Actuator model: First order differential equation with dead time: Refer to equation 3.34}

CRSS2=CRSS+crss1 {combining FF and FB control signals}

C=aa*tablevalue(runno-1,#c)+bB*tablevalue(runno-1,#crss2)

aa=exp(-3.33) {3.33 is the ratio between sample time and time constant. A high value is
selected intentionally to ensure that supply flow will reach its setpoint within 2 seconds}

bB=1-aa

{Valve/actuator model: Refer to equation 3.29 to 3.32}

{Frictional coefficients COEFF12, COEFF23, COEFF34 are arbitrarily chosen to achieve
desired flow rate at fuuly open valave position}
PW1=29.051 { Inlet pressure to the valve }
PW1-PW2=COEFF12*(abs(GPM))^2.0
PW2-PW3=COEFF23*(abs(GPM))^2.0
PW3-PW4=COEFF34*(abs(GPM))^2.0
PW4=29.0 {Outlet circuit pressure}
COEFF23=-.086
COEFF34=.08641
aw=(PW1-PW2)/(PW1-PW4)
{aw=0.01}
ETA=.000010 {Valve leakage parameter}
BETA=1 {Valve non-linearity}
GAMMA=.142 { Inverse of valve cv}
```

```
COEFF12=(PART1/PART2)+PART3
PART1=BETA*GAMMA
PART2=((1-ETA)*CVALVE+ETA)^2.0
PART3=(1-BETA)*GAMMA*ETA^(2.0*CVALVE-2.0)

{Actuator model}

Avalve=exp(-3.33)

{3.33 is the ratio between sample time and time constant. A high value is selected
intentionally to ensure that water flow will reach its setpoint within 2 seconds}

Bvalve=1-Avalve
crssv2=crssv+crssv1 {Combining FF and FB control signals}
CVALVE=Avalve*tablevalue(runno-1,#Cvalve)+Bvalve*tablevalue(runno-1,#crssv2)

{Transient heating coil model}

{Parameters}

CAD=42.0 {Design heat capacitance of air stream: btu/min-f}
CAW=9.0 {Design heat capacitance of water stream: btu/min-f}
CRD=CAW/CAD {CAW/CAD}
EPSD=0.70 {Design heating coil effectiveness}
UA=1.5*CAW {Btu/min f: calculated using chart}
TAI=55+460 {deg.r} {*********Things to change**********}
TWI=200+460 {deg.r}

{Calculation}

CW=GPM*0.13368*62.4*1.0 {gpm  is water flow rate in gpm}
CA=QDOTS*0.24*.075 {aflow is air flow rate in cfm}
CR=CW/CA
NTU=UA/CW
EPS=1-exp(-(1-exp(-CR*NTU))/cr) {Coil effectiveness}
DATss=(TAI+EPS*CR*(TWI-TAI))-460

{Coil transients}

Acoil=exp(-0.4)
Bcoil=1-Acoil

Dat=Acoil*tablevalue(runno-1,#DAT)+Bcoil*tablevalue(runno-1,#DATss)

{DAT is dischareg air temperature in deg.F}
{TS is supply temperature in Rankine}
TS=Dat+460

{normalization of data}

{
```

```
RAT is normalized coil temperature
DATSP is the discharge air setpoint
TAI is coil inlet air tempeature (515 deg.R)
TWI is coil inlet waterm temperature (660 deg.R)
}

RAT=(DATSP+460-TAI)/(TWI-TAI)
flow%=GPM/gpmax
gpmax=0.6
ST=TIME*60
flowsp%=GPMSP/gpmax

{ Call different procedures}

Call LOAD(runno,ST,tablevalue(runno-1,#rmtemp),tablevalue(runno-
5,#Rmtemp),tablevalue(runno-1,#qdots),tablevalue(runno-1,#qtx),tablevalue(runno-
1,#DAT),tablevalue(runno-1,#LOADP):loadp)

Call Sflow(runno,ST,QDOTSP,tablevalue(runno-1,#qdots),tablevalue(runno-
1,#qse),tablevalue(runno-1,#qsi):qsp,qskp,qski,Qsi,qsout,qse,CRSS)

Call Valve(runno,ST,tablevalue(runno-1,#RMTEMP),tablevalue(runno-
1,#Ve),tablevalue(runno-1,#Vi):Vp,Vkp,Vki,Vi,Vout,Ve,crssv)

Call Snet (runno,norm%,ST,tablevalue(runno-1,#CRSS1):crss1)
Call VCoil(runno,RAT:flowsp%)
Call Vnet( runno,flowsp%,ST,tablevalue(runno-1,#CRSSV1):crssv1)
```